**REPUBLIC OF TURKEY**
**UNIVERSITY OF GAZIANTEP**
**GRADUATE SCHOOL OF**
**NATURAL & APPLIED SCIENCES**

**MODELING AND ANALYSIS OF CENTRALLY LOADED**
**DOUBLE SKIN COMPOSITE COLUMNS**

**PhD. THESIS**
**IN**
**CIVIL ENGINEERING**

**BY**

**SÜLEYMAN İPEK**

**FEBRUARY 2019**

**Modeling and Analysis of Centrally Loaded Double Skin Composite Columns**

PhD. Thesis

in

Civil Engineering

University of Gaziantep

Supervisor

Assoc. Prof. Dr. Esra METE GÜNEYİSİ

by

Süleyman İPEK

February 2019

REPUBLIC OF TURKEY
UNIVERSITY OF GAZİANTEP
GRADUATE SCHOOL OF NATURAL & APPLIED SCIENCES
CIVIL ENGINEERING DEPARTMENT

Name of the thesis: Modeling and Analysis of Centrally Loaded Double Skin Composite Columns

Name of the student: Süleyman İPEK

Exam date: 06.02.2019

Approval of the Graduate School of Natural and Applied Sciences

Prof. Dr. Necmeddin YAZICI
Director

I certify that this thesis satisfies all the requirements as a thesis for the degree of Doctor of Philosophy.

Prof. Dr. Hanifi ÇANAKÇI
Head of Department

This is to certify that we have read this thesis and that in our opinion it is fully adequate, in scope and quality, as a thesis for the degree of Doctor of Philosophy.

Assoc. Prof. Dr. Esra METE GÜNEYİSİ
Supervisor

| Examining Committee Members | Signature |
|---|---|
| Prof. Dr. Mustafa GÜNAL | _____ |
| Assoc. Prof. Dr. Esra METE GÜNEYİSİ | _____ |
| Assoc. Prof. Dr. Mehmet İshak YÜCE | _____ |
| Assoc. Prof. Dr. Kasım MERMERDAŞ | _____ |
| Assist. Prof. Dr. Hatice Öznur ÖZ | _____ |

I hereby declare that all information in this document has been obtained and presented in accordance with academic rules and ethical conduct. I also declare that, as required by these rules and conduct, I have fully cited and referenced all material and results that are not original to this work.

Süleyman İPEK

**ABSTRACT**

**MODELING AND ANALYSIS OF CENTRALLY LOADED DOUBLE SKIN COMPOSITE COLUMNS**

İPEK, Süleyman

PhD. in Civil Engineering

Supervisor: Assoc. Prof. Dr. Esra METE GÜNEYİSİ

February 2019

219 pages

Composite columns offer several benefits for the earthquake resistant design. They are produced in a variety of cross-sections and by many methods. However, there are some limitations in the application since the behavior of such members under loading is quite different than traditional steel or concrete members. In this thesis, three new models for calculating the ultimate axial strength of centrally loaded composite columns were developed. For this, totally 103 experimental test results on circular hollow section (CHS) concrete-filled double skin steel tubular (CFDST) composite columns given in the previous studies was employed. The models presented herein were generated by using finite element method as well as gene expression programming and artificial neural network techniques. The yield strength, diameter, and thickness of outer and inner steel tubes, concrete compressive strength, length of test specimen, and ultimate axial strength of the CHS-CFDST columns were adopted as investigation parameters. The usefulness of available codes of ACI, Eurocode 4, and AISC, and some existing empirical models suggested by scientists were also statistically evaluated. Furthermore, to investigate the effect of diameter and thickness of outer and inner steel tubes, and concrete strength on such composite columns, a parametric study was performed through finite element analysis. All results were given and discussed comparatively.

**Keywords:** Analysis; Composite column; Concrete filled double skin tube; Finite element method; Genetic programming; Neural network.

# ÖZET

## MERKEZDEN YÜKLEMELİ ÇİFT KABUKLU KOMPOZİT KOLONLARIN MODELLENMESİ VE ANALİZİ

İPEK, Süleyman

Doktora Tezi, İnşaat Mühendisliği

Tez Yöneticisi: Doç. Dr. Esra METE GÜNEYİSİ

Şubat 2019

219 sayfa

Depreme dayanıklı yapı tasarımında kompozit kolonlar birçok fayda sağlamaktadırlar. Bunlar çeşitli kesitlerde ve farklı tiplerde üretilmektedirler. Ancak, kompozit elemanların geleneksel çelik veya beton elemanlardan yük altındaki davranışı oldukça farklı olduğu için uygulamada da bazı farklılıklar bulunmaktadır. Bu tezde, merkezden yüklemeli kompozit kolonların nihai eksenel mukavemetinin hesabı için üç yeni model geliştirildi. Bunun için, toplamda 103 adet dairesel boşluklu kesitli (DBK) beton dolgulu çift kabuklu tüp (BDÇKT) kompozit kolonları ile ilgili önceki çalışmalarda sunulan deneysel test sonuçları kullanıldı. Burada sunulan modeller, sonlu eleman metodunun yanı sıra gen ekspresyonu programı ve yapay sinir ağı teknikleri kullanılarak üretildi. DBK-BDÇKT kolonlarının dış ve iç çelik tüplerinin akma dayanımı, çapı ve kalınlığı, betonunun basınç dayanımı, numunenin boyu ve nihai eksenel mukavemeti araştırma parametreleri olarak kabul edildi. ACI, Eurocode 4 ve AISC gibi mevcut kodların ve bilim insanları tarafından önerilen bazı mevcut ampirik modellerin kullanışlıkları istatistiksel olarak değerlendirildi. Ayrıca, iç ve dış çelik tüplerin çapının ve kalınlığının ve beton dayanımının bu tip kompozit kolonlar üzerindeki etkisini incelemek için, sonlu eleman yöntemi aracılığıyla parametrik bir çalışma gerçekleştirildi. Bütün sonuçlar karşılaştırmalı olarak sunulup değerlendirildi.

**Anahtar Kelimeler:** Analiz; Kompozit kolon; Beton dolgulu çift kabuklu tüp; Sonlu eleman yöntemi; Genetik programlama; Sinir ağı.

*to my family
and Melek*

# ACKNOWLEDGEMENTS

# CONTENTS

# LIST OF FIGURES

xvii

## LIST OF SYMBOLS & ABBREVIATIONS

| | |
|---|---|
| $A_a$ | Cross-sectional area of structural steel section |
| $A_c$ | Cross-sectional area of concrete annulus |
| $A_{cc}$ | Cross-sectional area of concrete core |
| $A_{c,nominal}$ | Nominal cross-sectional area of concrete |
| $A_k$ | Cross-sectional area of hollow part |
| $A_s$ | Cross-sectional area of reinforcing bars |
| $A_{si}$ | Cross-sectional area of inner steel tube |
| $A_{so}$ | Cross-sectional area of outer steel tube |
| $A_{soc}$ | Cross-sectional area of outer steel tube and concrete annulus |
| $b$ | Bias value |
| B | Edge size of steel tube |
| $B_i$ | Edge size of inner steel tube |
| $B_o$ | Edge size of outer steel tube |
| $C_1$ | Strength coefficient |
| $C_2$ | Strength coefficient |
| D | Diameter of steel tube |
| $D_c$ | Diameter of concrete annulus |
| $D_i$ | Diameter of inner steel tube |
| $D_o$ | Diameter of outer steel tube |

| | |
|---|---|
| e | Euler number |
| $E_{cm}$ | Modulus of elasticity of concrete |
| $E_{cc}$ | Modulus of elasticity of confined concrete |
| $E_p$ | Plastic modulus of steel |
| $E_{si}$ | Modulus of elasticity of inner steel tube |
| $E_{so}$ | Modulus of elasticity of outer steel tube |
| $EI_{eff}$ | Effective stiffness of composite section |
| $f$ | Activation function |
| $f'$ | Confined concrete strength in nonlinear region |
| $f_1$ | Lateral confining pressure provided by steel tube |
| $f_c'$ | Compressive strength of concrete |
| $f_{cc}$ | Confined concrete strength |
| $f_{cd}$ | Design compressive strength of cylinder concrete |
| $f_{ck}$ | Characteristic compressive strength of cylinder concrete |
| $f_{cu}$ | Characteristic compressive strength of cube concrete |
| $f_{osc}$ | Strength characteristic of outer steel tube and concrete annulus |
| $f_{sd}$ | Design yield strength of reinforcing steel |
| $f_{sy}$ | Yield strength of steel tube |
| $f_{syi}$ | Yield strength of inner steel tube |
| $f_{syo}$ | Yield strength of outer steel tube |
| $f_y$ | Nominal yield strength of structural steel |
| $f_{yd}$ | Design yield strength of structural steel |
| $I_c$ | Second moment of area of concrete annulus |

| | | |
|---|---|---|
| $I_{si}$ | | Second moment of area of inner steel tube |
| $I_{so}$ | | Second moment of area of outer steel tube |
| $k_1$ | | Constant for ultimate compressive strength of confined concrete |
| $k_2$ | | Constant for strain at ultimate compressive strength of confined concrete |
| $k_3$ | | Coefficient for final compressive strength of confined concrete |
| K | | Effective length factor |
| $K_c$ | | Correction factor |
| L | | Length of column specimen |
| $L_u$ | | Laterally unbranced length of member |
| $m$ | | Coefficient of normalization |
| $n$ | | Coefficient of normalization |
| $P_{cr}$ | | Elastic critical normal force |
| $P_e$ | | Elastic critical buckling load |
| $P_{i,u}$ | | Capacity of inner steel tube |
| $P_o$ | | Nominal axial compressive strength without consideration of length effects |
| $P_{osc,u}$ | | Capacity of outer steel tube and concrete annulus |
| $P_u$ | | Ultimate axial strength of column specimen |
| $P_{pl,Rd}$ | | Characteristic value of plastic resistance |
| Q | | Square root |
| r | | Coefficient for final compressive strength of confined concrete |

| | |
|---|---|
| R | Coefficient for compressive strength of confined concrete in nonlinear region |
| $R_E$ | Coefficient for compressive strength of confined concrete in nonlinear region |
| $R_\varepsilon$ | Coefficient for compressive strength of confined concrete in nonlinear region |
| $R_\sigma$ | Coefficient for compressive strength of confined concrete in nonlinear region |
| $t$ | Thickness of structural steel |
| $t_i$ | Thickness of inner steel tube |
| $t_o$ | Thickness of outer steel tube |
| $u_x$ | Displacement in x-axis |
| $u_y$ | Displacement in y-axis |
| $u_z$ | Displacement in z-axis |
| $w$ | Weight parameter |
| $w_c$ | Unit weight of concrete |
| $w_i$ | Weight parameter |
| $x$ | Independent variable |
| $x_i$ | Independent variable |
| $y$ | Dependent variable |
| $\alpha$ | Imperfection factor |
| $\alpha'$ | Strength coefficient parameter |
| $\alpha_n$ | Strength coefficient parameter |
| $\beta$ | Actual value of input and output parameters |

| | |
|---|---|
| $\beta_{max}$ | Maximum actual value of input and output parameters |
| $\beta_{min}$ | Minimum actual value of input and output parameters |
| $\beta_{normalized}$ | Normalized value of input and output parameters |
| $\gamma_c$ | Strength reduction factor for concrete |
| $\gamma_{si}$ | Strain hardening factor for inner steel tube |
| $\gamma_{so}$ | Strain hardening factor for outer steel tube |
| $\varepsilon$ | Confined concrete strain in nonlinear region |
| $\varepsilon_c$ | Concrete strain |
| $\varepsilon_{cc}$ | Confined concrete strain |
| $\varepsilon_s$ | Steel strain |
| $\varepsilon_{sy}$ | Steel strain at yield point |
| $\eta_a$ | Reduction factor |
| $\eta_c$ | Enhancement factor |
| $\theta_z$ | Rotation against z-axis |
| $\bar{\lambda}$ | Slenderness |
| $\nu_c$ | Poisson's ratio of concrete |
| $\nu_o$ | Poisson's ratio of steel tube with concrete infill |
| $\nu_o'$ | Poisson's ratio parameter |
| $\nu_s$ | Poisson's ratio of steel tube |
| $\xi$ | Nominal confinement factor |
| $\sigma_i$ | Desired steel strength |
| $\Phi$ | Reduction factor parameter for Eurocode 4 |
| $\chi$ | Reduction factor for Eurocode 4 |

| | |
|---|---|
| Ω | Solid ratio |
| atan | Arctangent |
| ACI | American Concrete Institute |
| AIJ | Architectural Institute of Japan |
| AISC | American Institute of Steel Construction |
| ANN | Artificial neural network |
| CFDST | Concrete filled double skin steel tubular |
| CFT/CFST | Concrete filled steel tube |
| CHS | Circular hollow section |
| cos | Cosine |
| EC3 | Eurocode 3 |
| EC4 | Eurocode 4 |
| ET | Expression tree |
| FEM | Finite element method |
| GA | Genetic algorithm |
| GEP | Gene expression programming |
| GP | Genetic programming |
| IS | Insertion sequence |
| K-expression | Karva language expression |
| max | Maximum |
| nf | Neural-fuzzy |
| nn | Neural-network |
| ORF | Open reading frame |

| RC | Reinforced concrete |
| ReLU | Rectified linear unit |
| RIS | Root insertion sequence |
| SHS | Square hollow section |
| sin | Sine |
| tanh | Tangent hyperbolic |

# CHAPTER 1

# INTRODUCTION

## 1.1 General

The structural construction comprises various types of composite elements; concrete section including reinforcing bars named reinforced concrete members, tubular section filled with concrete named as concrete-filled tubes, beam section composing of different propertied materials known as composite beams, slabs and frames, panels consisting of steel and concrete called as double skin sandwich panels, the tubular section involving double steel tubes and concrete infill known as concrete-filled double skin tubes (Zhao and Han, 2006). The most widely used kind of the composite members in structural purposes is steel-concrete composites.

The concrete filled steel tubes (CFT or CFST), considered as precious structural members, are widely used as a structural member in composite construction because of their high strength and good deformability (Uenaka et al., 2010). Concrete filled double skin steel tubular (CFDST) members that can be accepted as a new generation of traditional CFST members distinguish from the conventional one. CFDST members include outer and inner steel tubes and concrete infill between these tubes whereas the traditional CFST members involve a steel tube and concrete infill (Zhao and Han, 2006). Although the double skin composite construction concept has been firstly designed for utilization in submerged tube tunnels (Tomlinson et al., 1989), it is also believed having potential to use in nuclear containment, liquid and gas retaining structures, and blast resistant shelters (Wright et al., 1991a; Wright et al. 1991b). Moreover, CFDST members can be applied for vessels to resist external pressure, for the legs of offshore constructions, for large diameter columns and structures exposed to ice loading (Lin and Tsai, 2001; Montague, 1975; Shakir-Khalil, 1991; Wei et al., 1995).

Compaction of concrete in the double skin tubular columns is one major adversity. The concrete compaction has different impact on composite tubular columns than the concrete including reinforcing bars or steel profiles (Han, 2000). The mechanical features of the concrete are influenced by the compaction of concrete during the construction of the reinforced concrete columns. The main objective of the concrete compaction in these kinds of columns is the improving of mechanical properties of concrete. Yet, the aim of compaction of concrete in the CFDST columns is not only improving the concrete characteristics but also the enhancing the adherence between the steel tubes and concrete annulus (Han and Zhao 2003; Zhao and Han, 2006). For this reason, self-compacting concrete utilization in this kind of construction may be a possible significant solution to achieve a good compaction (Han et al., 2005; Zhu and Peter, 2003).

CFST and CFDST members having the advantages of being economical and quickly constructed can be built in several shapes since the outer steel tube performs a formwork duty for concrete casting and can resist the loading during the hardening of concrete. By this way, the structure could be constructed quickly. Mainly, CFDST members consist of concentric thin steel tubes with concrete infill (called also as concrete annulus). In the past, a large number of studies have been conducted on this kind of elements to investigate the possibilities to be applied to different practices (Han et al., 2004; Lin and Tsai, 2001; Tao et al., 2004; Uenaka, 2010; Wei et al., 1995; Zhao et al., 2002a; Zhao et al., 2002b; Zhao et al., 2010). It was deduced from these studies that CFDST members indicate almost the same behavior as CFST members (Li et al., 2012). Besides, via the hollow section of CFDST elements, a lower structure weight was achieved while a large energy absorption capacity was still maintained (Li et al., 2012; Uenaka et al., 2010).

In addition to having lower self-weight, CFDST has higher bending stiffness, ductility, strength and cyclic performance (Elchalakani et al., 2002; Zhao and Grzebieta, 2002; Yagishita et al., 2000; Nakanishi et al., 1999; Lin and Tsai, 2003). One of the most significant benefits of using CFDST members in the structure is having reasonable fire resistance due to having the inner tube with lower temperature than outer tube that can be provided by the protection of inner tube from the fire by sandwiched concrete (Li et al., 2012; Tao et al., 2004). By this way, the inner steel

could resist to loads during the fire when the outer steel could not due to affected by high temperature. In high-rise buildings, the architects may use the CFDST columns by putting the center of the columns to good use for detailing the downpipes or other services such as electrical wiring (Essopjee and Dundu, 2015).

Moreover, the inner steel tube supplies high local and global stability owing to steel-concrete-steel interactions and having higher modulus of inner tube than the concrete (Zhao and Han, 2006). Besides, for different application purposes, several filler materials between the steel tubes could be utilized instead of concrete annulus.

## 1.2 Research Significance

This study includes the generation of novel models to predict the ultimate axial strength of a new type of composite members, concrete filled double skin steel tubular columns with outer and inner circular hollow section. From the previous studies in the literature, totally 103 data experimentally investigating the ultimate axial strength of concrete filled double skin tubular columns with outer and inner circular hollow section have been compiled. The models presented herein were developed by using soft computing techniques named as finite element method, gene expression programming, and artificial neural network handled the collected data as input and output parameters. The compressive strength of the infill concrete, the outer steel's yield strength, diameter, and thickness, inner steel's yield strength, diameter, and thickness, and the specimen length were considered as input parameters whereas the ultimate axial strength of concrete filled double skin tubular columns with outer and inner circular hollow section was computed as the output parameter namely was the target. Three models generated by finite element method, gene expression programming, and artificial neural network indicated a good prediction performance capacity. The prediction performance of the model proposed by artificial neural network was better than that created by finite element method and gene expression programming. In addition, the estimation performance of models created in the current study was compared with the modified formulas from the codes and proposed empirical models by the researchers. The comparisons indicated that the models proposed by finite element method, gene expression programming, and artificial neural network were performed the best predictivity among the modified formulas from the codes and proposed empirical models by the researchers.

Particularly, when the results of the finite element method, gene expression programming, and artificial neural network models were statistically evaluated, the estimation capability of these models could be obviously seen.

**1.3 Outline of the Thesis**

Chapter 1 - Introduction: Purposes and objectives of the thesis were introduced.

Chapter 2 - Literature review and background: A detailed literature review was carried out on single and double skin concrete filled tubular columns. The previous researches on the experimentally investigation of the concrete filled double skin tubular columns with outer and inner circular hollow section were submitted. The data used in the thesis were explained and presented in detail. The modified formulas from the codes and proposed empirical models recommended by the researchers were presented and explained. Furthermore, the detailed information about finite element method, gene expression programming, and the artificial neural network were given.

Chapter 3 – Research methodology: The soft computing techniques utilized in the thesis presented herein were described. The details of the software used in the generation of the models on the basis of finite element method, gene expression programming, and artificial neural network were explained. The models proposed by finite element method, gene expression programming, and artificial neural network were given and defined.

Chapter 4 - Results and discussions: Indication, evaluation, and discussion of the parametric test results were presented. The results were compared with the experimental test results and the modified formulas from the codes and proposed empirical models by the researchers. Moreover, the comparisons were supported by statistical evaluations.

Chapter 5 – Parametric study and statistical analysis: A parametric study, which includes the modeling and simulation of different propertied CFDST columns with CHS, was submitted. The parametric study was carried out regarding nonlinear analyzing method. The ultimate axial strength of each modeled CFDST column was presented in order to visualize the effect of input parameters on the load carrying capacity of such type of columns. In addition, the results attained from the parametric

study were statistically evaluated to see which input parameter has a remarkable impact on the ultimate axial strength of CFDST columns with CHS.

Chapter 6 - Conclusions: Conclusions of the thesis and recommendations for future studies were presented.

# CHAPTER 2

# LITERATURE REVIEW AND BACKGROUND

## 2.1 Introduction

Composite as a term means the materials that are made up of various elements and/or sections. The same definition could be done for the composites used in the structural construction. The most common and significant utilization areas of the composites in the structures are the using as structural members such as the composite beams, composite slabs, composite columns, etc. In the composites used as structural purposes use the compressive strength characteristic of the concrete and the tensile strength feature of the steel. By using these superior properties of the concrete and steel, a structural member resisting both compressive and tensile loads can be constructed. The utilization only the concrete in the construction of such type of structural members cannot resist the tensile loads since the concrete has negligible resistance in tension while constructing these members just using steel can cause to buckling problems because only steel utilization will provide small dimensioned sections producing the buckling problem.

The composite columns are the one of the most important structural members that is the combination of structural concrete and steel. The composite columns have various formation shapes as shown in Figure 2.1.

Reinforced concrete (RC) columns are the composite column in which the reinforcing (steel) bars are surrounded by the concrete in order to resist against to loads by acting together as shown in Figure 2.1a. Concrete encased steel columns are a special kind of composite columns in which H-shaped steel is encompassed by concrete or reinforced concrete to improve the load carrying capacity and earthquake resistance characteristic of columns as illustrated in Figure 2.1b. Concrete filled steel columns are special type of composite columns which consist of steel tube filled with concrete as shown in Figure 2.1c.
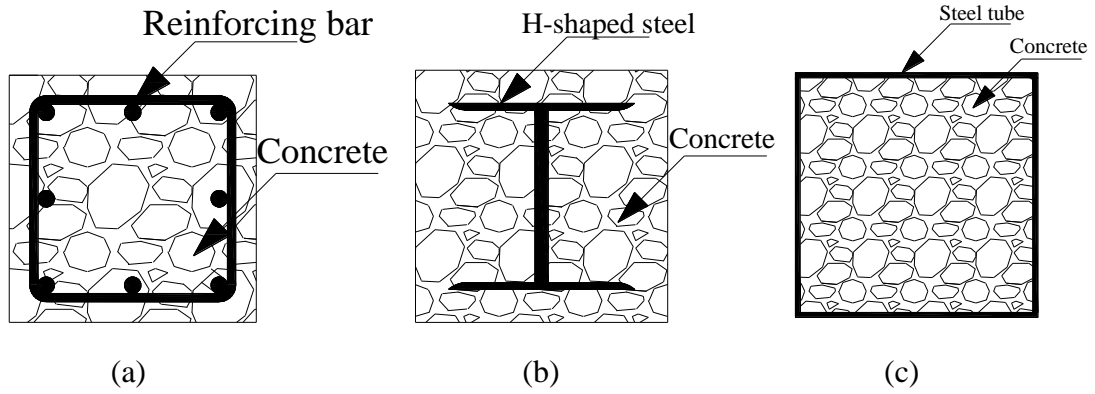
**Figure 2.1.** Typical composite columns sections: (a) reinforced concrete column, (b) concrete encased steel column, and (c) concrete filled steel column

Concrete filled steel tubes (CFT or CFST) have large strength and good deformability characteristics which makes it precious structural members (Uenaka et al., 2010). Construction of these types of the columns is quicker than that of traditional one since the steel tube is also playing formwork role during the construction (Zhao and Han, 2006). The CFST columns may be in various cross-sectional patterns. The common cross-sectional patterns of the CFST columns are given in Figure 2.2.



(a)



(b)
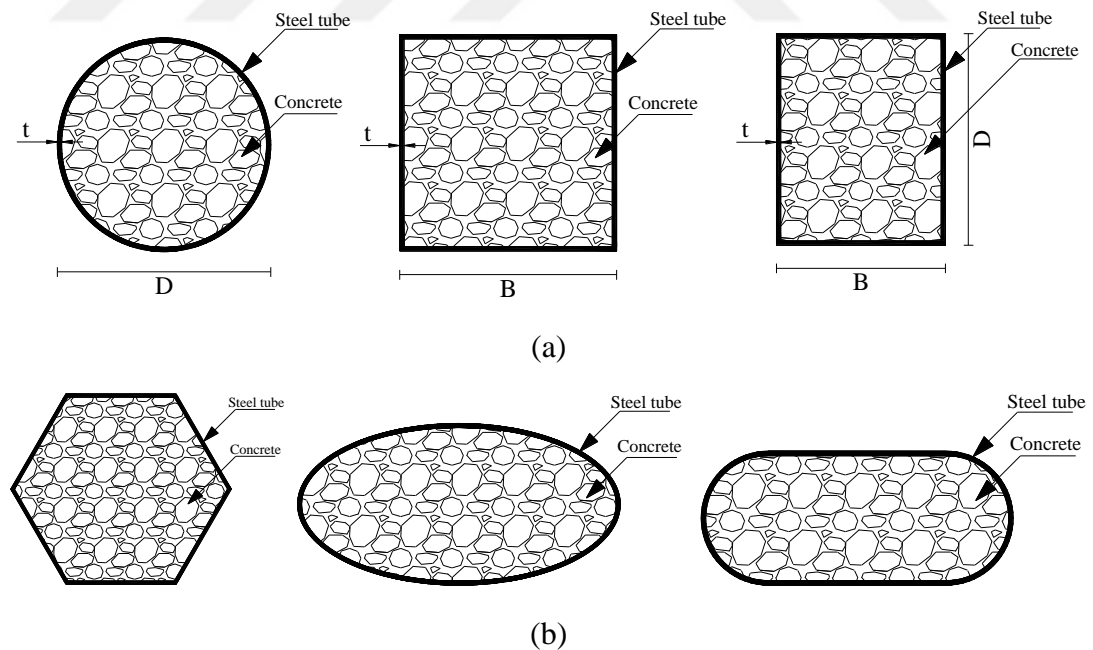
**Figure 2.2.** The cross-sectional patterns of the CFST columns: (a) common patterns and (b) special patterns

Figure 2.2a illustrates the common patterns of the CFST columns where B and D are the outer dimensions and t is the thickness of the steel tube. The patterns presented in

Figure 2.2b may be used for architectural purposes to achieve aesthetic view in the structures. Offshore and marine structures, bridge pipers, and multi-floor structures are some of the utilization area of CFST columns. The large lateral stiffness and strength as well as large load carrying capacity that are obtained by steel tube and concrete interaction are sufficiently procured in the CFST columns. Further, the steel tube secures the concrete that results in procrastination of the local buckling of the steel tube and also, the strength increment is provided to concrete by steel tube confinement effect (Hsiao et al., 2015). There have been many studies carried out to experimentally and analytically investigate the behaviors, characteristics, and applications of CFST members (Furlong, 1967; Gardner and Jacobson, 1967; Chen and Chen, 1973; Lin, 1988; Luksha and Nesterovich, 1991; Prion and Boehme, 1994; Boyd et al., 1995; Kato, 1995; Morino et al., 1997; O'Shea and Bridge, 2000; Elchalakani et al., 2001; Elremaily and Azizinamini, 2002; Han et al., 2003; Marson and Bruneau, 2004; Fujimoto et al., 2004; Han and Yang, 2005; Wheeler and Bridge, 2006; Goode and Lam, 2008; Zhang et al., 2009; Roeder et al., 2010; Lu and Zhao; 2010; Ho and Lai, 2013; D'Aniello et al., 2014; Güneyisi et al., 2016)

## 2.2 Concrete Filled Double Skin Steel Tubular (CFDST) Members

Concrete filled double skin steel tubular (CFDST) members could be acknowledged as a new generation of conventional CFST members differing in some points. The general phenomenon for these members is the steel-concrete-steel formation. Namely, they are formed by two eccentrically built steel tubes and a concrete annulus between the tubes. However, in some applications, the steel-concrete-steel-concrete phenomenon could be used. The general names for these phenomena are hollow section and solid section, respectively. Figure 2.3 presents some type of CFDST members sections in detail. In the figure, $D$, $D_o$, $D_i$, $B$, $B_o$, and $B_i$, are the outer and inner dimensions of circular and square steel tubes, $t_o$ and $t_i$ are the thickness of outer and inner steel tubes, respectively. The circular hollow section (CHS) and the square hollow section (SHS) are illustrated in Figure 2.3a and 2.3c, respectively. Figure 2.3b and 2.3d indicates the sections consisting of different shaped steel tube sections, as seen in Figure 2.3b, the section comprises of outer circular and inner square steel tubes whereas in Figure 2.3d, the section consists of outer square and inner circular tubes. All these sections are known as hollow section.

Besides, in Figure 2.3e and 2.3f, the steel-concrete-steel-concrete section, namely, double skin solid section is presented for circular and square members, respectively.
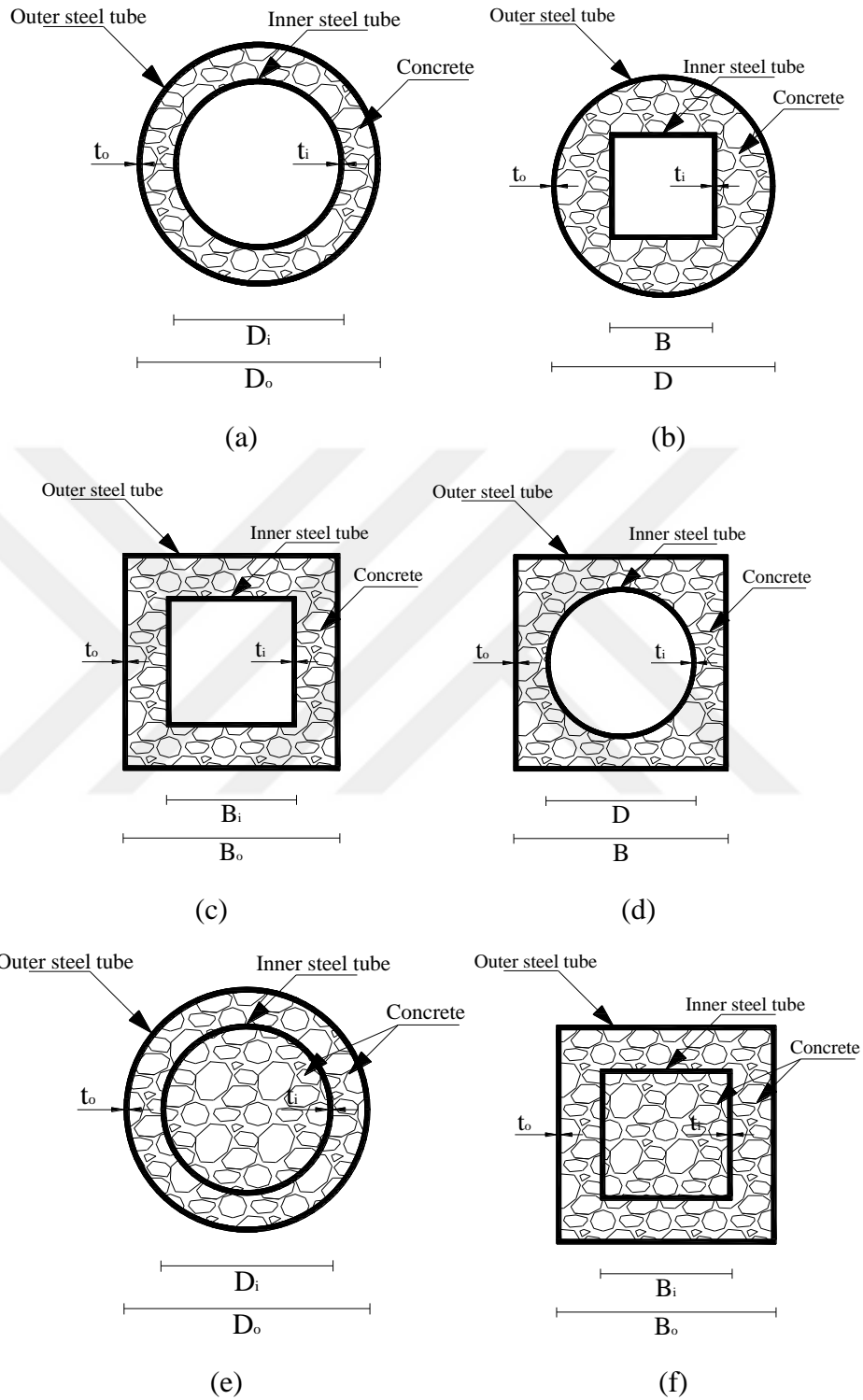


**Figure 2.3.** CFDST columns sections: (a) circular outer and inner hollow section, (b) circular outer and square inner hollow section, (c) square outer and inner hollow section, (d) square outer and circular inner hollow section, (e) circular outer and inner solid section, and (f) square outer and inner solid section

Since the last two decades, many experimental studies have been conducted on the CFDST members (Lin and Tsai, 2001; Elchalakani et al., 2002; Zhao and Grzebieta, 2002; Lin and Tsai, 2003; Han et al., 2004; Tao et al., 2004; Zhao et al., 2006; Lu et al., 2010b; Uenaka et al., 2010; Li et al., 2012; Essopjee and Dundu; 2015; ). Many properties of CFDST members were experimentally investigated. The CFDST members with hollow section consist of outer and inner steel tubes and concrete annulus between the tubes. For this reason, in these studies, the effects of strength characteristics of concrete, outer and inner steel tubes as well as the section properties such as the cross-section types and thicknesses of outer and inner steel tubes and the length of members on the properties of CFDST columns were the main researching point.

## 2.3 Advantages of CFDST Members

The CFDST members, which is the improved type of traditional CFST members, were achieved by the substituting the centralized part of the concrete with hollow sectioned steel tube (Dong and Ho, 2013). The CFDST members consisting of steel-concrete-steel sections carry almost same mechanical properties with conventional CFST members, moreover, in some points, indicates better performance than the CFST members (Tao et al., 2004; Uenaka et al., 2010; Li et al., 2012; Dong and Ho, 2013; Wang et al., 2014; Wang et al., 2016). The annulus concrete is supported by the inner tube and effectually confined by the outer tube before getting at the ultimate axial strength (Abbas et al., 2016).

The most obvious benefit of CFDST members compared to the RC (Dong and Ho, 2013) and the CFST members is its lighter weight that was attained by replacing the some part of concrete with thinner steel tube (Elchalakani et al., 2002; Zhao et al., 2002; Lin and Tsai, 2003; Tao et al., 2004; Nie and Liao, 2008; Han et al., 2009; Uenaka et al., 2010; Li et al., 2012; Wang et al., 2014; Abbas et al., 2016; Wang et al., 2016). Another significant advantage provided by the CFDST members is the having higher uni-axial strength (Zhao and Grzebieta, 2002; Zhao et al., 2002a; Yang et al., 2008; Uenaka et al., 2010; Han et al., 2011b; Dong and Ho, 2013; Wang et al., 2016), bending stiffness (Elchalakani et al., 2002; Lin and Tsai, 2003; Tao et al., 2004; Han et al., 2004; Nie and Liao, 2008; Lu et al., 2009; Han et al, 2012b; Wang et al., 2014) and moment carrying capacity (Lin and Tsai, 2001; Tao and Han, 2006;

Dong and Ho, 2013) as well as indicating better ductility behavior (Elchalakani et al., 2002; Wang et al. 2016) whilst the weight of these members is reduced. In addition, the CFDST members hold the similar torsional capacity with the CFST members (Dong and Ho, 2013).

The labor force, the formwork employee demand, and the time of construction comparing with traditional RC columns could be decreased in the case of the utilization of CFDST members in particular the columns (Lin and Tsai, 2003). The envelopment of the concrete by the steel tubes provides permanent formworks for concrete casting that eliminate the time consumed by the installation of temporary formworks (Han et al, 2012b; Abbas et al., 2016; Wang et al., 2016). By this way, the cost of the construction is also reduced (Dong and Ho, 2013). Besides, the size of the CFDST members is wispier than that of the traditional RC columns (Dong and Ho, 2013).

Another superior characteristic of the CFDST columns is its cyclic performance that is the indicating the brilliant performance against the earthquake loads (Zhao et al., 2002; Tao et al., 2004; Nie et al., 2008; Han et al., 2009; Li et al., 2012; Han et al., 2012b; Wang et al., 2014; Wang et al., 2016). Also, the energy absorption capacity, namely toughness, of the CFDST columns and its damping characteristics is better than that of the CFST columns (Li et al., 2012; Abbas et al., 2016; Uenaka et al., 2010). In addition, the CFDST columns indicate good deformability (Uenaka et al., 2010; Yagishita et al., 2000). All these properties of the CFDST columns were supplied by having two steel tubes (Li et al., 2012; Abbas et al., 2016).

Utilization of two steel tubes in the manufacturing of the CFDST members and compressing the concrete between these tubes alter the behavior of such members during the fire. While the outer tube directly exposed to the fire, the inner tube is protected from the fire by the concrete annulus. The temperature of the inner tube remains lower than the outer tube's. This situation effectively results in the increasing of the fire resistance capacity of such type of members (Tao et al., 2004; Lu et al., 2010a; Li et al., 2012; Han et al., 2012b; Wang et al., 2016).

In addition, when the ratio of the strength capacity-to-member weight of the CFDST and CFST member is compared, it can be obviously seen that the strength capacity-to-member weight of the CFDST members is greater than that of CFST columns.

This event is another benefit of the CFDST member utilization. Besides, when the CFDST members is considered in accordance with the environmental profit, it can be overemphasized that during the destruction of the structures constructed by the utilization of the CFDST members, less waste materials such as concrete will come out, since the utilization second steel skin, which is a recyclable material, decreased the concrete consumption in the construction (Dong and Ho, 2013). Furthermore, this type of members has esthetical and architectural benefit due to fact that the cavity in the members can be rewardingly utilized for some service works such as electrical lines, telecommunication wires, and plumbing pipes (Essopjee and Dundu, 2015).

## 2.4 Previous Studies on CFDST Columns with CHS

Since the main objective of this thesis is analyzing the centrally loaded CFDST columns with CHS, the literature review was given with respect to the studies performed on the CFDST columns with CHS.

Uenaka et al. (2010) experimentally tested CFDST stub columns with CHS. They regarded inner-to-outer diameter ratio and diameter-to-thickness ratio as testing parameters. They produced totally 12 stub columns specimen with changing the outer and inner steel tube thicknesses, the diameter of inner steel tube, and the yield strength value of outer and inner steel tubes. They grouped the specimens according to the changing of the diameter of inner steel tube. By this way, 3 groups were prepared and in each group, there were one specimen without inner steel tube. Table 2.1 provides the detail of specimens produced and tested in this study excluding the specimens without inner steel tube.

They concluded that failure mode of CFDST columns was local buckling occurring at both tubes that is due to accommodation to shear failure of the sandwiched concrete. Moreover, they inferred that the confinement effect that occurs on the concrete annulus significantly improves the strength of the CFST columns but in CFDST columns, the improvement thanks to confinement effect gradually decreased by increasing $D_i/D_o$. In addition, they observed that the plastic deformability of CFDST specimen is almost similar to that of CFST. As a result, they claimed that the inner tube has no confinement effect because of complex biaxial compression.

**Table 2.1.** Material and section properties and ultimate axial strength of CFDST columns with CHS tested in study of Uenaka et al. (2010)

| No. | $f_{syo}$ (MPa) | $d_o$ (mm) | $t_o$ (mm) | $f_{syi}$ (MPa) | $D_i$ (mm) | $t_i$ (mm) | $f_c'$ (MPa) | L (mm) | $P_u$ (kN) |
|---|---|---|---|---|---|---|---|---|---|
| 1 | 221 | 158 | 0.90 | 221 | 38 | 0.90 | 18.7 | 450 | 635.0 |
| 2 | 221 | 159 | 0.90 | 221 | 76 | 0.90 | 18.7 | 450 | 540.0 |
| 3 | 221 | 159 | 0.90 | 221 | 114 | 0.90 | 18.7 | 450 | 378.3 |
| 4 | 308 | 158 | 1.50 | 308 | 39 | 1.50 | 18.7 | 450 | 851.6 |
| 5 | 308 | 158 | 1.50 | 308 | 77 | 1.50 | 18.7 | 450 | 728.1 |
| 6 | 308 | 158 | 1.50 | 308 | 114 | 1.50 | 18.7 | 450 | 589.0 |
| 7 | 286 | 158 | 2.14 | 286 | 40 | 2.14 | 18.7 | 450 | 968.2 |
| 8 | 286 | 158 | 2.14 | 286 | 77 | 2.14 | 18.7 | 450 | 879.1 |
| 9 | 286 | 157 | 2.14 | 286 | 115 | 2.14 | 18.7 | 450 | 703.6 |

Zhao et al. (2002) performed a series of compression tests on CFDST stub columns with CHS regarding six different section sizes for the outer tube and two different section sizes for the inner tube. The detail of the specimen properties is given in Table 2.2. They experimentally investigated the failure modes, strength, ductility, and energy absorption characteristics of CFDST stub columns with CHS. They disclosed two failure modes for outer tube which was described as "elephant foot mode" and "diagonal shear mode" while there was only one type of failure mode for the inner tube which was defined as "distorted diamond". The failure modes of outer tubes and inner tube were demonstrated in Figure 2.4 and 2.5, respectively.



(a)                    (b)
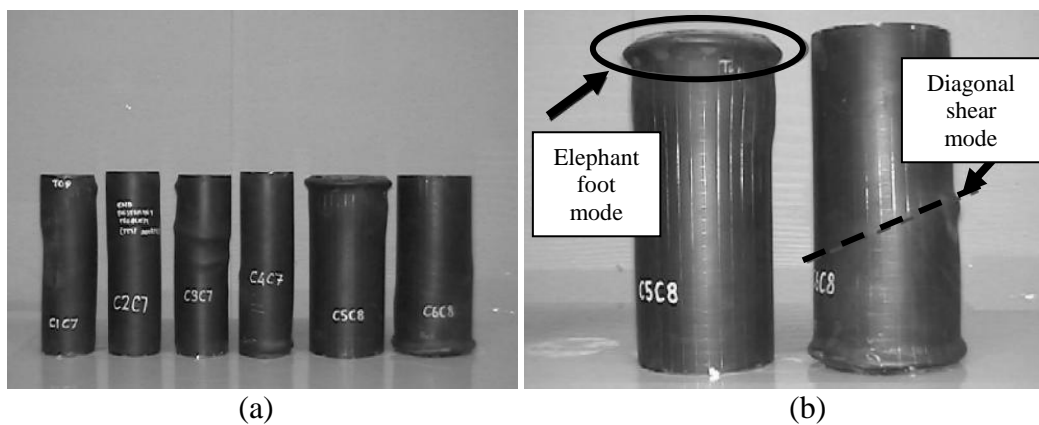
**Figure 2.4.** Typical failure modes: (a) CFDST specimen after testing and (b) indication (Zhao et al., 2002)

**Figure 2.5.** Failure modes of inner CHS in CFDST (a) after opening and (b) top view (Zhao et al., 2002)

**Table 2.2.** Material and section properties and ultimate axial strength of CFDST columns with CHS tested in studies of *Zhao et al. (2002) and **Zhao et al. (2010)

| No. | $f_{syo}$ (MPa) | $d_o$ (mm) | $t_o$ (mm) | $f_{syi}$ (MPa) | $D_i$ (mm) | $t_i$ (mm) | $f_c'$ (MPa) | L (mm) | $P_u$ (kN) |
|---|---|---|---|---|---|---|---|---|---|
| 1* | 454 | 114.5 | 2.80 | 425 | 48.4 | 5.9 | 63.4 | 400 | 1415 |
| 2* | 416 | 114.6 | 2.80 | 425 | 48.4 | 4.7 | 63.4 | 400 | 1380 |
| 3* | 453 | 114.4 | 2.80 | 425 | 48.4 | 3.5 | 63.4 | 400 | 1210 |
| 4* | 430 | 114.2 | 2.80 | 425 | 48.4 | 3.0 | 63.4 | 400 | 1110 |
| 5* | 433 | 165.1 | 3.10 | 410 | 101.8 | 3.5 | 63.4 | 400 | 1705 |
| 6* | 395 | 165.3 | 3.10 | 410 | 101.8 | 2.9 | 63.4 | 400 | 1605 |
| 7** | 454 | 114.3 | 6.00 | 425 | 48.3 | 2.9 | 63.4 | 400 | 1665 |
| 8** | 416 | 114.3 | 4.80 | 425 | 48.3 | 2.9 | 63.4 | 400 | 1441 |
| 9** | 453 | 114.3 | 3.60 | 425 | 48.3 | 2.9 | 63.4 | 400 | 1243 |
| 10** | 430 | 114.3 | 3.20 | 425 | 48.3 | 2.9 | 63.4 | 400 | 1145 |
| 11** | 433 | 165.1 | 3.50 | 394 | 101.6 | 3.2 | 63.4 | 400 | 1629 |
| 12** | 395 | 165.1 | 3.00 | 394 | 101.6 | 3.2 | 63.4 | 400 | 1613 |
| 13** | 395 | 163.8 | 2.35 | 394 | 101.6 | 3.2 | 63.4 | 400 | 1487 |
| 14** | 395 | 163.0 | 1.95 | 394 | 101.6 | 3.2 | 63.4 | 400 | 1328 |
| 15** | 395 | 162.5 | 1.70 | 394 | 101.6 | 3.2 | 63.4 | 400 | 1236 |

Tao et al. (2004) studied on CFDST stub columns and beam-columns. In this research, the sections of both inner and outer steel tubes were CHS. They considered the diameter-to-thickness and hollow section ratios for the stub columns and the slenderness ratio and the eccentricity of the load for the beam-columns as the main experimental parameters.

Totally 26 CFDST columns with CHS were tested and their ultimate axial strength, axial strain, and ductility index values as well as the buckling modes were determined in their study. Table 2.2 indicates some of tested columns in this research. They paid attention to "composite action" terms as conclusion. They revealed that both column types, stub column and beam-column, were indicated relatively ductile behavior and the structural behavior of stub columns were enhanced thanks to the composite action between the steel tube and the concrete core.

**Table 2.3.** Material and section properties and ultimate axial strength of CFDST columns with CHS tested in study of Thao et al. (2004)

| No. | $f_{syo}$ (MPa) | $d_o$ (mm) | $t_o$ (mm) | $f_{syi}$ (MPa) | $D_i$ (mm) | $t_i$ (mm) | $f_c'$ (MPa) | L (mm) | $P_u$ (kN) |
|---|---|---|---|---|---|---|---|---|---|
| 1 | 275.9 | 180 | 3 | 396.1 | 48 | 3 | 40 | 540 | 1790 |
| 2 | 275.9 | 180 | 3 | 396.1 | 48 | 3 | 40 | 540 | 1791 |
| 3 | 275.9 | 180 | 3 | 370.2 | 48 | 3 | 40 | 540 | 1648 |
| 4 | 275.9 | 180 | 3 | 370.2 | 48 | 3 | 40 | 540 | 1650 |
| 5 | 275.9 | 180 | 3 | 342.0 | 48 | 3 | 40 | 540 | 1435 |
| 6 | 275.9 | 180 | 3 | 342.0 | 48 | 3 | 40 | 540 | 1358 |
| 7 | 294.5 | 114 | 3 | 374.5 | 58 | 3 | 40 | 342 | 904 |
| 8 | 294.5 | 114 | 3 | 374.5 | 58 | 3 | 40 | 342 | 898 |
| 9 | 275.9 | 240 | 3 | 294.5 | 114 | 3 | 40 | 720 | 2421 |
| 10 | 275.9 | 240 | 3 | 294.5 | 114 | 3 | 40 | 720 | 2460 |
| 11 | 275.9 | 300 | 3 | 320.5 | 165 | 3 | 40 | 900 | 3331 |
| 12 | 275.9 | 300 | 3 | 320.5 | 165 | 3 | 40 | 900 | 3266 |
| 13 | 294.5 | 114 | 3 | 374.5 | 58 | 3 | 40 | 1770 | 620 |
| 14 | 294.5 | 114 | 3 | 374.5 | 58 | 3 | 40 | 1770 | 595 |

**Table 2.4.** Material and section properties and ultimate axial strength of CFDST columns with CHS tested in study of Li et al. (2012)

| No. | $f_{syo}$ (MPa) | $d_o$ (mm) | $t_o$ (mm) | $f_{syi}$ (MPa) | $D_i$ (mm) | $t_i$ (mm) | $f_c'$ (MPa) | L (mm) | $P_u$ (kN) |
|---|---|---|---|---|---|---|---|---|---|
| 1 | 439.3 | 350 | 3.82 | 396.5 | 231 | 2.92 | 50 | 1050 | 5499 |
| 2 | 439.3 | 350 | 3.82 | 396.5 | 231 | 2.92 | 50 | 1050 | 5396 |

Li et al. (2012) studied on CFDST tapered columns with CHS. They tested 12 tapered columns with different section sizes. However, two of them were straight

CFDST columns with CHS and they were manufactured on the purpose of comparison. The details of two straight CFDST columns with CHS are presented in Table 2.4. In this research, it was concluded that CFDST tapered columns with CHS have the similar failure mode with straight one.

Lin and Tsai (2003) aimed to experimentally investigate the CFDST columns with CHS in terms of the strength, stiffness, and ductility. They tested three CHS column specimen; one is the CFST and two of them are the CFDST columns. The details of material and section properties are presented in Table 2.5. They concluded that the ductility performance of the CFDST columns is almost same with that of the CFST columns. Moreover, they mentioned on the confinement effect provided by the outer steel. Besides, they verbalized that the occurrence of the local buckling of the steel could be postponed by the concrete between the tubes.

**Table 2.5.** Material and section properties and ultimate axial strength of CFDST columns with CHS tested in study of Lin and Tsai (2003)

| No. | $f_{syo}$ (MPa) | $d_o$ (mm) | $t_o$ (mm) | $f_{syi}$ (MPa) | $D_i$ (mm) | $t_i$ (mm) | $f_c'$ (MPa) | L (mm) | $P_u$ (kN) |
|---|---|---|---|---|---|---|---|---|---|
| 1 | 250 | 300 | 4 | 250 | 180 | 2 | 28 | 1100 | 2311 |
| 2 | 250 | 300 | 2 | 250 | 180 | 2 | 28 | 1100 | 2750 |

Essopjee and Dundu (2015) manufactured 32 CFDST slender columns with CHS to measure their ultimate axial capacity under compressive loading. They altered the length and diameters of the specimens and the yield strength of the outer steel tube. The specimen properties are given in Table 2.6.

According to their test results, it was concluded that the CFDST columns having length of 1 m failed due to the yield strength of the steel tubes whereas the columns having length of more than 1 m failed owing to overall buckling that is the result of large slenderness. In addition, they verbalized that increasing the length of the columns specimens resulted in the reducing of the compressive capacity of the CFDST columns. Besides, they observed that the ultimate compressive strength of the specimens was increased by increasing the diameters.

**Table 2.6.** Material and section properties and ultimate axial strength of CFDST columns with CHS tested in study of Essopjee and Dundu (2015)

| No. | $f_{syo}$ (MPa) | $d_o$ (mm) | $t_o$ (mm) | $f_{syi}$ (MPa) | $D_i$ (mm) | $t_i$ (mm) | $f_c'$ (MPa) | L (mm) | $P_u$ (kN) |
|---|---|---|---|---|---|---|---|---|---|
| 1 | 418 | 139.2 | 3.0 | 324 | 76 | 2 | 30.8 | 998 | 1059.2 |
| 2 | 418 | 139.2 | 3.0 | 324 | 76 | 2 | 30.8 | 1001 | 1056.1 |
| 3 | 418 | 139.2 | 3.0 | 324 | 76 | 2 | 30.8 | 1500 | 905.5 |
| 4 | 418 | 139.2 | 3.0 | 324 | 76 | 2 | 30.8 | 1503 | 901.6 |
| 5 | 418 | 139.2 | 3.0 | 324 | 76 | 2 | 30.8 | 2000 | 831.7 |
| 6 | 418 | 139.2 | 3.0 | 324 | 76 | 2 | 30.8 | 1998 | 837.4 |
| 7 | 418 | 139.2 | 3.0 | 324 | 76 | 2 | 30.8 | 2502 | 732.1 |
| 8 | 418 | 139.2 | 3.0 | 324 | 76 | 2 | 30.8 | 2498 | 729.0 |
| 9 | 549 | 152.4 | 3.0 | 324 | 76 | 2 | 30.8 | 1003 | 1263.5 |
| 10 | 549 | 152.4 | 3.0 | 324 | 76 | 2 | 30.8 | 1002 | 1254.9 |
| 11 | 549 | 152.4 | 3.0 | 324 | 76 | 2 | 30.8 | 1497 | 1195.6 |
| 12 | 549 | 152.4 | 3.0 | 324 | 76 | 2 | 30.8 | 1503 | 1191.2 |
| 13 | 549 | 152.4 | 3.0 | 324 | 76 | 2 | 30.8 | 1997 | 1047.3 |
| 14 | 549 | 152.4 | 3.0 | 324 | 76 | 2 | 30.8 | 2000 | 1041.6 |
| 15 | 549 | 152.4 | 3.0 | 324 | 76 | 2 | 30.8 | 2498 | 941.4 |
| 16 | 549 | 152.4 | 3.0 | 324 | 76 | 2 | 30.8 | 2500 | 949.0 |
| 17 | 516 | 165.1 | 3.0 | 324 | 76 | 2 | 30.8 | 998 | 1512.3 |
| 18 | 516 | 165.1 | 3.0 | 324 | 76 | 2 | 30.8 | 999 | 1510.6 |
| 19 | 516 | 165.1 | 3.0 | 324 | 76 | 2 | 30.8 | 1504 | 1286.4 |
| 20 | 516 | 165.1 | 3.0 | 324 | 76 | 2 | 30.8 | 1498 | 1275.1 |
| 21 | 516 | 165.1 | 3.0 | 324 | 76 | 2 | 30.8 | 2003 | 1187.2 |
| 22 | 516 | 165.1 | 3.0 | 324 | 76 | 2 | 30.8 | 1998 | 1199.8 |
| 23 | 516 | 165.1 | 3.0 | 324 | 76 | 2 | 30.8 | 2498 | 1028.0 |
| 24 | 516 | 165.1 | 3.0 | 324 | 76 | 2 | 30.8 | 2502 | 1036.5 |
| 25 | 391 | 193.7 | 3.5 | 324 | 76 | 2 | 30.8 | 1003 | 2010.0 |
| 26 | 391 | 193.7 | 3.5 | 324 | 76 | 2 | 30.8 | 1000 | 2030.0 |
| 27 | 391 | 193.7 | 3.5 | 324 | 76 | 2 | 30.8 | 1502 | 1730.0 |
| 28 | 391 | 193.7 | 3.5 | 324 | 76 | 2 | 30.8 | 1500 | 1720.0 |
| 29 | 391 | 193.7 | 3.5 | 324 | 76 | 2 | 30.8 | 1998 | 1581.6 |
| 30 | 391 | 193.7 | 3.5 | 324 | 76 | 2 | 30.8 | 2003 | 1584.1 |
| 31 | 391 | 193.7 | 3.5 | 324 | 76 | 2 | 30.8 | 2503 | 1451.4 |
| 32 | 391 | 193.7 | 3.5 | 324 | 76 | 2 | 30.8 | 2497 | 1458.7 |

Han et al. (2011a) studied on long-term sustained loading and ultimate strength test of the CFDST columns. For this purpose, 8 CFDST columns with CHS and 8 CFDST columns with SHS were manufactured. From each section, 5 column specimens were tested regarding to only ultimate strength. Table 2.7 presents the details of 5 CFDST columns with CHS. It was specified that when the column

specimens tested under long-term sustained load were compared with that tested under ultimate strength, lower ultimate axial capacity was observed.

In another study conducted by Han et al. (2011b), a series of test on the CFDST columns with different sectional type and column type was performed. They produced the columns with respect to circular, square, round-end rectangular, and elliptical sections with straight, inclined, and tapered column types. Totally they manufactured 80 CFDST columns in order to investigate their performance. The details of CFDST straight columns with CHS are given in Table 2.7. It was concluded according to the experimental test results that all column types indicated the ductile behavior. Furthermore, the failure mode of the outer tube was the outward local buckling whereby that of the inner tube was the inward local buckling.

**Table 2.7.** Material and section properties and ultimate axial strength of CFDST columns with CHS tested in studies of *Han et al. (2011a) and **Han et al. (2011b)

| No. | $f_{syo}$ (MPa) | $d_o$ (mm) | $t_o$ (mm) | $f_{syi}$ (MPa) | $D_i$ (mm) | $t_i$ (mm) | $f_c'$ (MPa) | L (mm) | $P_u$ (kN) |
|-----|------|-----|------|------|-----|------|------|------|-------|
| 1*  | 311.0 | 120 | 1.96 | 380.0 | 60 | 1.96 | 39.3 | 1324 | 578 |
| 2*  | 311.0 | 120 | 1.96 | 380.0 | 60 | 1.96 | 66.4 | 1324 | 789.9 |
| 3*  | 311.0 | 120 | 1.96 | 380.0 | 60 | 1.96 | 66.4 | 1324 | 715.4 |
| 4** | 319.6 | 220 | 3.62 | 380.6 | 159 | 3.72 | 60.0 | 660 | 2537 |
| 5** | 319.6 | 220 | 3.62 | 380.6 | 159 | 3.72 | 60.0 | 660 | 2566 |
| 6** | 319.6 | 220 | 3.62 | 380.6 | 106 | 3.72 | 60.0 | 660 | 3436 |
| 7** | 319.6 | 220 | 3.62 | 380.6 | 106 | 3.72 | 60.0 | 660 | 3506 |

Wang et al. (2016) conducted an experimental study on CFDST stub columns with CHS in order to investigate their strength and behavior. In total, 14 column specimens were manufactured with various concrete class and inner tube diameter and thickness. The gap between outer and inner steel tube was filled with three different concrete cylinder strengths of 40, 80, and 120 MPa. The strength of CFDST stub columns with CHS was measured by applying uniform axial loading whereas the behavior was studied with respect to failure mode and load-axial strain relationship. The details of the specimen properties excluding columns with 120 MPa concrete are presented in Table 2.8. It was reported that the collapsing shape of the columns was ductile failure.

**Table 2.8.** Material and section properties and ultimate axial strength of CFDST columns with CHS tested in study of Wang et al. (2016)

| No. | $f_{syo}$ (MPa) | $d_o$ (mm) | $t_o$ (mm) | $f_{syi}$ (MPa) | $D_i$ (mm) | $t_i$ (mm) | $f_c'$ (MPa) | L (mm) | $P_u$ (kN) |
|---|---|---|---|---|---|---|---|---|---|
| 1 | 300 | 140.2 | 2.92 | 794 | 22.1 | 4.09 | 40.5 | 350 | 1450.0 |
| 2 | 300 | 140.3 | 2.89 | 619 | 32.0 | 5.48 | 40.5 | 350 | 1562.0 |
| 3 | 300 | 140.1 | 2.91 | 433 | 38.1 | 7.63 | 40.5 | 350 | 1838.4 |
| 4 | 300 | 140.2 | 2.90 | 739 | 55.1 | 10.62 | 40.5 | 350 | 2724.0 |
| 5 | 300 | 140.1 | 2.87 | 1029 | 89.0 | 3.91 | 40.5 | 350 | 2024.9 |
| 6 | 300 | 140.2 | 2.91 | 794 | 22.1 | 4.10 | 79.9 | 350 | 1845.1 |
| 7 | 300 | 140.2 | 2.92 | 619 | 31.9 | 5.27 | 79.9 | 350 | 2012.5 |
| 8 | 300 | 140.1 | 2.90 | 433 | 38.0 | 7.51 | 79.9 | 350 | 2083.4 |
| 9 | 300 | 140.1 | 2.90 | 739 | 55.2 | 10.76 | 79.9 | 350 | 2775.0 |
| 10 | 300 | 140.1 | 2.86 | 1029 | 89.1 | 3.91 | 79.9 | 350 | 2107.4 |

Hastemoğlu (2017) studied on CFST and CFDST columns with CHS. A total of 5 CFDST columns with CHS were manufactured in this study. The load carrying capacity of the specimens, then, was measured. In order to observe the effect of slenderness ratio on the ultimate axial strength of CFDST columns, various specimen lengths were utilized in the production. The details of three specimens manufactured in this study are given in Table 2.9. It was concluded that the columns performed the ductile behavior since the gap between the tubes was filled with concrete and there was a hollow core.

**Table 2.9.** Material and section properties and ultimate axial strength of CFDST columns with CHS tested in study of Hastemoğlu (2017)

| No. | $f_{syo}$ (MPa) | $d_o$ (mm) | $t_o$ (mm) | $f_{syi}$ (MPa) | $D_i$ (mm) | $t_i$ (mm) | $f_c'$ (MPa) | L (mm) | $P_u$ (kN) |
|---|---|---|---|---|---|---|---|---|---|
| 1 | 250 | 139 | 2 | 250 | 75 | 3 | 55 | 351 | 807 |
| 2 | 250 | 139 | 2 | 250 | 75 | 3 | 55 | 468 | 810 |
| 3 | 250 | 139 | 2 | 250 | 75 | 3 | 55 | 585 | 877 |

Dong and Ho (2012) and (2013) experimentally investigated CFST and CFDST columns with CHS including rings to obtain additional confinement. Totally, 30 column specimens were manufactured to examine the effect of confining-rings and second skin on the ultimate axial strength of the columns. The properties of CFDST columns with CHS excluding confining-rings are stated in Table 2.10. According to

their experimental results, it was revealed that the compressive strength of the CFDST columns with CHS was higher than that of CFST columns.

**Table 2.10.** Material and section properties and ultimate axial strength of CFDST columns with CHS tested in studies of *Dong and Ho (2012) and **Dong and Ho (2013)

| No. | $f_{syo}$ (MPa) | $d_o$ (mm) | $t_o$ (mm) | $f_{syi}$ (MPa) | $D_i$ (mm) | $t_i$ (mm) | $f_c'$ (MPa) | L (mm) | $P_u$ (kN) |
|---|---|---|---|---|---|---|---|---|---|
| 1* | 360 | 168.3 | 5 | 450 | 88.9 | 5 | 50 | 330 | 2852 |
| 2** | 450 | 168.3 | 5 | 360 | 88.9 | 5 | 50 | 330 | 2865 |
| 3** | 430 | 168.3 | 5 | 360 | 114.3 | 5 | 50 | 330 | 2674 |
| 4** | 450 | 168.3 | 5 | 360 | 88.9 | 5 | 85 | 330 | 3218 |
| 5** | 430 | 168.3 | 5 | 360 | 114.3 | 5 | 85 | 330 | 2994 |

Abbas et al. (2016) studied on the CFDST columns with CHS exposure to temperature with different cooling regimes. In order to investigate and observe the temperature and cooling regime effect on the ultimate axial capacity of the CFDST columns with CHS, one control specimen was also manufactured. Table 2.11 presents the detail of the control specimen.

**Table 2.11.** Material and section properties and ultimate axial strength of CFDST column with CHS tested in study of Abbas et al. (2016)

| No. | $f_{syo}$ (MPa) | $d_o$ (mm) | $t_o$ (mm) | $f_{syi}$ (MPa) | $D_i$ (mm) | $t_i$ (mm) | $f_c'$ (MPa) | L (mm) | $P_u$ (kN) |
|---|---|---|---|---|---|---|---|---|---|
| 1 | 307 | 150 | 6 | 307 | 26.7 | 2.87 | 40 | 600 | 1805 |

Wang et al. (2014) investigated the effect of fiber reinforced polymer on the ultimate axial capacity of the CFDST stub columns with CHS. They covered the CFDST stub columns with different orientated fiber reinforced polymer to increase the confinement effect. For this reason, they produced two CFDST stub columns with CHS excluding the fiber reinforced polymers. The detailed specimen properties of these specimens are given in Table 2.12. It was observed that decreasing the concrete annulus cross section resulted in lower ultimate axial strength capacity of the CFDST stub columns with CHS.
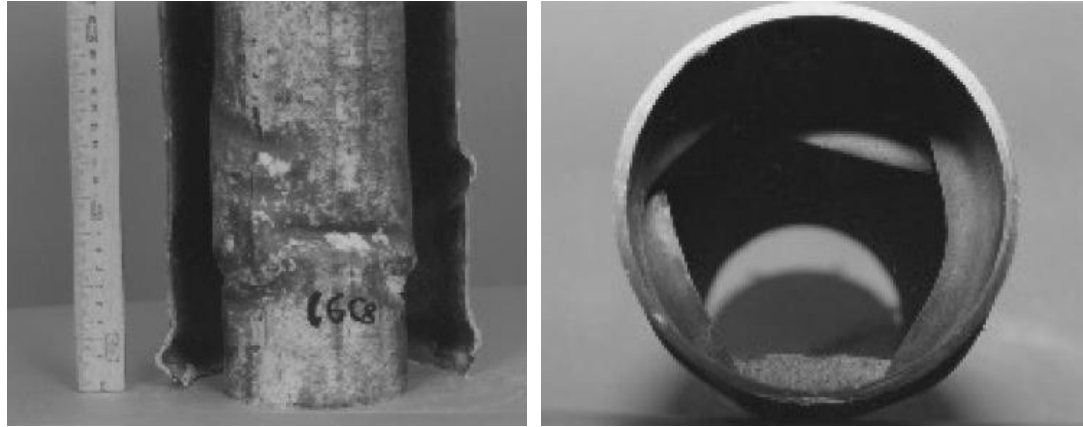
**Table 2.12.** Material and section properties and ultimate axial strength of CFDST columns with CHS tested in study of Wang et al. (2014)

| No. | $f_{syo}$ (MPa) | $d_o$ (mm) | $t_o$ (mm) | $f_{syi}$ (MPa) | $D_i$ (mm) | $t_i$ (mm) | $f_c'$ (MPa) | L (mm) | $P_u$ (kN) |
|-----|------|------|-----|------|------|-----|-------|-----|-----|
| 1 | 350 | 165 | 1.7 | 350 | 76 | 1.2 | 22.48 | 500 | 980 |
| 2 | 350 | 165 | 1.7 | 350 | 114 | 1.7 | 22.48 | 500 | 715 |

Lu et al. (2010a) also examined the fire effect on the CFDST columns. In total, 18 CFDST columns with circular and square cross section were manufactured during the study. Two of total specimens were reference specimens which were not exposure to fire. One specimen was reference for circular series whereas the other was for square series. The detailed specimen properties of the reference of circular series are presented in Table 2.13.

**Table 2.13.** Material and section properties and ultimate axial strength of CFDST column with CHS tested in study of Lu et al. (2010a)

| No. | $f_{syo}$ (MPa) | $d_o$ (mm) | $t_o$ (mm) | $f_{syi}$ (MPa) | $D_i$ (mm) | $t_i$ (mm) | $f_c'$ (MPa) | L (mm) | $P_u$ (kN) |
|-----|------|-------|----|------|-------|-----|-------|-----|------|
| 1 | 426 | 219.1 | 5 | 426 | 101.6 | 3.2 | 44.38 | 800 | 3333 |

## 2.5 Utilization Areas of CFDST Members

Montague (1971, 1978) presented the CFDST members for the vessel building that exposed to external pressure. Tomlinson et al. (1989) introduced the possibilities of utilization of such members in the immersed tube tunnels. Wright et al. (1991a, 1991b) believed that the CFDST members may have the opportunity to be used in structures apart from vessels and immersed tube tunnels. They provide an opportunity for the using such type of members in the structures aimed the repression of nuclear, retainment of liquid and gas as well as in the shelter resistive to blasts. After these progresses in the utilization area of the CFDST members, the double skin phenomenon aroused attention of many researchers and then great numbers of studied have been carried out to investigate the characteristics of the CFDST members under different types of loading (Lin and Tsai, 2001; Elchalakani et al., 2002; Yagishita et al., 2002; Zhao and Grzebieta, 2002; Zhao et al., 2002a; Zhao et

al., 2002b; Lin and Tsai, 2003; Tao et al., 2004; Tao and Han, 2006; Nie and Liao, 2008; Yang et al., 2008; Lu et al., 2010a; Lu et al., 2010b; Uenaka et al., 2010; Zhao et al., 2010; Han et al., 2011a; Han et al., 2011b; Dong and Ho, 2012; Li et al., 2012; Wang et al., 2014; Essopjee and Dundu, 2015; Hsiao et al., 2015; Abbas et al., 2016; Wang et al., 2016; Hastemoğlu, 2017). These studies pave the way for using these members in the construction of offshore platforms and marine structures. In addition, the bridge piers construction, especially high-rise viaducts, electricity pylon, and multi-storey buildings are other usage areas of the CFDST members.

## 2.6 Prediction of Ultimate Axial Strength of CFDST Columns with CHS

The ultimate axial strength of the concrete filled steel tubular columns could be predicted by the empirical methods recommended by codes or researchers. However, there is no any code that standardized the formula estimating the ultimate axial capacity of the concrete filled double skin tubular columns. For this reason, the model that can be used for the prediction of the ultimate axial strength of the CFDST columns is urgently necessary. Although there is no any empirical formula for the prediction of the CFDST columns by codes, there are formulas modified from the codes by which the ultimate axial strength of CFST columns could be calculated. In addition to the modified formulas from the codes, in the literature, there are also some proposed empirical models which was developed or derived by the researchers. The modified formulas from the codes and the proposed empirical models by the researchers were given in the following sections.

## 2.6.1 Formula Modified from ACI (2002)

ACI code (2002) proffers an equation by which the ultimate axial strength of single skin composite columns containing a reinforcing bar can be determined. However, the concrete confinement effect is disregarded in formula suggested by the ACI code (2002). The equation modified from ACI code (2002) in order to determine the ultimate axial strength of the CFDST stub column involving the contribution of the inner steel tube expressed as follows (ACI, 2002):

$$(P_u)_{ACI} = f_{syo} A_{so} + 0.85 f_c^{'} A_c + f_{syi} A_{si} \tag{2.1}$$

where;

$f_{syo}$ is the yield strength of the outer steel tube,

$A_{so}$ is the cross-sectional area of outer steel tube

$f_c'$ is the unconfined cylindrical concrete compressive strength,

$A_c$ is the cross-sectional area of concrete infill between both tubes

$f_{syi}$ is the yield strength of inner steel tube, and

$A_{si}$ is the cross-sectional area of inner steel tube.

## 2.6.2 Formula Modified from Eurocode 4 (2004)

The equation suggested by Eurocode 4 (EC4) (2004) for the calculation of the ultimate axial strength of the CFST columns includes the outer steel tube, reinforcing bars and concrete as well as confinement effect. EC4 (2004) approach has two different equations according to relative slenderness criteria. The recommended formula to determine the ultimate axial strength of CFST columns with respect to two relative slenderness criteria is given as follows (Eurocode 4, 2004):

In the case of $\bar{\lambda} > 0.5$

$$P_u = f_{yd} A_a + f_{cd} A_c + f_{sd} A_s \tag{2.2}$$

In the case of $\bar{\lambda} \leq 0.5$

$$P_u = \eta_a f_{yd} A_a + f_{cd} A_{cc} \left[1 + \eta_c \left(\frac{t}{D}\right)\left(\frac{f_y}{f_{ck}}\right)\right] + f_{sd} A_s \tag{2.3}$$

where;

$f_{yd}$ is the design value of the yield strength of the structural steel,

$A_a$ is the cross-sectional area of the structural steel section,

$f_{cd}$ is the design value of the compressive strength of the cylinder concrete,

$A_{cc}$ is the cross-sectional area of the concrete core,

$f_{sd}$ is the design value of the yield strength of the reinforcing steel,

$A_s$ is the cross-sectional area of the reinforcing bars,

$t$ is the thickness of the structural steel,

$D$ is the diameter of the structural steel,

$f_y$ is the nominal value of the yield strength of the structural steel, and

$f_{ck}$ is the characteristic value of the compressive strength of the cylinder concrete at 28 days.

The approach in EC4 (2004) uses a reduction factor, $\eta_a$, and an enhancement factor, $\eta_c$, for the contribution of the steel to the cross-section resistance and for the concrete contribution, respectively, for regarding the confinement effect of concrete. In these formulations, firstly, the reinforcement part was considered as a second steel skin. For this reason, in Eqn. 2.3, the strength provided by this section was multiplied with $\eta_a$, the factor related to the confinement of concrete as Pagoulatou et al. (2014) recommended. Then, terminological conversion was carried out. Finally, the following expressions were obtained for both conditions:

In the case of $\bar{\lambda} > 0.5$

$$(P_u)_{EC4} = f_{syo} A_{so} + f_c' A_c + f_{syi} A_{si} \tag{2.4}$$

In the case of $\bar{\lambda} \leq 0.5$

$$(P_u)_{EC4} = \eta_a f_{syo} A_{so} + f_c' A_c \left[1 + \eta_c \left(\frac{t_o}{D_o}\right)\left(\frac{f_{syo}}{f_c'}\right)\right] + \eta_a f_{syi} A_{si} \tag{2.5}$$

where;

$t_o$ is the thickness of the outer steel tube,

$D_o$ is the diameter of the outer steel tube,

$\eta_a$ is the reduction factor for the contribution of the steel to the cross-section resistance, and

$\eta_c$ is the enhancement factor for the concrete contribution.

$\eta_a$ and $\eta_c$ are to be calculated as follows:

$$\eta_a = 0.25(3 + 2\bar{\lambda}) \quad (but \ \leq 1.0) \tag{2.5a}$$

$$\eta_c = 4.9 - 18.5\bar{\lambda} + 17\bar{\lambda}^2 \quad (but \geq 0) \tag{2.5b}$$

where;

$\bar{\lambda}$ is the relative slenderness and to be determined by the following expression:

$$\bar{\lambda} = \sqrt{P_{pl,Rd,(6.30)}\Big/P_{cr}} \tag{2.5c}$$

where;

$P_{pl,Rd,(6.30)}$ is the characteristic value of the plastic resistance given in EC4 (2004) as 6.30[th] equation and this expression applies for concrete encased and partially concrete encased steel sections, to be determined by the following expression:

$$P_{pl,Rd,(6.30)} = f_{syo}A_{so} + 0.85f_c'A_c + f_{syi}A_{si} \tag{2.5d}$$

$P_{cr}$ is the elastic critical normal force for relevant buckling mode and to be determined by following expression:

$$P_{cr} = \frac{\pi^2(EI)_{eff}}{(KL_u)^2} \tag{2.5e}$$

where;

$K$ is the effective length factor (for pin-pin connection can be taken as 1.0),

$L_u$ is the laterally unbraced length of the member, and

$EI_{eff}$ is the effective stiffness of composite section and to be calculated by the following expression:

$$EI_{eff} = E_{so}I_{so} + K_cE_{cm}I_c + E_{si}I_{si} \tag{2.5f}$$

where;

$E_{so}$ is the modulus of elasticity of outer steel tube,

$I_{so}$ is the second moments of area of outer steel tube section,

$K_c$ is a correction factor that should be taken as 0.6,

$E_{cm}$ is the modulus of elasticity of concrete,

25

$I_c$ is the second moments of area of concrete annulus section,

$E_{si}$ is the modulus of elasticity of inner steel tube, and

$I_{si}$ is the second moments of area of inner steel tube section.

Herein, the modulus of elasticity of concrete could be calculated by the following equation provided by ACI-318 (2002):

$$E_{cm} = w_c^{1.5} 0.043 \sqrt{f_c'} \tag{2.5g}$$

where;

$w_c$ is the unit weight of the concrete (between 2300 and 2500 kg/m$^3$)

At the end of the calculation of the ultimate axial strength of the CFDST columns, the strength value should be multiplied with the reduction factor ($\chi$) for the relevant buckling mode. The formula for the reduction factor according to Eurocode 3 (EC3) (2004) is as follows:

$$\chi = \frac{1}{\phi + \sqrt{\phi^2 - \bar{\lambda}^2}} \quad but \; \chi \leq 1.0 \tag{2.6}$$

where;

$$\phi = 0.5\left[1 + \alpha(\bar{\lambda} - 0.2) + \bar{\lambda}^2\right] \tag{2.6a}$$

$\alpha$ is an imperfection factor depending on a buckling curve and can be taken from Table 6.1 in EC3 (2004). As Hassanein and Kharoob (2014a) mentioned in their study, the imperfection factor was taken according to buckling curve (b) as 0.34.

**2.6.3 Formula Modified from AISC (2010)**

The equations by AISC (2010) are suggested for the single skin composite columns involving reinforcing bars. AISC (2010) also recommends two different expressions for determination of the ultimate axial strength of encased composite columns that subjected to axial loading:

In the case of $P_e < 0.44 P_o$

$$(P_u)_{AISC} = 0.877 P_e \tag{2.7}$$

where;

$$P_e = \frac{\pi^2 (EI)_{eff}}{(KL)^2} \tag{2.7a}$$

and where;

$EI_{eff}$ can be calculated by using Eqn. 2.5f with a small alteration in the correction factor, $K_c$.

$$K_c = 0.6 + 2 \left( \frac{A_{so}}{A_c + A_{so}} \right) \le 0.9 \tag{2.7b}$$

In the case of $P_e \ge 0.44 P_o$

$$(P_u)_{AISC} = P_o \left[ 0.658^{\left( \frac{P_o}{P_e} \right)} \right] \tag{2.8}$$

where;

$$P_o = f_{syo} A_{so} + 0.95 f_c' A_c + f_{syi} A_{si} \tag{2.8a}$$

Herein, in the calculation of $P_o$ and $P_e$, a steel tubular section instead of reinforcing bars was considered a second skin. After these modifications, $P_o$ and $P_e$ can be expressed as above.

### 2.6.4 Empirical Model Proposed by Uenaka et al. (2010)

Uenaka et al. (2010) derived the equation determining the ultimate axial strength of the CFDST columns from the equation that was proposed by AIJ (2002) for CFST stub columns. Uenaka et al. (2010) elementally superposed strength of the tubes and the concrete infill between tubes. The following expression was first asserted to temporarily estimate the ultimate axial strength of CFDST:

$$P_u = f_{syo} A_{so} + f_c' A_c + f_{syi} A_{si} \tag{2.9}$$

After the experimental tests, it was overemphasized that the confinement effect of the outer tube is more effective on the ultimate axial strength of the CFDST columns than that of the inner tube (Uenaka et al., 2010). Regarding the experimental results, the estimated ultimate axial strength derived from AIJ (2002) is modified to the following expression by Uenaka et al. (2010).

$$(P_u)_{UENAKA} = \left(2.86 - 2.59\left(\frac{D_i}{D_o}\right)\right)f_{yo}A_{so} + f_c'A_c + f_{yi}A_{si} \quad \left(0.2 < {D_i}/{D_o} < 0.7\right) \quad (2.10)$$

where;

$D_i$ is the diameter of the inner steel tube.

## 2.6.5 Empirical Model Proposed by Han et al. (2011b)

In addition to modifying the formula recommended by the codes, some researchers proposed some equations for the calculation of the ultimate axial strength of the CFDST columns. Han et al. (2011b) are one of these researchers who proposed an equation regarding the inner tube capacity and a capacity containing the outer steel tube and sandwiched concrete. The formula given by Han et al. (2011b) is as follows:

$$(P_u)_{HAN} = P_{osc,u} + P_{i,u} \quad (2.11)$$

where;

$P_{i,u}$ is the capacity of the inner steel tube and to be determined by the following expression:

$$P_{i,u} = f_{syi}A_{si} \quad (2.11a)$$

$P_{osc,u}$ is the capacity of the outer steel tube and concrete annulus and to be determined by the following expression:

$$P_{osc,u} = f_{osc}A_{soc} \quad (2.11b)$$

where;

$f_{osc}$ is the strength characteristic of outer steel tube and concrete annulus and to be determine by the following expression:

$$f_{osc} = C_1\chi^2 f_{syo} + C_2(1.14 + 1.02\xi)f_{ck} \tag{2.11c}$$

where;

$C_1$ is the strength coefficient of the outer steel tube and to be determined by the following expression:

$$C_1 = \frac{\alpha'}{1+\alpha'} \tag{2.11d}$$

in which $\alpha'$ can be determined by the following expression:

$$\alpha' = \frac{A_{so}}{A_c} \tag{2.11e}$$

$\chi$ is the hollow section ratio and to be determined by the following expression:

$$\chi = \frac{D_i}{D_o - 2t_o} \tag{2.11f}$$

$C_2$ is the strength coefficient of the concrete annulus and to be determined by the following expression:

$$C_2 = \frac{1+\alpha_n}{1+\alpha'} \tag{2.11g}$$

in which $\alpha_n$ can be determined by the following expression:

$$\alpha_n = \frac{A_{so}}{A_{c,nominal}} \tag{2.11h}$$

$\xi$ is the nominal confinement factor and to be determined by the following expression:

$$\xi = \frac{f_{syo} A_{so}}{f_{ck} A_{c,nominal}} \tag{2.11i}$$

$f_{ck}$ is the characteristic compressive strength and to be determined by the following expression:

$$f_{ck} = 0.67 f_{cu} \tag{2.11j}$$

and where $f_{cu}$ is the characteristic cube strength of concrete.

$A_{c,nominal}$ is the nominal cross-sectional area of the concrete and to be determined by the following expression:

$$A_{c,nominal} = \frac{\pi(D_o - 2t_o)^2}{4} \tag{2.11k}$$

$A_{soc}$ is the cross-sectional area of the outer steel tube and concrete annulus and to be determined by the following expression:

$$A_{soc} = A_{so} + A_c \tag{2.11l}$$

### 2.6.6 Empirical Model Proposed by Yu et al. (2013)

Yu et al. (2013) proposed an equation confirming the experimental ultimate axial strength results. The formula was for the single skin solid and hollow section CFST columns and presented as follows:

$$P_u = \left(1 + 0.5\frac{\xi}{1+\xi}\Omega\right)\left(f_{sy}A_s + f_{ck}A_c\right) \tag{2.12}$$

where;

$\xi$ is the confinement coefficient and to be determined by the following expression:

$$\xi = \frac{f_{syo}A_{so}}{f_{ck}A_c} \tag{2.12a}$$

$\Omega$ is the solid ratio and to be determined by the following expression:

$$\Omega = \frac{A_c}{A_c + A_k} \tag{2.12b}$$

$f_{sy}$ is the yield strength of steel tube,

$f_{ck}$ is the characteristic strength of concrete, and

$A_k$ is the cross-sectional area of the hollow part.

Herein, the formula proposed by Yu et al. (2013) was modified to be applicable on the double skin CFST columns. As Hassanein and Kharoob (2014b) recommended, the modified formula includes the combination of circular hollow CFST column and inner steel tube as follows:

$$(P_u)_{YU} = \left(1 + 0.5\frac{\xi}{1+\xi}\Omega\right)\left(f_{syo}A_{so} + f_{ck}A_c\right) + P_{i,u} \tag{2.13}$$

30

where;

$P_{i,u}$ is the capacity of the inner steel tube and to be determined by Eqn. 2.11a.

### 2.6.7 Empirical Model Proposed by Hassanein et al. (2013b)

Hassanein et al. (2013b) proposed a new design model for calculation of the ultimate axial strength of circular CFDST short columns based on Liang and Fragomeni's (2009) design models for determining the ultimate axial strength of circular CFST short columns and Hassanein et al.'s (2013a) design models for calculating the ultimate axial strength of concrete filled stainless steel tubular short columns and concrete filled-stainless steel-carbon steel tubular short columns. The new design model proposed by Hassanein et al. (2013b) is presented as follows:

$$(P_u)_{HASSANEIN} = \gamma_{so} f_{syo} A_{so} + (\gamma_c f_c' + 4.1 f_1) A_c + \gamma_{si} f_{syi} A_{si} \qquad (2.14)$$

where;

$\gamma_{so}$ is the factor used to account for the influence of strain hardening on outer steel tube and to be determined by the following expression:

$$\gamma_{so} = 1.458 \left(\frac{D_o}{t_o}\right)^{-0.1} \qquad 0.9 \le \gamma_{so} \le 1.1 \qquad (2.14a)$$

$\gamma_c$ is a strength reduction factor proposed by Liang (2009) and to be determined by the following expression:

$$\gamma_c = 1.85 D_c^{-0.135} \qquad 0.85 \le \gamma_c \le 1.0 \qquad (2.14b)$$

where;

$D_c$ is the diameter of the concrete annulus and to be determined by the following expression:

$$D_c = D_o - 2t_o \qquad (2.14c)$$

$f_1$ is the lateral confining pressure and to be determined by the following expressions:

$$f_1 = \begin{cases} 0.7(v_o - v_s)\frac{2t_o}{D_o - 2t_o} f_{syo} & for \ \frac{D_o}{t_o} \le 47 \\ \left(0.006241 - 0.0000357\frac{D_o}{t_o}\right) f_{syo} & for \ 47 < \frac{D_o}{t_o} \le 150 \end{cases} \qquad (2.14d)$$

$v_o$ is the Poisson's ratio of steel tube with concrete infill and to be determined by the following expression given by Tang et al. (1996):

$$v_o = 0.2312 + 0.3582v_o' - 0.1524\left(\frac{f_c'}{f_{syo}}\right) + 4.843v_o'\left(\frac{f_c'}{f_{syo}}\right) - 9.169\left(\frac{f_c'}{f_{syo}}\right)^2 \qquad (2.14e)$$

in which;

$$v_o' = 0.881x10^{-6}\left(\frac{D_o}{t_o}\right)^3 - 2.58x10^{-4}\left(\frac{D_o}{t_o}\right)^2 + 1.953x10^{-2}\left(\frac{D_o}{t_o}\right) + 0.4011 \qquad (2.14f)$$

$v_s$ is the Poisson's ratios of steel tube without concrete infill and at the maximum strength point, it is taken as 0.5.

$\gamma_{si}$ is the factor used to account for the influence of strain hardening on inner steel tube and to be determined by the following expression:

$$\gamma_{si} = 1.458\left(\frac{D_i}{t_i}\right)^{-0.1} \qquad 0.9 \leq \gamma_{si} \leq 1.1 \qquad (2.14g)$$

where;

$t_i$ is the thickness of inner steel tube.

## 2.7 Soft Computing and Numerical Analysis Methods

Soft computing could be described as a summation of techniques which are purposed to utilize the toleration for erroneous and uncertainness to attain tractability, robustness, and low solution cost (Zadeh, 1994). Engineering problems, financial estimations, diagnostic tools in medicine etc. are some of the application areas of soft computing techniques. The gene expression programming (GEP) and artificial neural network (ANN) are two of the most popular soft-computing techniques used in the derivation of the predictive model. In this thesis, GEP and ANN were used to propose an empirical model that could be used in the prediction of the ultimate axial strength of the CFDST columns with CHS. In addition, finite element method (FEM) was used to model the CFDST columns with CHS in order to analyze and predict the ultimate axial strength. The predictive formula of GEP was obtained by using GeneXproTools 5.0 (2018) software while that of ANN was derived by using Neural-Fuzzy Tool (nf tool) and Neural-Network Tool (nn tool) on MATLAB v.17

(2012) software. The analysis of the CFDST columns with CHS was carried out by using ABAQUS CAE 16 (2014) software.

**2.7.1 Finite Element Method (FEM)**

Finite element method (FEM), which is an applicative tool for the solving the engineering and physic application problems that cannot be solved by analytical solutions, is a very strong and contemporary numerical method. The complicated geometry, nonuniform loading conditions, complex boundary conditions, and nonlinear material behaviors incapacitate the analytical solutions. Because the analytical solutions makes several assumptions in order to solve the simplified and stripped mathematical models.

*2.7.1.1 History of the FEM*

Although it is very difficult to say exactly when the FEM is invented, Hrennkoff (1941) and Courant (1943) can be accepted as the pioneers of this method. At the beginning of the 1950s, the method was first applied on the stress analysis occurring on the aircraft bodies. In the course of time, this method has been used to solve a wide variety of the complicated engineering problems, particularly by the development of the computers.

*2.7.1.2 Application Area of the FEM*

The FEM found a great deal of application area. It has been effectively used in many engineering fields, especially in mechanical, aerospace, civil, and automotive engineering. Besides, the applicability of this method on not only linear but also on nonlinear problems made it valuable. The capability to analyze the static and the dynamic as well as the explicit models is its another useful side. In addition, it has been influentially applied for the solutions of fluid flow, heat transfer, acoustics, biomechanics, electromagnetic, and soil mechanic problems.

*2.7.1.3 Discretization in the FEM*

The continuous equations, variables, functions, and models in the applied mathematics are discrete into counterpart pieces in order to make them appropriate

for numerical solution. This transferring process is known as discretization. The FEM also initiates the procedures of the solution based on the discretization process.

In the first stage of the FEM, the model body consisting of infinite points is divided into a large number of soluble small sub-regions or units. In order to constitute approximate equation system, these sub-regions are connected each other from the nodes or nodal points. By this way, one-dimensional (line), two-dimensional (plane), and/or three-dimensional (solid) elements could be constructed. Figure 2.6 indicates typical one-, two-, and three-dimensional elements used in the FEM. In addition to Figure 2.6, the typical sub-regioned and nodal pointed member is illustrated in Figure 2.7.

(LINE)

(a)

(4-NODE PLANE)         (3-NODE PLANE)

(b)

(8-NODE SOLID)

(4-NODE SOLID)

(6-NODE SOLID)

(c)
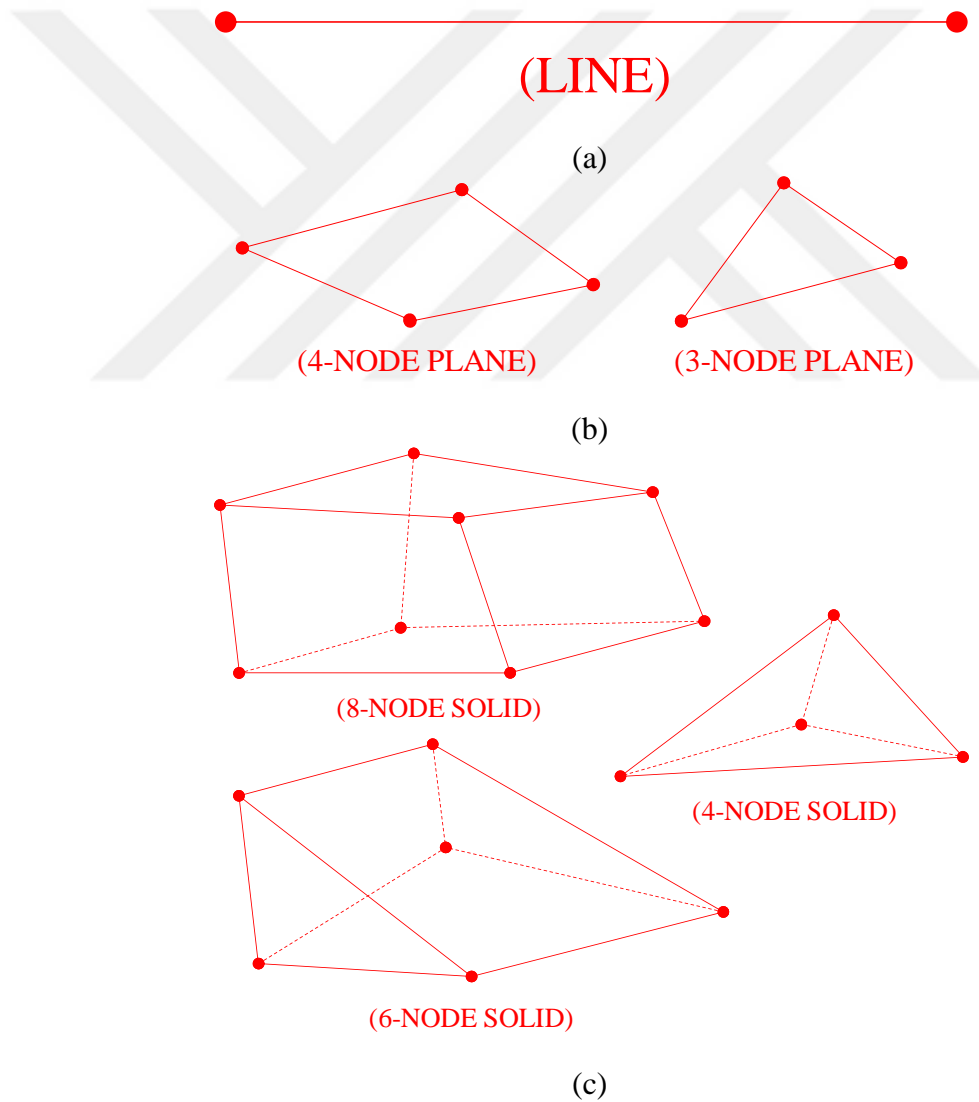
**Figure 2.6.** The element types used in discretization: (a) line, (b) plane, and (c) solid element type

34

The one-dimensional elements is used in the modeling of spring, truss, beam, pipe, etc. while two and three-dimensional elements are utilized for modeling the membrane, plate, shell, etc. and temperature, displacement, stress, flow velocity, etc., respectively. As a result, briefly it can be said about the FEM that this method divides and solves the problems.
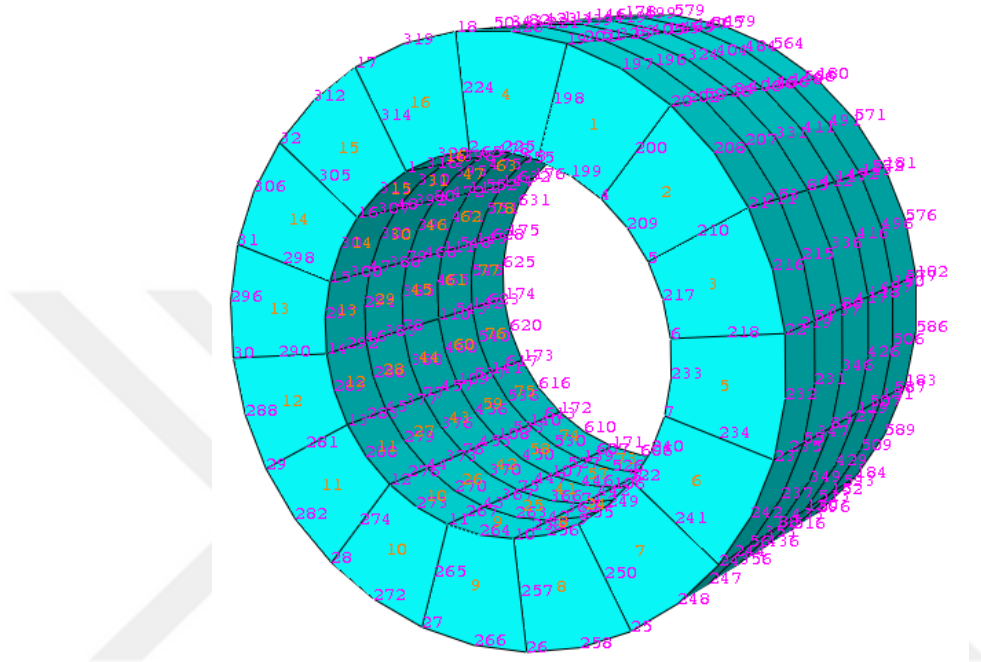


**Figure 2.7.** The solid element and nodal point numbers (orange colored numbers indicates the element number while purple colored number indicates the nodal point number)

### 2.7.1.4 Advantageous and Disadvantageous of the FEM

The ability of the FEM to be applied on complex geometry is the most significant advantageous. Workableness of the FEM to a wide range of engineering difficulties and complex restraints such as indeterminate structures is its another advantageous. In addition, complex loading condition can also be solved by using the FEM and this can be accepted as its crucial benefit.

The fatality of the mistakes done by users and inherent errors in the FEM could be accepted as its main disadvantageous. The investigation of the system response in the case of changing in the several parameters is not possible and the solution attained from the FEM is approximate result. These could also be its disadvantageous.

35

## 2.7.2 Gene Expression Programming (GEP)

The gene expression programming functionally is similar to genetic algorithm (GA) and genetic programming (GP). The population of individuals is utilized during the operations by GEP, they are selected in accordance with fitness, and the genetic variation is presented by utilizing the one or more genetic operators (Mitchell, 1996).
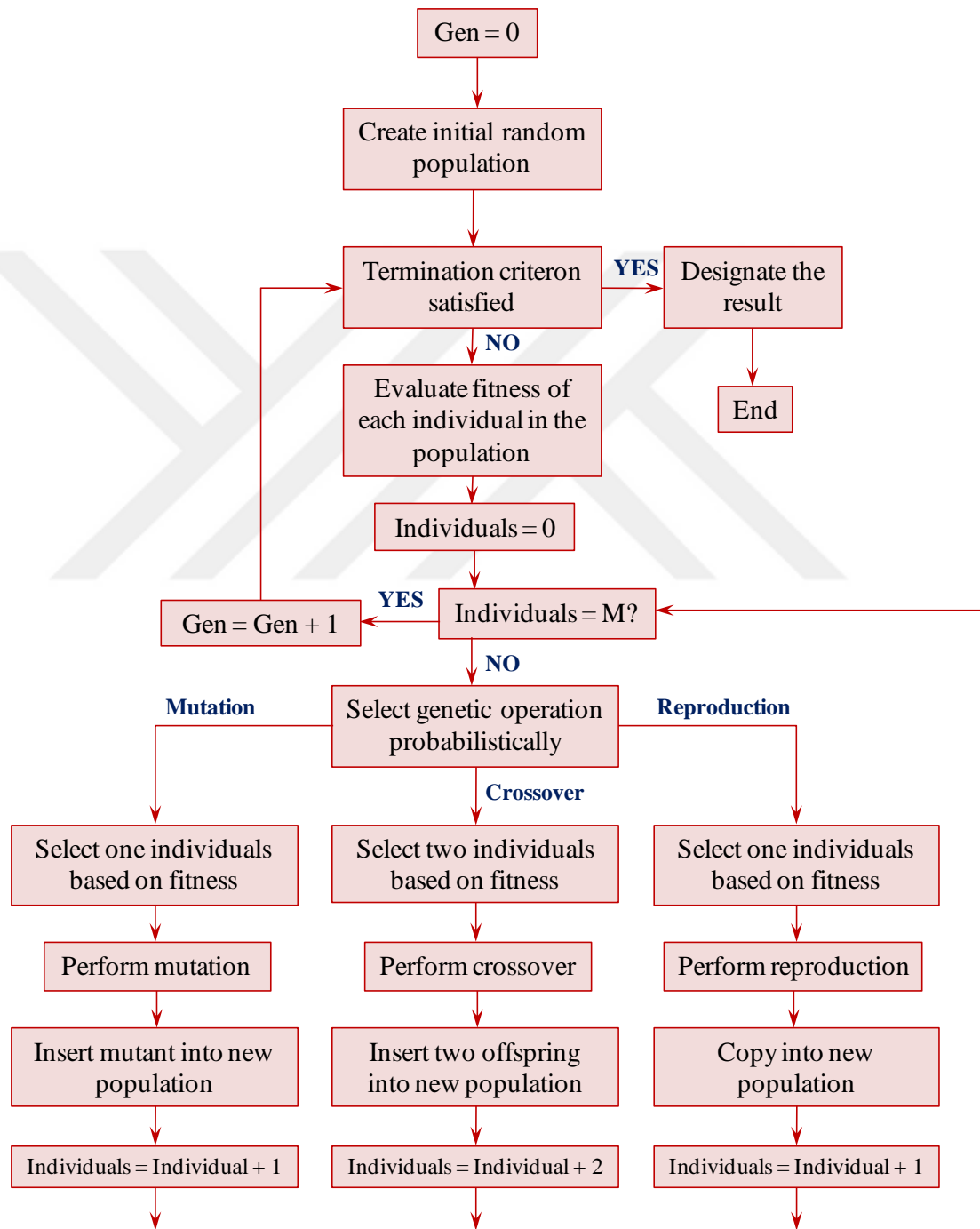


**Figure 2.8.** The flowchart presentation of a genetic programming paradigm (Koza, 1992)

In the GEP, linear strings of fixed length namely the genome or chromosomes are used to codify the individuals and then nonlinear entities of different sizes such as simple diagram expressions or expression trees are used to represent these individuals. However, the individuals in GA and GP are linear strings of fixed length and nonlinear entities of different sizes and shapes, respectively (Ferreira, 2001). In other words, in the dialectic of genetic programming and algorithms, the problem must be described at the beginning, thereafter the solution of the problem is endeavored in a problem-independent mode by the program (Koza, 1992; Gen and Cheng, 1997). This is the basic differentiation among these algorithms (Ferreira, 2001). Therefore, it could be stated that the GEP is the enhanced form of GA and GP. Ferreira (2001) is the inventor of this enhanced form of GA and GP. Koza (1992) represents the flowchart of the gene expression algorithm as given in Figure 2.8. At the beginning of the process, the chromosomes of the preliminary population are arbitrarily generated. Afterwards, the executing the each program starts as next step of the expression of the chromosomes. After the expression of the chromosomes and the executing of the each program, the fitness of each individual is estimated. Regarding the fitness of the each individual, the selection of the individuals for modification step begins for reproduction. This process is maintained and repeated to enhance the individuals that obtained from new generation till the exact number of generations or a solution is achieved (Ferreira, 2001). On the basis of the solution, all aforementioned techniques use the almost same genetic operator with minor differences.

### 2.7.2.1 K-expressions and Expression Trees

The GEP uses open reading frames (ORFs) that permit better comprehending of structural organization. Ferreira (2001) denominated the ORFs as K-expressions that got this name from the Karva language. The K-expressions is an important advantage of the GEP since it provides an opportunity for inferring of phenotype achieved from gene sequences. Also, the GEP allow to translation of K-expressions to expression trees (ETs) that is the diagramming illustration of the phenotype of the GEP sequence as shown in Figure 2.9. Besides, the inverse process such as translation of the ET to K-expression is also possible. For instance, the following mathematical expression can be:

$$\sqrt{(a-b)/(a+b)} \tag{2.15}$$

predicated in K-expression or in ET as below:

```
01234567
Q/-+abab
```
(2.16)

where Q represents the square root.
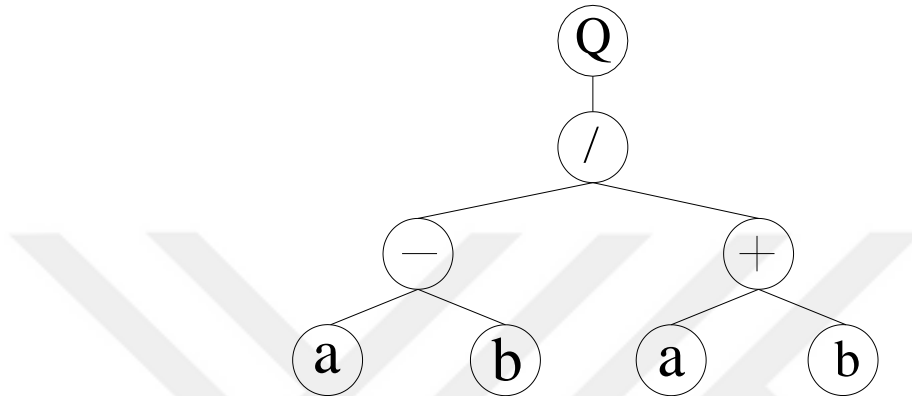


**Figure 2.9.** Typical expression tree configuration

The GEP chromosomes consisting of one or more genes with equal length are in the fixed length. However, the length of K-expressions (or ORFs) is changeable while the length of a gene is constant. This situation is the advanatage of the K-expression.

### 2.7.2.2 Mutation and Inversion Operators

The mutation that can happen in anyplace of the chromosomes must keep the structural organization of the chromosomes as untouched. During the mutation, any symbol in the head could alter to the function or terminal while the terminals in the tail could alter into just terminals. The head, which consists of symbols that reflect the functions and terminals, and tail, which includes only the terminals, constitute the GEP genes. A typical gene which consists of "*Q, \*, /, -, +, a, b*" is presented below (the tail part is given in bold) (Ferreira, 2001):

```
012345678901234567890
+Q-/b*abQbabbababbaab
```
(2.17)

While the mutation can be taken place in both head and tail, the inversion is limitative to the gene head. Both mutation and inversion operators are generally used

38

together. Inversion operator arbitrarily selects any sequence in the gene to be veered and mirrors this sequence and sets it to same place.

In order to illustrate how mutation change the element in the gene, 2-genic chromosome is presented as follows:

$$\begin{array}{l} \texttt{012345678012345678} \\ \texttt{-+-+}\textbf{abaaa}\texttt{/ab/}\textbf{ababb} \end{array} \qquad (2.18)$$

Assume that the elements in position 0 in gene 1 and in position 3 in gene 2 were altered by the mutation to '*Q*'. By this way, the following expression is to be obtained:

$$\begin{array}{l} \texttt{012345678012345678} \\ \texttt{Q+-+}\textbf{abaaa}\texttt{/abQ}\textbf{ababb} \end{array} \qquad (2.19)$$

In order to understand the inversion operator as powerful as mutation, the following 2-genic expression indicates how inversion alters the genes:

$$\begin{array}{l} \texttt{012345678012345678} \\ \texttt{-/Qababaabbaaa*ab+} \end{array} \qquad (2.20)$$

Suppose that the elements between positions 2 and 4 in gene 1 were removed to be inverted from the sequence of "*Qab*" to "*baQ*". By this way, the following expression is to be obtained:

$$\begin{array}{l} \texttt{012345678012345678} \\ \texttt{-/baQabaabbaaa*ab+} \end{array} \qquad (2.21)$$

### 2.7.2.3 Transpositions

Insertion sequence (IS) transposition, root insertion sequence (RIS) transposition, and gene transposition are other powerful operators in the generation of GEP gene. In the fundamental, these three transpositions perform the similar operation on the GEP gene with small differences. The IS transposition randomly chooses a block of element in the gene and then copies it to paste another places of the gene except at the beginning position. Also, the gene, the start of IS element, and its length are arbitrarily selected (Ferreira, 2001). This operator can be clearly seen in the following 2-genic expression:

```
012345678901234567890012345678901234567890
*a+ba-+/*bbabbbaaababQ*/+ab/bbQaababaaabba        (2.22)
```

Assume that the sequence between positions 12 and 14 in gene 2 "*bab*" was selected to be transposed by IS. The target point of this sequence is the bond between positions 6 and 7 in gene 1. Afterwards, the bond between positions 6 and 7 is cut and the copied sequence is pasted on broken point. By this way, the following expression is to be obtained:

```
012345678901234567890012345678901234567890
*a+ba-+/bababbbaaababQ*/+ab/bbQaababaaabba        (2.23)
```

In order to achieve syntatically correct programs and maintain the structural organization of the chromosomes, the element at position 6 keeps its place whereas the element at position 7 shifts to right according to the element number of the IS and subsequently the elements after this position are deleted as much as the element number in the IS. In other words, "*bb*" between positions 8 and 10 in gene 1 is erased from the chromosome.

The RIS is also using the same method to create proper chromoses but the sequence in the RIS begins with a function. Like the IS transposition, the all selections in the RIS transposition are also randomly picked (Ferreira, 2001). The following 2-genic expression is given to obviously see RIS transposition:

```
012345678901234567890012345678901234567890
-bb*++/-Q/abbaabbbaaa/*b/*babaabaabaaaabbb        (2.24)
```

Assume that the sequence between positions 4 and 6 in gene 2 "*\*ba*" was selected to be transposed by RIS. The target point of this sequence is the root of the gene. By this way, the following expression is to be obtained:

```
012345678901234567890012345678901234567890
-bb*++/-Q/abbaabbbaaa*ba/*b/*babaabaaaabbb        (2.25)
```

The program is also syntactically valid and its structural organization is still continued since the elements following the RIS sequence is deleted as soon as the transposition is completed. In other words, "*baa*" between positions 7 and 9 in gene 2 on original chromosome is directly discarded.

As can be understood from its name, gene transposition is the transferring of a gene on the chromosome from one place to another place. In order to clearly see how gene transposition occurs, the following 3-genic expression is presented:

```
0123456780123456780123456 78
/a-+aaaab-Q*+bbaabQ+bbaba+a
```
(2.26)

As in the previous transposition types, the gene is also arbitrarily selected to experience the gene transposition. The gene is replaced with another gene in the chromosome. Assume that the gene 2 is randomly selected and substituted with the gene 1. By this way, the following expression is to be obtained:

```
0123456780123456780123456 78
-Q*+bbaab/a-+aaaabQ+bbaba+a
```
(2.27)

Again, the validation of the program is kept and the structural organization is still maintained.

### 2.7.2.4 Recombination

The recombination in which randomly selected two parent chromosomes are matched to interchange some materials between them is another operator that GEP uses to achieve suitable chromosome. One-point recombination, two-point recombination, and gene recombination are the types of recombination used in the GEP (Ferreira, 2001).

In one-point recombination, the cross over operation is performed between two parent chromosomes only from one point while the operation is carried out from two points in two-point recombination. As a result, newly generated two daughter chromosomes are acquired (Ferreira, 2001). In aid of clearly understanding of these two operators, the following expressions are given:

```
012345678012345678
Qa+*bbaba-aQbababb
*-b/aba+bbaa-aabab
```
(2.28)

Assume that the crossover point is arbitrarily selected at the bond between positions 4 and 5. The interchanging between the parent chromosomes happens at this cut

41

point and two new crossover daughter chromosomes are attained as shown in the following expression:

```
012345678012345678
Qa+*bba+bbaa-aabab
*-b/ababa-aQbababb
```
(2.29)

This process is known as one-point recombination since it undergoes at one point. When the process takes at two points; for instance, the bond between positions 3 and 4 in gene 1 and the bond between positions 5 and 6 in gene 2 is randomly selected to perform two-point recombination, the interchanging is to be as follows:

```
012345678012345678
Qa+*aba+bbaa-aaabb
*-b/bbaba-aQbabbab
```
(2.30)

While the recombination of one- and two-point occurs at any place of the chromosomes, the gene recombination takes place only among the genes. According to this phenomenon, the following expression illustrates the gene recombination happening between two parent chromosomes:

```
012345678012345678
Qa+*bbababaa-aabab
*-b/aba+b-aQbababb
```
(2.31)

### 2.7.3 Artificial Neural Network (ANN)

Artificial neural networks, which was developed by inspiring from human brain, are the computer programs that are imitating the biological neural networks by collecting the information, generalizing, and then deciding about the instances when faced with the examples never saw before (Ergezer et al., 2003; Elmas, 2003). The synaptic connections between among the neurons manage the learning process in the biological systems. However, in the ANN, the training based on the back propagation consists of three stages (Schalkoff, 1997): (i) the input training pattern progress through the forward, (ii) the relevant errors is calculated and propagated through backward, and (iii) the weights are arranged. Many varied optimization methods can be used to manage this process. The weights of the previous layers are modernized by the back propagation of the error that is between the target value and the output of the network as illustrated in Figure (Hebb, 1949; Haykin, 2000; Susac et al., 2005).
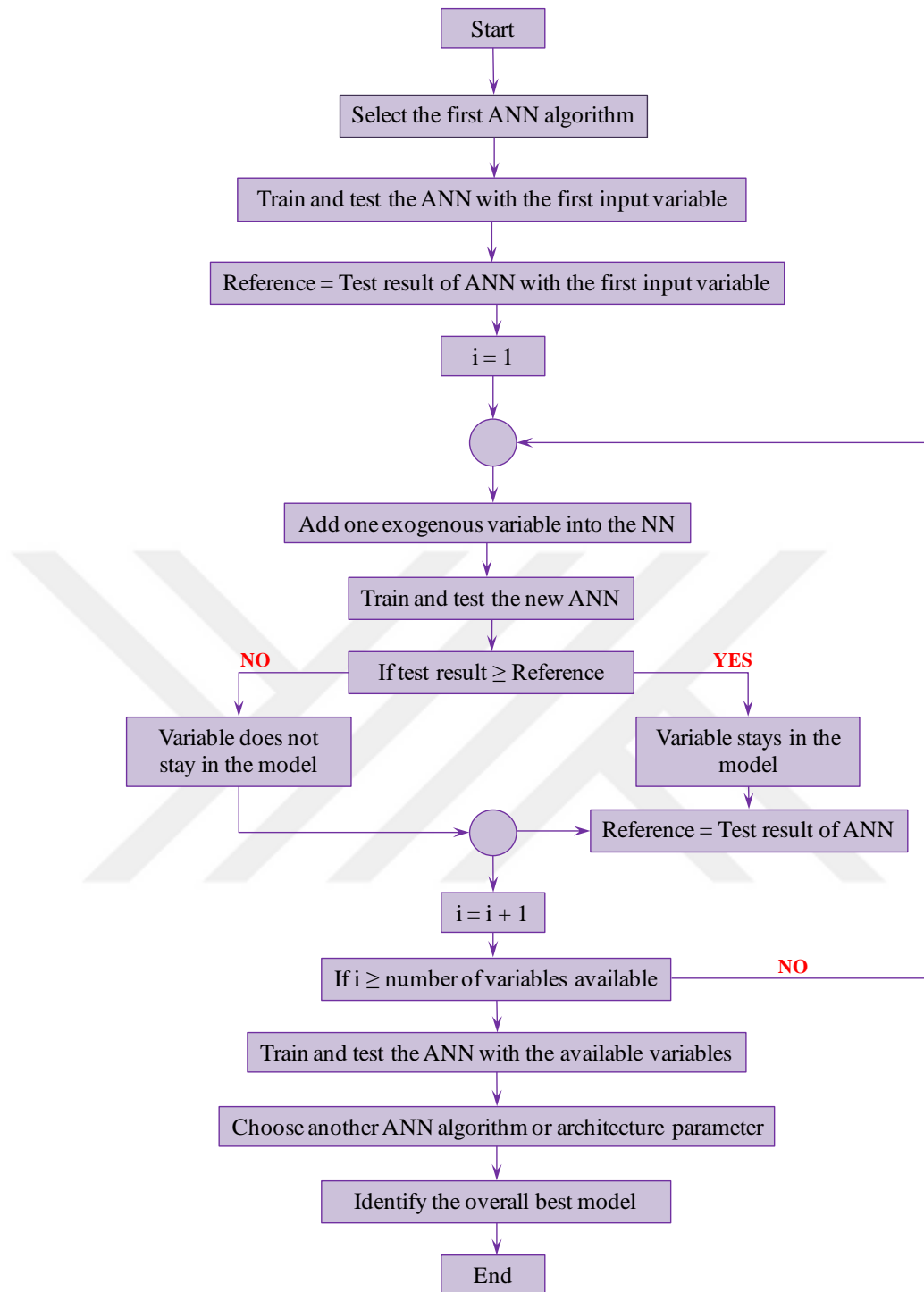
**Figure 2.10.** ANN architecture and model selection in the forward methods (Susac et al., 2005)

### 2.7.3.1 History of the ANN

The first attempts for the theory of the artificial neural networks were done by McCulloch and Pitts at the beginning of 1940s and the first technical paper about the artificial neural networks was published in 1943 by McCulloch and Pitts (1943). By

the time, this basic theory was developed and applied on many areas. In 1960, the first neural computers were emerged. After that time, the deficiencies in the basic theory was discerned but the successive results were achieved during the 1970s and 1980s. After these years, intense researches have started about the highly recognized artificial neural networks (Wah and Mehra, 1992).

### *2.7.3.2 The Mechanism of ANN*

The ANN was produced with respect to the rules that were established during the learning process by input and output information. The calculations in the ANN are asynchronous and parallel to the learning process. Additionally, the ANNs have the faults tolerance. It was aimed to model the learning structure of human brain with the ANNs, which are educable, adaptive, and able to learn and evaluate by self-organizing (Kızrak, 2018). The main elements of the biological nervous systems are neural cells named as neurons. The human nervous systems compose of approximately 86 billion of neural cells that connected with approximately $10^{14}$ and $10^{15}$ synapses. In Figure 2.10, the demonstration of a biological nerve cell and its mathematical model are represented, respectively.

The neurons consist of nucleus, myelin sheath, synapse, dendrite, and axon. The nucleus provides periodical reproduction of the signs through the axons. The axons are one-way electrically active body in which the output impacts are produced, namely they are the exit of the systems while the dendrites are the electrically passive branches in which the signs coming from the other cells are collected, in other words, they are the entrance of the systems. The synapse ensures the connection of the axons with other dendrites (Kızrak, 2018).



(a)

(b)
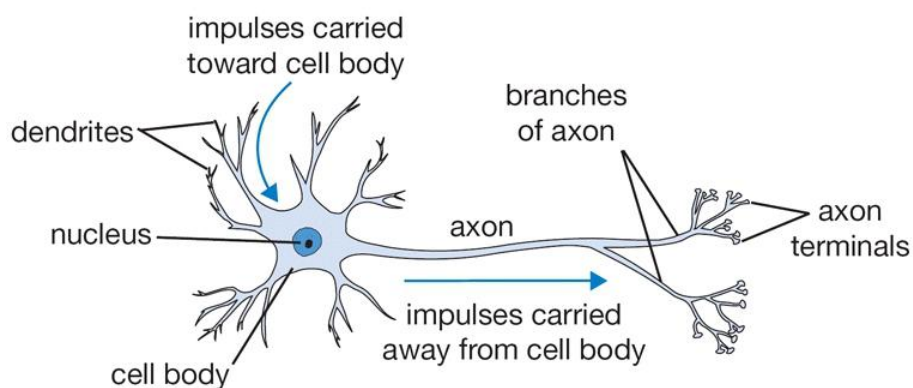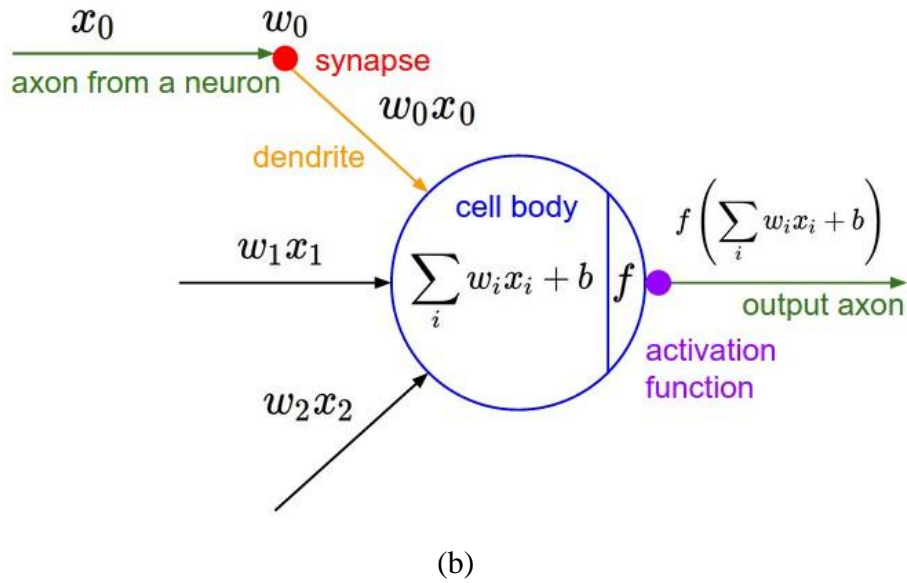
**Figure 2.11.** The demonstration of: (a) a biological nerve cell and (b) a typical mathematical model of nerve cell (Convolutional Neural Networks for Visual Recognition, 2018)

The signals that pass through the axons are illustrated by $x_i$ in the mathematical model. The dendrites, which are connected to axons on the synapse, are interplayed with these signals with respect to synaptic strength denoted as $w_i$. The interaction between the signals traveling through the axons and the dendrites is expressed as $x_i w_i$ in the mathematical representation. These signals passed through the axons and carried by the dendrites are collected at the cell body. At the end, the collected signals are activated with the function that illustrated with the symbol of $f$ in the mathematical model (Convolutional Neural Networks for Visual Recognition, 2018). As a result, the output of the node can be expressed as follows:

$$y = f(\textstyle\sum_i w_i x_i + b) \tag{2.32}$$

where;

$y$ is the dependent variable

$f$ is the activation function

$w_i$ is the weight parameter

$x_i$ is the independent variables

$b$ is the bias value

The bias value is a parameter used to better fitting the output data by altering the activation data to the right or left since there is no any interaction between the bias value and the actual input data.

### 2.7.3.3 Activation Functions

In the ANN, the activation functions have an important role on the solution. The linear, step, sign (signum), sigmoid, tangent hyperbolic, piece-wise linear, sine, and rectified linear unit (ReLU) are the types of the activation functions could be used in the model. The sigmoid, tangent hyperbolic, and ReLU are the commonly used activation functions (Convolutional Neural Networks for Visual Recognition, 2018). The detailed explanation about these activation functions is given in the following sections.

### Sigmoid Activation Function

The sigmoid activation function is a nonlinear function in which the values range between 0 and 1 according to a threshold (Maladkar, 2018). This function is continuous and can be derived. This activation function is mathematically expressed as follows and its graphically representation is presented in Figure 2.11.

$$f(x) = \frac{1}{1+e^{-x}} \qquad (2.33)$$
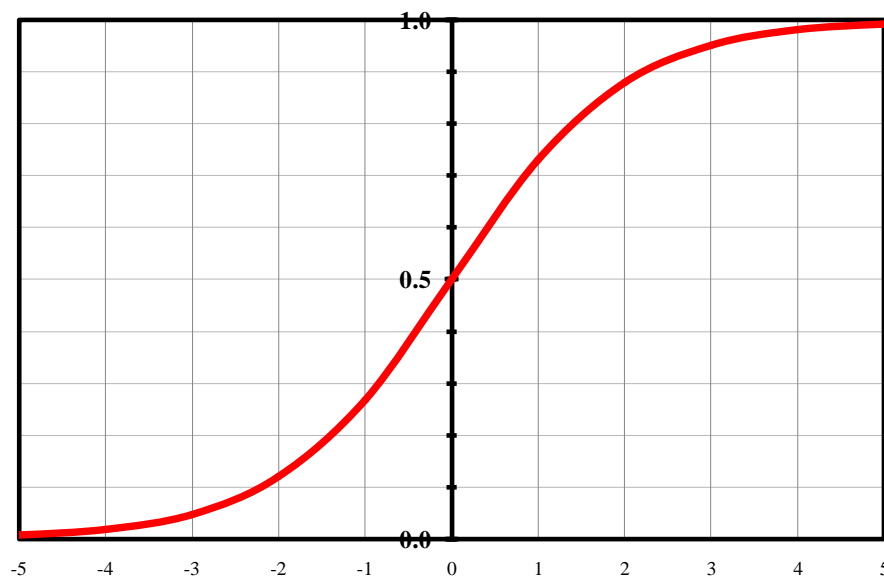


**Figure 2.12.** The graphical illustration of sigmoid activation function

### *Tangent Hyperbolic Activation Function*

Tangent hyperbolic activation function is also a nonlinear function similar to sigmoid function. The only difference is that the values range between -1 and 1 according to the threshold (Maladkar, 2018). This activation function is mathematically expressed as follows and its graphically representation is presented in Figure 2.12.

$$f(x) = \frac{e^x - e^{-x}}{e^x + e^{-x}} \tag{2.34}$$
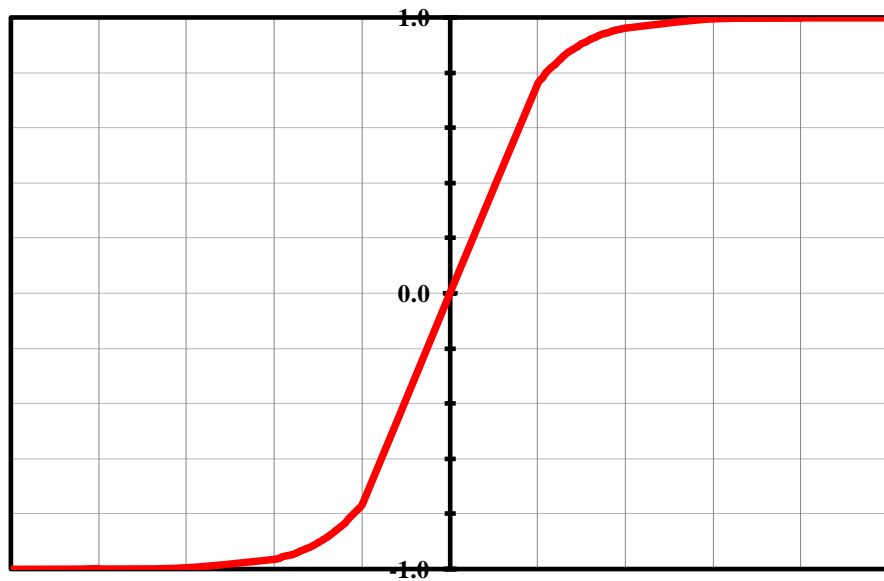


**Figure 2.13.** The graphical illustration of tangent hyperbolic activation function

### *Rectified Linear Unit (ReLU) Activation Function*

The ReLU activation function is another most used activation function. In this activation function, only the positive values are permitted to pass while the passing of the negative values is blocked. By this way, the speed of model is increased and the dead neuron occurrence is extinguished (Maladkar, 2018). This activation function is mathematically expressed as follows and its graphically representation is presented in Figure 2.13.

$$f(x) = \max(0, x) \tag{2.35}$$
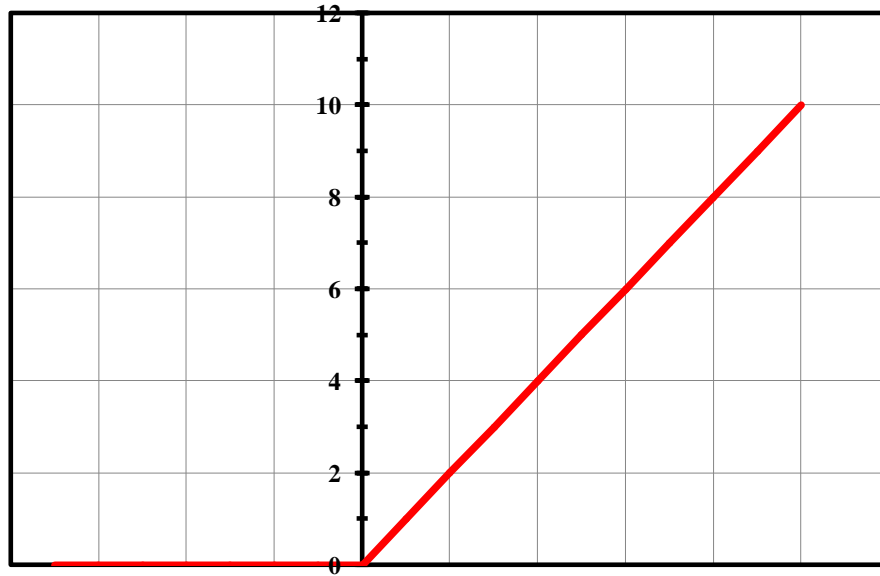
**Figure 2.14.** The graphical illustration of rectified linear unit (ReLU) activation function

### *2.7.3.4 Single-layer and Multi-layer Neural Networks*

When the single-layer and multi-layer neural networks are investigated, it would be noticed that there is a critical difference between them. This crucial distinction is the interactions of the layers. There is only one hidden layer in the single-layer neural networks whereas in the multi-layer neural networks, there are at least two hidden layers as illustrated in Figure 2.10.



INPUT LAYER     HIDDEN LAYER     OUTPUT LAYER

(a)

|  |  |  |  |
|---|---|---|---|
| INPUT<br>LAYER | HIDDEN<br>LAYER I | HIDDEN<br>LAYER II | OUTPUT<br>LAYER |
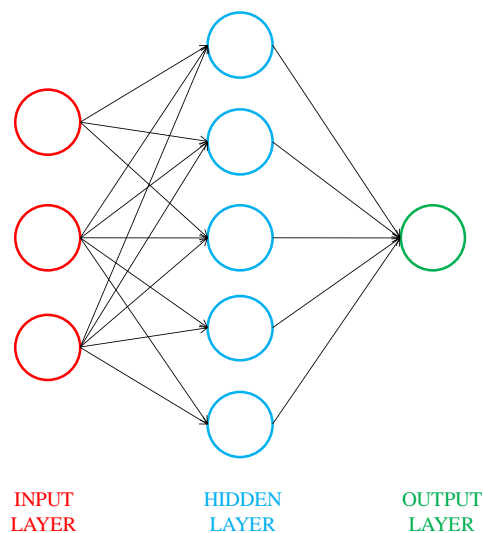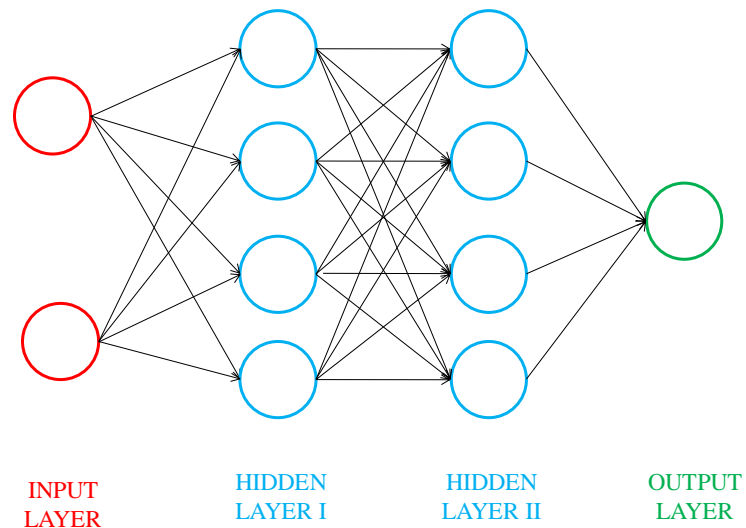
(b)

**Figure 2.15.** The neural networks structure of: (a) single-layer and (b) multi-layer

There is no any relation and interactions between the neurons in a layer. They directly actualize the transferring of the memorable knowledge to the other layers or the exit. On the other hand, the neurons in the two different hidden layers affect the each other regarding various activation values and actualize a transferring determining the learning level of the model (Kızrak, 2018). In both single-layer and multi-layer neural networks, the main operation done in the layer is the improving the *w* and *b* parameters, which enhances the model (Kızrak, 2018).

In Figure 2.14a, there is 6 (5+1) neurons (excluding the input layer). It includes 20 (3x5+5x1) weigh values and 6 (5+1) bias values and as a result, there is totally 26 parameters that should be learned. On the other hand, in Figure 2.14b, the number of neurons (excluding the input layer) is 9 (4+4+1). It contains 28 (2x4+4x4+4x1) weigh values and 9 (4+4+1) bias value and in total, there is 37 parameters that should be learned.

# CHAPTER 3

## RESEARCH METHODOLOGY

### 3.1 Dataset Preparation

The thesis herein presents the numerical analysis of the composite columns, which compose of two steel tube and concrete in-fill between them with circular hollow section (CHS). The concrete filled double skin steel tubular (CFDST) columns were analyzed as regards the column specimens experimentally investigated in the literature. For this reason, the column specimen section properties and ultimate axial strength values were compiled for modeling and analyzing. Totally 16 studies available in the literature were used with the intent to prepare the data source. From 16 studies: Zhao (2002), Lin and Tsai (2003), Tao et al. (2004), Lu et al. (2010a), Uenaka (2010), Zhao (2010), Han et al. (2011a), Han et al. (2011b), Dong and Ho (2012), Li et al. (2012), Dong and Ho (2013), Wang et al. (2014), Essopjee and Dundu (2015), Abbas et al. (2016), Wang et al. (2016), and Hastemoğlu (2017), the data number of 6, 2, 14, 1, 9, 9, 3, 4, 1, 2, 4, 2, 32, 1, 10, and 3 were obtained, respectively. As a result, totally 103 data were gathered up and they presented in Table 3.1. The collection of the data was firstly done with respect to the loading condition and section properties as shown in Figure 3.1.
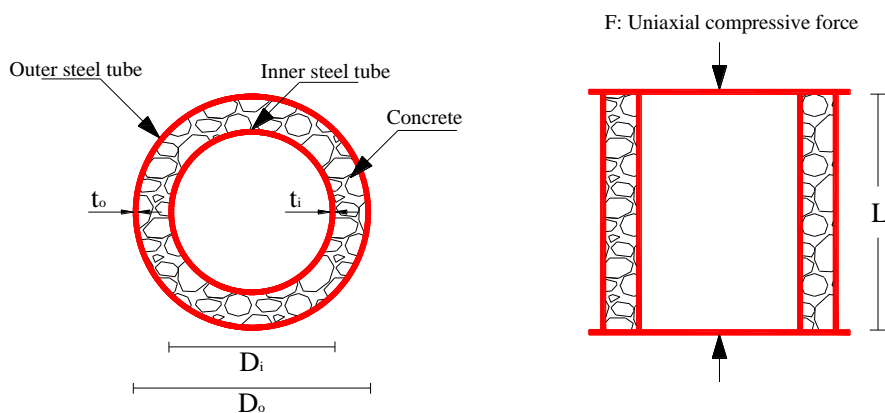


**Figure 3.1.** Specimen details and test configuration of CFDST columns with CHS

**Table 3.1.** Experimental data set used in generation of predictive models

| Reference | Number | Sample ID | Yield strength $f_{syo}$ (MPa) | Outer steel | | Yield strength $f_{syi}$ (MPa) | Inner steel | | Concrete compressive strength $f_c'$ (MPa) | Length of specimen L (mm) | Ultimate axial strength $P_u$ (kN) |
|---|---|---|---|---|---|---|---|---|---|---|---|
| | | | | Diameter $D_o$ (mm) | Thickness $t_o$ (mm) | | Diameter $D_i$ (mm) | Thickness $t_i$ (mm) | | | |
| Zhao et al. (2002) | 1 | C1C7 | 454.0 | 114.5 | 2.80 | 425.0 | 48.4 | 5.90 | 63.4 | 400 | 1415.0 |
| | 2 | C2C7 | 416.0 | 114.6 | 2.80 | 425.0 | 48.4 | 4.70 | 63.4 | 400 | 1380.0 |
| | 3 | C3C7 | 453.0 | 114.4 | 2.80 | 425.0 | 48.4 | 3.50 | 63.4 | 400 | 1210.0 |
| | 4 | C4C7 | 430.0 | 114.2 | 2.80 | 425.0 | 48.4 | 3.00 | 63.4 | 400 | 1110.0 |
| | 5 | C5C8 | 433.0 | 165.1 | 3.10 | 410.0 | 101.8 | 3.50 | 63.4 | 400 | 1705.0 |
| | 6 | C6C8 | 395.0 | 165.3 | 3.10 | 410.0 | 101.8 | 2.90 | 63.4 | 400 | 1605.0 |
| Lin and Tsai (2003) | 7 | DS-06-2-2-C | 250.0 | 300.0 | 2.00 | 250.0 | 180.0 | 2.00 | 28.0 | 1100 | 2311.0 |
| | 8 | DS-06-4-2-C | 250.0 | 300.0 | 4.00 | 250.0 | 180.0 | 2.00 | 28.0 | 1100 | 2750.0 |
| Tao et al. (2004) | 9 | cc2a | 275.9 | 180.0 | 3.00 | 396.1 | 48.0 | 3.00 | 40.0 | 540 | 1790.0 |
| | 10 | cc2b | 275.9 | 180.0 | 3.00 | 396.1 | 48.0 | 3.00 | 40.0 | 540 | 1791.0 |
| | 11 | cc3a | 275.9 | 180.0 | 3.00 | 370.2 | 48.0 | 3.00 | 40.0 | 540 | 1648.0 |
| | 12 | cc3b | 275.9 | 180.0 | 3.00 | 370.2 | 48.0 | 3.00 | 40.0 | 540 | 1650.0 |
| | 13 | cc4a | 275.9 | 180.0 | 3.00 | 342.0 | 48.0 | 3.00 | 40.0 | 540 | 1435.0 |
| | 14 | cc4b | 275.9 | 180.0 | 3.00 | 342.0 | 48.0 | 3.00 | 40.0 | 540 | 1358.0 |
| | 15 | cc5a | 294.5 | 114.0 | 3.00 | 374.5 | 58.0 | 3.00 | 40.0 | 342 | 904.0 |
| | 16 | cc5b | 294.5 | 114.0 | 3.00 | 374.5 | 58.0 | 3.00 | 40.0 | 342 | 898.0 |
| | 17 | cc6a | 275.9 | 240.0 | 3.00 | 294.5 | 114.0 | 3.00 | 40.0 | 720 | 2421.0 |

**Table 3.1.** (cont'd) Experimental data set used in generation of predictive models

| Reference | Number | Sample ID | Yield strength $f_{syo}$ (MPa) | Outer steel | | Yield strength $f_{syi}$ (MPa) | Inner steel | | Concrete compressive strength $f_c'$ (MPa) | Length of specimen L (mm) | Ultimate axial strength $P_u$ (kN) |
|---|---|---|---|---|---|---|---|---|---|---|---|
| | | | | Diameter $D_o$ (mm) | Thickness $t_o$ (mm) | | Diameter $D_i$ (mm) | Thickness $t_i$ (mm) | | | |
| Tao et al. (2004) | 18 | cc6b | 275.9 | 240.0 | 3.00 | 294.5 | 114.0 | 3.00 | 40.0 | 720 | 2460.0 |
| | 19 | cc7a | 275.9 | 300.0 | 3.00 | 320.5 | 165.0 | 3.00 | 40.0 | 900 | 3331.0 |
| | 20 | cc7b | 275.9 | 300.0 | 3.00 | 320.5 | 165.0 | 3.00 | 40.0 | 900 | 3266.0 |
| | 21 | pcc2-1a | 294.5 | 114.0 | 3.00 | 374.5 | 58.0 | 3.00 | 40.0 | 1770 | 620.0 |
| | 22 | pcc2-1b | 294.5 | 114.0 | 3.00 | 374.5 | 58.0 | 3.00 | 40.0 | 1770 | 595.0 |
| Lu et al. (2010) | 23 | C2-C4-SCC1-Ref | 426.0 | 219.1 | 5.00 | 426.0 | 101.6 | 3.20 | 46.6 | 800 | 3333.0 |
| Uenaka et al. (2010) | 24 | c10-375 | 221.0 | 158.0 | 0.90 | 221.0 | 38.0 | 0.90 | 18.7 | 450 | 635.0 |
| | 25 | c10-750 | 221.0 | 159.0 | 0.90 | 221.0 | 76.0 | 0.90 | 18.7 | 450 | 540.0 |
| | 26 | c10-1125 | 221.0 | 159.0 | 0.90 | 221.0 | 114.0 | 0.90 | 18.7 | 450 | 378.3 |
| | 27 | c16-375 | 308.0 | 158.0 | 1.50 | 308.0 | 39.0 | 1.50 | 18.7 | 450 | 851.6 |
| | 28 | c16-750 | 308.0 | 158.0 | 1.50 | 308.0 | 77.0 | 1.50 | 18.7 | 450 | 728.1 |
| | 29 | c16-1125 | 308.0 | 158.0 | 1.50 | 308.0 | 114.0 | 1.50 | 18.7 | 450 | 589.0 |
| | 30 | c23-375 | 286.0 | 158.0 | 2.14 | 286.0 | 40.0 | 2.14 | 18.7 | 450 | 968.2 |
| | 31 | c23-750 | 286.0 | 158.0 | 2.14 | 286.0 | 77.0 | 2.14 | 18.7 | 450 | 879.1 |
| | 32 | c23-1125 | 286.0 | 157.0 | 2.14 | 286.0 | 115.0 | 2.14 | 18.7 | 450 | 703.6 |
| Zhao et al. (2010) | 33 | O1I1-S | 454.0 | 114.3 | 6.00 | 425.0 | 48.3 | 2.90 | 63.4 | 400 | 1665.0 |
| | 34 | O2I1-S | 416.0 | 114.3 | 4.80 | 425.0 | 48.3 | 2.90 | 63.4 | 400 | 1441.0 |

**Table 3.1.** (cont'd) Experimental data set used in generation of predictive models

| Reference | Number | Sample ID | Yield strength $f_{syo}$ (MPa) | Outer steel | | Yield strength $f_{syi}$ (MPa) | Inner steel | | Concrete compressive strength $f_c'$ (MPa) | Length of specimen L (mm) | Ultimate axial strength $P_u$ (kN) |
|---|---|---|---|---|---|---|---|---|---|---|---|
| | | | | Diameter $D_o$ (mm) | Thickness $t_o$ (mm) | | Diameter $D_i$ (mm) | Thickness $t_i$ (mm) | | | |
| Zhao et al. (2010) | 35 | O3I1-S | 453.0 | 114.3 | 3.60 | 425.0 | 48.3 | 2.90 | 63.4 | 400 | 1243.0 |
| | 36 | O4I1-S | 430.0 | 114.3 | 3.20 | 425.0 | 48.3 | 2.90 | 63.4 | 400 | 1145.0 |
| | 37 | O5I2-S | 433.0 | 165.1 | 3.50 | 394.0 | 101.6 | 3.20 | 63.4 | 400 | 1629.0 |
| | 38 | O6I2-S | 395.0 | 165.1 | 3.00 | 394.0 | 101.6 | 3.20 | 63.4 | 400 | 1613.0 |
| | 39 | O7I2-S | 395.0 | 163.8 | 2.35 | 394.0 | 101.6 | 3.20 | 63.4 | 400 | 1487.0 |
| | 40 | O8I2-S | 395.0 | 163.0 | 1.95 | 394.0 | 101.6 | 3.20 | 63.4 | 400 | 1328.0 |
| | 41 | O9I2-S | 395.0 | 162.5 | 1.70 | 394.0 | 101.6 | 3.20 | 63.4 | 400 | 1236.0 |
| Han et al. (2011a) | 42 | DCc-0 | 311.0 | 120.0 | 1.96 | 380.0 | 60.0 | 1.96 | 39.3 | 1324 | 578.0 |
| | 43 | DCc-1 | 311.0 | 120.0 | 1.96 | 380.0 | 60.0 | 1.96 | 66.4 | 1324 | 789.0 |
| | 44 | DCc-2 | 311.0 | 120.0 | 1.96 | 380.0 | 60.0 | 1.96 | 66.4 | 1324 | 715.0 |
| Han et al. (2011b) | 45 | C1-1 | 319.6 | 220.0 | 3.62 | 380.6 | 159.0 | 3.72 | 60.0 | 660 | 2537.0 |
| | 46 | C1-2 | 319.6 | 220.0 | 3.62 | 380.6 | 159.0 | 3.72 | 60.0 | 660 | 2566.0 |
| | 47 | C2-1 | 319.6 | 220.0 | 3.62 | 380.6 | 106.0 | 3.72 | 60.0 | 660 | 3436.0 |
| | 48 | C2-2 | 319.6 | 220.0 | 3.62 | 380.6 | 106.0 | 3.72 | 60.0 | 660 | 3506.0 |
| Dong and Ho (2012) | 49 | D50-5-0 | 360.0 | 168.3 | 5.00 | 450.0 | 88.9 | 5.00 | 50.0 | 330 | 2852.0 |
| Li et al. (2012) | 50 | C1-1 | 439.3 | 350.0 | 3.82 | 396.5 | 231.0 | 2.92 | 50.0 | 1050 | 5499.0 |
| | 51 | C1-2 | 439.3 | 350.0 | 3.82 | 396.5 | 231.0 | 2.92 | 50.0 | 1050 | 5396.0 |

**Table 3.1.** (cont'd) Experimental data set used in generation of predictive models

| Reference | Number | Sample ID | Yield strength $f_{syo}$ (MPa) | Outer steel | | Yield strength $f_{syi}$ (MPa) | Inner steel | | Concrete compressive strength $f_c'$ (MPa) | Length of specimen L (mm) | Ultimate axial strength $P_u$ (kN) |
| | | | | Diameter $D_o$ (mm) | Thickness $t_o$ (mm) | | Diameter $D_i$ (mm) | Thickness $t_i$ (mm) | | | |
|---|---|---|---|---|---|---|---|---|---|---|---|
| Dong and Ho (2013) | 52 | D-A-50-0 | 450.0 | 168.3 | 5.00 | 360.0 | 88.9 | 5.00 | 50.0 | 330 | 2865.0 |
| | 53 | D-B-50-0 | 430.0 | 168.3 | 5.00 | 360.0 | 114.3 | 5.00 | 50.0 | 330 | 2674.0 |
| | 54 | D-A-85-0 | 450.0 | 168.3 | 5.00 | 360.0 | 88.9 | 5.00 | 85.0 | 330 | 3218 |
| | 55 | D-B-85-0 | 430.0 | 168.3 | 5.00 | 360.0 | 114.3 | 5.00 | 85.0 | 330 | 2994 |
| Wang et al. (2014) | 56 | 0HA0 | 350.0 | 165.0 | 1.70 | 350.0 | 76.0 | 1.20 | 28.1 | 500 | 980.0 |
| | 57 | 0HB0 | 350.0 | 165.0 | 1.70 | 350.0 | 114.0 | 1.70 | 28.1 | 500 | 715.0 |
| Essopjee and Dundu (2015) | 58 | S139.2-1.0 | 418.0 | 139.2 | 3.00 | 324.0 | 76.0 | 2.00 | 30.8 | 998 | 1059.2 |
| | 59 | S139.2-1.0 | 418.0 | 139.2 | 3.00 | 324.0 | 76.0 | 2.00 | 30.8 | 1001 | 1056.1 |
| | 60 | S139.2-1.5 | 418.0 | 139.2 | 3.00 | 324.0 | 76.0 | 2.00 | 30.8 | 1500 | 905.5 |
| | 61 | S139.2-1.5 | 418.0 | 139.2 | 3.00 | 324.0 | 76.0 | 2.00 | 30.8 | 1503 | 901.6 |
| | 62 | S139.2-2.0 | 418.0 | 139.2 | 3.00 | 324.0 | 76.0 | 2.00 | 30.8 | 2000 | 831.7 |
| | 63 | S139.2-2.0 | 418.0 | 139.2 | 3.00 | 324.0 | 76.0 | 2.00 | 30.8 | 1998 | 837.4 |
| | 64 | S139.2-2.5 | 418.0 | 139.2 | 3.00 | 324.0 | 76.0 | 2.00 | 30.8 | 2502 | 732.1 |
| | 65 | S139.2-2.5 | 418.0 | 139.2 | 3.00 | 324.0 | 76.0 | 2.00 | 30.8 | 2498 | 729.0 |
| | 66 | S152.4-1.0 | 549.0 | 152.4 | 3.00 | 324.0 | 76.0 | 2.00 | 30.8 | 1003 | 1263.5 |
| | 67 | S152.4-1.0 | 549.0 | 152.4 | 3.00 | 324.0 | 76.0 | 2.00 | 30.8 | 1002 | 1254.9 |
| | 68 | S152.4-1.5 | 549.0 | 152.4 | 3.00 | 324.0 | 76.0 | 2.00 | 30.8 | 1497 | 1195.6 |

**Table 3.1.** (cont'd) Experimental data set used in generation of predictive models

| Reference | Number | Sample ID | Yield strength $f_{syo}$ (MPa) | Outer steel | | Yield strength $f_{syi}$ (MPa) | Inner steel | | Concrete compressive strength $f_c'$ (MPa) | Length of specimen L (mm) | Ultimate axial strength $P_u$ (kN) |
|---|---|---|---|---|---|---|---|---|---|---|---|
| | | | | Diameter $D_o$ (mm) | Thickness $t_o$ (mm) | | Diameter $D_i$ (mm) | Thickness $t_i$ (mm) | | | |
| Essopjee and Dundu (2015) | 69 | S152.4-1.5 | 549.0 | 152.4 | 3.00 | 324.0 | 76.0 | 2.00 | 30.8 | 1503 | 1191.2 |
| | 70 | S152.4-2.0 | 549.0 | 152.4 | 3.00 | 324.0 | 76.0 | 2.00 | 30.8 | 1997 | 1047.3 |
| | 71 | S152.4-2.0 | 549.0 | 152.4 | 3.00 | 324.0 | 76.0 | 2.00 | 30.8 | 2000 | 1041.6 |
| | 72 | S152.4-2.5 | 549.0 | 152.4 | 3.00 | 324.0 | 76.0 | 2.00 | 30.8 | 2498 | 941.4 |
| | 73 | S152.4-2.5 | 549.0 | 152.4 | 3.00 | 324.0 | 76.0 | 2.00 | 30.8 | 2500 | 949.0 |
| | 74 | S165.1-1.0 | 516.0 | 165.1 | 3.00 | 324.0 | 76.0 | 2.00 | 30.8 | 998 | 1512.3 |
| | 75 | S165.1-1.0 | 516.0 | 165.1 | 3.00 | 324.0 | 76.0 | 2.00 | 30.8 | 999 | 1510.6 |
| | 76 | S165.1-1.5 | 516.0 | 165.1 | 3.00 | 324.0 | 76.0 | 2.00 | 30.8 | 1504 | 1286.4 |
| | 77 | S165.1-1.5 | 516.0 | 165.1 | 3.00 | 324.0 | 76.0 | 2.00 | 30.8 | 1498 | 1275.1 |
| | 78 | S165.1-2.0 | 516.0 | 165.1 | 3.00 | 324.0 | 76.0 | 2.00 | 30.8 | 2003 | 1187.2 |
| | 79 | S165.1-2.0 | 516.0 | 165.1 | 3.00 | 324.0 | 76.0 | 2.00 | 30.8 | 1998 | 1199.8 |
| | 80 | S165.1-2.5 | 516.0 | 165.1 | 3.00 | 324.0 | 76.0 | 2.00 | 30.8 | 2498 | 1028.0 |
| | 81 | S165.1-2.5 | 516.0 | 165.1 | 3.00 | 324.0 | 76.0 | 2.00 | 30.8 | 2502 | 1036.5 |
| | 82 | S193.7-1.0 | 391.0 | 193.7 | 3.50 | 324.0 | 76.0 | 2.00 | 30.8 | 1003 | 2010.0 |
| | 83 | S193.7-1.0 | 391.0 | 193.7 | 3.50 | 324.0 | 76.0 | 2.00 | 30.8 | 1000 | 2030.0 |
| | 84 | S193.7-1.5 | 391.0 | 193.7 | 3.50 | 324.0 | 76.0 | 2.00 | 30.8 | 1502 | 1730.0 |
| | 85 | S193.7-1.5 | 391.0 | 193.7 | 3.50 | 324.0 | 76.0 | 2.00 | 30.8 | 1500 | 1720.0 |

**Table 3.1.** (cont'd) Experimental data set used in generation of predictive models

| Reference | Number | Sample ID | Yield strength $f_{syo}$ (MPa) | Outer steel | | Yield strength $f_{syi}$ (MPa) | Inner steel | | Concrete compressive strength $f_c'$ (MPa) | Length of specimen L (mm) | Ultimate axial strength $P_u$ (kN) |
|---|---|---|---|---|---|---|---|---|---|---|---|
| | | | | Diameter $D_o$ (mm) | Thickness $t_o$ (mm) | | Diameter $D_i$ (mm) | Thickness $t_i$ (mm) | | | |
| Essopjee and Dundu (2015) | 86 | S193.7-2.0 | 391.0 | 193.7 | 3.50 | 324.0 | 76.0 | 2.00 | 30.8 | 1998 | 1581.6 |
| | 87 | S193.7-2.0 | 391.0 | 193.7 | 3.50 | 324.0 | 76.0 | 2.00 | 30.8 | 2003 | 1584.1 |
| | 88 | S193.7-2.5 | 391.0 | 193.7 | 3.50 | 324.0 | 76.0 | 2.00 | 30.8 | 2503 | 1451.4 |
| | 89 | S193.7-2.5 | 391.0 | 193.7 | 3.50 | 324.0 | 76.0 | 2.00 | 30.8 | 2497 | 1458.7 |
| Abbas et al. (2016) | 90 | CB2-40NG-AB-CP | 307.0 | 150.0 | 6.00 | 307.0 | 26.7 | 2.87 | 40.0 | 600 | 1805.0 |
| Wang et al. (2016) | 91 | HC22X4-C40 | 300 | 140.2 | 2.92 | 794.0 | 22.1 | 4.09 | 40.5 | 350 | 1450.0 |
| | 92 | HC32X6-C40 | 300 | 140.3 | 2.89 | 619.0 | 32.0 | 5.48 | 40.5 | 350 | 1562.0 |
| | 93 | HC38X8-C40 | 300 | 140.1 | 2.91 | 433.0 | 38.1 | 7.63 | 40.5 | 350 | 1838.4 |
| | 94 | HC55X11-C40 | 300 | 140.2 | 2.90 | 739.0 | 55.1 | 10.62 | 40.5 | 350 | 2724.0 |
| | 95 | HC89X4-C40 | 300 | 140.1 | 2.87 | 1029.0 | 89.0 | 3.91 | 40.5 | 350 | 2024.9 |
| | 96 | HC22X4-C80 | 300 | 140.2 | 2.91 | 794.0 | 22.1 | 4.10 | 79.9 | 350 | 1845.1 |
| | 97 | HC32X6-C80 | 300 | 140.2 | 2.92 | 619.0 | 31.9 | 5.27 | 79.9 | 350 | 2012.5 |
| | 98 | HC38X8-C80 | 300 | 140.1 | 2.90 | 433.0 | 38.0 | 7.51 | 79.9 | 350 | 2083.4 |
| | 99 | HC55X11-C80 | 300 | 140.1 | 2.90 | 739.0 | 55.2 | 10.76 | 79.9 | 350 | 2775.0 |
| | 100 | HC89X4-C80 | 300 | 140.1 | 2.86 | 1029.0 | 89.1 | 3.91 | 79.9 | 350 | 2107.4 |
| Hastemoğlu (2017) | 101 | DSCFT 3 | 250.0 | 139.0 | 2.00 | 250.0 | 75.0 | 3.00 | 55.0 | 351 | 807.0 |
| | 102 | DSCFT 4 | 250.0 | 139.0 | 2.00 | 250.0 | 75.0 | 3.00 | 55.0 | 468 | 810.0 |
| | 103 | DSCFT 5 | 250.0 | 139.0 | 2.00 | 250.0 | 75.0 | 3.00 | 55.0 | 585 | 877.0 |

The axially loading condition and circular hollow section were fixed parameters in all data. However, the yield strength of both outer and inner tubes, their diameters and thicknesses, the concrete compressive strength, and the length of the column specimens were variable parameters. The ultimate strength of the circular hollow section column specimens with these changeable parameters under axially loading condition was the investigated parameter.

The yield strength of the outer steel tube was in the range of 221 and 549 MPa while that of the inner steel tube was in the range of 221 and 1029 MPa. The diameter and thickness of the outer steel tube ranged between 114 and 350 mm and 0.9 and 6.0 mm, respectively, whereas the inner steel tube's ranged between 22.1 and 231 mm and 0.90 and 10.76 mm, respectively. The maximum compressive strength value was 85.0 MPa and the minimum was 18.7 MPa. The length of the specimens aligned between 330 and 2503 mm. According to these section properties and material strengths, the ultimate axial strength values were in the range in 378.3 kN and 5499 kN.

In addition, the variable parameters and the investigated parameter were also statistically analyzed regarding to mean, standard deviation and coefficient of variation. The statistical analysis results are tabulated in Table 3.2.

**Table 3.2.** Statistics of experimental data used in analysis and production of models

|  | $f_{syo}$ (MPa) | $D_o$ (mm) | $t_o$ (mm) | $f_{syi}$ (MPa) | $D_i$ (mm) | $t_i$ (mm) | $f_c$ (MPa) | L (mm) | $P_{u,exp}$ (kN) |
|---|---|---|---|---|---|---|---|---|---|
| Total data |  |  |  |  |  |  |  |  |  |
| Number of data | 103 | 103 | 103 | 103 | 103 | 103 | 103 | 103 | 103 |
| Mean | 374.9 | 167.1 | 3.02 | 380.6 | 81 | 2.99 | 37.1 | 938.1 | 1608 |
| Standard deviation | 93.2 | 47.2 | 0.93 | 137.4 | 38.2 | 1.64 | 18.4 | 686.5 | 929.4 |
| COV | 0.25 | 0.28 | 0.31 | 0.36 | 0.47 | 0.55 | 0.50 | 0.73 | 0.58 |
| Min. value | 221 | 114 | 0.9 | 221 | 22.1 | 0.9 | 18.7 | 330 | 378.3 |
| Max. value | 549 | 350 | 6 | 1029 | 231 | 10.76 | 85 | 2503 | 5499 |

## 3.2 Finite Element Modeling and Soft Computing Methods

In the thesis herein, the samples were modeled in ABAQUS CAE 16 named software in which the samples were model with the logic of the finite element method (FEM). In addition, the gene expression programming (GEP) and the artificial neural network (ANN) were used in order to derive the predictive model. The MATLAB

v.17 named software was handled to generate the predictive model by using the ANN method while the GeneXproTools 5.0 named software was handled to achieve the predictive model by using the GEP method. In the following sections, the detailed explanations about the modeling and analyzing are given.

### 3.2.1 Modeling by FEM

The finite element program named ABAQUS CAE 16 (2014) was employed to simulate and analyze the nonlinear behavior of the CFDST columns with CHS under axial loading condition. The verification and calibration of the developed material model is a crucial issue in order to truthfully estimate the behavior of such columns. For this reason, the previously conducted experimental test results given in Table 3.1 were regarded for verification and calibration of the proposed model. The material definition especially the nonlinear behaviors, interaction and surface identifications, the element type and mesh selection, and loading and boundary conditions are presented in detail in the following sections.

#### 3.2.1.1 Material Modeling

The CFDST columns with CHS analyzed in this study consist of two steel tubes named as outer and inner, two end plates placed at top and bottom of columns, and concrete annulus between the steel tubes. The material behaviors of the steel and concrete are explained in the following sections.

#### Modeling of Steel

In ABAQUS, bilinear elastic-plastic material behavior with isotropic hardening was considered for modeling of both end plates and steel tubes. According to the recommendation by Han and Huo (2003), the stress-strain relationship consists of two regions as shown in Figure 3.2. The elastic characteristics of the steel were specified in the first region, which starts from the origin and ends at the yield point. The elastic constants such as modulus of elasticity and Poisson's ratio were set in this region. The modulus of elasticity was directly obtained from some studies but for the others in which the moduli of elasticity values were not given, it was used as $200 \times 10^3$ N/mm$^2$. Poisson's ratio, $v_s$, for all steel tubes was considered as 0.3.
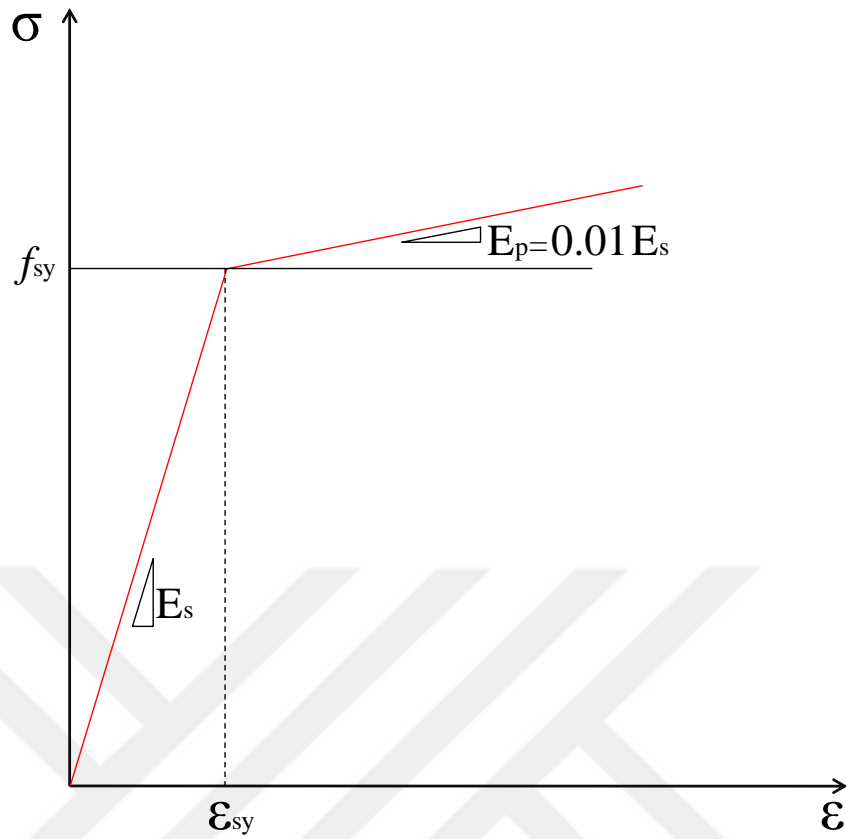
**Figure 3.2.** Stress-strain curve for steel end plates and tubes

The modulus of elasticity of the steel was used for the determination of modulus in plastic region that was assumed to be equal to 1% of elastic modulus. First and second regions, namely elastic and plastic regions, could be easily achieved by using the following equations (Pagoulatou et al., 2014):

$$\sigma_i = E_s \varepsilon_s \qquad for \; \varepsilon_s \leq \varepsilon_{sy} \; (elastic \; region) \qquad (3.1)$$

$$\sigma_i = f_{sy} + E_p\left(\varepsilon_s - \varepsilon_{sy}\right) \qquad for \; \varepsilon_s > \varepsilon_{sy} \; (plastic \; region) \qquad (3.2)$$

where;

$\sigma_i$ is the desired steel strength,

$\varepsilon_s$ is the steel strain,

$\varepsilon_{sy}$ is the steel strain at yield point and can be calculated by $f_{sy}/E_s$.

59

As a result, the steel behavior was defined in ABAQUS as elastic till its yield strain and plastic between yield and final strain that was assumed to be 3% in this study.

*Modeling of Concrete*

The confinement effect provided by the surrounding steel can be considered in the case of lower diameter-to-thickness ratio ($D_o/t_o$) of outer steel tube. Otherwise, the confinement effect on concrete procured by steel would be insufficient. For this reason, the strength improvement in concrete ensured by confinement effect could be considered in the case of $D_o/t_o$ is less than or equal to 150. In the modeling of concrete in ABAQUS, two different concrete stress-strain relationships, confined and unconfined, could be identified as indicated in Figure 3.3.
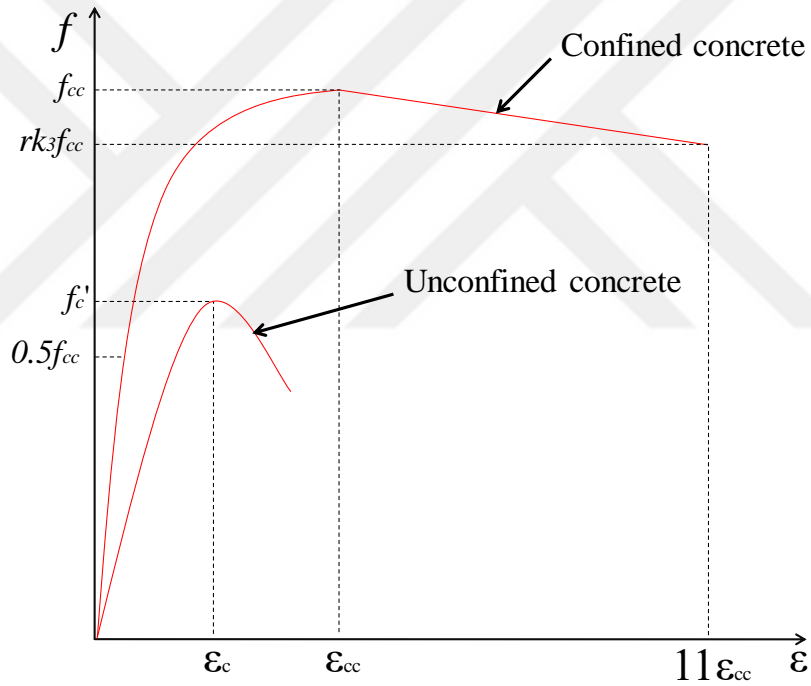


**Figure 3.3.** Stress-strain curves for confined and unconfined concrete

In Figure 3.3, $f_c'$ and $f_{cc}$ are the unconfined compressive strength of cylinder concrete, which is equal to 80% of compressive strength of cube concrete, and confined compressive strength, respectively. The corresponding strains of unconfined and confined concretes are demonstrated by $\varepsilon_c$ and $\varepsilon_{cc}$, respectively. The compressive strength of cylinder concrete can be obtained by experimental test and the unconfined concrete strain, $\varepsilon_c$, can be considered as 0.003 regarding ACI (2002)

suggestion. However, the following formulas proposed by Mander et al. (1988) could be used in the calculation of the confined concrete parameters, strength and corresponding strain:

$$f_{cc} = f_c^{'} + k_1 f_1 \tag{3.3}$$

$$\varepsilon_{cc} = \varepsilon_c \left(1 + k_2 \frac{f_1}{f_c}\right) \tag{3.4}$$

where;

$k_1$ and $k_2$ are constants and recommended to be taken as 4.1 and 20.5, respectively, by Richart et al. (1928),

$f_1$ is the lateral confining pressure provided by the steel tube and can be calculated by the following expressions recommended by Hu et al. (2003):

In the case of $21.7 \leq D_o/t_o \leq 47$

$$f_1 = f_{syo} \left[0.043646 - 0.000832 \left(\frac{D_o}{t_o}\right)\right] \tag{3.5}$$

In the case of $47 < D_o/t_o \leq 150$

$$f_1 = f_{syo} \left[0.006421 - 0.0000357 \left(\frac{D_o}{t_o}\right)\right] \tag{3.6}$$

As clearly be seen from Figure 3.5, the confined concrete stress-strain curve contains three zones. The elastic region, which begins from origin and ends at the proportional limit stress, is the first zone of the curve while the nonlinear region, which falls between the proportional limit and confined concrete stresses, is the second zone of the stress-strain curve of the confined concrete. In this study, the proportional limit stress was taken as $0.5 f_{cc}$ according to Hu et al. (2003) proposed and corresponding strain was calculated by dividing the proportional limit stress to confined concrete's modulus of elasticity, $E_{cc}$. The empirical equation given as follows and suggested by ACI (2002) was used to determine the acceptedly elastic modulus for the confined concrete. In addition to that, the Poisson's ratio for conventional concrete, $v_c$, ranges between 0.15 and 0.22 and it was presumed to be 0.20 for confined concrete in this numerical analysis.

$$E_{cc} = 4700\sqrt{f_{cc}} \tag{3.7}$$

The nonlinear region of the stress-strain curve of the confined concrete could be determined by the following expression that was recommended by Saenz (1964):

$$f' = \frac{E_{cc}\,\varepsilon}{1+(R+R_E-2)\left(\frac{\varepsilon}{\varepsilon_{cc}}\right)-(2R-1)\left(\frac{\varepsilon}{\varepsilon_{cc}}\right)^2+R\left(\frac{\varepsilon}{\varepsilon_{cc}}\right)^3} \qquad (3.8)$$

where;

R and $R_E$ coefficients can be calculated by the following expressions:

$$R = \frac{R_E(R_\sigma-1)}{(R_\varepsilon-1)^2} - \frac{1}{R_\varepsilon} \qquad (3.8a)$$

$$R_E = \frac{E_{cc}\,\varepsilon_{cc}}{f_{cc}} \qquad (3.8b)$$

and where;

$R_\sigma$ and $R_\varepsilon$ are set to be equivalent to 4 according to suggestion by Hu and Schnobrich (1989).

In this situation, in the formula proposed by Saenz (1964), only the strain, $\varepsilon$, value is unknown in order to calculate the stress. The stress values for nonlinear region could be easily computed by postulating the strain values which must be between the proportional strain and the confined strain.

The third zone of the stress-strain curve of confined concrete could be named as descending region which starts from the confined concrete strength and decline throughout the terminated stress value of the curve that can be computed as $rk_3 f_{cc}$. The strain value at the terminated stress was formulized to be $11\varepsilon_{cc}$. It was recommended by Hu et al. (2003) that the coefficient, $k_3$, used in the calculation of last point of descending region can be computed by the following expressions:

In the case of $21.7 \le D_o/t_o \le 47$

$$k_3 = 1 \qquad (3.9)$$

In the case of $47 < D_o/t_o \le 150$

$$k_3 = 0.0000339\left(\frac{D_o}{t_o}\right)^2 - 0.0100085\left(\frac{D_o}{t_o}\right) + 1.3491 \qquad (3.10)$$

The other coefficient in the final stress calculation, r, was proposed to be taken as 1.0 for the concrete having 30 MPa cube strength, $f_{cu}$, and 0.5 for the concrete having the cube strength, $f_{cu}$, more than 100 MPa. This recommendation by Ellobody and Young (2006a, 2006b) depends on the experimental study carried out by Giakoumelis and Lam (2004). The linear interpolation may be carried out to determine the concrete having the cube strength, $f_{cu}$, between 30 and 100 MPa.

The confined concrete was also identified as a material consisting of elastic and plastic region. In the ABAQUS, Drucker Prager yield criterion model was used to compute the plastic characteristics of the confined concrete which was the second and third zone of the sress-strain curve of the confined concrete. The shear criterion in Drucker Prager model was chosen as linear and flow potential eccentricity was selected as default value of 0.1. Furthermore, other three parameters in Drucker Prager model were the material angle of friction, the flow stress ratio of material, and dilation angle. The material angle of friction and the flow stress ratio in triaxial tension to that in compression were computed as 20 degrees and 0.8 regarding to recommendation by Hu et al. (2003) whereas the dilation angle was selected according to Damaraju (2013) as 30 degrees. In addition to Drucker Prager parameters, Drucker Prager Hardening was chosen as a suboption in order to accurately define the yield region of the confined concrete.

### 3.2.1.2 Interaction and Surface Identifications

In the modeling of each specimen, endplates, which were placed at the top and bottom of columns, were used in order to attain equal contractions. By this way, each specimen consisted of five components such as outer and inner steel tubes, concrete annulus between the tubes, and the top and bottom endplates as indicated in Figure 3.4. The surfaces of the components were used to identify the interactions. The surface-to-surface contact and Tie constraint available in ABAQUS CAE were employed to govern the bond between the specimen components. By using these methods, the surfaces should be firstly identified according to their characterizations namely it should be decided that which surface will penetrate to other. For this condition, in ABAQUS, the surfaces can be defined as master or slave. In this study, the steel tube surfaces were selected as master surface during the interaction with concrete whereas they were designated as slave surface when interacted with

endplates. The surfaces of endplates were treated as master surface while the surfaces of the concrete annulus were chosen as slave surface in all interactions with other components. Normal and Tangential behaviors were computed for the surface-to-surface contact properties. Pressure-Overclosure model with Hard Contact feature was used for Normal behavior whereas Penalty Friction model with friction coefficient of 0.4 and directionality of isotropic was applied for Tangential behavior. The surface-to-surface contact was designated to define the interactions between the surfaces of the steel tubes and the concrete annulus and also between the surfaces of the end plates and the concrete annulus. Tie constraint, however, was used to identify only the interactions between the steel tubes and endplates surfaces.

### 3.2.1.3 Finite Element Type and Mesh Selection

The components in this study were modeled with respect to the solid and shell shapes. The solid shaped components were sketched by using extrusion type while the shell shaped elements were drawn by using planar type. The outer and inner steel tubes and the concrete annulus between tubes were deformable solid shaped whereby the endplates were discrete rigid shell shaped. R3D3 element type with geometric order of linear was used for the endplates while C3D8 element type with reduced integration and geometric order of linear was used for the outer and inner steel tubes and the concrete annulus. The element shape for R3D3 and C3D8 were triangle and hexahedron, respectively. However, in despite of the outer steel tube being C3D8, the element shape was hexahedron-dominated in order to achieve representative meshing. The approximate global size of the mesh was 4 for the endplates. However, in order to achieve good meshing, the approximate global size of the mesh was between 20 and 24 for concrete annulus, 5 and 10 for inner and 24 and 32 for outer steel tubes. The representative meshing of each component is illustrated in Figure 3.4.

### 3.2.1.4 Boundary and Loading Conditions

There was a reference (RF) point in the top and bottom endplates in order to specify the centre of the plates and create a rigid body constraint. The boundary and loading were applied on the specimens from these RF points. Encastre type boundary condition in ABAQUS was used at the bottom endplates in order to obtain a fixed

support against all degrees of freedom. However, at the top plate on which the load was applied were unrestrained in the loading direction. The nodes remained in the specimen were free to displace or rotate in any direction. The static uniform loading by designating a displacement on RF point of top endplate was applied to each specimen. An example of boundary and loading condition on the CFDST column specimen with CHS is presented in Figure 3.5.
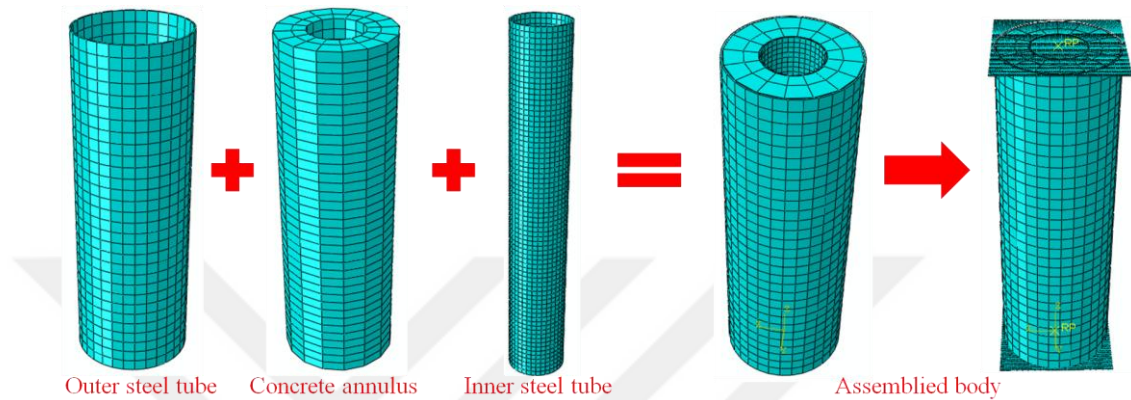


**Figure 3.4.** Typical meshing of CFDST columns with CHS



(a)                                                                 (b)
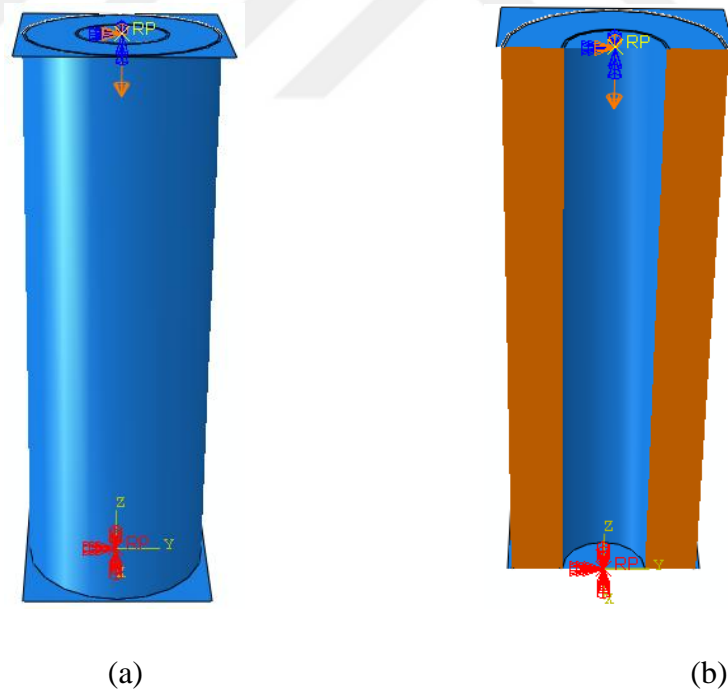
**Figure 3.5.** Boundary and loading conditions of typical CFDST column with CHS: (a) normal and (b) section views

However, for the samples that were anticipated to fail due to the buckling, the boundary condition at the bottom was fixed against 4 degrees of freedom ($u_x = u_y =$

$u_z = \theta_z = 0$). In other words the deformations in x, y, and z axes as well as rotation about z axis were restrained. Namely, the bottom plate of the model was allowed to rotate just about x and y axes. On the other hand, at the top plate on which the load was applied were allowed to deform in z direction and rotate about x and y axes. In other words, the deformations were inhibited in x and y direction and the rotation was forbidden about z axis at the top plate ($u_x = u_y = \theta_z = 0$). The loading was applied similar to aforementioned way.

### 3.2.2 Modeling by GEP

Software named as GeneXproTools.5.0 (GepSoft, 2018) was used in the derivation of a mathematical model based predictive equation. The data presented in Table 3.1 was used in the developing the model. As seen in Table 3.1, a total of eight crucial parameters, which are the yield strengths ($f_{syo}$, $f_{syi}$), diameters ($D_o$, $D_i$) and thicknesses ($t_o$, $t_i$) of the outer and inner steel tubes, the 28-day compressive strength of concrete ($f_c$), and the length of the specimen (L), were used in the producing the mathematical model. In the generation of the model, the steel tube yield strengths were used in the unit of megapascals (MPa) and the diameters, thicknesses, and the specimen length were in the unit of milimeter (mm). Besides, the 28-day concrete compressive strength tested on Ø150x300-mm cylindrical specimen with unit of MPa was used in the generation of the model. The concrete compressive strength given in these studies were carried out on different geometric and sized samples. Thereby, the compressive strengths measured on different geometric and sized samples were transformed from the given specimen geometry and size to Ø150x300-mm cylindrical specimens regarding conversion coefficients recommended by Ersoy et al. (2010).

After the concrete compressive strength conversion, the data source was arbitrarily divided into two groups as train and test sub-datasets. The train dataset was handled to employ for the enhancement of the developed model whereas the test dataset was used to observe the fitness, predictability, robustness and repeatability of the proposed mathematical model. The test dataset constitutes approximately 25% (26 data) of the total dataset. To observe the train and test datasets represent the whole data or not, both sub-datasets were also statistically analyzed and the results are given in Table 3.3. It can be obviously seen from the table that, there is a good

agreement between the train and test sub-datasets such that both sub-datasets represent the nearly same populations.

**Table 3.3.** Statistics of train and test sub-datasets used in modeling by GEP

| | $f_{syo}$ (MPa) | $D_o$ (mm) | $t_o$ (mm) | $f_{syi}$ (MPa) | $D_i$ (mm) | $t_i$ (mm) | $f_c$ (MPa) | L (mm) | $P_{u,exp}$ (kN) |
|---|---|---|---|---|---|---|---|---|---|
| **Train data** | | | | | | | | | |
| Number of data | 77 | 77 | 77 | 77 | 77 | 77 | 77 | 77 | 77 |
| Mean | 375 | 169.5 | 3.08 | 373.5 | 81.6 | 2.97 | 37.4 | 955.2 | 1642.9 |
| Standard deviation | 93.1 | 47.5 | 0.97 | 127.6 | 37.6 | 1.56 | 19.1 | 691.6 | 901.5 |
| COV | 0.25 | 0.28 | 0.31 | 0.34 | 0.46 | 0.52 | 0.52 | 0.72 | 0.55 |
| Min. value | 221 | 114 | 0.9 | 221 | 22.1 | 0.9 | 18.7 | 330 | 378.3 |
| Max. value | 549 | 350 | 6 | 1029 | 231 | 10.62 | 85 | 2503 | 5499 |
| **Test data** | | | | | | | | | |
| Number of data | 26 | 26 | 26 | 26 | 26 | 26 | 26 | 26 | 26 |
| Mean | 374.7 | 159.7 | 2.87 | 401.6 | 79.3 | 3.03 | 36.3 | 887.5 | 1504.9 |
| Standard deviation | 95.5 | 46.7 | 0.80 | 164.1 | 40.8 | 1.90 | 16.5 | 682.1 | 1019.3 |
| COV | 0.25 | 0.29 | 0.28 | 0.41 | 0.51 | 0.63 | 0.45 | 0.77 | 0.68 |
| Min. value | 221 | 114 | 0.9 | 221 | 32 | 0.9 | 18.7 | 330 | 578 |
| Max. value | 549 | 350 | 5 | 1029 | 231 | 10.76 | 77.6 | 2500 | 5396 |

In the developing of the mathematical model, several mathematical operations such as addition (+), substraction (-), multiplication (*), division (/), square root ($\sqrt{}$), exponential ($e^{\wedge}$), sine (*sin*), cosine (*cos*), and arctangent (*atan*) were used so as to increase the accuracy and reliability of the model as presented in Table 3.4. In addition to the function set, Table 3.4 also includes the number of generation as *499999* at which the model was achieved, the number of chromosomes as 140 and head size as *10* that were used in the generation of the model.

The number of genes and linking function of these genes were *8* and *addition* as presented in Table 3.4. Besides, the number of constant that was used in each gene and the upper and lower limits for these constants were given in Table 3.4. Both the mutation, which is equal to two point mutations per chromosome, and the inversion rates were also given in Table 3.4. In addition, the transposition rates and recombination rates were also tabulated in the table.

By using these properties, the model was generated with the coefficient of determination (R-squared) value of 0.987. The ETs of this predictive model is illustrated in Figure 3.6. In each ET, the green ballonets were used for the indication

of the input parameters whereas the blue and red ballonets were designated for the mathematical operations and the constants used in the genes, respectively.

**Table 3.4.** GEP parameters used in the proposed model

| | | |
|---|---|---|
| **P1** | Function set | +,-,*,/,Sqrt,Exp,Sin,Cos,Arctan |
| **P2** | Number of generation | 499999 |
| **P3** | Chromosomes | 140 |
| **P4** | Head size | 10 |
| **P5** | Number of genes | 8 |
| **P6** | Linking function | Addition |
| **P7** | Constants per gen | 5 |
| **P8** | Lower/Upper bound of constants | -50/60 |
| **P9** | Mutation rate | 0.00206 |
| **P10** | Inversion rate | 0.00546 |
| **P11** | IS transposition rate | 0.00546 |
| **P12** | RIS transposition rate | 0.00546 |
| **P13** | Gene transposition rate | 0.00277 |
| **P14** | One-point recombination rate | 0.00277 |
| **P15** | Two-point recombination rate | 0.00277 |
| **P16** | Gene recombination rate | 0.00277 |

Sub-ET 1



$c_1$ = - 47.4016208

(a)

68
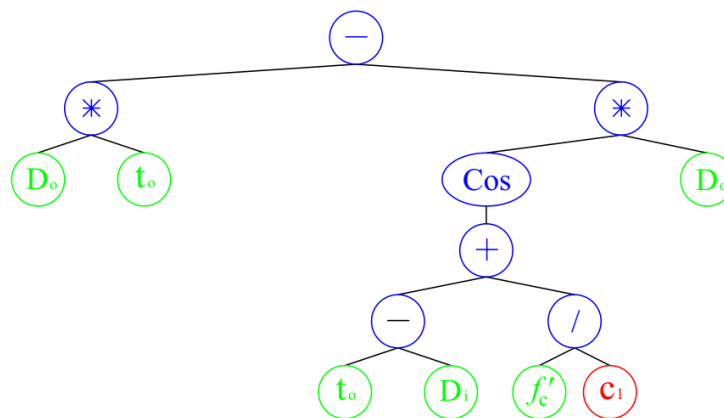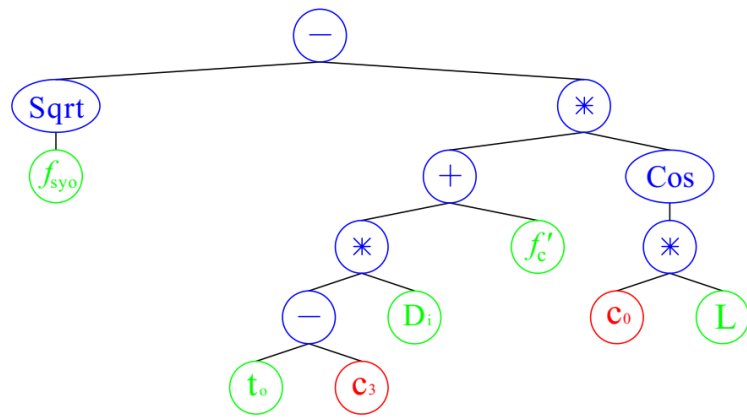
Sub-ET 2



$c_0 = 27.565796$    $c_3 = 1.9217768$

(b)

Sub-ET 3
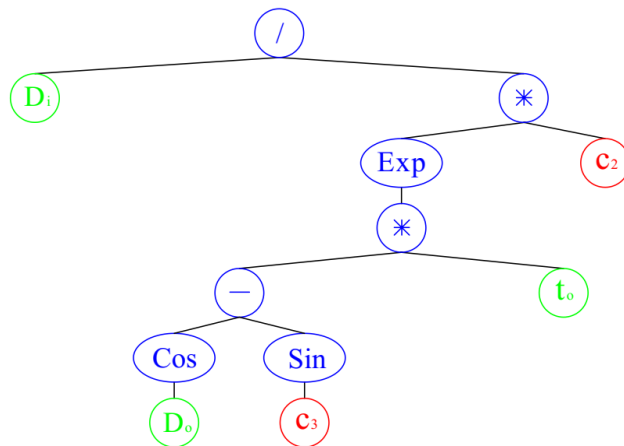


$c_2 = 18.452453$    $c_3 = 26.026295$

(c)

Sub-ET 4
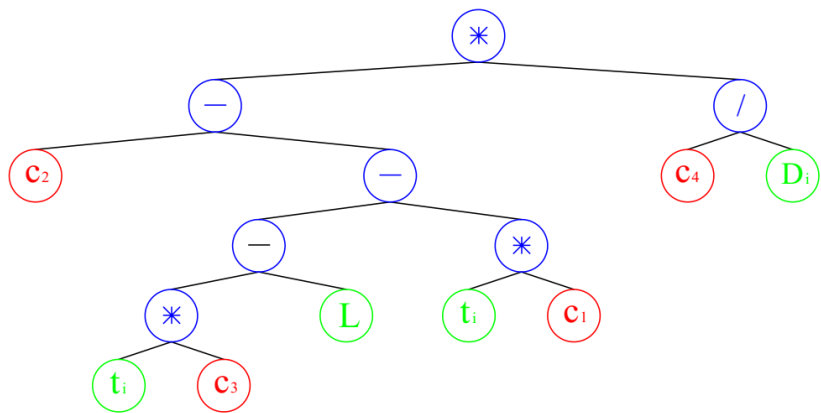


$c_1 = 47.6205805$    $c_2 = -20.245728$    $c_3 = -50.617881$    $c_4 = -25.1921737$

(d)

69

$c_3 = -0.470241$

(e)

(f)
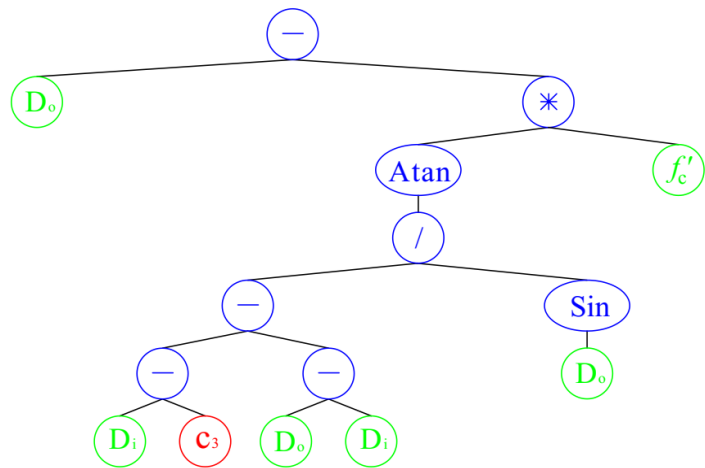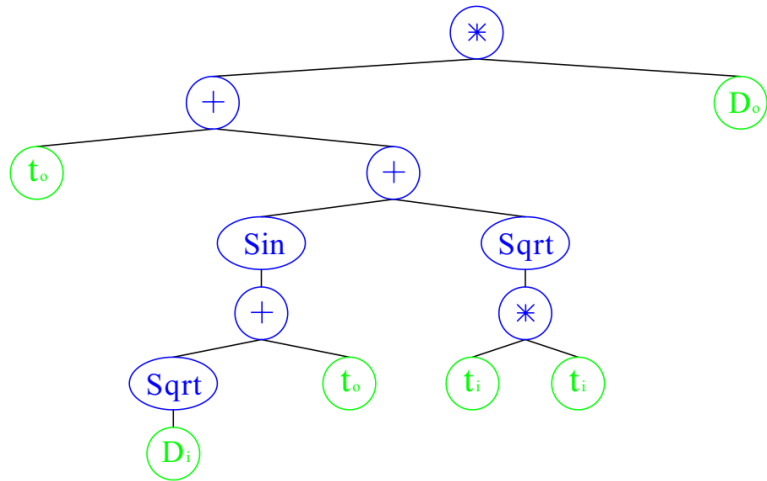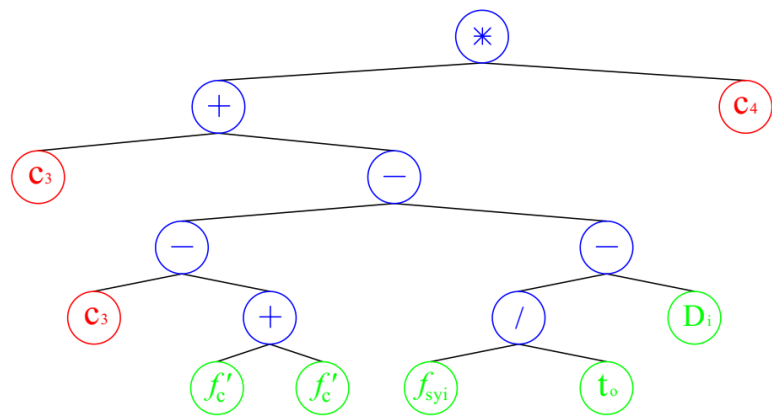
$c_3 = 33.8517421$    $c_4 = -1.5067511$

(g)

$C_1 = 38.175287$ $C_2 = 12.718897$ $C_3 = 52.9959407$
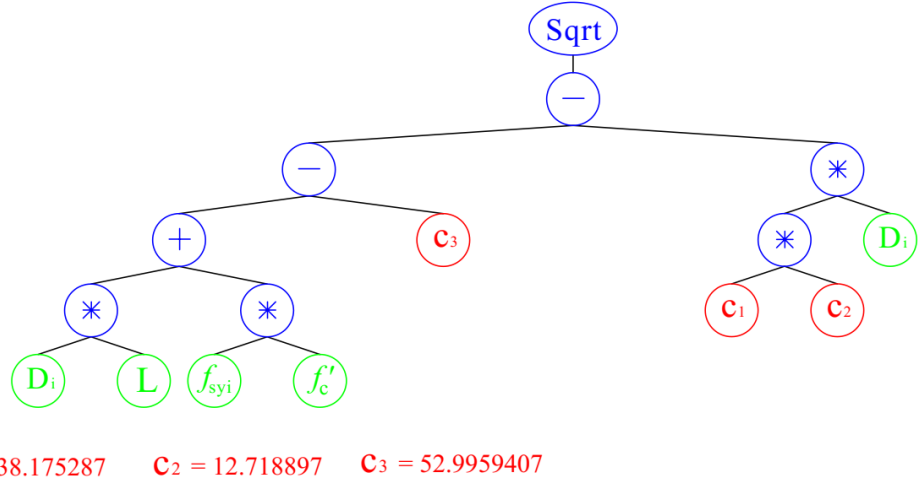
(h)

**Figure 3.6.** Expression trees for GEP model: (a) Function 1, (b) Function 2, (c) Function 3, (d) Function 4, (e) Function 5, (f) Function 6, (g) Function 7, and (h) Function 8

The equation attained from the ETs, which were employed to present the GEP model formulation, is given as follows.

$$(P_u)_{GEP} = P_1 + P_2 + P_3 + P_4 + P_5 + P_6 + P_7 + P_8 \tag{3.11}$$

where $(P_u)_{GEP}$ is the ultimate axial strength of the CFDST columns with CHS proposed by the help of GEP, and the functions from $P_1$ to $P_8$ are given as follows:

$$P_1 = D_o t_o - D_o \cos\left(t_o - D_i - \frac{f_c}{47.401621}\right) \tag{3.11a}$$

$$P_2 = \sqrt{f_{syo}} - [D_i(t_o - 1.9217768) + f_c]\cos(27.565796L) \tag{3.11b}$$

$$P_3 = \frac{D_i}{18.452453\, e^{t_o[\cos(D_o) - 0.779304]}} \tag{3.11c}$$

$$P_4 = (L + 98.2384615 t_i - 20.245728)\left(\frac{-25.1921737}{D_i}\right) \tag{3.11d}$$

$$P_5 = D_o - f_c \tan^{-1}\left(\frac{2D_i - D_o + 0.470241}{\sin(D_o)}\right) \tag{3.11e}$$

$$P_6 = D_o\left[t_o + t_i + \sin\left(\sqrt{D_i} + t_o\right)\right] \tag{3.11f}$$

$$P_7 = (-1.5067511)\left(D_i + 67.7034842 - 2f_c - \frac{f_{syi}}{t_o}\right) \tag{3.11g}$$

$$P_8 = \sqrt{D_i L + f_c f_{syi} - 52.9959407 - 485.5475433 D_i} \qquad (3.11h)$$

Some mathematical terms given in the expression tree were abbreviated in the formula presentation. As an example, $2f_c$ was used instead of writing $f_c + f_c$ in Sub-ET7 (Figure 3.8g). Although some input parameters can sometimes be neglected by software owing to their negligible influence on the entire model when the optimum model evaluation was trained for the best fitness, all input variables were used in the current study during the development of GEP model.

### 3.2.3 Modeling by ANN

MatlabV.R2017, which provides a neural-fuzzy tool (nf tool) and neural-network tool (nn tool) as a soft-computing tool, was used in the derivation of the model (MathWorks, 2018). The same data (given in Table 3.1) handled in the developing the GEP model was used in the derivation of the ANN model. The independent variables were the yield strengths ($f_{syo}$, $f_{syi}$), diameters ($D_o$, $D_i$) and thicknesses ($t_o$, $t_i$) of the outer and inner steel tubes, the 28-day compressive strength of concrete ($f_c$), and the length of the specimen (L). In the generation of the model, the steel tube yield strengths were used in the unit of megapascals (MPa) and the diameters, thicknesses, and the specimen length were in the unit of milimeter (mm). The concrete compressive strength conversion as in the derivation of the GEP model was done in the generation of the ANN model.

As in the GEP model generation, the training and test sub-datasets were constituted by randomly dividing of the data source. The data source was divided into two group as in the dividing objective of the GEP model. To observe the training and testing datasets represent the whole data or not, both sub-datasets were also statistically analyzed and the results are given in Table 3.5. It can be obviously seen from the table that, there is a good agreement between the train and test sub-datasets such that both sub-datasets reflect the nearly same populations.

In the ANN model generation, Bayesian Regularization back propagation algorithm was used in order to train the model. Besides, tangent hyperbolic was used as an activation function. The number of nodes in the input layer, hidden layer, and output layer was 8, 5, and 1, respectively. It was aimed to determine the ultimate axial

72

strength by the output layer. The neural network structure produced in this model according to aforementioned layers and nodes was demonstrated in Figure 3.7.

**Table 3.5.** Statistics of train and test sub-datasets used in modeling by ANN

| | $f_{syo}$ (MPa) | $D_o$ (mm) | $t_o$ (mm) | $f_{syi}$ (MPa) | $D_i$ (mm) | $t_i$ (mm) | $f_c'$ (MPa) | L (mm) | $P_{u,exp}$ (kN) |
|---|---|---|---|---|---|---|---|---|---|
| **Train data** | | | | | | | | | |
| Number of data | 77 | 77 | 77 | 77 | 77 | 77 | 77 | 77 | 77 |
| Mean | 378.0 | 165.5 | 3.02 | 379.5 | 78.0 | 2.97 | 36.2 | 943.4 | 1589.6 |
| Standard deviation | 94.4 | 45.0 | 0.96 | 134.0 | 35.6 | 1.71 | 17.8 | 690.7 | 890.0 |
| COV | 0.25 | 0.27 | 0.32 | 0.35 | 0.46 | 0.58 | 0.49 | 0.73 | 0.57 |
| Min. value | 221 | 114 | 0.9 | 221 | 22.1 | 0.90 | 18.7 | 330 | 378.3 |
| Max. value | 549 | 350 | 6 | 1029 | 231 | 10.76 | 85.0 | 2503 | 5499 |
| **Test data** | | | | | | | | | |
| Number of data | 26 | 26 | 26 | 26 | 26 | 26 | 26 | 26 | 26 |
| Mean | 366.1 | 171.7 | 3.04 | 383.9 | 89.9 | 3.03 | 39.7 | 922.5 | 1662.6 |
| Standard deviation | 90.9 | 53.9 | 0.85 | 149.9 | 44.9 | 1.42 | 20.3 | 687.0 | 1028.6 |
| COV | 0.25 | 0.31 | 0.28 | 0.39 | 0.50 | 0.47 | 0.51 | 0.74 | 0.62 |
| Min. value | 250 | 114 | 1.5 | 250 | 31.9 | 1.20 | 18.7 | 330 | 620 |
| Max. value | 549 | 350 | 5 | 1029 | 231 | 7.63 | 85.0 | 2500 | 5396 |
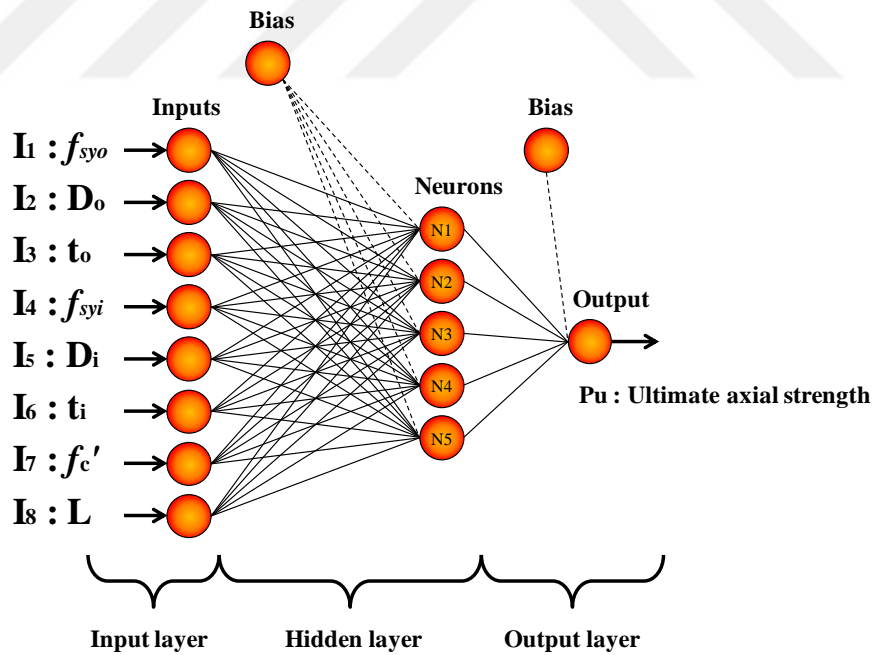


**Figure 3.7.** Structure of proposed ANN model

The bias values are used in the model to better fitting the output data by altering the activation data to the right or left because of no any interaction between the bias value and the actual input data as given in Equation 3.12. Besides, the mathematical

demonstration of Figure 3.7 was given in Equation 3.13 by using the generalized algebraic matrix operation.

$$P_k = \sum_{j=1}^{n} w_{j,k} I_j + Bias_k \tag{3.12}$$

$$P_k = \begin{bmatrix} w_{11} & w_{12} & . & . & . & w_{1n} \\ w_{21} & . & & & & . \\ . & & . & & & . \\ . & & & . & & . \\ . & & & & . & . \\ w_{m1} & . & . & . & . & w_{mn} \end{bmatrix}_{mxn} \begin{bmatrix} I_1 \\ I_2 \\ . \\ . \\ . \\ I_n \end{bmatrix}_{nx1} + \begin{bmatrix} Bias_1 \\ Bias_2 \\ . \\ . \\ . \\ Bias_m \end{bmatrix}_{mx1} = \begin{bmatrix} P_1 \\ P_2 \\ . \\ . \\ . \\ P_m \end{bmatrix}_{mx1} \tag{3.13}$$

In order to predict the results, nf tool operates the processes of model generation by using normalized values that are between -1 and 1. For this reason, Equation 3.14 was used in the calculation of the normalized values of the input parameters. After the generation of the model, nf tool provides the results again in the normalized form. Therefore, to achieve the non-normalized results, m and n coefficients used in the calculation of the normalized values were utilized to de-normalize the results. By using the maximum and minimum values of the each input parameter, m and n coefficients for each one were determined.

$$\beta_{normalized} = m\beta + n \tag{3.14}$$

where;

$\beta$ is the actual value of the input or output parameters

$\beta_{normalized}$ is the normalized value of the input or output parameters vary between -1 and 1

$m$ and $n$ are the coefficients of normalization

The following expressions are used to determine the coefficients of normalization, m and n.

$$m = \frac{2}{\beta_{max} - \beta_{min}} \tag{3.14a}$$

$$n = -\frac{\beta_{max} + \beta_{min}}{\beta_{max} - \beta_{min}} \tag{3.14b}$$

74

where;

$\beta_{\max}$ is the maximum actual value of the input and output parameters

$\beta_{\min}$ is the minimum actual value of the input and output parameters

By using the normalization parameters, the highest numeric value becomes 1 while the lowest value becomes -1. The maximum and minimum actual values and the coefficients of normalization for input and output parameters are given in Table 3.6.

The simplified equation of the model proposed by the ANN and its structural formula are given by Equations 3.15 and 3.16, respectively.

$$(P_u)_{ANN} = Bias_{output\ layer} + \sum_{k=1}^{m} W_k f(U_k) \qquad (3.15)$$

$$(P_u)_{ANN} = 1.2504 + 1.0321\tanh(P_1) - 0.28765\tanh(P_2) + 0.24148\tanh(P_3) - 1.281\tanh(P_4) + 0.50319\tanh(P_5) \qquad (3.16)$$

where;

$Bias_{output\ layer}$ is 1.2504 for the ANN model proposed in this thesis

$P_1$, $P_2$, $P_3$, $P_4$, and $P_5$ are the output parameters, which are in the normalized form

*tanh* is the tangent hyperbolic used as activation function

**Table 3.6.** Normalization coefficients for database

| Input and output variables | Normalization parameters | | | |
|---|---|---|---|---|
| | $\beta_{max}$ | $\beta_{min}$ | $m$ | $n$ |
| $f_{syo}$ (MPa) | 549 | 221 | 0.006098 | - 2.34756 |
| $D_o$ (mm) | 350 | 114 | 0.008475 | - 1.9661 |
| $t_o$ (mm) | 6.0 | 0.9 | 0.392157 | - 1.35294 |
| $f_{syi}$ (MPa) | 1029 | 221 | 0.002475 | - 1.54703 |
| $D_i$ (mm) | 231.0 | 22.1 | 0.009574 | - 1.21158 |
| $t_i$ (mm) | 10.76 | 0.90 | 0.20284 | - 1.18256 |
| $f_c'$ (MPa) | 85.0 | 18.7 | 0.030166 | - 1.5641 |
| L (mm) | 2503 | 330 | 0.00092 | - 1.30373 |
| $P_{u,exp}$ (kN) | 5499.0 | 378.3 | 0.000391 | - 1.14775 |

The following algebraic matrix (Equation 3.17) and the expression (Equation 3.18) are used to calculate the output parameters and the tangent hyperbolic value, respectively.

$$\begin{bmatrix} 0.59019 & 2.7882 & -4.904 & -0.37728 & 3.4189 & 0.11149 & 1.6412 & 2.4088 \\ 1.9187 & -2.3882 & -0.51551 & 1.6955 & 0.97003 & -1.1306 & -3.9182 & -0.92553 \\ 0.3469 & 2.5879 & -0.02123 & 6.138 & -0.72143 & 2.2498 & -0.59073 & -0.22808 \\ -0.0234 & -0.58639 & -0.54234 & -0.13114 & 0.80317 & -0.53623 & 0.35448 & 0.14106 \\ 0.44102 & -0.85343 & -0.79207 & -0.46916 & 3.1564 & -1.8282 & 0.31751 & 0.016073 \end{bmatrix} \begin{bmatrix} f_{syo} \\ D_o \\ t_o \\ f_{syi} \\ D_i \\ t_i \\ f_c^{'} \\ L \end{bmatrix} + \begin{bmatrix} -4.3746 \\ -0.24361 \\ 5.9176 \\ 0.64673 \\ 1.0156 \end{bmatrix} = \begin{bmatrix} P_1 \\ P_2 \\ P_3 \\ P_4 \\ P_5 \end{bmatrix} \quad (3.17)$$

$$\tanh(x) = \frac{2}{1-e^{-2x}} - 1 \qquad (3.18)$$

As a result, $(P_u)_{ANN}$ values calculated according to Equation 3.16 are in the normalized form that requires to be de-normalized by using Equation 3.14 and coefficients of normalization tabulated in Table 3.6.

## 3.3 The Statistical Evaluation

The statistical examination of the developed models in this thesis were carried out on behalf of the mean absolute percent error (MAPE), mean square error (MSE), root mean square error (RMSE), coefficient of variation (COV), and coefficient of determination (R-squared) values which were calculated according to following equations:

$$MAPE = \frac{1}{n}\sum_{i=1}^{n}\left|\frac{m_i-p_i}{m_i}\right| x100 \qquad (3.19)$$

$$MSE = \frac{\sum_{i=1}^{n}(m_i-p_i)^2}{n} \qquad (3.20)$$

$$RMSE = \sqrt{\frac{\sum_{i=1}^{n}(m_i-p_i)^2}{n}} \qquad (3.21)$$

$$COV = \frac{SD}{\bar{X}} \qquad (3.22)$$

$$R-squared = \left(\frac{\sum(m_i-m)(p_i-p)}{\sqrt{\sum(m_i-m)^2 \sum(p_i-p)^2}}\right)^2 \qquad (3.23)$$

where;

m is the value of the measured ($m_i$) values

p is the value of the predicted ($p_i$) values

SD is the standard deviation

$\bar{X}$ is the mean value

# CHAPTER 4

# RESULTS AND DISCUSSIONS

The detailed comparisons of the generated models with the formulas modified from the codes and the existing models proposed by other researchers as well as experimental test results are submitted and discussed in this section. The results and discussions achieved from the comparative assessments were also evaluated statistically in terms of the mean absolute percent error (MAPE), mean square error (MSE), root mean square error (RMSE), coefficient of variation (COV), and coefficient of determination (R-squared) values, which were calculated by using Equations 3.19, 3.20, 3.21, 3.22, and 3.23, respectively.

In order to clearly comprehend the prediction capability of the models, the generated models by the finite element method (FEM), the gene expression programming (GEP), and the artificial neural network (ANN) were individually compared with the experimental test results, the formulas modified from the codes, and the existing models proposed by other researchers. Immediately after, the models were compared and evaluated among each other.

## 4.1 Finite Element Method (FEM) Model Results

The concrete filled double skin steel tubular (CFDST) columns with circular hollow section (CHS) were modeled by using the FEM in order to predict the ultimate axial strength values and simulate the behavior under axially loading. The ultimate axial strength values attained from the FEM are tabulated in Table 4.1 including also the experimental test results. The normalized ultimate axial strength values of the FEM model, which were calculated by dividing the experimental strength to the predicted strength given in Table 4.1, are also presented in Figure 4.1 in order to reveal how the normalized values are dispersed on the normalization line.

77

**Table 4.1.** Ultimate axial strength values of experiment and FEM prediction

| Sample | | | Experimental ultimate axial strength $(P_u)_{exp}$, kN | Predicted ultimate axial strength $(P_u)_{FEM}$, kN |
|---|---|---|---|---|
| Reference | Number | Identification | | |
| Zhao et al. (2002a) | 1 | C1C7 | 1415.0 | 1443.0 |
| | 2 | C2C7 | 1380.0 | 1326.0 |
| | 3 | C3C7 | 1210.0 | 1313.0 |
| | 4 | C4C7 | 1110.0 | 1235.0 |
| | 5 | C5C8 | 1705.0 | 1961.0 |
| | 6 | C6C8 | 1605.0 | 1811.0 |
| Lin and Tsai (2003) | 7 | DS-06-2-2-C | 2311.0 | 1838.0 |
| | 8 | DS-06-4-2-C | 2750.0 | 2400.0 |
| Tao et al. (2004) | 9 | cc2a | 1790.0 | 1436.0 |
| | 10 | cc2b | 1791.0 | 1436.0 |
| | 11 | cc3a | 1648.0 | 1425.0 |
| | 12 | cc3b | 1650.0 | 1425.0 |
| | 13 | cc4a | 1435.0 | 1413.0 |
| | 14 | cc4b | 1358.0 | 1413.0 |
| | 15 | cc5a | 904.0 | 835.7 |
| | 16 | cc5b | 898.0 | 835.7 |
| | 17 | cc6a | 2421.0 | 2086.0 |
| | 18 | cc6b | 2460.0 | 2086.0 |
| | 19 | cc7a | 3331.0 | 2871.0 |
| | 20 | cc7b | 3266.0 | 2871.0 |
| | 21 | pcc2-1a | 620.0 | 709.8 |
| | 22 | pcc2-1b | 595.0 | 709.8 |
| Lu et al. (2010b) | 23 | C2-C4-SCC1-Ref | 3333.0 | 3424.0 |
| Uenaka et al. (2010) | 24 | c10-375 | 635.0 | 558.5 |
| | 25 | c10-750 | 540.0 | 516.6 |
| | 26 | c10-1125 | 378.3 | 334.5 |
| | 27 | c16-375 | 851.6 | 774.6 |
| | 28 | c16-750 | 728.1 | 658.6 |
| | 29 | c16-1125 | 589.0 | 594.8 |
| | 30 | c23-375 | 968.2 | 884.2 |
| | 31 | c23-750 | 879.1 | 790.6 |
| | 32 | c23-1125 | 703.6 | 753.0 |
| Zhao et al. (2010) | 33 | O1I1-S | 1665.0 | 1837.0 |
| | 34 | O2I1-S | 1441.0 | 1543.0 |

**Table 4.1.** (cont'd) Ultimate axial strength values of experiment and FEM prediction

| | Sample | | Experimental ultimate axial strength $(P_u)_{exp}$, kN | Predicted ultimate axial strength $(P_u)_{FEM}$, kN |
|---|---|---|---|---|
| Reference | Number | Identification | | |
| Zhao et al. (2010) | 35 | O3I1-S | 1243.0 | 1376.0 |
| | 36 | O4I1-S | 1145.0 | 1232.0 |
| | 37 | O5I2-S | 1629.0 | 1905.0 |
| | 38 | O6I2-S | 1613.0 | 1715.0 |
| | 39 | O7I2-S | 1487.0 | 1519.0 |
| | 40 | O8I2-S | 1328.0 | 1320.0 |
| | 41 | O9I2-S | 1236.0 | 1368.0 |
| Han et al. (2011a) | 42 | DCc-0 | 578.0 | 638.1 |
| | 43 | DCc-1 | 789.0 | 796.0 |
| | 44 | DCc-2 | 715.0 | 796.0 |
| Han et al. (2011b) | 45 | C1-1 | 2537.0 | 2324.0 |
| | 46 | C1-2 | 2566.0 | 2324.0 |
| | 47 | C2-1 | 3436.0 | 2865.0 |
| | 48 | C2-2 | 3506.0 | 2865.0 |
| Dong and Ho (2012) | 49 | D50-5-0 | 2852.0 | 2669.0 |
| Li et al. (2012) | 50 | C1-1 | 5499.0 | 4982.0 |
| | 51 | C1-2 | 5396.0 | 4982.0 |
| Dong and Ho (2013) | 52 | D-A-50-0 | 2865.0 | 2856.0 |
| | 53 | D-B-50-0 | 2674.0 | 2648.0 |
| | 54 | D-A-85-0 | 3218 | 3484.0 |
| | 55 | D-B-85-0 | 2994 | 3077.0 |
| Wang et al. (2014) | 56 | 0HA0 | 980.0 | 820.9 |
| | 57 | 0HB0 | 715.0 | 786.0 |
| Essopjee and Dundu (2015) | 58 | S139.2-1.0 | 1059.2 | 1042.0 |
| | 59 | S139.2-1.0 | 1056.1 | 1041.0 |
| | 60 | S139.2-1.5 | 905.5 | 887.4 |
| | 61 | S139.2-1.5 | 901.6 | 887.3 |
| | 62 | S139.2-2.0 | 831.7 | 826.7 |
| | 63 | S139.2-2.0 | 837.4 | 826.9 |
| | 64 | S139.2-2.5 | 732.1 | 699.4 |
| | 65 | S139.2-2.5 | 729.0 | 699.8 |
| | 66 | S152.4-1.0 | 1263.5 | 1388.0 |
| | 67 | S152.4-1.0 | 1254.9 | 1388.0 |
| | 68 | S152.4-1.5 | 1195.6 | 1251.0 |

**Table 4.1.** (cont'd) Ultimate axial strength values of experiment and FEM prediction

| Sample | | | Experimental ultimate axial strength $(P_u)_{exp}$, kN | Predicted ultimate axial strength $(P_u)_{FEM}$, kN |
|---|---|---|---|---|
| Reference | Number | Identification | | |
| Essopjee and Dundu (2015) | 69 | S152.4-1.5 | 1191.2 | 1250.0 |
| | 70 | S152.4-2.0 | 1047.3 | 1212.0 |
| | 71 | S152.4-2.0 | 1041.6 | 1212.0 |
| | 72 | S152.4-2.5 | 941.4 | 1075.0 |
| | 73 | S152.4-2.5 | 949.0 | 1075.0 |
| | 74 | S165.1-1.0 | 1512.3 | 1472.0 |
| | 75 | S165.1-1.0 | 1510.6 | 1472.0 |
| | 76 | S165.1-1.5 | 1286.4 | 1364.0 |
| | 77 | S165.1-1.5 | 1275.1 | 1365.0 |
| | 78 | S165.1-2.0 | 1187.2 | 1245.0 |
| | 79 | S165.1-2.0 | 1199.8 | 1246.0 |
| | 80 | S165.1-2.5 | 1028.0 | 1100.0 |
| | 81 | S165.1-2.5 | 1036.5 | 1099.0 |
| | 82 | S193.7-1.0 | 2010.0 | 1779.0 |
| | 83 | S193.7-1.0 | 2030.0 | 1779.0 |
| | 84 | S193.7-1.5 | 1730.0 | 1641.0 |
| | 85 | S193.7-1.5 | 1720.0 | 1641.0 |
| | 86 | S193.7-2.0 | 1581.6 | 1611.0 |
| | 87 | S193.7-2.0 | 1584.1 | 1610.0 |
| | 88 | S193.7-2.5 | 1451.4 | 1551.0 |
| | 89 | S193.7-2.5 | 1458.7 | 1552.0 |
| Abbas et al. (2016) | 90 | CB2-40NG-AB-CP | 1805.0 | 2001.0 |
| Wang et al. (2016) | 91 | HC22X4-C40 | 1450.0 | 1283.0 |
| | 92 | HC32X6-C40 | 1562.0 | 1366.0 |
| | 93 | HC38X8-C40 | 1838.4 | 1541.0 |
| | 94 | HC55X11-C40 | 2724.0 | 2024.0 |
| | 95 | HC89X4-C40 | 2024.9 | 1793.0 |
| | 96 | HC22X4-C80 | 1845.1 | 1717.0 |
| | 97 | HC32X6-C80 | 2012.5 | 1815.0 |
| | 98 | HC38X8-C80 | 2083.4 | 1838.0 |
| | 99 | HC55X11-C80 | 2775.0 | 2548.0 |
| | 100 | HC89X4-C80 | 2107.4 | 2165.0 |
| Hastemoğlu (2017) | 101 | DSCFT 3 | 807.0 | 823.4 |
| | 102 | DSCFT 4 | 810.0 | 849.9 |
| | 103 | DSCFT 5 | 877.0 | 860.5 |
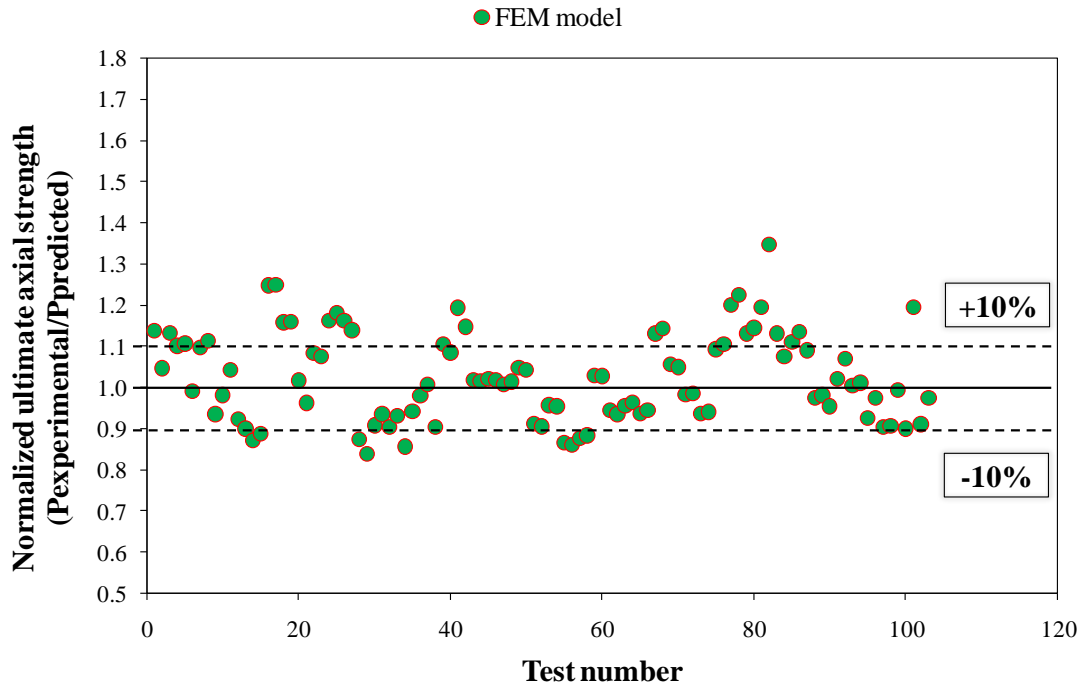
**Figure 4.1.** Prediction performance of FEM model based on normalized ultimate axial strength values

Figure 4.1 demonstrates the estimation capability of the FEM model with respect to chosen ±10% normalization limits. The normalized ultimate axial strength values are well scattered between the designated normalization limit lines. However, in some cases, the model has the underestimated ultimate axial strength values which can be easily understood from the interspersion of the normalized values above the upper normalization limit of +10%. Yet, when the number of normalized ultimate axial strength falling to the out of normalization limit lines is compared with that remaining between these lines, it would be overtly seen that the number of normalized ultimate axial strength falling in the normalization limit lines are much more than that falling to the out of these lines.

### 4.1.1 Comparison of FEM Model with Element Properties

In order to indicate how the prediction performance of FEM model varies with respect to the mechanical properties of elements, the ultimate axial strengths extrapolated by applying the FEM model are shown in Figure 4.2a, 4.2b, and 4.2c according to the yield strength of outer/inner steel tubes and compressive strength of concrete annulus, respectively. The yield strengths are approximately between 200 and 600 MPa for outer steel tube and 200 and 1050 MPa for inner steel tube. When

Figures 4.2a and 4.2b are examined, it could be obviously seen that the model generated by FEM has a good prediction performance for each yield strength value. The same estimation capability of model could be also seen in Figure 4.2c, which given for the concrete compressive strength. It can be certainly stated that the proposed FEM model has a good prediction capability whatever the strengths of elements are.



(a)



(b)
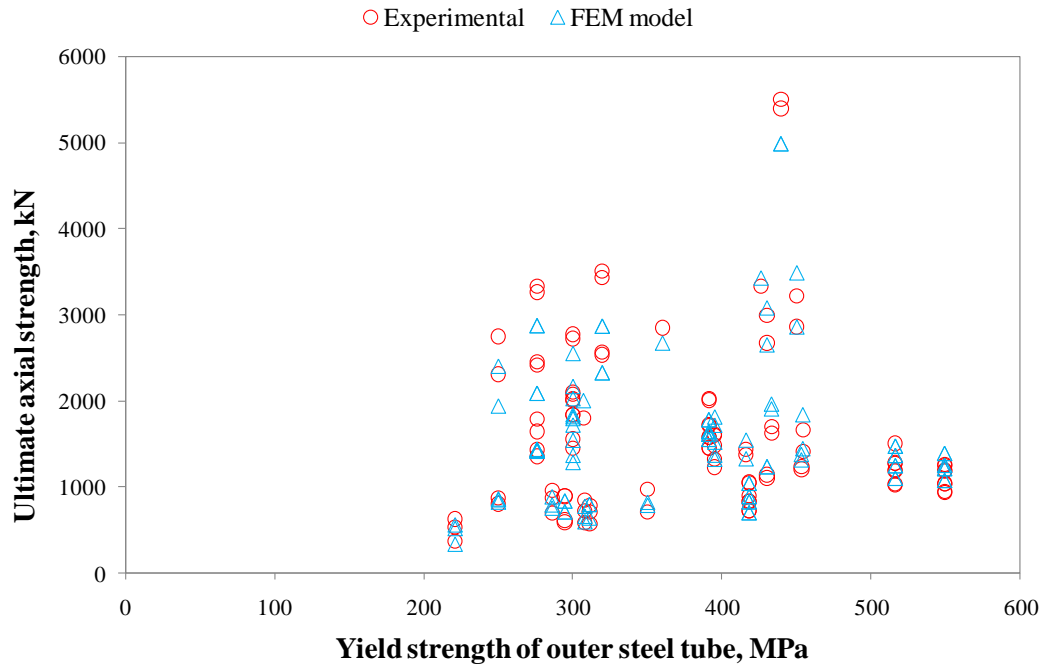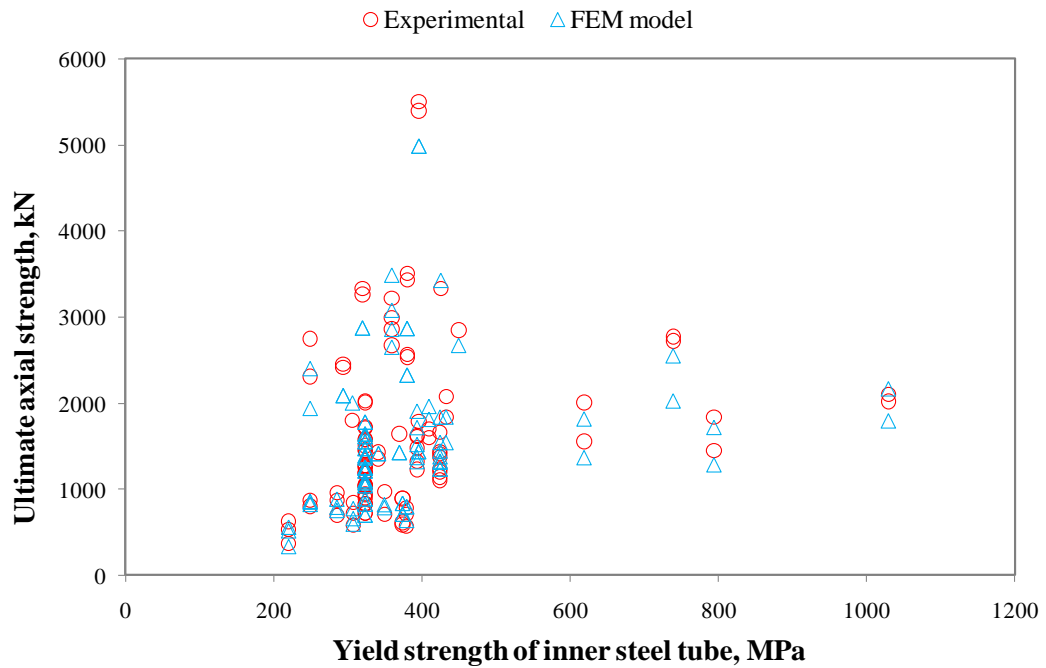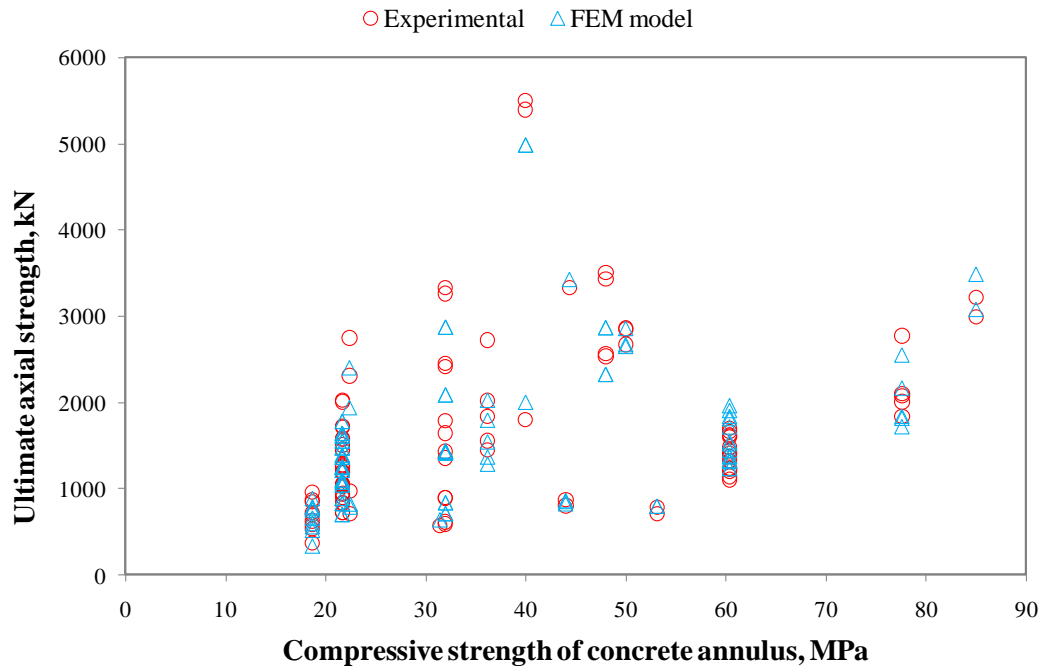
**Figure 4.2.** Experimental and FEM prediction ultimate axial strengths versus: (a) yield strength of outer steel tube, (b) yield strength of inner steel tube, and (c) compressive strength of concrete annulus

As well, the cross-sectional areas of the outer/inner steel tubes and concrete annulus have remarkable influences on the load carrying capacity of the CFDST columns with CHS as much as the yield strength of steel tubes and compressive strength of concrete. Therefore, the graphical comparison of the actual and predicted ultimate axial strength values versus the cross-sectional area of the outer steel tube, the inner steel tube, and the concrete annulus are illustrated in Figure 4.3a, 4.3b, and 4.3c, respectively.

The graphical presentation revealed that there is a relative relation between the ultimate axial strength of the CFDST columns and cross-sectional area of materials. Especially, increasing the cross-sectional area of the steel tubes has trend to increase the ultimate axial strength of the columns. But the same does not remarkably occur by the increasing in the cross-sectional area of concrete annulus, namely this tendency to increase the load carrying capacity by increasing the concrete cross-sectional area remains weak. This increasing of the ultimate axial strength by the increment of cross-sectional area can be observed in both experimental and predicted results, which means the model shows similar trend with the experimental.
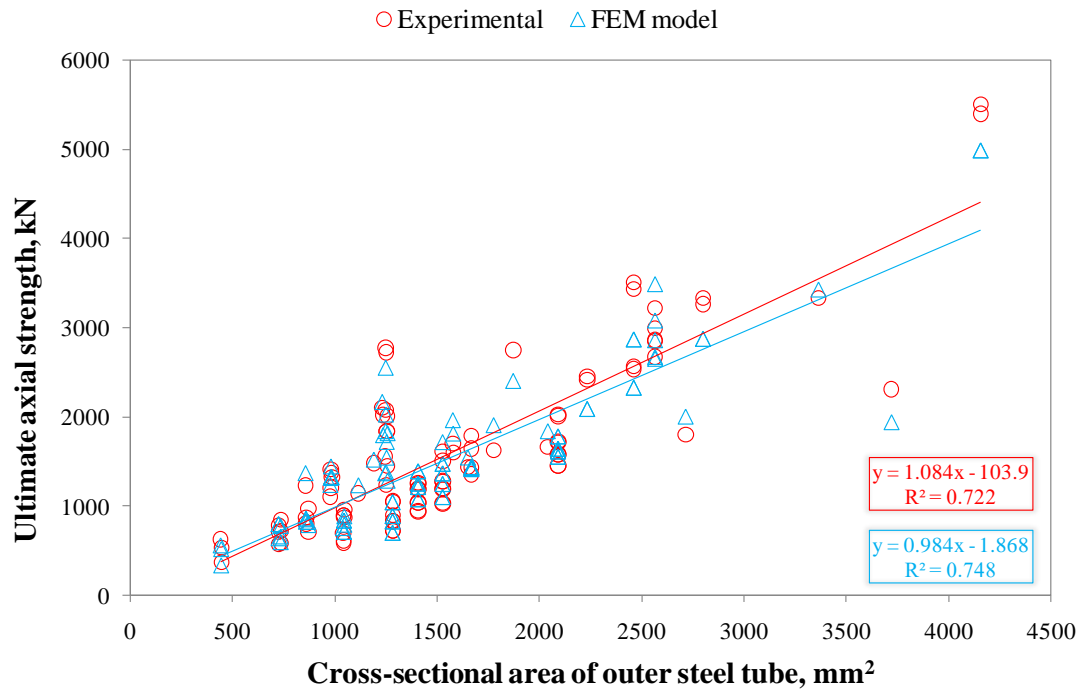
(a)
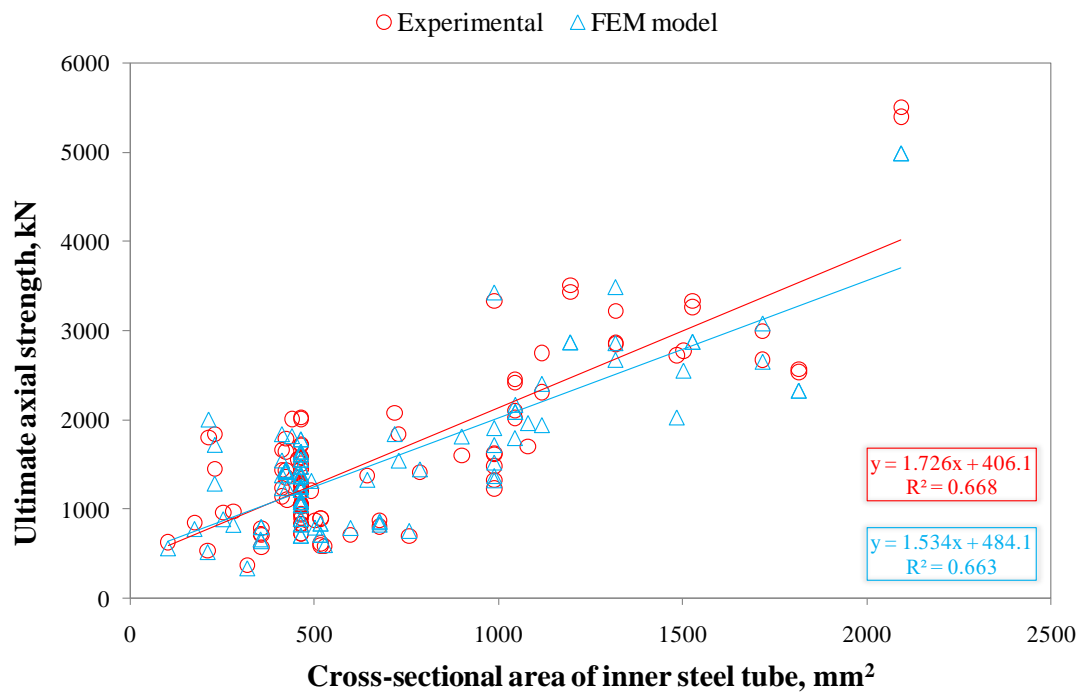


(b)
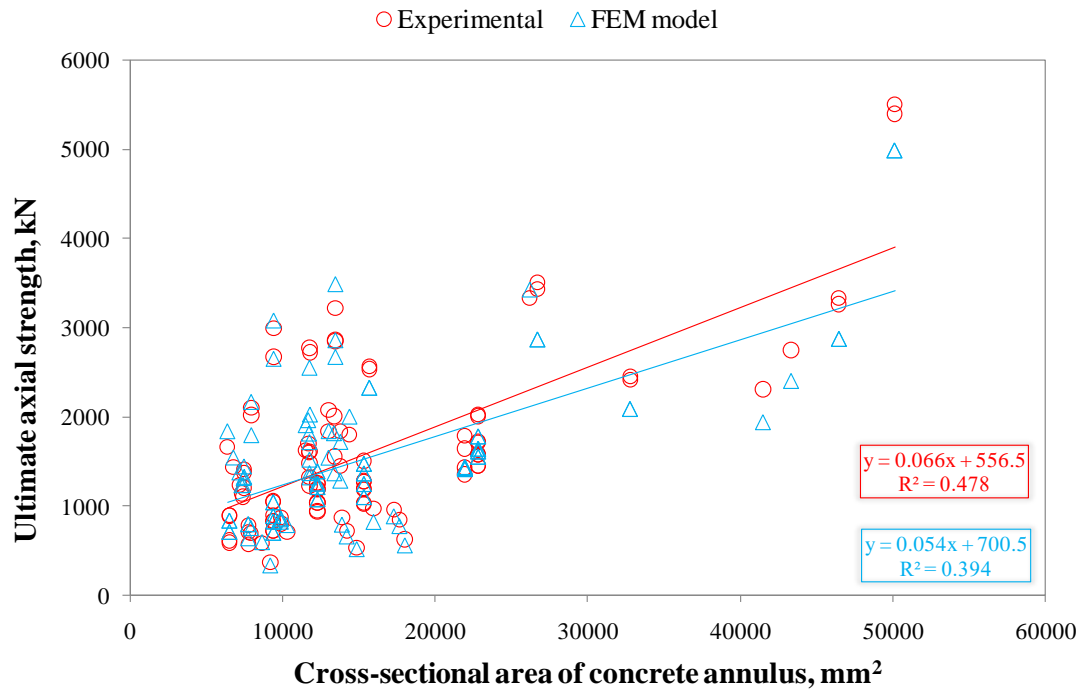
(c)

**Figure 4.3.** Experimental and FEM prediction ultimate axial strengths versus cross-sectional area of: (a) outer steel tube, (b) inner steel tube, and (c) concrete annulus

In Figure 4.3, R-squared values are also presented to exhibit the relation between the ultimate axial strength and cross-sectional areas. The R-squared values between the experimental ultimate axial strength and the cross-sectional area of the materials are close to R-squared values between the predicted ultimate axial strength and the cross-sectional area of the materials. According to this information, it can be overtly articulated that the proposed FEM model has a good prediction performance.

Although the load carrying capacity of the CFDST columns are significantly determined by the mechanical properties of the used materials and their cross-sectional areas, the length and diameter of elements used in the preparation of specimen as well as the amount of hollow part have also important influences on the ultimate axial strength of these columns. Because of that, Figures 4.4a, 4.4b, and 4.4c are presented to comprehend the effect of these parameters and how the proposed FEM model results vary according to the changing in these parameters. While Figures 4.4a and 4.4b illustrate the relation between the ultimate axial strength and length-to-outer steel tube diameter ratio and outer steel diameter-to-outer steel

85

thickness, respectively, Figure 4.4c demonstrates the relation between ultimate axial strength and hollow ratio.
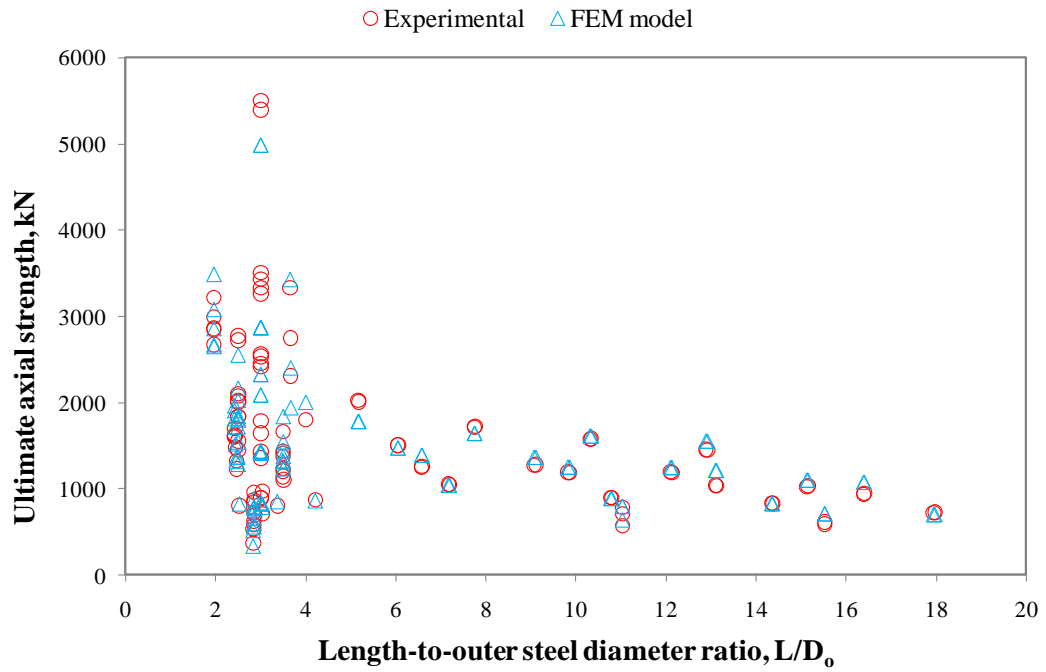


(a)
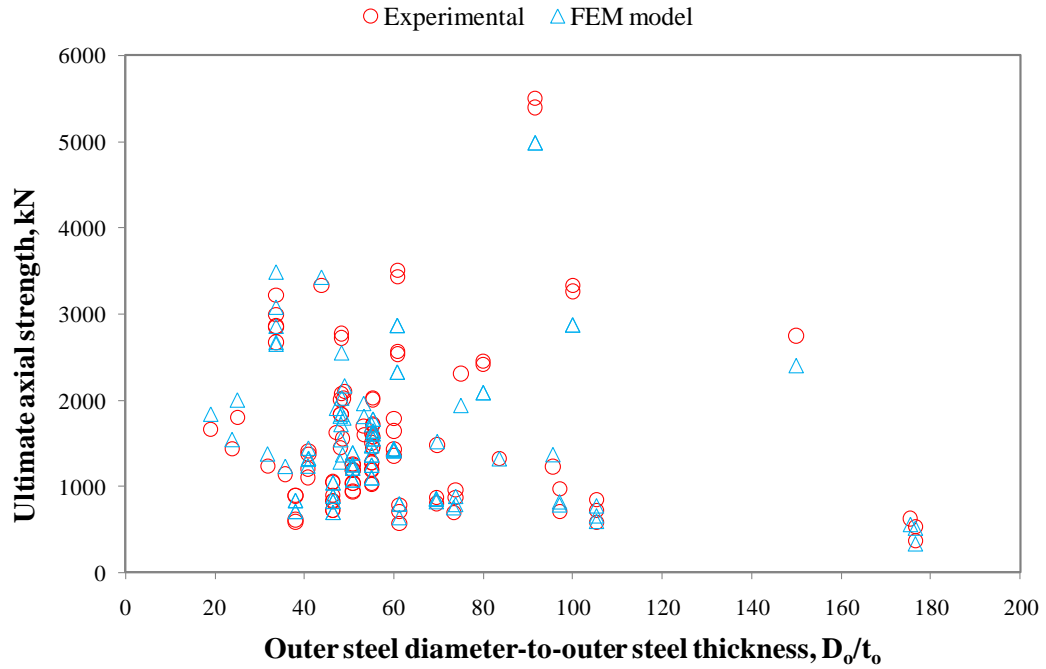


(b)
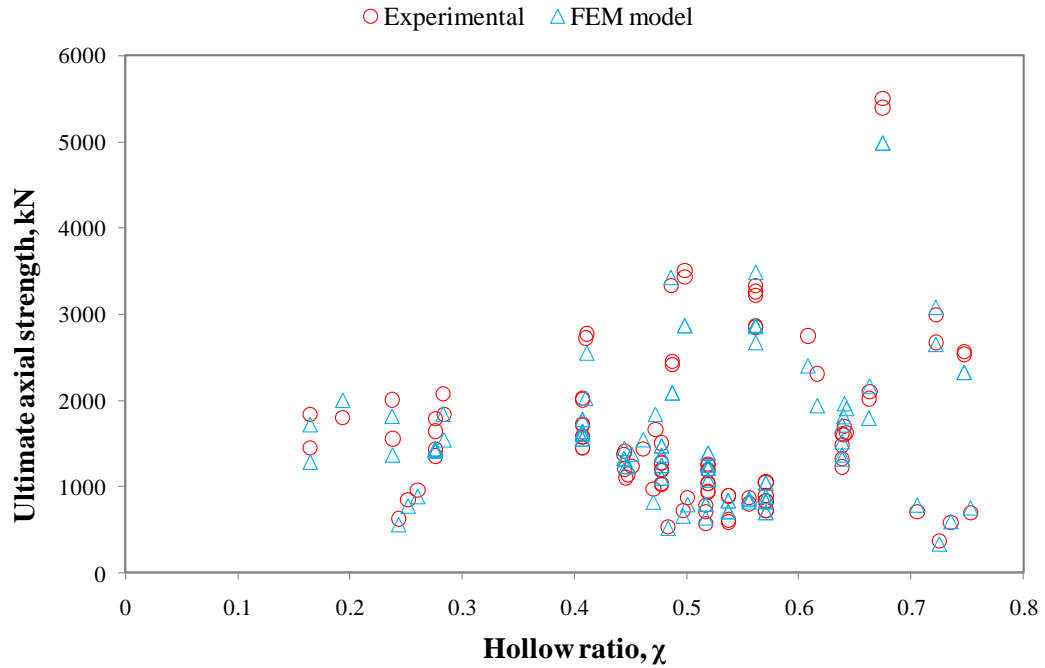
(c)

**Figure 4.4.** Experimental and FEM prediction ultimate axial strengths versus: (a) length-to-outer steel tube ratio ($L/D_o$), (b) outer steel diameter-to-outer steel thickness ($D_o/t_o$), and (c) hollow ratio ($\chi$)

Figure 4.4a indicates that the column specimen used in this thesis has the $L/D_o$ values ranging approximately between 2 and 18. The great amount of the specimens has the $L/D_o$ value ranging between 2 and 3.8 and this type of specimens are known as stub columns. While the specimens having the $L/D_o$ value varying between 2 and 3.8 have the various load carrying capacity values, the specimens with the $L/D_o$ value greater than 3.8 have the ultimate axial strength values approximately less than 2000 kN. It can be also stated that the FEM model predicts the ultimate axial strength with similar trend observed in the experimental results.

Besides, the results reveal that the proposed model can predict the ultimate axial strength within a large scale of $L/D_o$. The prediction performance of the model can be obviously seen when Figures 4.4b and 4.4c are also examined. The model generated in this study by using FEM is not affected from the sectional and geometric properties of the members utilized in the construction of the specimen. As a result, the findings demonstrate that the proposed FEM model has general prediction capableness.

### 4.1.2 Comparison of FEM Model with Experimental Results

In addition to the ultimate axial strength, the software used in the generation of the FEM model also provides displacement and corresponding strain as well on the specimen arisen by loading. In addition to all these, the deformed shape of the specimen can be simulated as well by the software. In order to reveal the robustness and correctitude of the proposed FEM model, the load, displacement, and strain results attained from the analyzing by software are also compared with the experimental results. The load versus displacement curve achieved from the experimental test conducted by Zhao et al. (2002a) is compared with that was obtained from the FEM model in Figure 4.5.
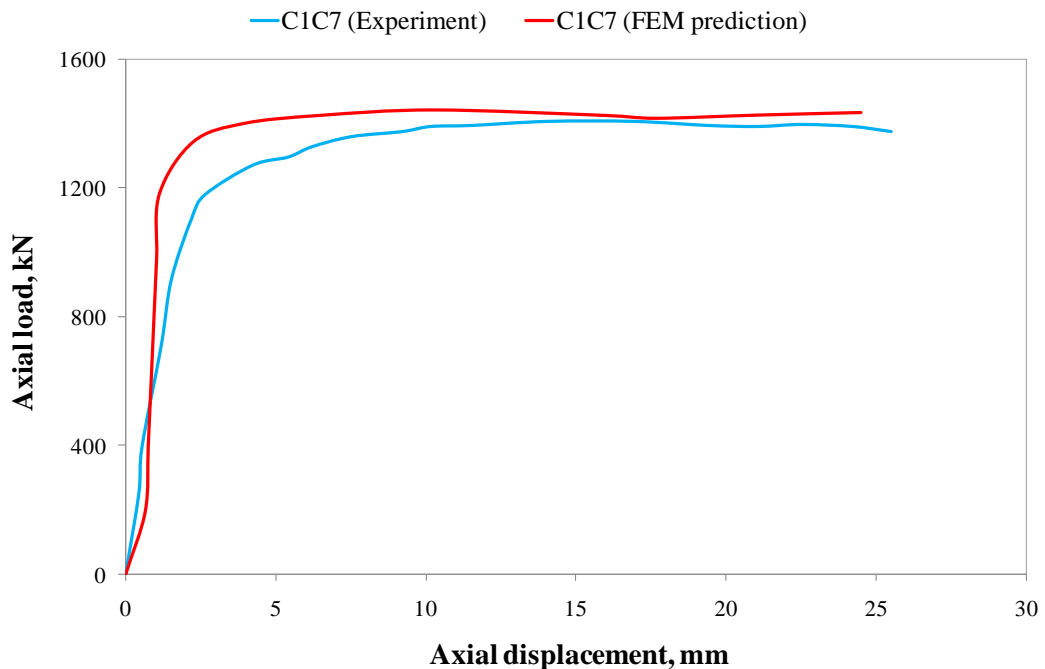


**Figure 4.5.** Axial load versus axial displacement of the experimental and modeled C1C7 specimen (Zhao et al., 2002a)

The blue curve in the figure belongs to experimental results of C1C7 named specimen from the study of Zhao et al. (2002a) while the red curve is plotted by using the data attained from the FEM model. The graphically comparison of the experimental and predicted load-displacement values strongly indicates that the model predicts not only the ultimate axial strength but also the displacement change with corresponding loading. The proposed FEM model gives almost same axial

displacement and similar load-displacement behavior as performed in the experiment.

The specimen labeled as DS-06-2-2-C, from the study carried out by Lin and Tsai (2003), is used to compare the axial load and axial strain of experimental result with that of the predicted result. The graphically comparison is presented in Figure 4.6. It can be obviously seen from the figure that the axial strain of the specimen could also be estimated by using the proposed FEM model. Although the ultimate axial strength value of the model is less than that of the experimental result, the strain at the pick point and the behavior after the pick point are almost same with the experimental result. Namely, both axial load-strain curves indicate similar behavior.
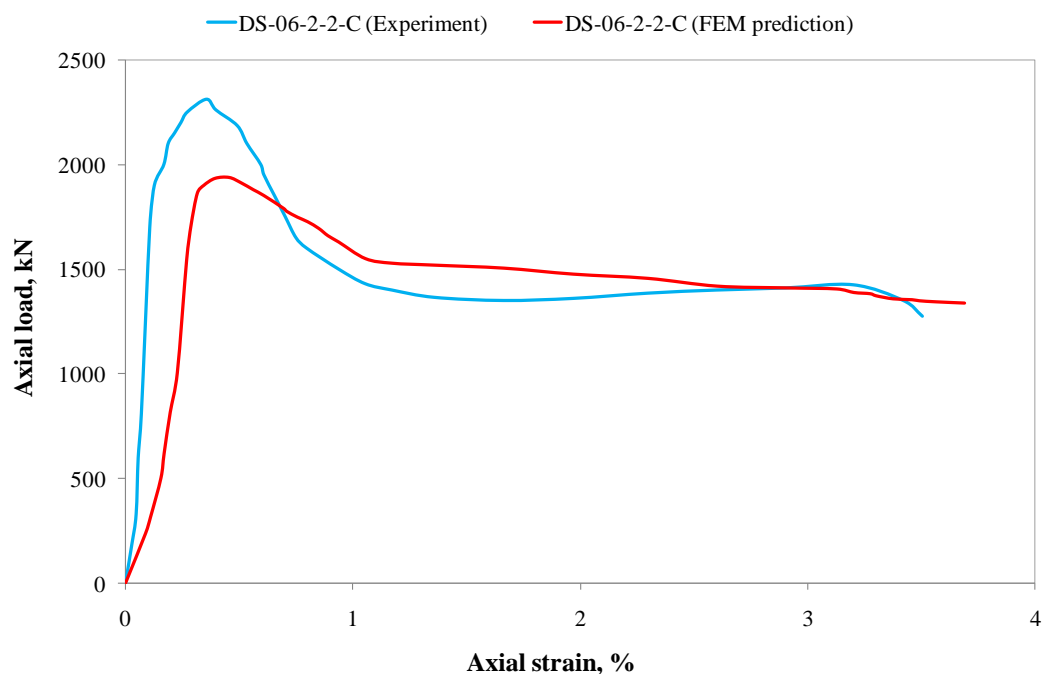


**Figure 4.6.** Axial load versus axial strain of the experimental and modeled DS-06-2-2-C specimen (Lin and Tsai, 2003)

The load-displacement and the load-strain curves are not the only demonstration of the good prediction performance of the proposed FEM model. The failure mode simulation gotten from the software indicates also almost same behavior with that observed in the experiments. For this reason, the beam-column specimen tested in the study of Thao et al. (2004) was used in order to compare the experimental and simulated failure mode of the typical beam-column specimens as shown in Figure 4.7.

(a)                                                    (b)
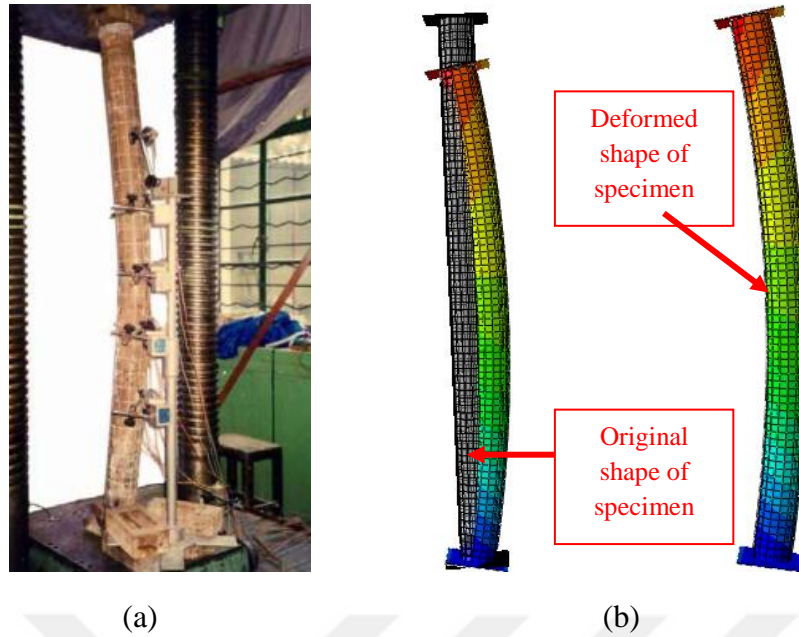
**Figure 4.7.** Failure mode comparison of the experimental and modeled beam-column specimen (Thao et al., 2004): (a) experimental and (b) modeled by FEM

The beam-column specimen tested by Thao et al. (2004) had the L/Do values of more than 15. For this reason, such type of CFDST column specimens generally fails due to the buckling. As shown in Figure 4.7a, the experimentally tested typical beam-column specimen performed buckling type failure. Also, the same type of specimen analyzed by the proposed FEM model failed because of the buckling failure mode as illustrated in Figure 4.7b. On the other hand, the failure mode of stub column specimens is different than that of beam-column specimens. In the same study conducted by Thao et al. (2004), the stub column specimens were also experimentally tested. Generally, the buckling of outer steel tube and/or inner steel tube in the stub column specimens is the main reason of specimen failure. This buckling mode could be observed at the sections near to top and/or bottom surface or mid-height of the specimens. The typical failure mode of stub column specimen that was experimentally tested by Thao et al. (2004) is presented in Figures 4.8a and 4.8b. The corresponding failure mode achieved from the FEM analysis is demonstrated in Figures 4.8c and 4.8d. The failure modes acquired from the proposed FEM model are nearly similar to that observed after the experimentally testing.

As shown in Figure 4.8a, there are buckling on the outer steel tube of experimentally tested stub column specimen. The similar failure mode can be clearly seen on the specimen analyzed according to the proposed FEM model. Moreover, the failure

modes of inner steel tube of the experimentally tested and simulated stub column specimen are almost same. These findings about the failure mode of both stub column and beam-column specimens support that the results of proposed FEM model are strongly reliable and consistent.



(a)                                                                 (b)
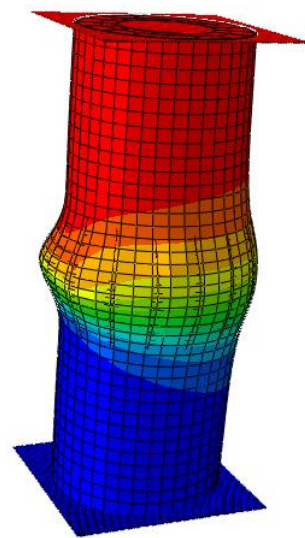


(c)
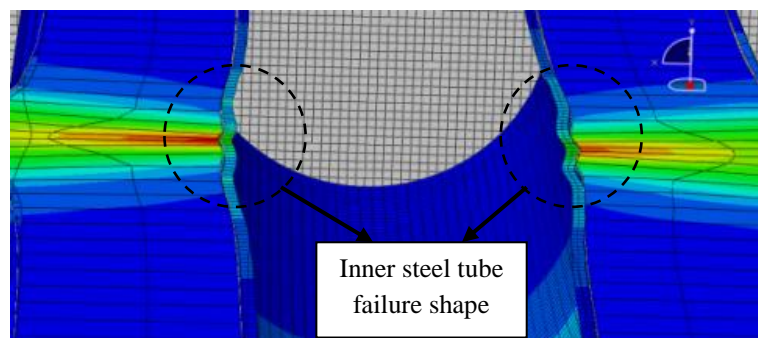


(d)

**Figure 4.8.** Typical failure mode comparison of the experimental and modeled stub specimen (Thao et al., 2004): (a) deformed specimen after experimentally testing, (b) failure mode of inner steel tube after experimentally testing, (c) deformed specimen after analyzing with FEM, and (d) failure mode of inner steel tube after analyzing with FEM

In order to support the reliability and prediction capability of the model, the load-displacement curves of other specimens gotten from the different experimental studies are compared with the curves achieved from the analyzing by FEM in Figures 4.9a -4.9f.
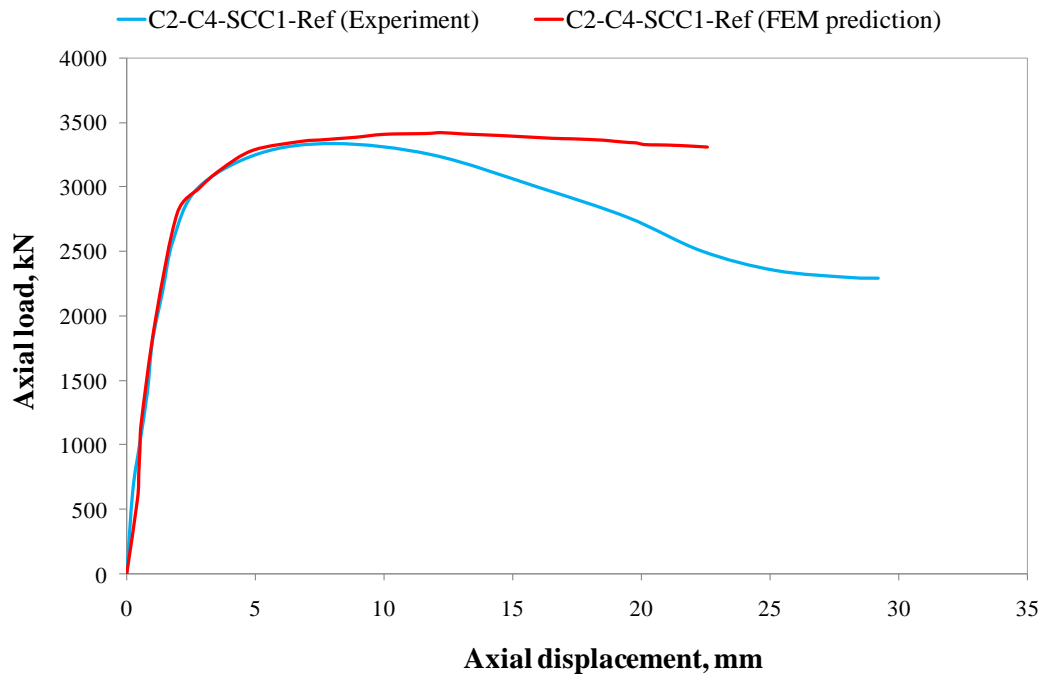


(a)
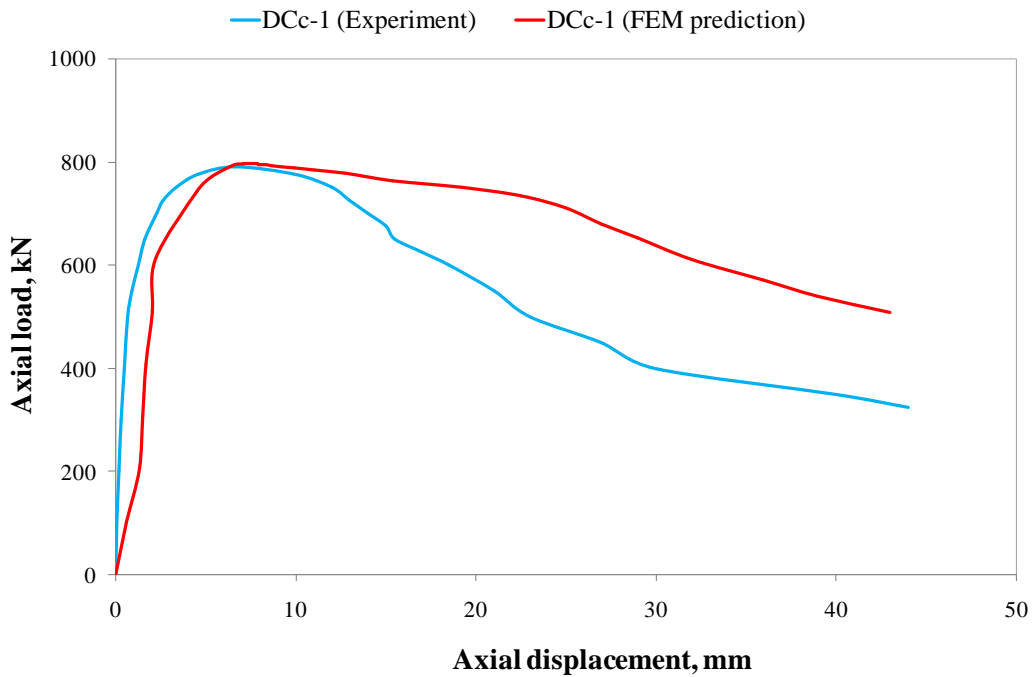


(b)
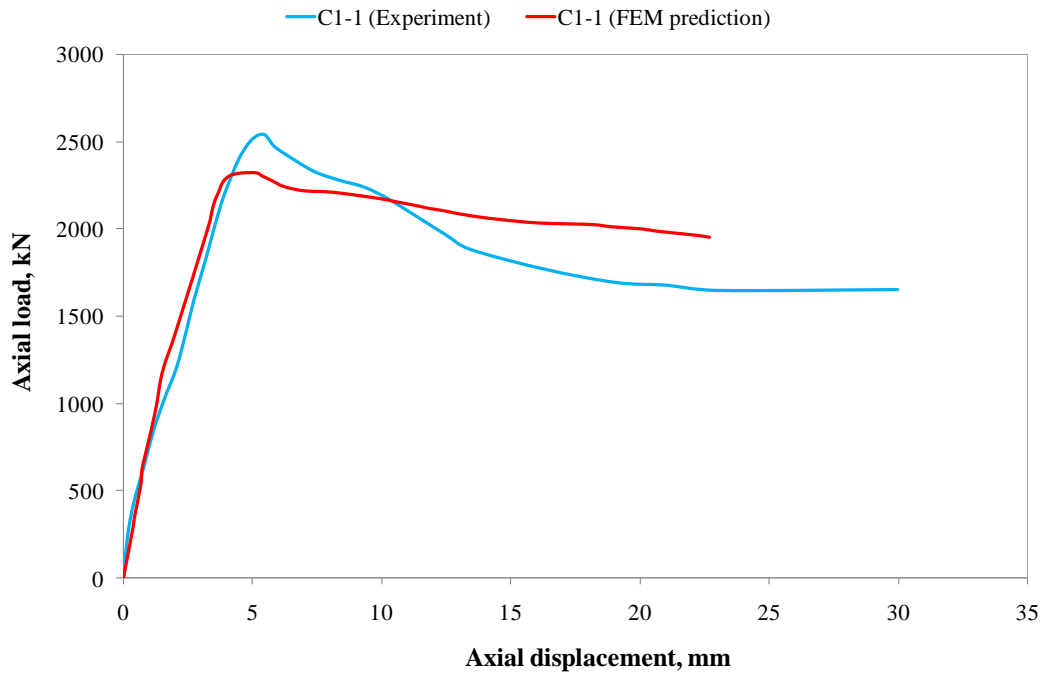
(c)
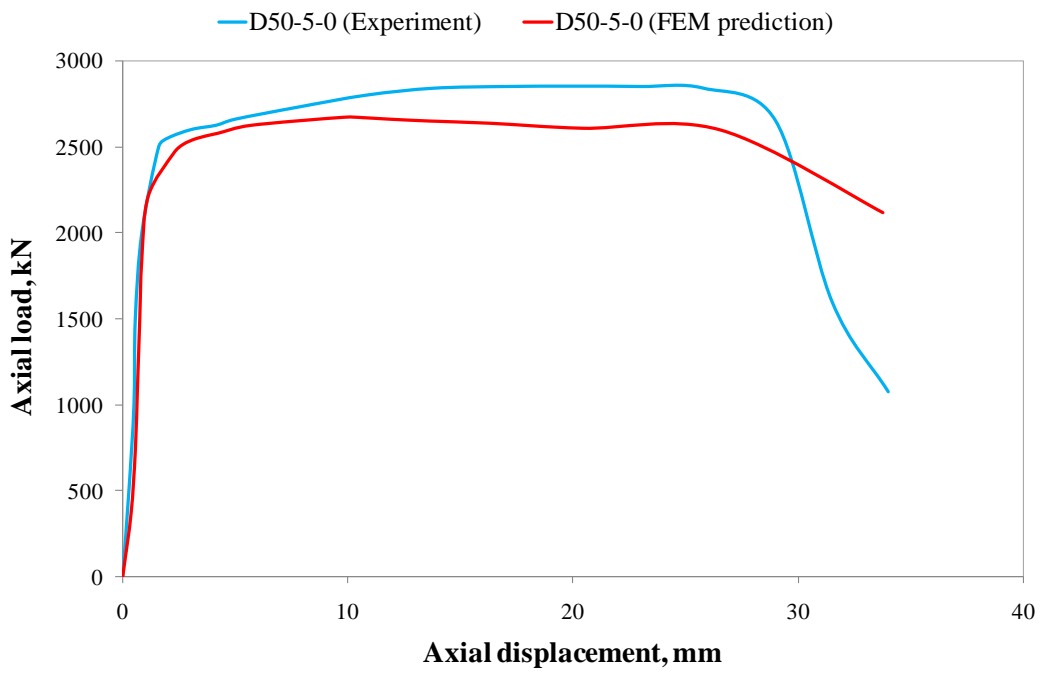


(d)
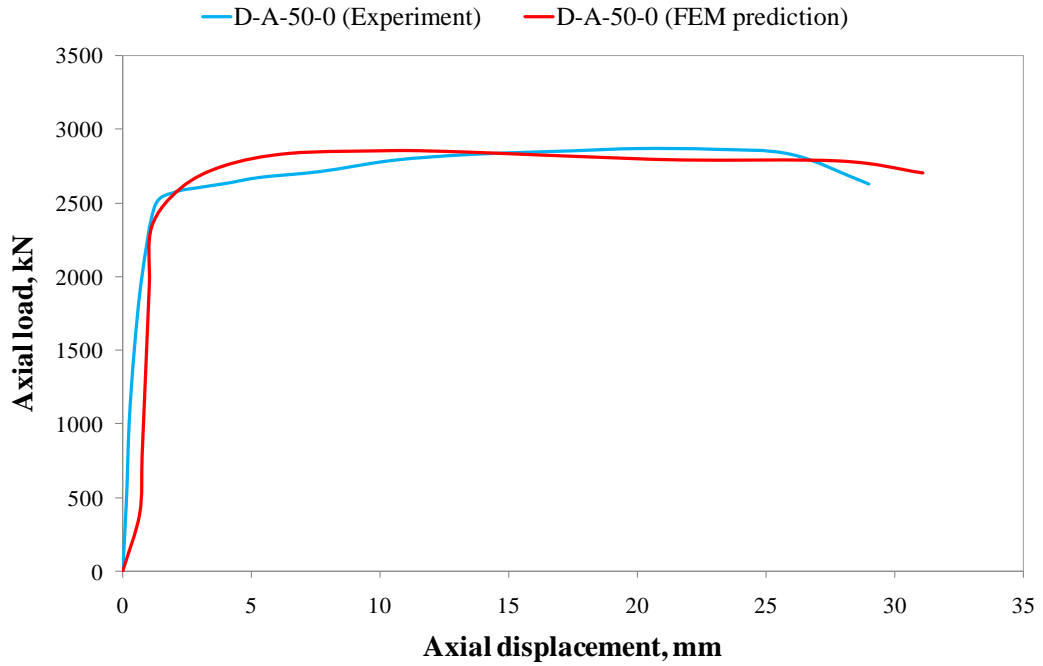
(e)
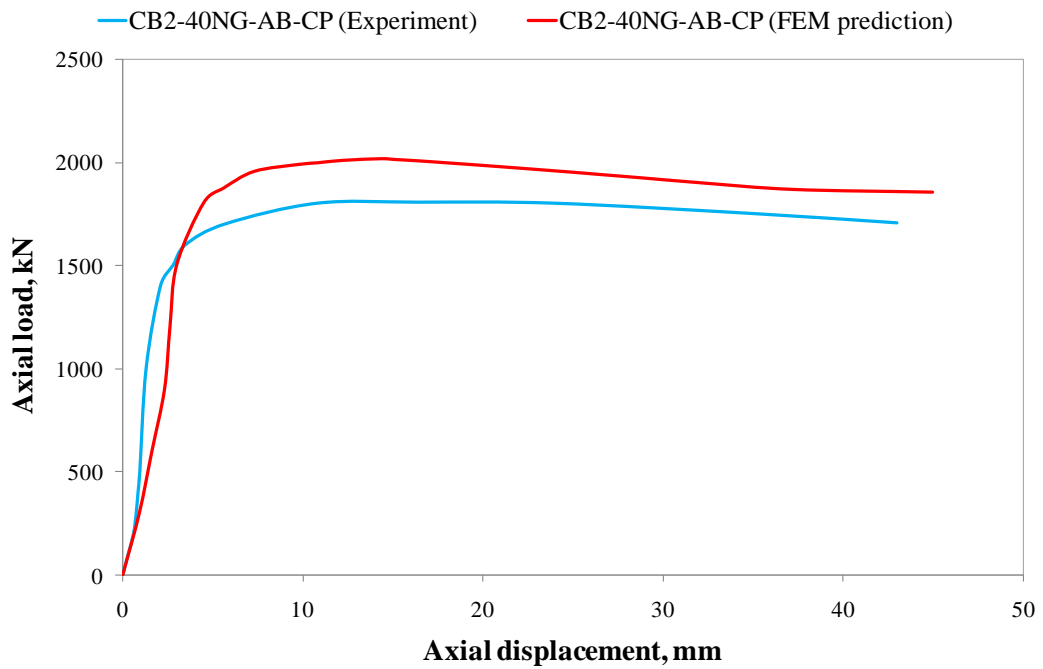


(f)

**Figure 4.9.** Axial load versus axial displacement of the experimental and modeled: (a) C2-C4-SCC1-Ref specimen (Lu et al., 2010b), (b) DCc-1 specimen (Han et al., 2011a), (c) C1-1 specimen (Han et al., 2011b), (d) D50-5-0 specimen (Dong and Ho, 2012), (e) DA-50-0 specimen (Dong and Ho, 2013), and (f) CB2-40NG-AB-CP specimen (Abbas et al., 2016)

When the all above figures are examined, it can be revealed that the load-displacement prediction of the proposed FEM model is almost similar to the experimental one. Especially, the specimen denoted as C2-C4-SCC1-Ref from the study of Lu et al. (2010b) indicates perfectly same load-displacement behavior till the ultimate point as indicated in Figure 4.9a. In addition, the experimental and predicted load-displacement curves for DCc-1 labeled specimen from the study of Han et al. (2011a) shows same demeanor against to axially loading with minor differences as presented in Figure 4.9b. On the other hand, the experimental and predicted curves for C1-1 named specimen from another study of Han et al. (2011b) shows admissible differences after the ultimate axial strength value reached as illustrated in Figure 4.9c.

The load-displacement curves of D50-5-0 and DA-50-0 labeled specimens from two different studies conducted by Dong and Ho (2012 and 2013) are presented in Figures 4.9d and 4.9e, respectively. In both CFDST specimens with CHS, the load increases till about 90% of the ultimate axial strength values with small amount of displacement and both perform a large deformation from this point to the ultimate axial strength point then after the load carrying capacities of both specimens tend to sharply decrease. The load-displacement curves achieved from the simulation by the proposed FEM model show similar result. Additionally, the experimental and predicted load-displacement curves plotted for the specimen denoted as CB2-40NG-AB-CP from the study of Abbas et al. (2016) demonstrate similar demeanor with small amount of overestimated ultimate axial load value of the proposed model.



0 mm    10 mm    20 mm    30 mm    40 mm

(a)

| 0 mm | 10 mm | 20 mm | 30 mm | 40 mm |
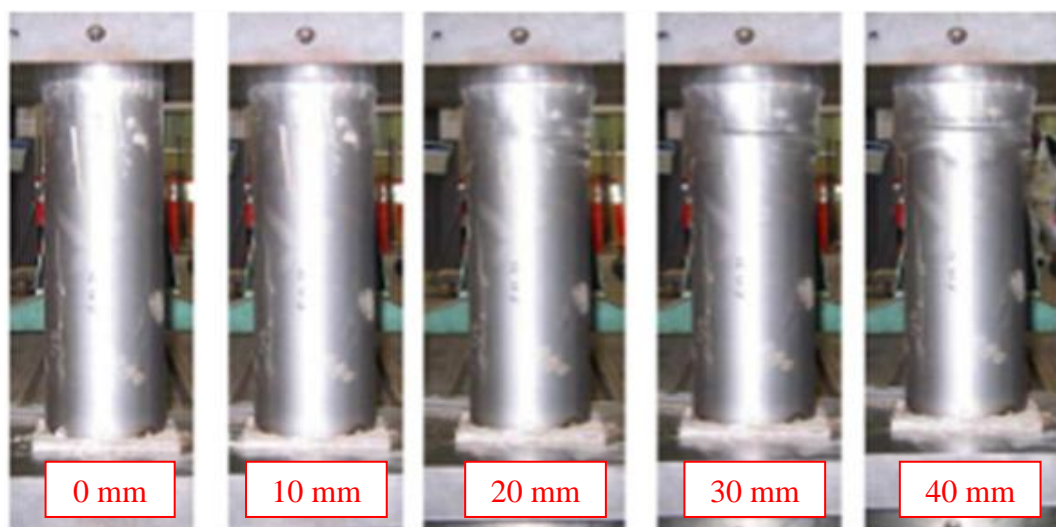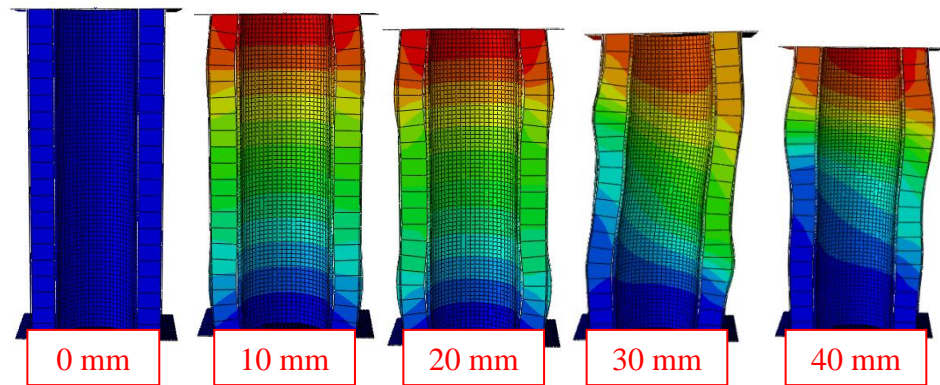
(b)

**Figure 4.10.** Failure progress comparison of the experimental and modeled O9I2S specimen (Zhao et al., 2010)

In another study carried out by Zhao et al. (2010), the specimens were loaded till 100 mm deformation value. From this study, experimentally attained failure progress of O9I2S labeled specimen is compared with that achieved from the simulation by the proposed FEM model as presented in Figure 4.10.

While Zhao et al. (2010) submitted the failure progress of the specimen until 100-mm displacement, the analyzing the specimen with FEM could accomplish only till 40-mm displacement. For this reason, the comparison herein is done till 40-mm displacement level. As shown in the figure, the specimen does not indicate visible deformation at 10-mm displacement. However, after this level of displacement in both experimental and modeled specimens perform overt deformation and outward buckling of the outer steel tube can be clearly seen at the displacement levels of 30 and 40 mm.

The similar buckling mode on the outer steel tube can also be obviously seen in specimen named C1-1 (Han et al., 2011b) as shown in Figure 4.11. For this specimen, the load-displacement curve is also presented in Figure 4.9c. The photo for C1-1 specimen given in the study conducted by Han et al. (2011b) indicates that the concrete near to top surface of the specimen swelled out through the outer steel tube direction and led to its buckling as demonstrated in Figure 4.11a. In order to show the failure mode of the modeled C1-1 specimen, the cut views for C1-1 specimen simulation with the configuration of stress, lateral strain, and axial deformation are

96

shown in Figure 4.11b, respectively. The highest stress value occurs on the concrete annulus at the region where the concrete efforts to buckle the outer steel tube. The lateral strain on the specimen also occurs at that region. However, at the middle region of specimen, the concrete applies the stress to the inner steel tube and by this way, inner steel tube at the middle region of the specimen is forced to deform through the inward direction.
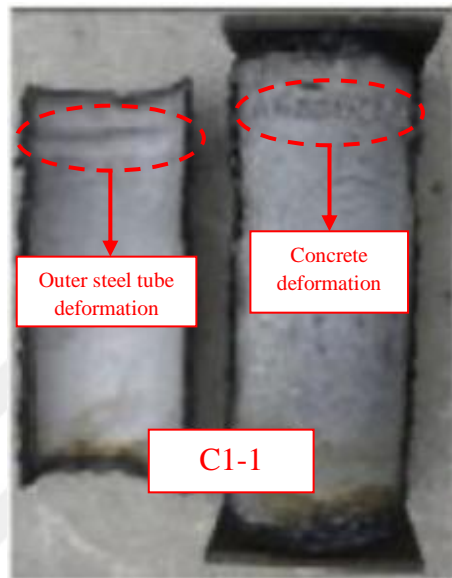


(a)
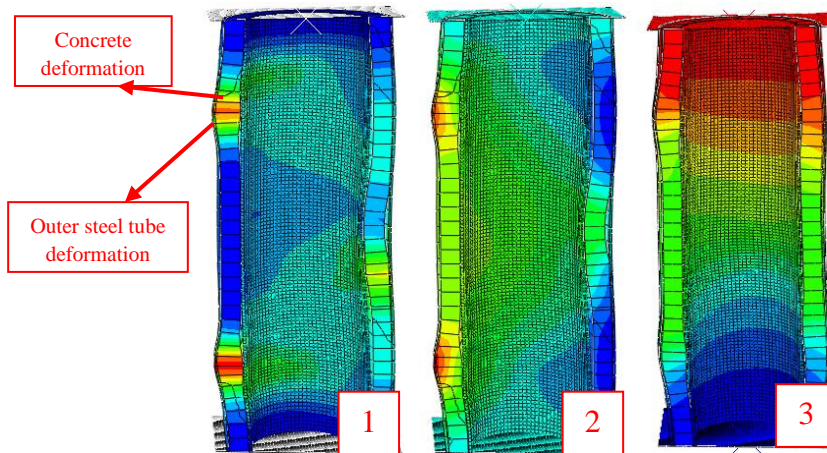


(b)

**Figure 4.11.** Failure mode comparison for the experimental and modeled C1-1 specimen (Han et al., 2011b): (a) after experimental test and (b) after FEM analysis (with configuration of: 1 – stress, 2 – lateral strain, and 3 – axial deformation distributions)

Li et al. (2012) also submitted the photographic view of typical failure mode of specimen as presented in Figure 4.12. The concrete is also swelled out at the top region of the specimen. Nevertheless, it can be clearly seen that the concrete forced both outer and inner steel tubes to buckle at the top region of specimens as shown in Figure 4.12a. The similar forcing of concrete to the steel tubes can also be viewed in the modeled specimens after simulation. The concrete swelled out through the outer steel tube near to the top surface of specimen and this caused the weak region occurrence on the inner steel tube at the same region. This situation also induced to the buckling of the inner steel tube near to the top surface region.



(a)



(b)
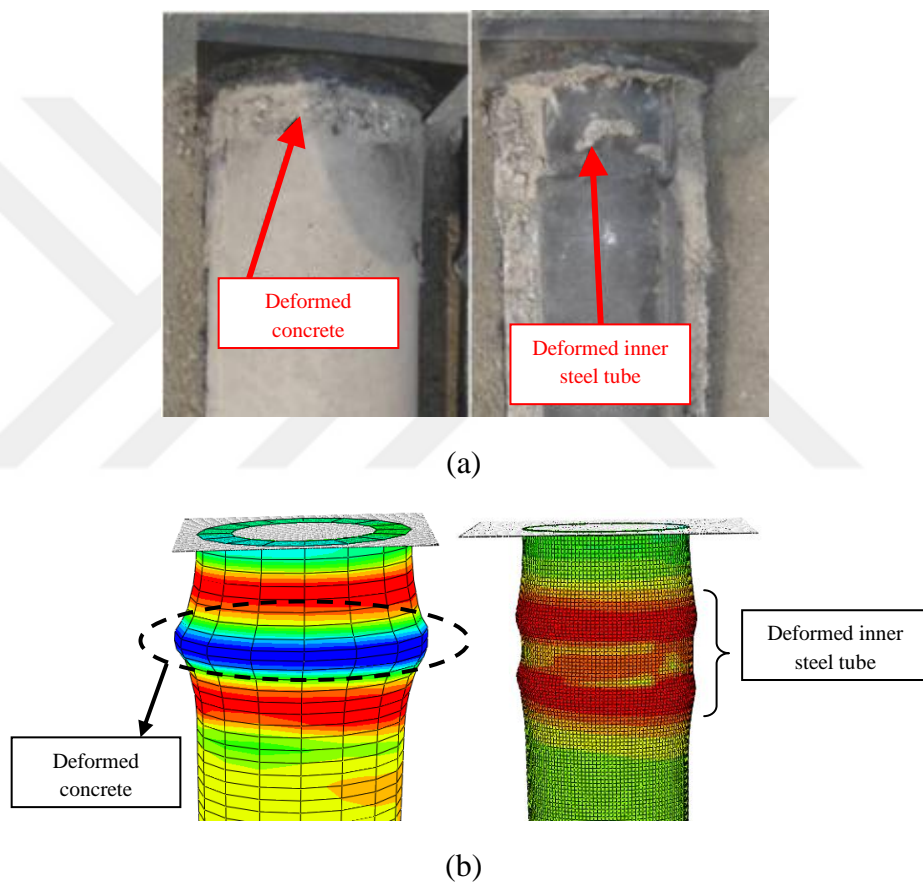
**Figure 4.12.** Typical failure mode comparison for concrete annulus and inner steel tube of the experimental and modeled specimens (Li et al., 2012): (a) after experimental test and (b) after FEM analysis

Contrarily, the study conducted by Wang et al. (2014) pointed out that the outward buckling of the outer steel tube occurred at the mid-height of the specimen as shown in Figure 4.13a. The simulated specimen by the proposed FEM model performed a similar failure mode as in the experimentally tested specimen as indicated in Figure

4.13b with configuration of stress and axial displacement level. The concrete of 0HA0 labeled specimen started to swell out from the mid-height of the specimen that also forced to outer steel tube to deform through the outward. All these findings could be accepted to be evidence for the well prediction performance of the proposed FEM model.



(a)
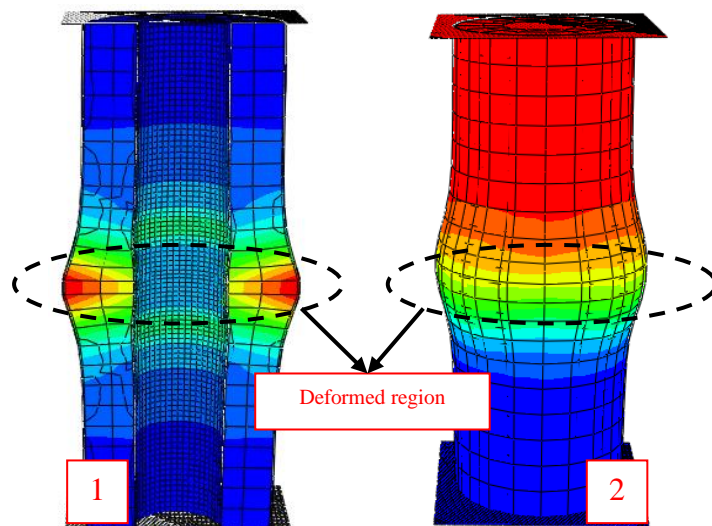


(b)

**Figure 4.13.** Failure mode comparison for the experimental and modeled 0HA0 specimen (Wang et al., 2014): (a) after experimental test and (b) after FEM analysis (with configuration of: 1 – stress and 2 – axial deformation distributions)

In many studies, the authors provided the load-displacement curves of the experimentally tested specimens whereas in some, instead of the load-displacement curves, the load-strain curves were submitted. The comparisons of the load-strain curves of experimental specimen with simulated specimens are presented in Figures 4.14a-4.14e.



(a)



(b)

(c)



(d)

101
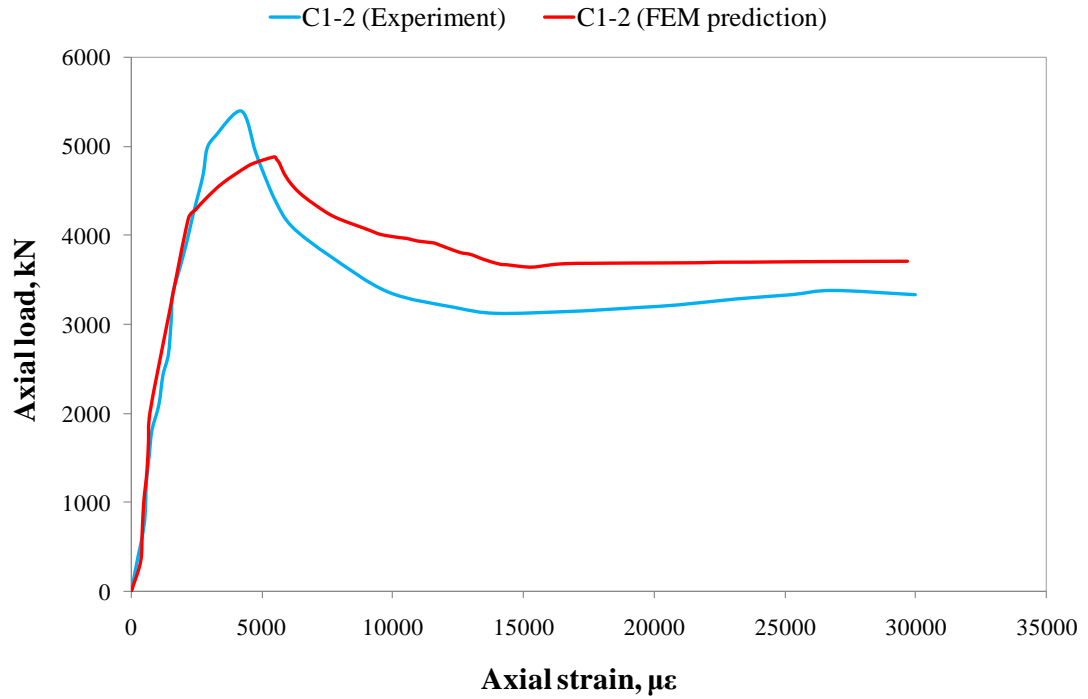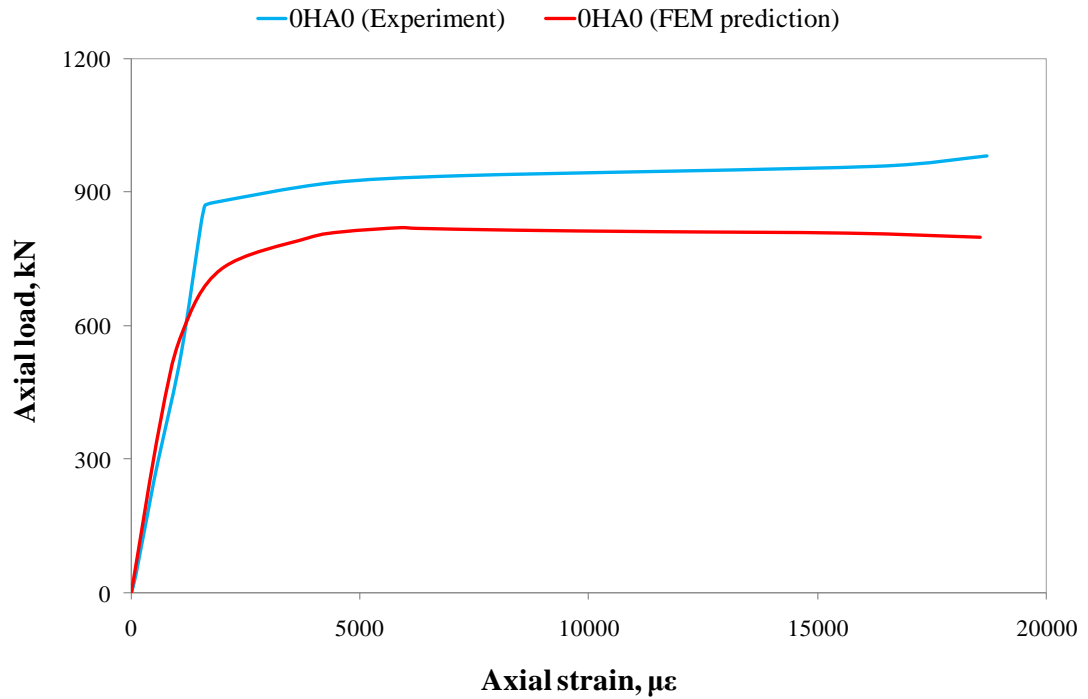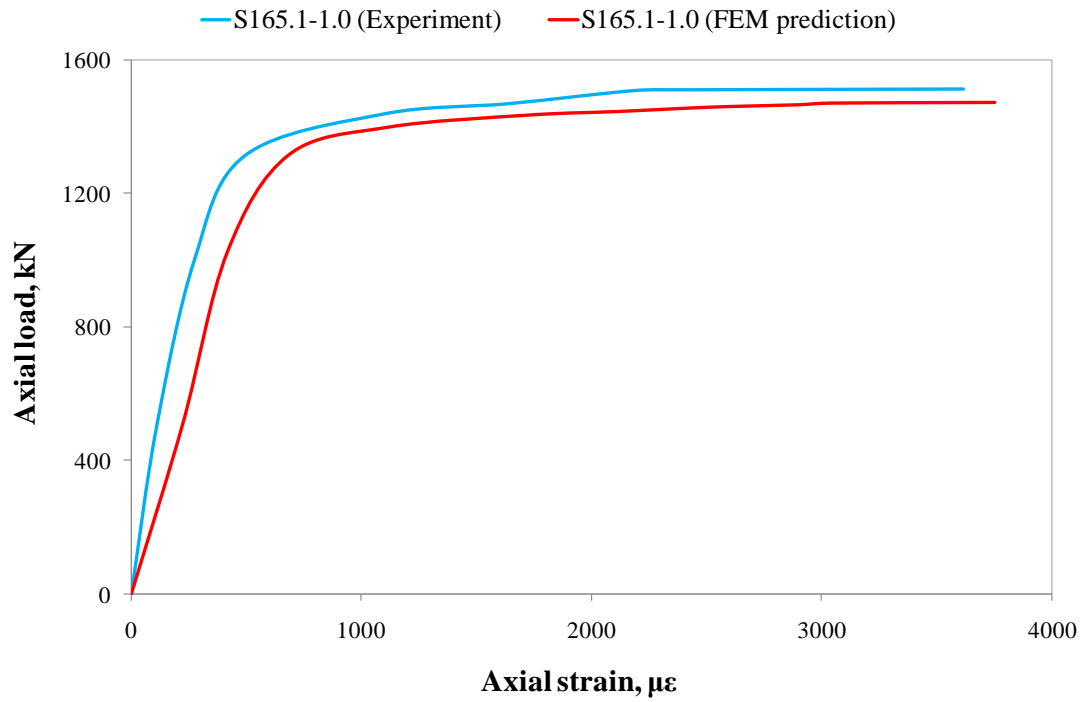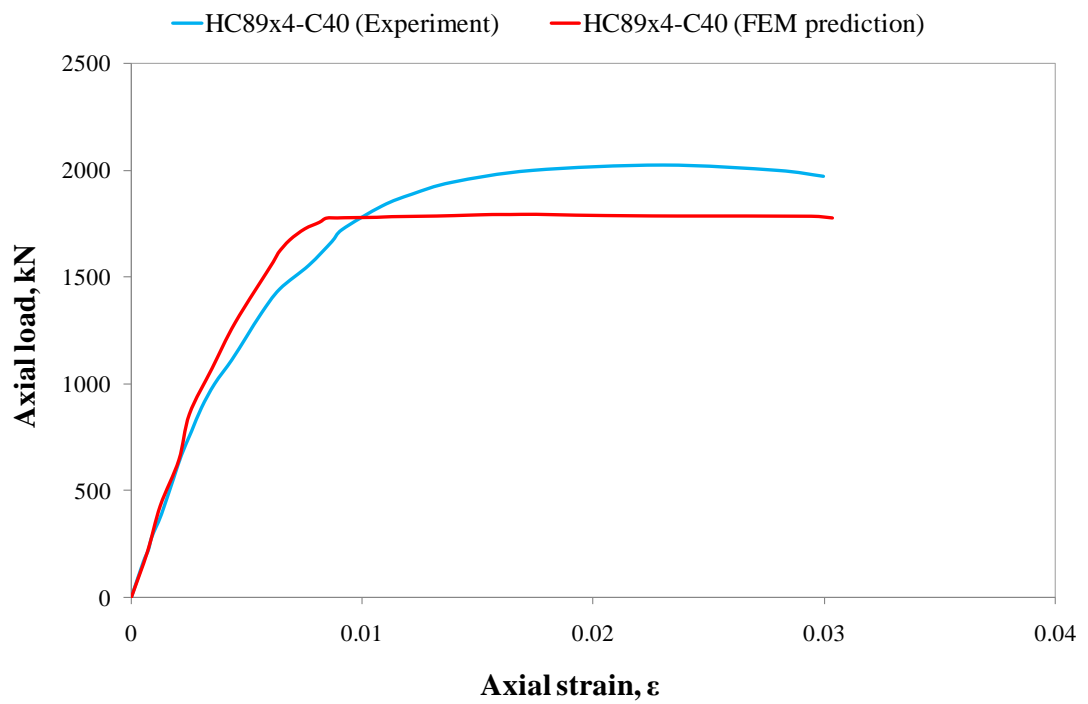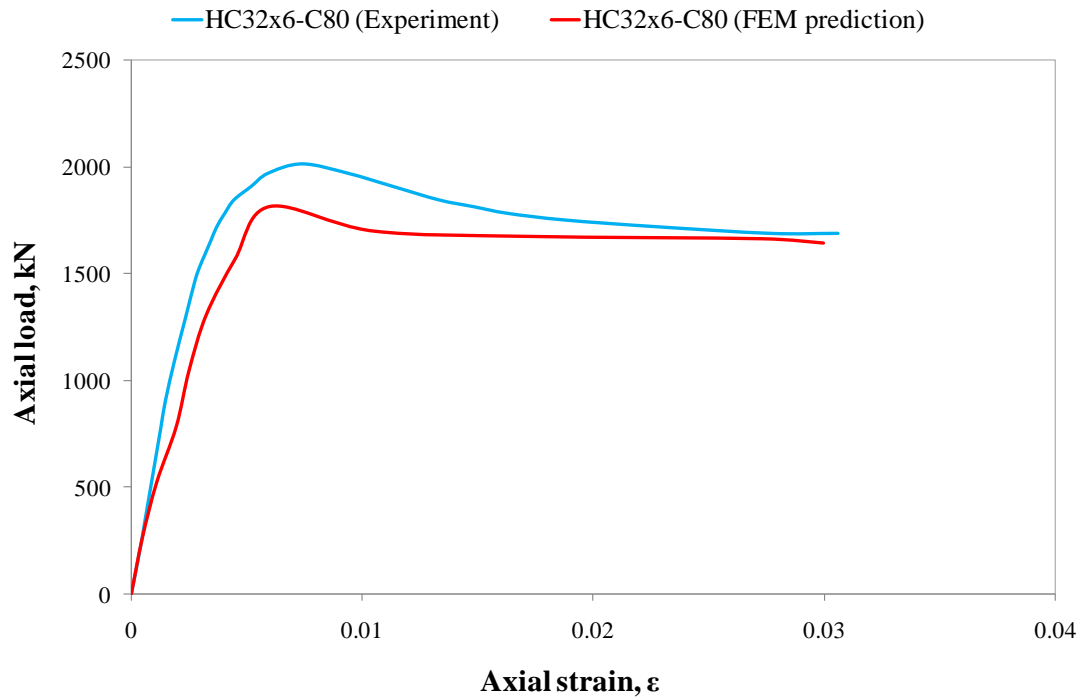
(e)

**Figure 4.14.** Axial load versus axial strain of the experimental and modeled: (a) C1-2 specimen (Li et al., 2012), (b) 0HA0 specimen (Wang et al., 2014), (c) S165.1-1.0 specimen (Essopjee and Dundu, 2015), (d) HC89x4-C40, and (e) HC32x6-C80 specimens (Wang et al., 2016)

The figures given above indicate that the load-strain curves achieved from the simulation by the proposed FEM model are almost same with that obtained from the experimental results. When Figure 4.14a is observed, it would be obviously seen that increasing in the axial strain by increasing the load about ultimate strength level is almost same for both curves achieved from experiment and simulation. As well, after reaching the ultimate strength value, the behavior of curves for both results is similar but the model has a small amount of overestimated load values. In other figures, the curves acquired from the model shows similar demeanor with experimental curves, however, the predicted load-strain values are under the exact results with slight values. This prediction capableness of proposed FEM model can be accepted as good, reliable and consistent according to the aforementioned findings.

**4.1.3 Comparison of FEM Model with Modified ACI (2002) Formula**

For ACI (2002), the ultimate axial strength of the CFDST columns with CHS was extrapolated by using Equation 2.1 that was procured by the modifying ACI (2002) formula, which was suggested to determine the ultimate axial strength of single skin composite columns involving a reinforcing bar. This modification on the original formula was performed so that it could be practicable to the CFDST columns with CHS.

Figure 4.15a indicates the predicted ultimate strengths of the FEM model and the modified ACI (2002) formula versus experimental ultimate axial strengths while Figure 4.15b shows the normalized ultimate strength values of the FEM model and the modified ACI (2002) formula. The purpose of the presenting the results as graph is the easily visual comparison for the prediction performance of the FEM model against to the modified ACI (2002) formula.

When the results of the FEM model are compared with the results calculated by using the modified (2002) ACI formula, it can be clearly seen that the FEM model showed better performance than the modified ACI formula (2002) since the ultimate axial strength values predicted by the FEM formula were amassed near to the 100% agreement line as demonstrated in Figure 4.15a.

Besides, when the coefficient of determination (R-squared) values of the proposed FEM model and the modified ACI formula (2002) are compared, it would be clearly appeared that the prediction performance of the FEM model is significantly better than the modified ACI formula (2002). Because the R-squared value of the FEM model is 0.963 while that of the modified ACI (2002) formula is 0.936 and the R-squared value is directly numerical representation of prediction capability.

In addition, observing Figure 4.15b can reveal that after the ultimate strength value of about 1500 kN, the modified ACI formula (2002) performs many underestimated values and a great number of the modified ACI (2002) results fall outside of normalization limit lines of ±10% while a few results of the proposed FEM model fall to the out of the normalization lines.
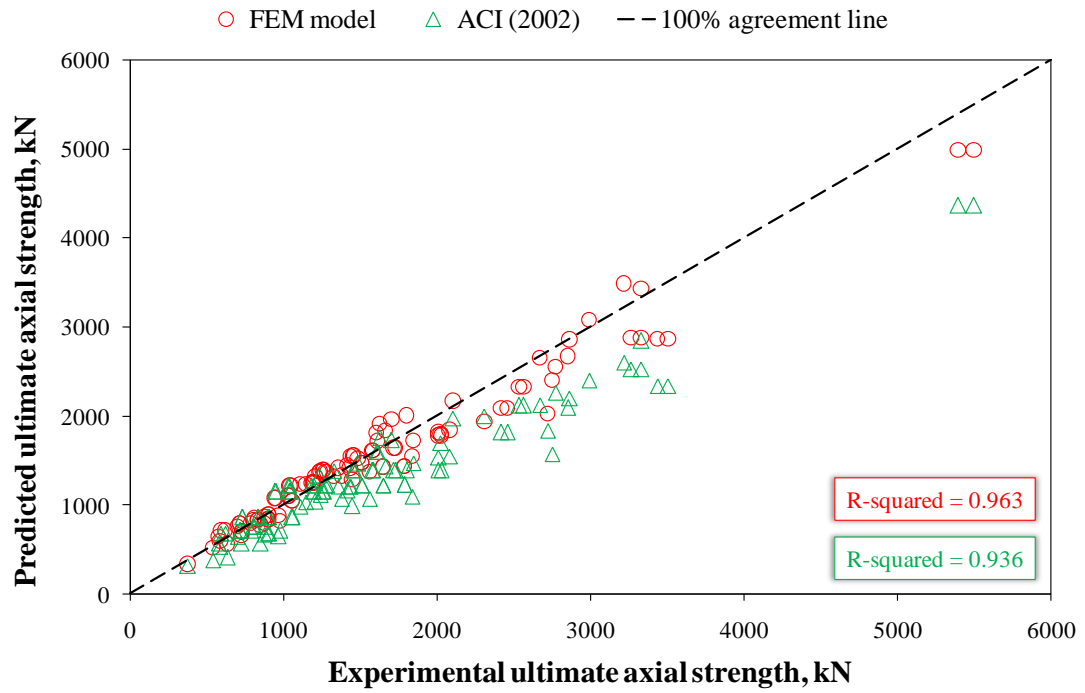
(a)
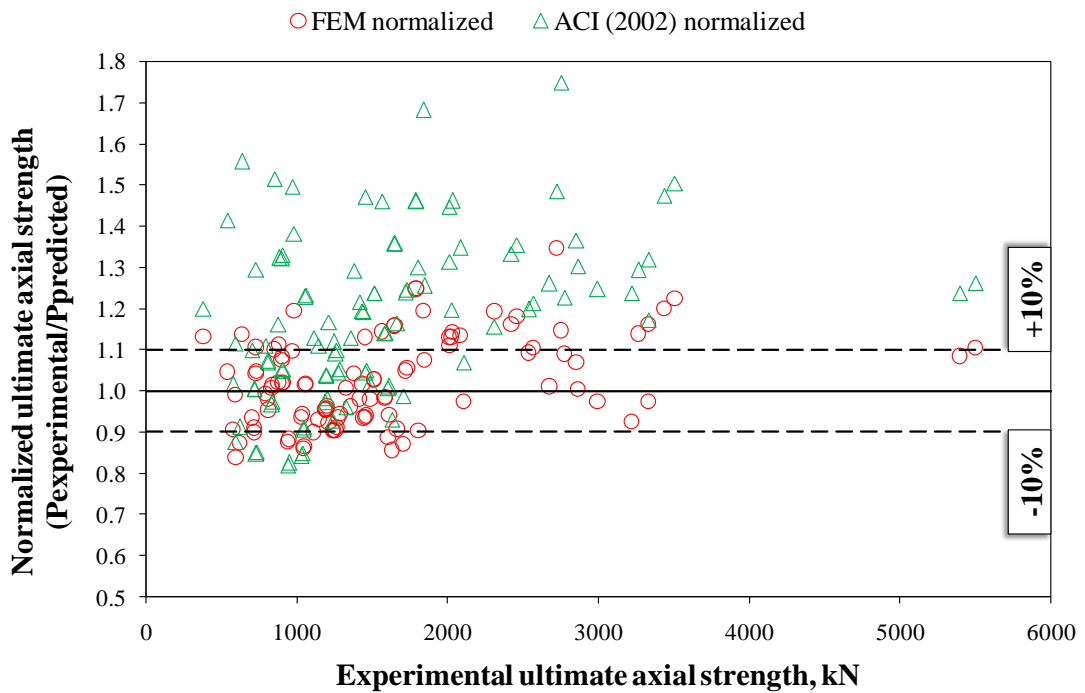


(b)

**Figure 4.15.** (a) predicted and (b) normalized ultimate axial strengths of FEM model and modified ACI (2002) formula versus experimental ultimate axial strengths

**4.1.4 Comparison of FEM Model with Modified Eurocode 4 (2004) Formula**

For Eurocode 4 (2004), the ultimate axial strength of the CFDST columns with CHS was extrapolated by using Equations 2.4 and 2.5 that were procured by the modifying Eurocode 4 (2004) formulas, which were given to determine the ultimate axial strength of the concrete filled steel tubular columns involving the outer steel tube, reinforcing bars and concrete as well as confinement effect. This modification on the original formulas was performed so that it could be practicable to the CFDST columns with CHS.

Figure 4.16a indicates the predicted ultimate strengths of the FEM model and the modified Eurocode 4 (2004) formula versus experimental ultimate axial strengths while Figure 4.16b shows the normalized ultimate strength values of the FEM model and the modified Eurocode 4 (2004) formula. The purpose of the presenting the results as graph is the easily visual comparison for the prediction performance of the FEM model against to the modified Eurocode (2004) formula.

According to these figures, it could be forthrightly stated that the modified Eurocode 4 formula (2004) performed almost near prediction capability with the proposed FEM model. Especially, when the R-squared values given in Figure 4.16a are considered, it would be noticed that the prediction performance of both models are similar, yet, the proposed FEM model is better than the modified Eurcode (2004) 4 formula even in small amount. The results of the proposed FEM model and the modified Eurocode 4 (2004) formula are amassed around the 100% agreement line along all ultimate axial strength values of the CFDST columns with CHS. The difference in the predictivity of the proposed FEM model and the modified Eurocode 4 (2004) formula can be clearly seen by the time Figure 4.16b is taken into account. Both, the proposed FEM model and the modified Eurocode 4 (2004) formula, had the underestimated and overestimated values but the residual ultimate axial strength values of the modified Eurocode 4 (2004) formula are greater than that of the proposed FEM model.

Besides, it can be easily seen that both, the proposed FEM model and the modified Eurocode 4 (2004) formula can be used to estimate all ultimate axial strength values. Only at the ultimate axial strength values ranging between 2000 and 4000 kN, the

modified Eurocode 4 (2004) formula gives more underestimated results than the proposed FEM model.
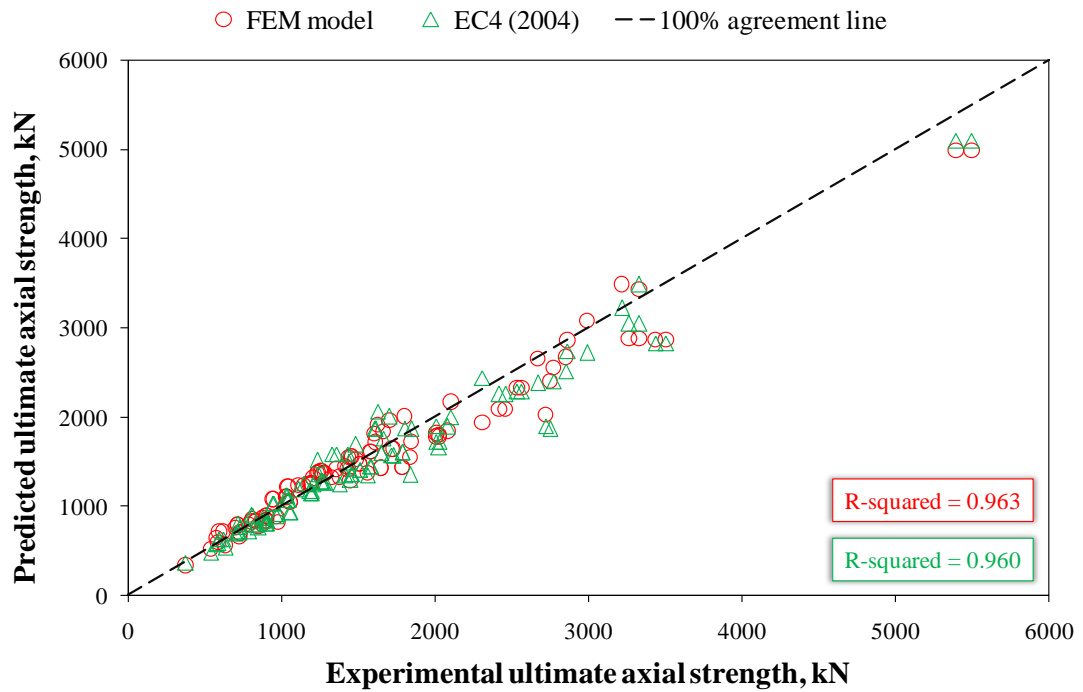


(a)
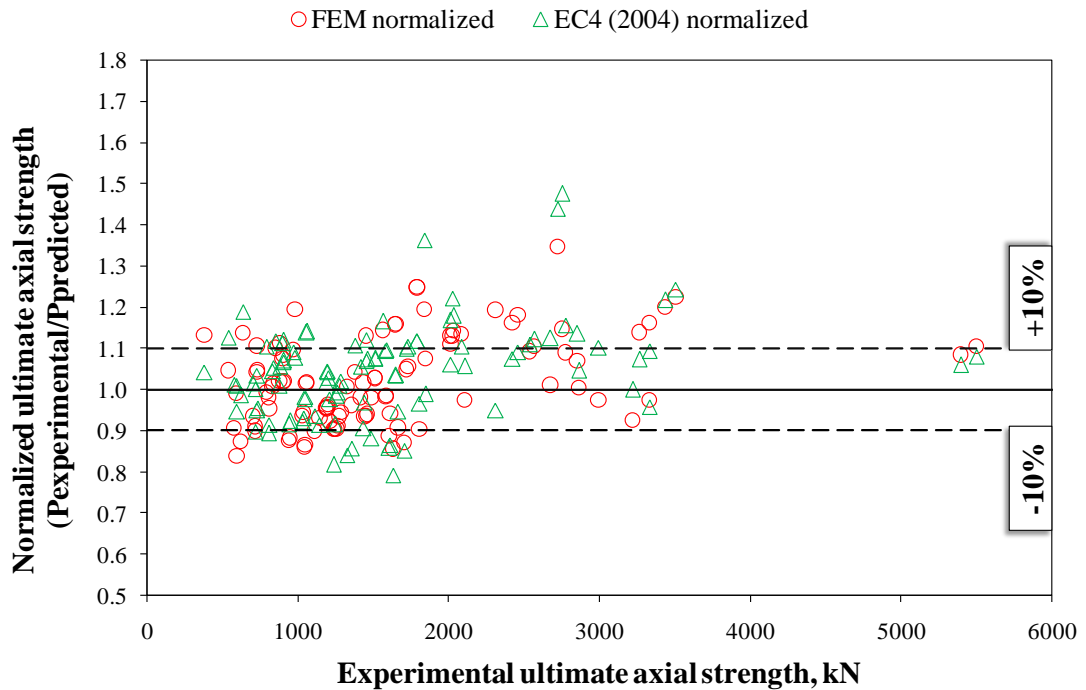


(b)

**Figure 4.16.** (a) predicted and (b) normalized ultimate axial strengths of FEM model and modified EC4 (2004) formula versus experimental ultimate axial strengths

**4.1.5 Comparison of FEM Model with Modified AISC (2010) Formula**

For AISC (2010), the ultimate axial strength of the CFDST columns with CHS was extrapolated by using Equations 2.7 and 2.8 that were procured by the modifying AISC (2010) formulas, which were given to determine the ultimate axial strength of the single skin composite columns involving reinforcing bars. This modification on the original formulas was performed so that it could be practicable to the CFDST columns with CHS.

Figure 4.17a indicates the predicted ultimate strengths of the FEM model and the modified AISC (2010) formula versus experimental ultimate axial strengths while Figure 4.17b shows the normalized ultimate strength values of the FEM model and the modified AISC (2010) formula. The purpose of the presenting the results as graph is the easily visual comparison for the prediction performance of the FEM model against to the modified AISC (2010) formula.

The estimation capability of the proposed FEM model is also better than the modified AISC (2010) formula. The R-squared value of the FEM model is greater than that of the modified ASIC (2010) formula as can be seen in Figure 4.17a. This indicates that the reliability and accuracy of the proposed FEM model are better than that of the modified AISC (2010) formula since the R-squared value is directly give a numerical idea about the prediction performance of model.

When Figure 4.17a is examined, it would be seen that the modified AISC (2010) formula estimations became bad after the ultimate axial strength value of 1500 kN. However, the consistency of the proposed FEM model to estimate the ultimate axial strength of the CFDST columns with CHS could be easily observed along almost all strength values.

In the case of the examining Figure 2.17b where the normalized values are plotted, it can be obviously seen that the modified AISC (2010) formula has so much underestimated ultimate axial strength values while the pretty much ultimate axial strength values predicted by the proposed FEM model fall between ±10% normalization limit lines. Besides, it is clear that many estimated results by the modified AISC (2010) formula are above the +10% normalization limit line and this decreases the reliability and accuracy of the modified AISC (2010) formula.
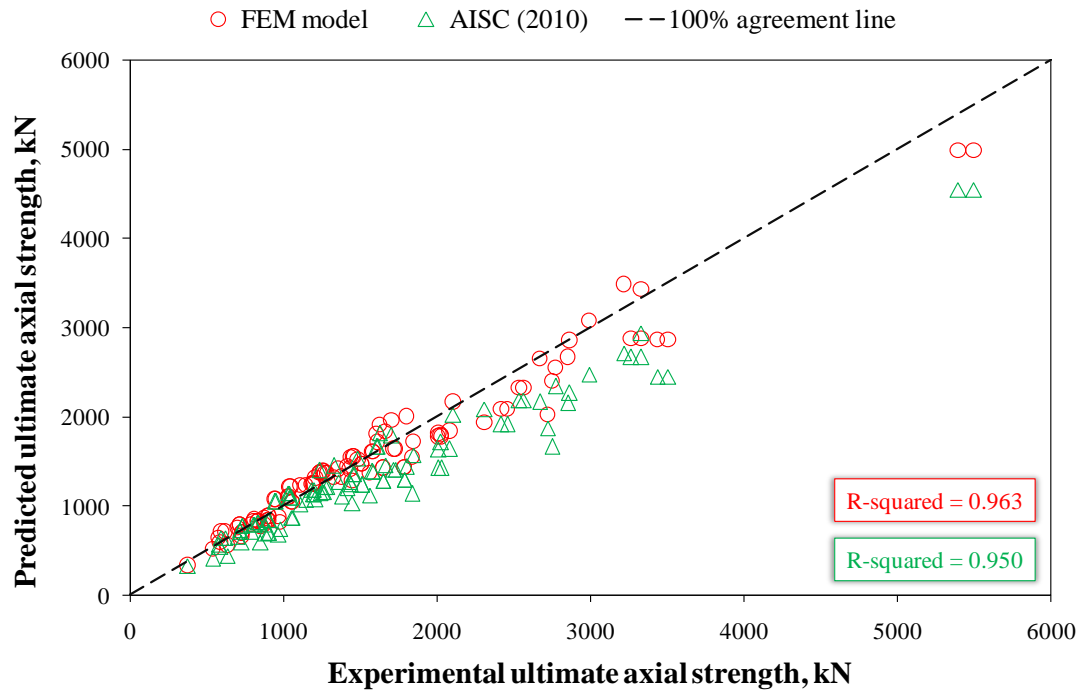
(a)
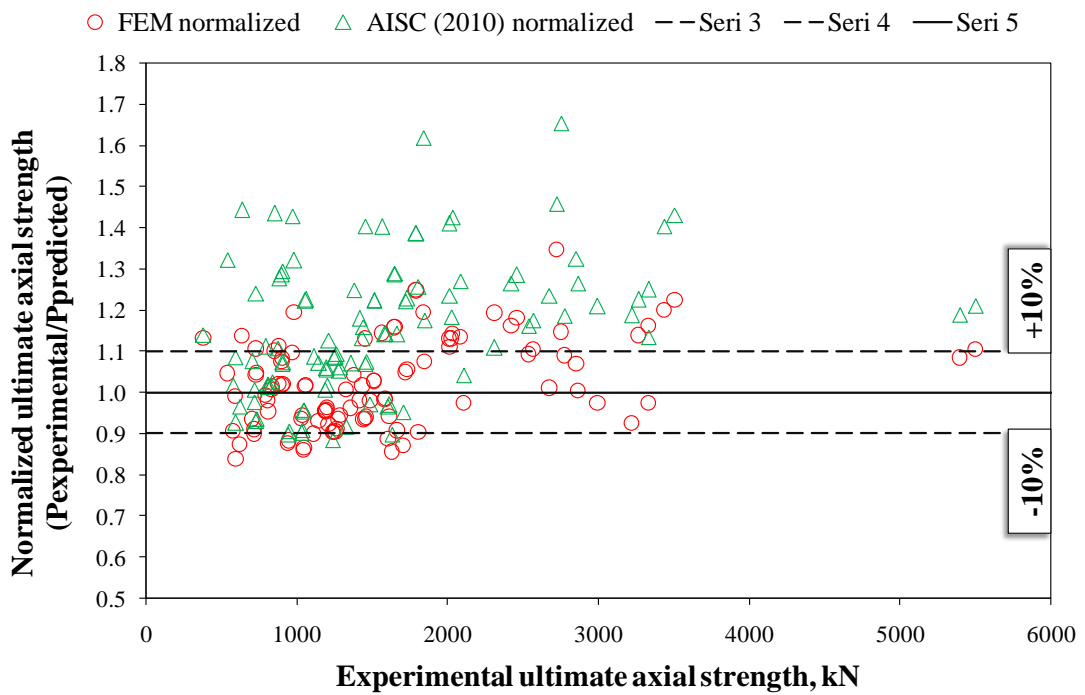


(b)

**Figure 4.17.** (a) predicted and (b) normalized ultimate axial strengths of FEM model and modified AISC (2010) formula versus experimental ultimate axial strengths

### 4.1.6 Comparison of FEM Model with Model of Uenaka et al. (2010)

In addition to the modified formulas, some researchers developed empirical models that also extrapolate the ultimate axial strength of the CFDST columns with CHS. Equation 2.10 was proposed by Uenaka et al. (2010) to determine the ultimate axial strength of the CFDST columns with CHS.

Figure 4.18a indicates the predicted ultimate strengths of the proposed FEM model and the model of Uenaka et al. (2010) versus experimental ultimate axial strengths while Figure 4.18b shows the normalized ultimate strength values of the FEM model and the model of Uenaka et al. (2010). The purpose of the presenting the results as graph is the easily visual comparison for the prediction performance of the FEM model against to the model of Uenaka et al. (2010) formula.

The R-squared value gotten from the results determined by the empirical model suggested by Uenaka et al. (2010) is far less than that achieved from the proposed FEM model as shown in Figure 4.18a. As well, when Figure 4.18b is observed, it is explicit that the prediction performance of the proposed FEM model is much better than that of Uenaka et al. (2010).



(a)
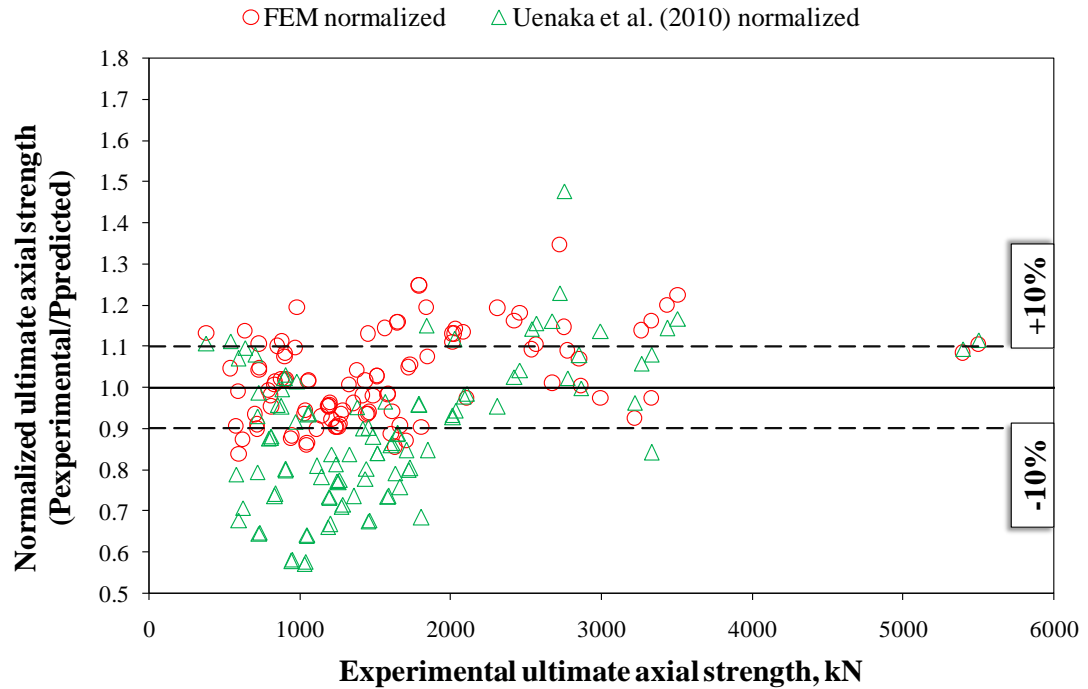
(b)

**Figure 4.18.** (a) predicted and (b) normalized ultimate axial strengths of FEM model and Uenaka et al. (2010) model versus experimental ultimate axial strengths

Furthermore, the results estimated by the model of Uenaka et al. (2010) are more than the experimental results that could be openly seen in Figure 4.18b in which the normalized ultimate axial strength values are plotted. For this reason, the validity and reliability of the proposed FEM model is much better than that of the model suggested by Uenaka et al. (2010).

Additionally, by viewing Figure 4.18b, it can be overtly observed that the model by Uenaka is no suitable especially for the CFDST columns having the ultimate axial strength value less than 200 kN. In fact, the proposed FEM model also has some underestimated and overestimated ultimate axial strength values but these strength values are not accomplished any strength intervals.

**4.1.7 Comparison of FEM Model with Model of Han et al. (2011b)**

Han et al. (2011b) also proposed an empirical model extrapolating the ultimate axial strength of the CFDST columns with CHS. Equation 2.11 was used to determine the ultimate axial strengths of the CFDST columns with CHS.

(a)
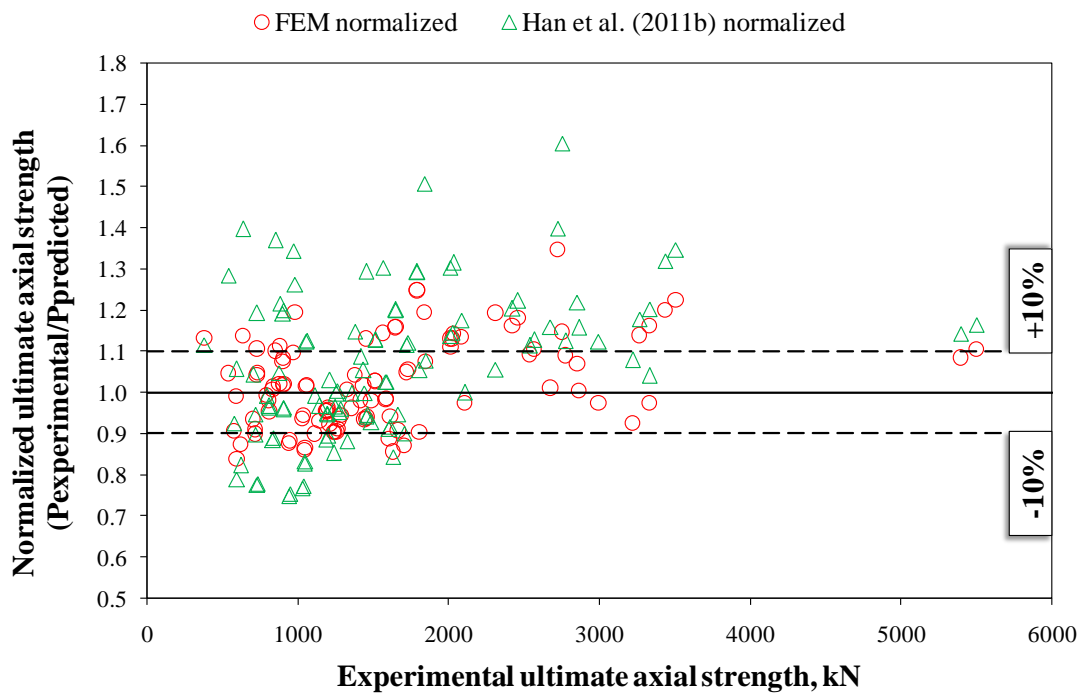


(b)

**Figure 4.19.** (a) predicted and (b) normalized ultimate axial strengths of FEM model and Han et al. (2011b) model versus experimental ultimate axial strengths

Figure 4.19a indicates the predicted ultimate strengths of the proposed FEM model and the model of Han et al. (2011b) versus experimental ultimate axial strengths

while Figure 4.19b shows the normalized ultimate strength values of the proposed FEM model and the model of Han et al. (2011b). The purpose of the presenting the results as graph is the easily visual comparison for the prediction performance of the proposed FEM model against to the model of Han et al. (2011b) formula.

It can be overtly seen in Figure 4.19a that the good prediction performance of the model proposed by Han et al. (2011b) can be succeed up to 2000 kN value of the ultimate strength. However, after this level of ultimate axial strength, the prediction capability of the model decreases.

In Figure 4.19a, the R-squared values of both models are also given. The R-squared value of the proposed FEM model is 0.963 while that of the model of Han et al. (2011b) is 0.939. According to the R-squared values, it can be articulated that the estimation performance of the proposed FEM model is better than that of the model suggested by Han et al. (2011b).

When Figure 4.19b is observed, it can be easily noticed that the model proposed by Han et al. (2011b) has many underestimated ultimate axial strength values. Although the proposed FEM model also has overestimated and underestimated ultimate axial strength values, the number of these over and underestimated values were less than the empirical model proposed by Han et al. (2011b) has. For this reason, good normalized strength value scattering of the proposed FEM model increases its reliability and robustness.

**4.1.8 Comparison of FEM Model with Model of Yu et al. (2013)**

Yu et al. (2013) proposed an empirical model that extrapolates the ultimate axial strength of single skin solid and hollow section concrete filled steel tubular columns. The effect of inner steel tube was added to this formula so that it could be practicable to the CFDST columns with CHS. As a final, Equation 2.13 was obtained and it was used determine the ultimate axial strength of the CFDST columns CHS.

Figure 4.20a indicates the predicted ultimate strengths of the proposed FEM model and the model of Yu et al. (2013) versus experimental ultimate axial strengths while Figure 4.20b shows the normalized ultimate strength values of the proposed FEM model and the model of Yu et al. (2013). The purpose of the presenting the results as

graph is the easily visual comparison for the prediction performance of the FEM model against to the model of Yu et al. (2013) formula.
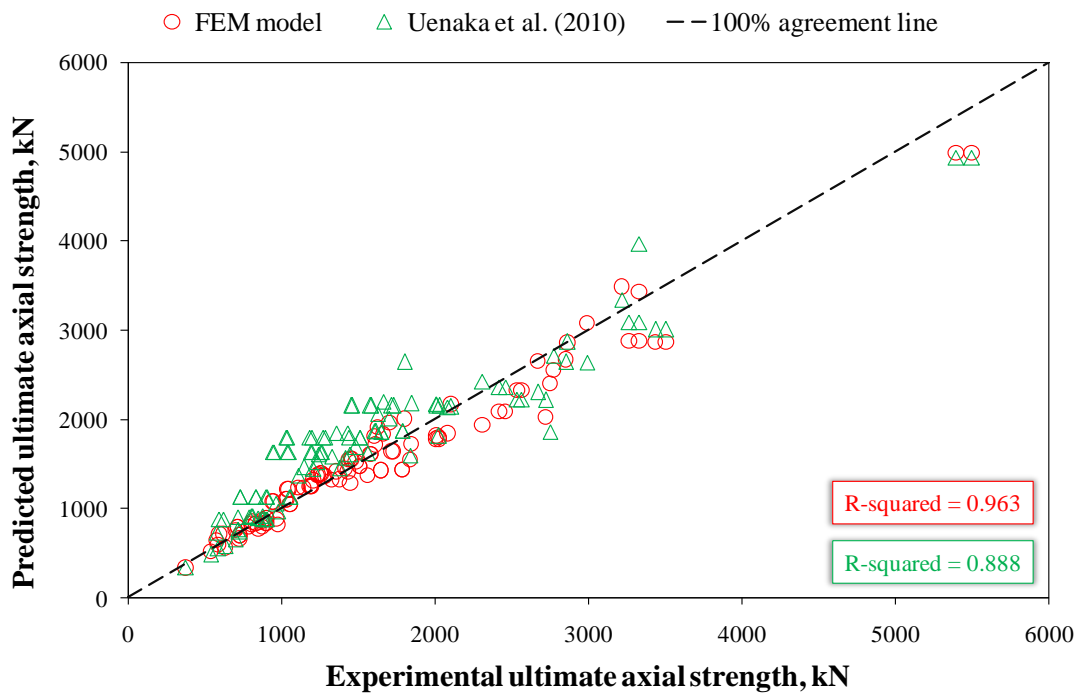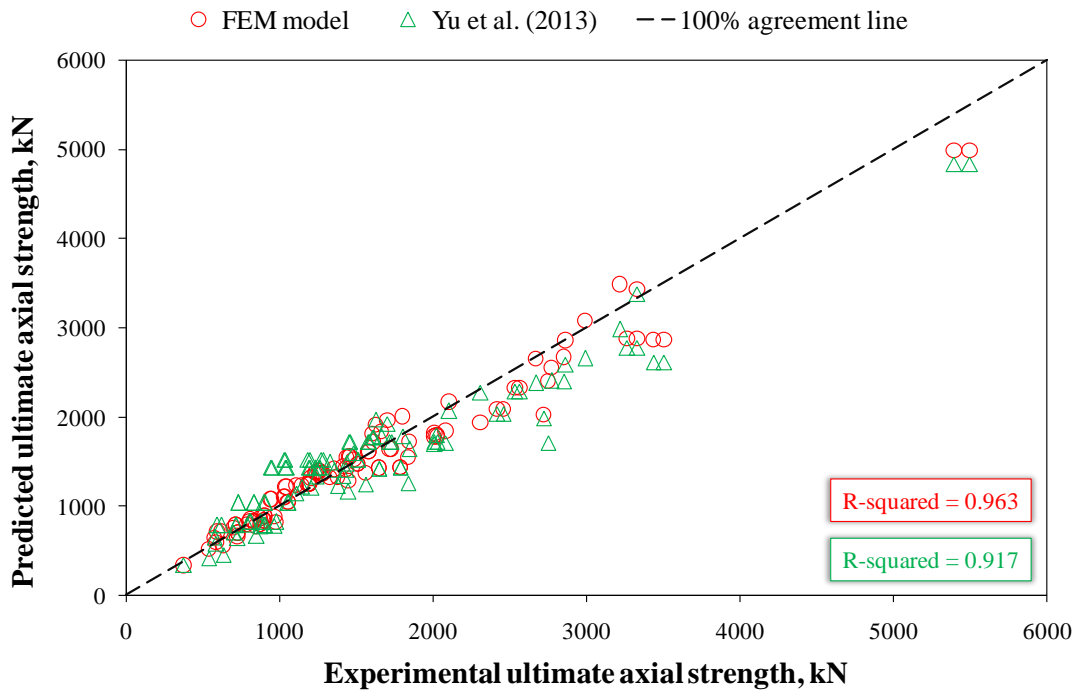


(a)
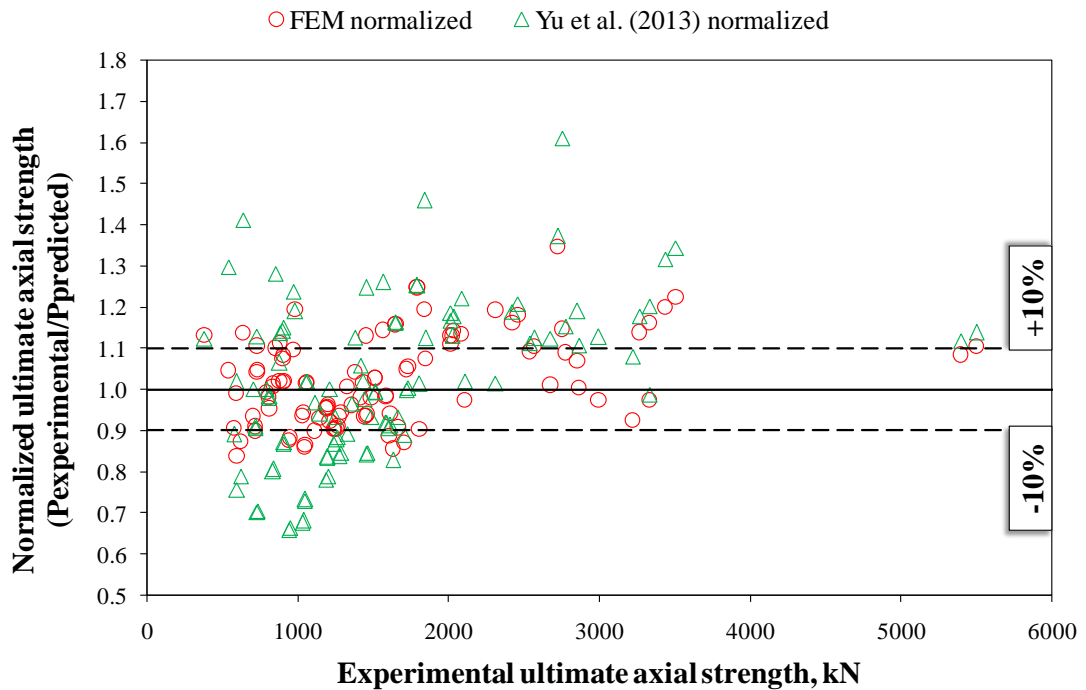


(b)
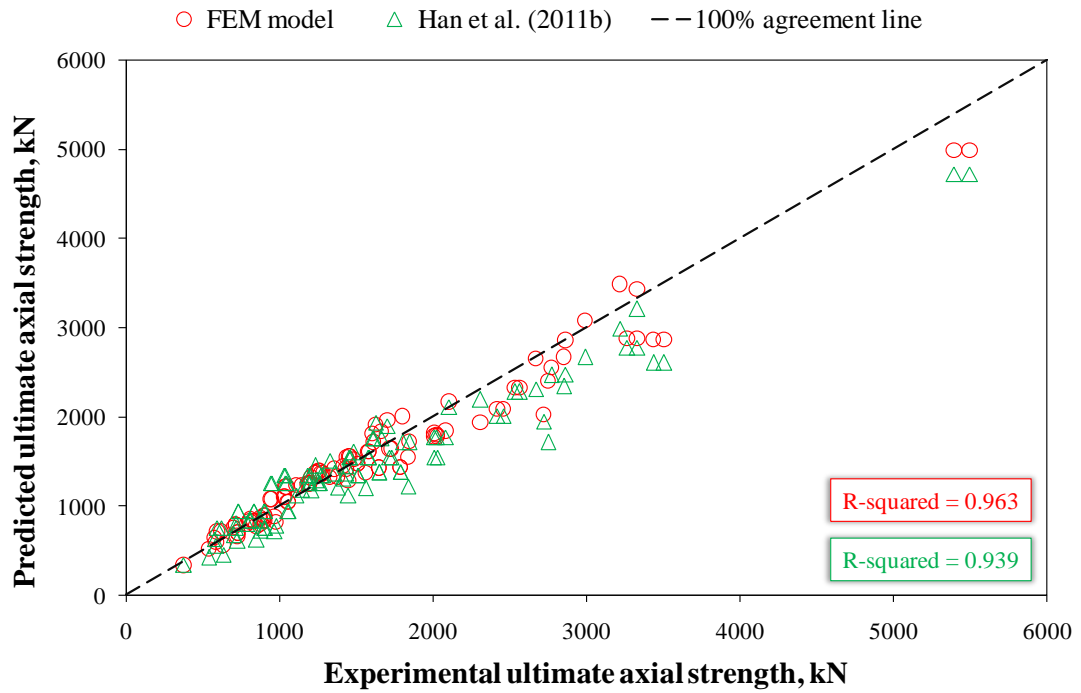
**Figure 4.20.** (a) predicted and (b) normalized ultimate axial strengths of FEM model and Yu et al. (2013) model versus experimental ultimate axial strengths

According to observation of Figure 4.20a, it can be seen that the predicted strength values are amassed around the 100% agreement line, yet, when Figure 4.20b, in which the normalized versus the experimental ultimate axial strength values are plotted, is observed, it can be obviously seen that a great number of normalized ultimate strength values predicted by model of Yu et al. (2013) are at the outside of the normalization limit lines. This situation indicates that the empirical model proposed by Yu et al. (2013) has a lot of over and underestimated ultimate axial strength values. Additionally, by the time, the R-squared values given in Figure 2.20a are compared, the estimation capability of the proposed FEM model would be easily revealed.

### 4.1.9 Comparison of FEM Model with Model of Hassanein et al. (2013b)

The final empirical model extrapolating the ultimate axial strength of the CFDST columns with CHS was proposed by Hassanein et al. (2013b). Equation 2.14 was used to determine the ultimate axial strengths of the CFDST columns with CHS.

Figure 4.21a indicates the predicted ultimate strengths of the proposed FEM model and the model of Hassanein et al. (2013b) versus experimental ultimate axial strengths while Figure 4.21b shows the normalized ultimate strength values of the FEM model and the model of Hassanein et al. (2013b). The purpose of the presenting the results as graph is the easily visual comparison for the prediction performance of the FEM model against to the model of Hassanein et al. (2013b) formula.

The R-squared value of the FEM model is also greater than that of the model suggested by Hassanein et al. (2013b). It means that the ultimate axial strength values predicted by the proposed FEM model are closer to the exact results than the values estimated by the model of Hassanein et al. (2013b). Generally, the model proposed by Hassanein et al. (2013b) performs underestimated ultimate axial strength values when Figure 4.21 is observed. This is another indication for how the prediction capability of the FEM model is better.

As seen in Figure 4.21a, the predicted ultimate axial strengths are accumulated around the 100% agreement line but when the normalized values given in Figure 4.21b are considered, it would be clearly seen that the model proposed by Hassanein

et al. (2013b) has many ultimate axial strength results falling to the outside of normalization limit lines.
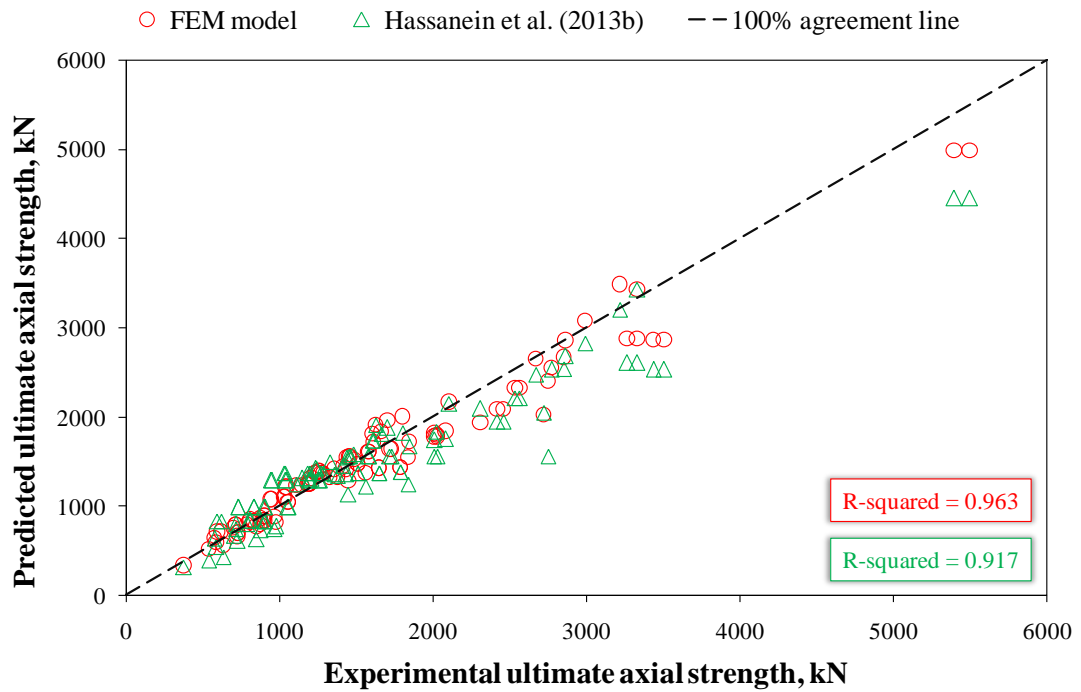


(a)
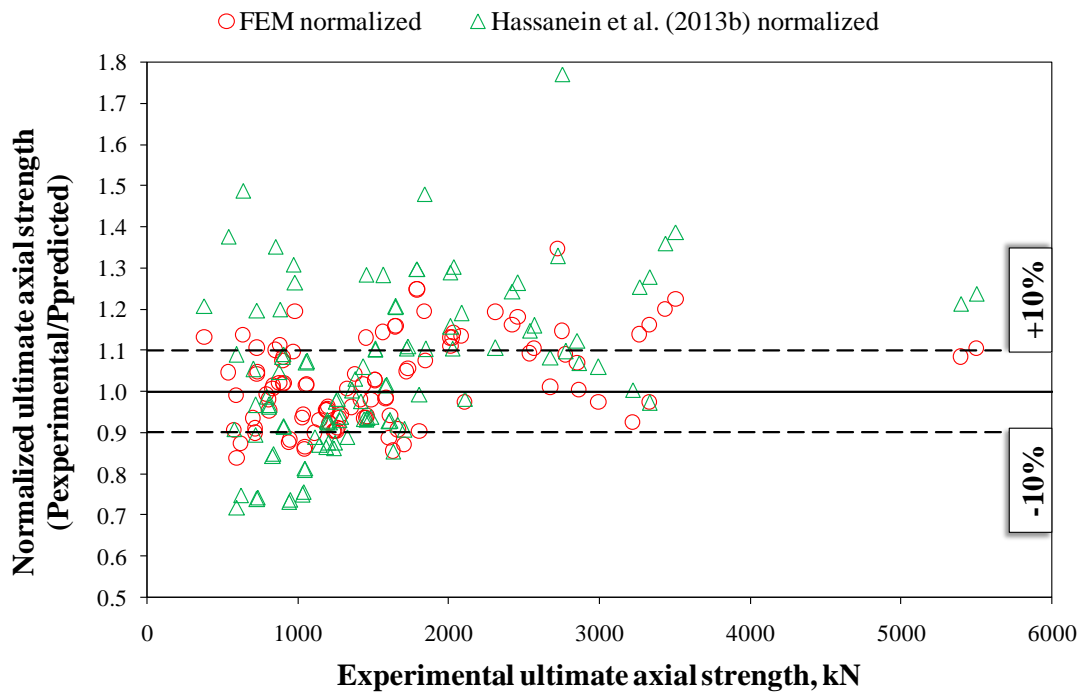


(b)

**Figure 4.21.** (a) predicted and (b) normalized ultimate axial strengths of FEM model and Hassanein et al. (2013b) model versus experimental ultimate axial strengths

**4.1.10 Statistical Comparison of Models**

In addition to graphical comparison of the results, the statistically evaluation of the model is crucially necessary. Therefore, the ultimate axial strength results extrapolated by the proposed FEM model, the modified formulas, and the proposed empirical models are statistically evaluated in this section. The fundamental statistical parameters such as MAPE, MSE, RMSE, COV, and R-squared values of which formulas were given in Chapter 3 are used to evaluate the prediction performance of the models and compare their capabilities. The values of these parameters are tabulated in Table 4.2. In order to visualize these tabulated values, MAPE, MSE, and RMSE values are shown in Figure 4.22a, 4.22b, and 4.22c, respectively, while COV and R-squared values are indicated in Figure 4.23a and 4.23b, respectively.

**Table 4.2.** Statistical parameters of the prediction performance of proposed FEM model and existing design codes and suggested empirical models in the previous studies

| Statistical parameters | Mean absolute percent error (MAPE) | Mean square error (MSE) | Root mean square error (RMSE) | Coefficient of variation (COV) | Coefficient of determination (R-squared) |
|---|---|---|---|---|---|
| FEM | 8.52 | 41515 | 145.9 | 0.104 | 0.963 |
| ACI (2002) | 16.81 | 168726 | 301.0 | 0.192 | 0.936 |
| EC4 (2004) | 8.68 | 45291 | 151.4 | 0.104 | 0.960 |
| AISC (2010) | 14.41 | 129403 | 262.5 | 0.139 | 0.950 |
| Uenaka et al. (2010) | 21.46 | 128636 | 291.2 | 0.186 | 0.888 |
| Han et al. (2011b) | 13.48 | 87481 | 220.6 | 0.160 | 0.939 |
| Yu et al. (2013) | 15.43 | 90708 | 234.3 | 0.180 | 0.917 |
| Hassanein et al. (2013b) | 14.54 | 104162 | 232.5 | 0.178 | 0.917 |

(a)



(b)

(c)

**Figure 4.22.** Statistically comparison FEM model with the modified formulas and suggested empirical models with regard to: (a) MAPE, (b) MSE, and (c) RMSE

The estimation performance of the proposed FEM model is also supported statistically. The lower MAPE, MSE, and RMSE values are the indication of the lower prediction error of the model and the proposed FEM model has the lowest MAPE, MSE, and RMSE values among other modified formulas and proposed empirical models as can be seen in Table 4.2 and Figure 4.22. Within the modified equations of the codes and the proposed empirical models, the highest MAPE, MSE, and RMSE values belong to the model of Uenaka et al. (2010) while the lowest values belong to the modified Eurocode 4 (2004).

Besides, the COV of the normalized ultimate axial strengths and R-squared values are remarkable statistical parameters for such types of models. These two parameters directly give an idea about the estimation capability of the model. The R-squared value is the measurement proportion of a predicted outcome variance. It has to be between 0 and 1 that indicates the performance of prediction. Namely, approaching the value of 1 means better prediction performance while moving away from the value of 1 indicates worse prediction. The lower the COV value, the higher the reliability to the model while the higher the R-squared value, the higher the

118

consistent of model. The proposed FEM model has the lowest COV value and the highest R-squared value as shown in Table 4.2 and Figure 4.23.
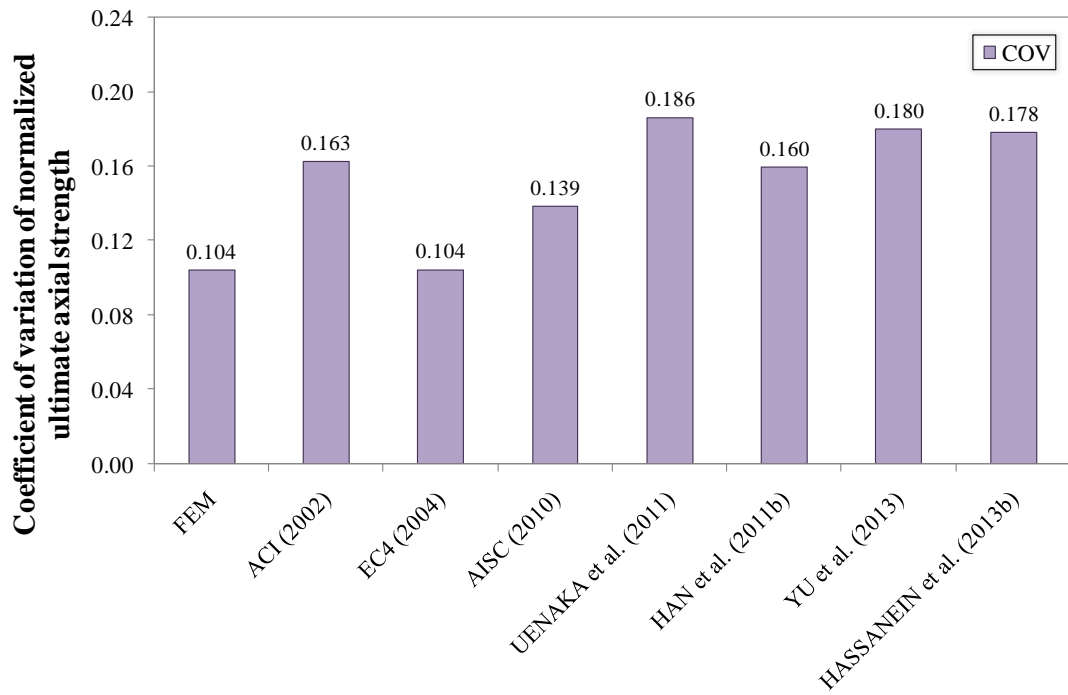


(a)
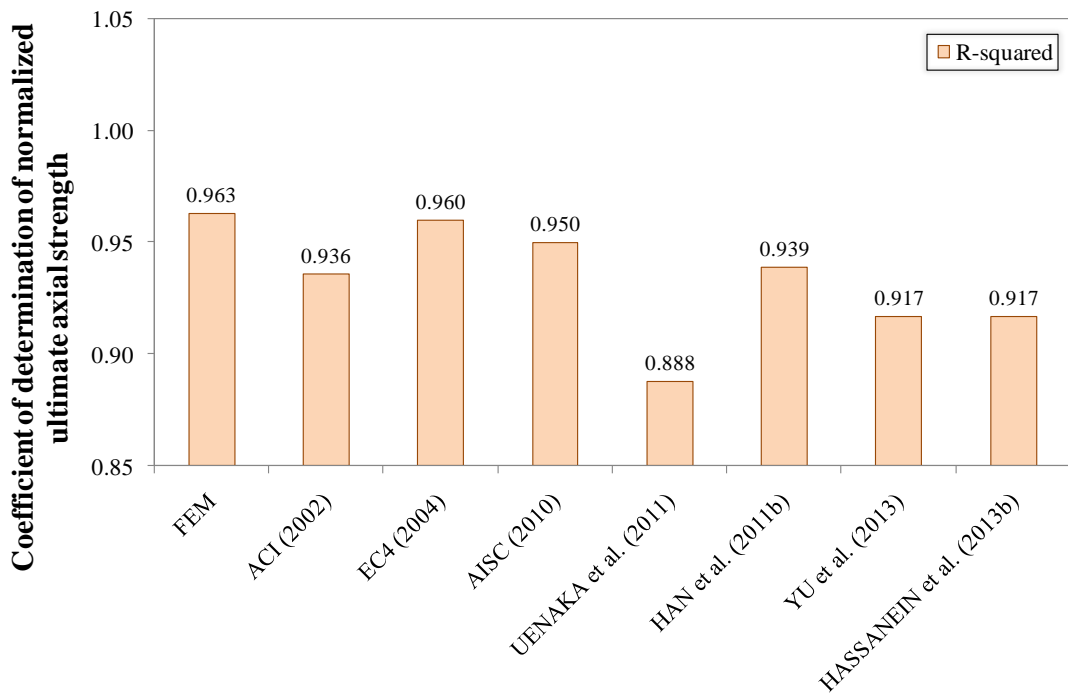


(b)

**Figure 4.23.** Statistically comparison FEM model with the modified formulas and suggested empirical models with regard to: (a) COV and (b) R-squared

Among the existing models, the nearest estimation capableness to the proposed FEM model can be seen in the modified Eurocode 4 (2004) formula with MAPE value of 8.68 and R-squared value of 0.960. Although the statistical results of some models are near to that of the proposed FEM model, the proposed FEM model is still the best than any other proposed model with respect to estimation performance.

Finally, the percent error caused by the models during the prediction of the ultimate axial strength is grouped according to the strength partitions and they are given in Figure 4.24. The ultimate axial strength values are divided into five partitions with the range of 750 kN and the number of data falling in each partition class is also shown in Figure 4.24 as frequency. It can be obviously seen that the modified EC4 (2004) formula has lower percent error value only in the case of the ultimate axial strength value ≤ 750 kN and > 3000 kN while the proposed FEM model performs lower percent error values in the other intervals. For the ultimate axial strength values ≤ 1500 kN, the higher percent error results are achieved from the model suggested by Uenaka et al. (2011) whereas for the strength values > 1500 kN, the worst percent error results are attained from the modified ACI (2002) formula.
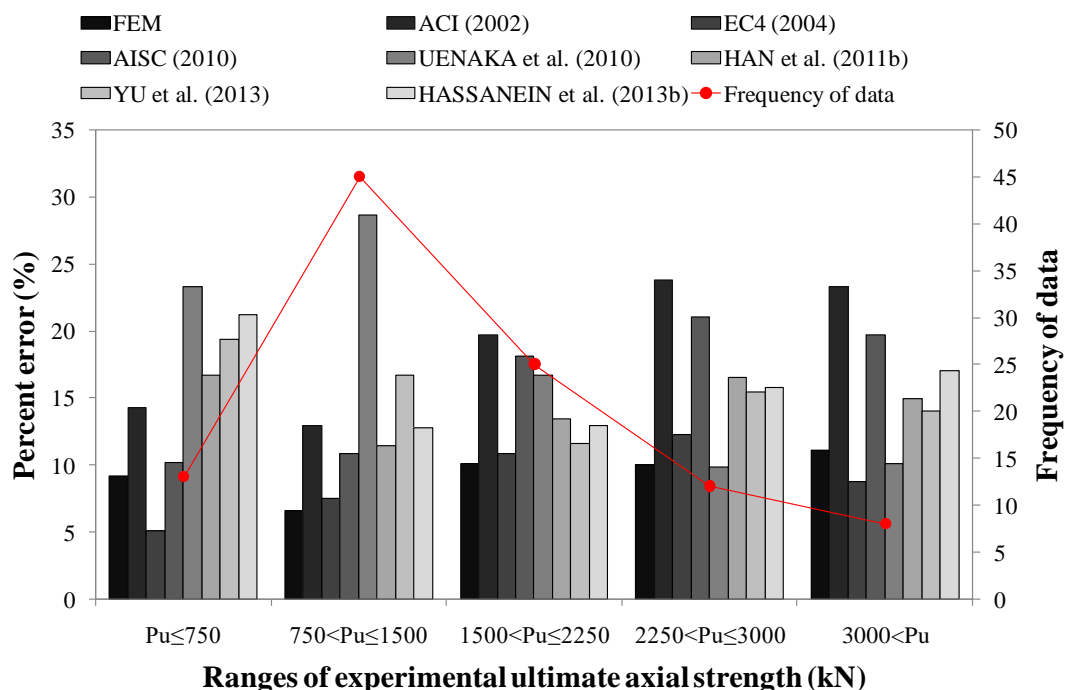


**Figure 4.24.** Error analysis of proposed FEM model, modified code formulas, and suggested empirical models

## 4.2 Gene Expression Programming (GEP) Model Results

In this section, modeling the CFDST columns with CHS regarding the GEP is going to be compared with the formulas modified from the codes and existing proposed empirical models as well as mechanical and sectional properties of elements used in the production of CFDST column specimens. As mentioned in Chapter 3, the data set used in the developing of GEP model was arbitrarily divided into train and test sub-datasets. The train dataset was handled to employ for the enhancement of the developed model whereas the test dataset was used to observe the fitness, predictability, robustness, and repeatability of the proposed mathematical model. Besides, the train and test sub-datasets are also statistically analyzed in order to examine these sub-datasets represent the whole data or not and the results are given in Table 3.3. In this section, firstly the predicted values for the train and test sub-datasets are compared with actual values obtained from the experiments. Then after, the whole predicted values is firstly compared with the material properties and then compared with the existing formulas that were used to predict the ultimate axial strength of the CFDST columns with CHS. The ultimate axial strength values calculated by using Equation 3.11, which was achieved by using GEP technique including both train and test values, are tabulated in Table 4.3 containing also the experimental test results. The normalized ultimate axial strength values of the GEP model, which are calculated by dividing the experimental strength to the predicted strength given in Table 4.3, are presented in Figure 4.25 in order to reveal how the normalized values are dispersed on the normalization line.

**Table 4.3.** Ultimate axial strength values of experiment and GEP prediction

| | Sample | | Experimental ultimate axial strength $(P_u)_{exp}$, kN | Predicted ultimate axial strength $(P_u)_{GEP}$, kN |
|---|---|---|---|---|
| Reference | Number | Identification | | |
| Zhao et al. (2002a) | 1 | C1C7 | 1415.0 | 1434.5 |
| | 2 | C2C7 | 1380.0 | 1363.3 |
| | 3 | C3C7 | 1210.0 | 1277.9 |
| | 4 | C4C7 | 1110.0 | 1239.3 |
| | 5 | C5C8 | 1705.0 | 1685.6 |
| | 6 | C6C8 | 1605.0 | 1686.5 |

**Table 4.3.** (cont'd) Ultimate axial strength values of experiment and GEP prediction

| | Sample | | Experimental ultimate axial strength $(P_u)_{exp}$, kN | Predicted ultimate axial strength $(P_u)_{GEP}$, kN |
|---|---|---|---|---|
| Reference | Number | Identification | | |
| Lin and Tsai (2003) | 7 | DS-06-2-2-C | 2311.0 | 2542.9 |
| | 8 | DS-06-4-2-C | 2750.0 | 2606.6 |
| Tao et al. (2004) | 9 | cc2a | 1790.0 | 1615.0 |
| | 10 | cc2b | 1791.0 | 1615.0 |
| | 11 | cc3a | 1648.0 | 1598.6 |
| | 12 | cc3b | 1650.0 | 1598.6 |
| | 13 | cc4a | 1435.0 | 1580.6 |
| | 14 | cc4b | 1358.0 | 1580.6 |
| | 15 | cc5a | 904.0 | 916.6 |
| | 16 | cc5b | 898.0 | 916.6 |
| | 17 | cc6a | 2421.0 | 2553.9 |
| | 18 | cc6b | 2460.0 | 2553.9 |
| | 19 | cc7a | 3331.0 | 3109.3 |
| | 20 | cc7b | 3266.0 | 3109.3 |
| | 21 | pcc2-1a | 620.0 | 521.0 |
| | 22 | pcc2-1b | 595.0 | 521.0 |
| Lu et al. (2010b) | 23 | C2-C4-SCC1-Ref | 3333.0 | 3299.1 |
| Uenaka et al. (2010) | 24 | c10-375 | 635.0 | 562.8 |
| | 25 | c10-750 | 540.0 | 525.8 |
| | 26 | c10-1125 | 378.3 | 351.9 |
| | 27 | c16-375 | 851.6 | 818.5 |
| | 28 | c16-750 | 728.1 | 672.5 |
| | 29 | c16-1125 | 589.0 | 654.9 |
| | 30 | c23-375 | 968.2 | 972.2 |
| | 31 | c23-750 | 879.1 | 788.6 |
| | 32 | c23-1125 | 703.6 | 984.3 |
| Zhao et al. (2010) | 33 | O1I1-S | 1665.0 | 1612.9 |
| | 34 | O2I1-S | 1441.0 | 1295.4 |
| | 35 | O3I1-S | 1243.0 | 1211.2 |
| | 36 | O4I1-S | 1145.0 | 1219.0 |
| | 37 | O5I2-S | 1629.0 | 1875.0 |
| | 38 | O6I2-S | 1613.0 | 1597.0 |
| | 39 | O7I2-S | 1487.0 | 1250.2 |
| | 40 | O8I2-S | 1328.0 | 1337.0 |
| | 41 | O9I2-S | 1236.0 | 1307.3 |

**Table 4.3.** (cont'd) Ultimate axial strength values of experiment and GEP prediction

| Sample | | | Experimental ultimate axial strength $(P_u)_{exp}$, kN | Predicted ultimate axial strength $(P_u)_{GEP}$, kN |
|---|---|---|---|---|
| Reference | Number | Identification | | |
| Han et al. (2011a) | 42 | DCc-0 | 578.0 | 684.5 |
| | 43 | DCc-1 | 789.0 | 795.7 |
| | 44 | DCc-2 | 715.0 | 795.7 |
| Han et al. (2011b) | 45 | C1-1 | 2537.0 | 2599.2 |
| | 46 | C1-2 | 2566.0 | 2599.2 |
| | 47 | C2-1 | 3436.0 | 3350.7 |
| | 48 | C2-2 | 3506.0 | 3350.7 |
| Dong and Ho (2012) | 49 | D50-5-0 | 2852.0 | 3033.3 |
| Li et al. (2012) | 50 | C1-1 | 5499.0 | 5466.4 |
| | 51 | C1-2 | 5396.0 | 5466.4 |
| Dong and Ho (2013) | 52 | D-A-50-0 | 2865.0 | 2979.8 |
| | 53 | D-B-50-0 | 2674.0 | 2778.5 |
| | 54 | D-A-85-0 | 3218 | 3135.6 |
| | 55 | D-B-85-0 | 2994 | 2946.0 |
| Wang et al. (2014) | 56 | 0HA0 | 980.0 | 783.4 |
| | 57 | 0HB0 | 715.0 | 885.2 |
| Essopjee and Dundu (2015) | 58 | S139.2-1.0 | 1059.2 | 1130.9 |
| | 59 | S139.2-1.0 | 1056.1 | 1106.0 |
| | 60 | S139.2-1.5 | 905.5 | 879.7 |
| | 61 | S139.2-1.5 | 901.6 | 836.1 |
| | 62 | S139.2-2.0 | 831.7 | 935.0 |
| | 63 | S139.2-2.0 | 837.4 | 871.8 |
| Essopjee and Dundu (2015) | 64 | S139.2-2.5 | 732.1 | 654.2 |
| | 65 | S139.2-2.5 | 729.0 | 755.7 |
| | 66 | S152.4-1.0 | 1263.5 | 1298.8 |
| | 67 | S152.4-1.0 | 1254.9 | 1113.8 |
| | 68 | S152.4-1.5 | 1195.6 | 1167.6 |
| | 69 | S152.4-1.5 | 1191.2 | 1023.2 |
| | 70 | S152.4-2.0 | 1047.3 | 1055.9 |
| | 71 | S152.4-2.0 | 1041.6 | 1122.1 |
| | 72 | S152.4-2.5 | 941.4 | 942.8 |
| | 73 | S152.4-2.5 | 949.0 | 815.6 |
| | 74 | S165.1-1.0 | 1512.3 | 1483.6 |
| | 75 | S165.1-1.0 | 1510.6 | 1324.9 |
| | 76 | S165.1-1.5 | 1286.4 | 1375.0 |

**Table 4.3.** (cont'd) Ultimate axial strength values of experiment and GEP prediction

| Sample | | | Experimental ultimate axial strength $(P_u)_{exp}$, kN | Predicted ultimate axial strength $(P_u)_{GEP}$, kN |
|---|---|---|---|---|
| Reference | Number | Identification | | |
| Essopjee and Dundu (2015) | 77 | S165.1-1.5 | 1275.1 | 1200.7 |
| | 78 | S165.1-2.0 | 1187.2 | 1258.1 |
| | 79 | S165.1-2.0 | 1199.8 | 1224.5 |
| | 80 | S165.1-2.5 | 1028.0 | 1108.4 |
| | 81 | S165.1-2.5 | 1036.5 | 1006.9 |
| | 82 | S193.7-1.0 | 2010.0 | 1941.3 |
| | 83 | S193.7-1.0 | 2030.0 | 1814.8 |
| | 84 | S193.7-1.5 | 1730.0 | 1840.4 |
| | 85 | S193.7-1.5 | 1720.0 | 1657.2 |
| | 86 | S193.7-2.0 | 1581.6 | 1685.3 |
| | 87 | S193.7-2.0 | 1584.1 | 1731.6 |
| | 88 | S193.7-2.5 | 1451.4 | 1511.9 |
| | 89 | S193.7-2.5 | 1458.7 | 1395.0 |
| Abbas et al. (2016) | 90 | CB2-40NG-AB-CP | 1805.0 | 1770.7 |
| Wang et al. (2016) | 91 | HC22X4-C40 | 1450.0 | 1481.6 |
| | 92 | HC32X6-C40 | 1562.0 | 1761.8 |
| | 93 | HC38X8-C40 | 1838.4 | 1851.3 |
| | 94 | HC55X11-C40 | 2724.0 | 2527.9 |
| | 95 | HC89X4-C40 | 2024.9 | 1943.0 |
| | 96 | HC22X4-C80 | 1845.1 | 1911.0 |
| | 97 | HC32X6-C80 | 2012.5 | 1946.8 |
| Wang et al. (2016) | 98 | HC38X8-C80 | 2083.4 | 2031.4 |
| | 99 | HC55X11-C80 | 2775.0 | 2826.9 |
| | 100 | HC89X4-C80 | 2107.4 | 2070.4 |
| Hastemoğlu (2017) | 101 | DSCFT 3 | 807.0 | 802.3 |
| | 102 | DSCFT 4 | 810.0 | 867.5 |
| | 103 | DSCFT 5 | 877.0 | 922.5 |

The normalized results procured from the GEP model perform a good scattering around the normalization line. Only a few numbers of the normalized values are at the outside of the normalization limit lines of ±10%. According to this good dispersion, it could be absolutely expressed that the model developed by using GEP has a good estimation performance.
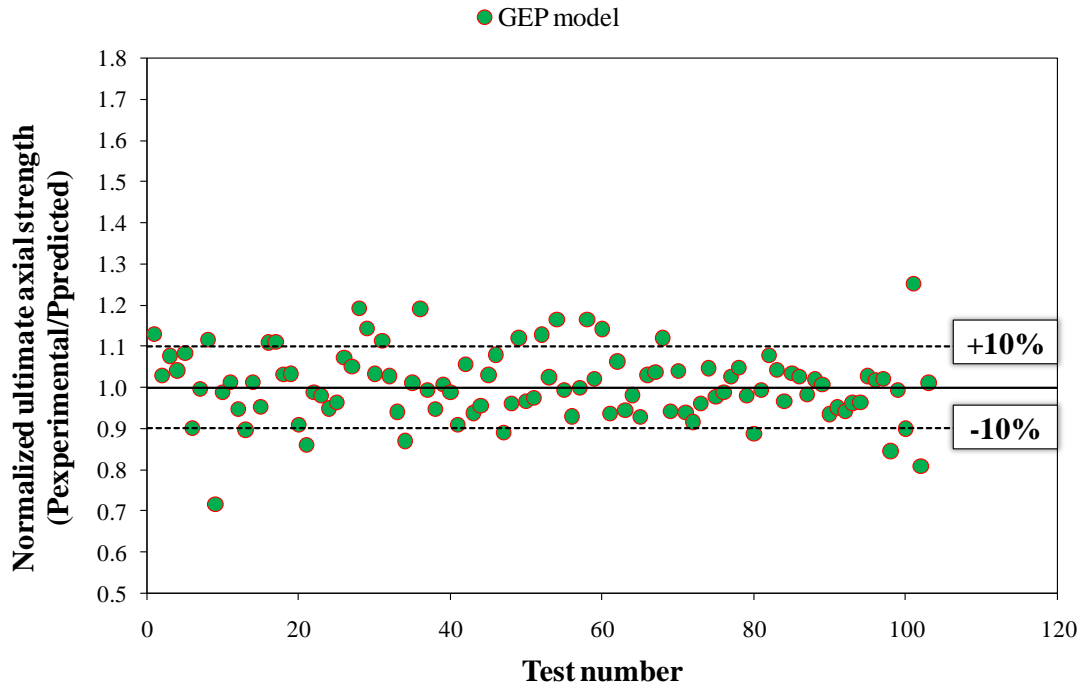
**Figure 4.25.** Prediction performance of GEP model based on normalized ultimate axial strength values

### 4.2.1 Comparison of Train and Test Sub-datasets for GEP Model

The comparisons of predicted ultimate axial strengths for train and test sub-datasets with the experimental results are submitted in Figure 4.26a and 4.26b, respectively. The graphically presentation indicates a good matching of the experimental results with the predicted results. The model developed by using GEP has the capability to predict the ultimate axial strength value at various strength levels as can be seen in Figure 4.26. From the lowest strengths to the highest, the GEP model performs a good predictivity for both train and test sub-datasets.

In order to evaluate the correlation between the experimental and the predicted strength values with respect to the R-squared values, they are also presented in Figure 4.27, where the experimental versus predicted ultimate axial strength values are plotted. As seen from Figure 4.27a and 4.27b, the R-squared values of 0.987 were achieved for the both train and test sub-datasets, respectively, in the developing of the GEP model. This indicates that the train and test sub-datasets strongly reflects all dataset and also it is the manifestation of a strong correlation between actual and predicted values. In addition, the robustness and appropriate correctitude of the GEP model could be manifested by obtaining the proximate R-squared values.
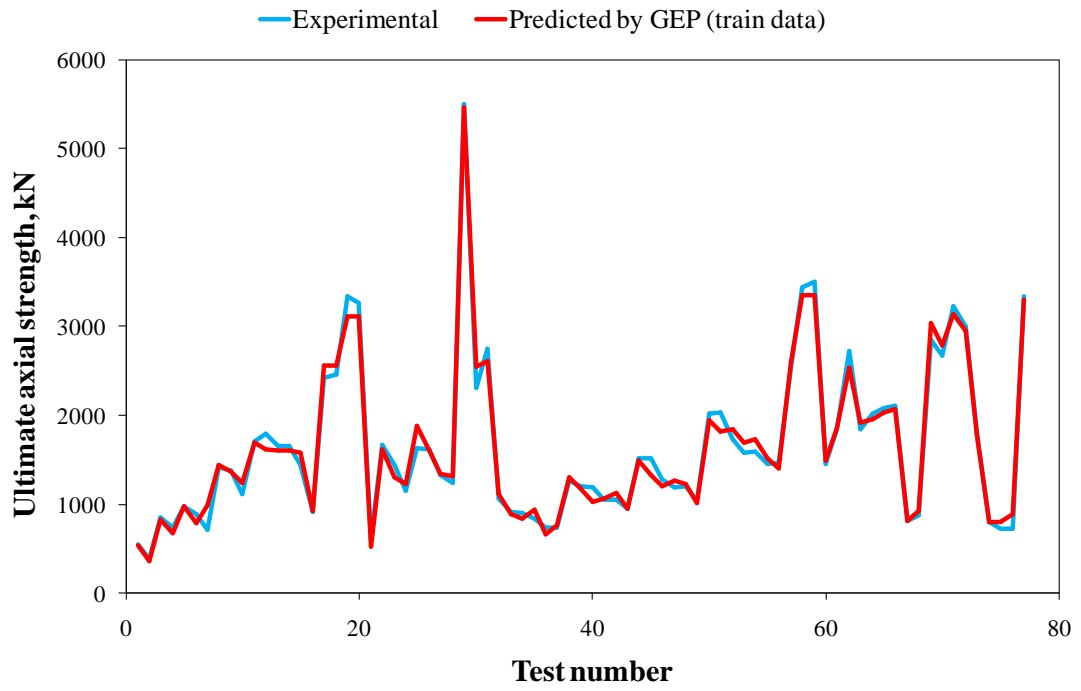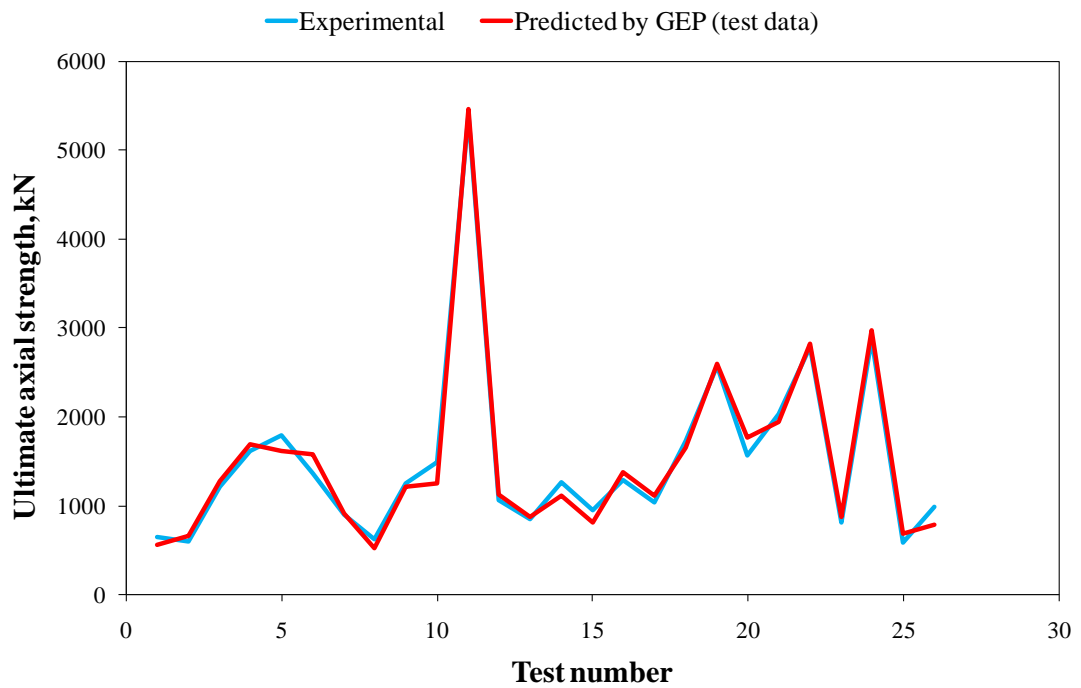
**Figure 4.26.** GEP prediction and experimental ultimate axial strength values of: (a) train and (b) test sub-datasets
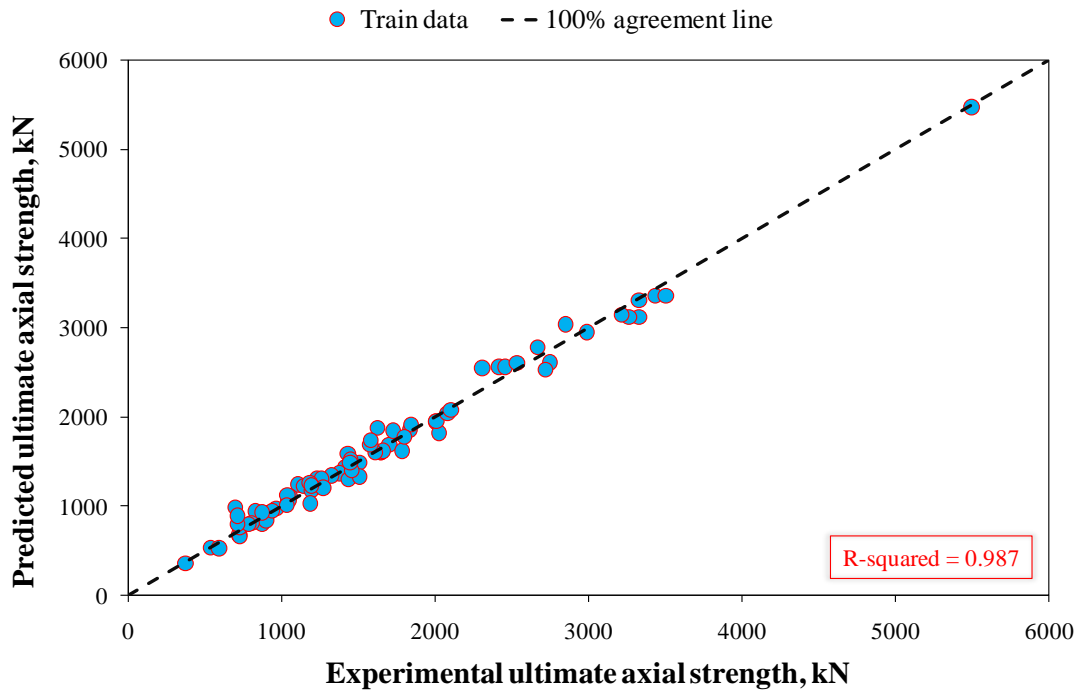
(a)
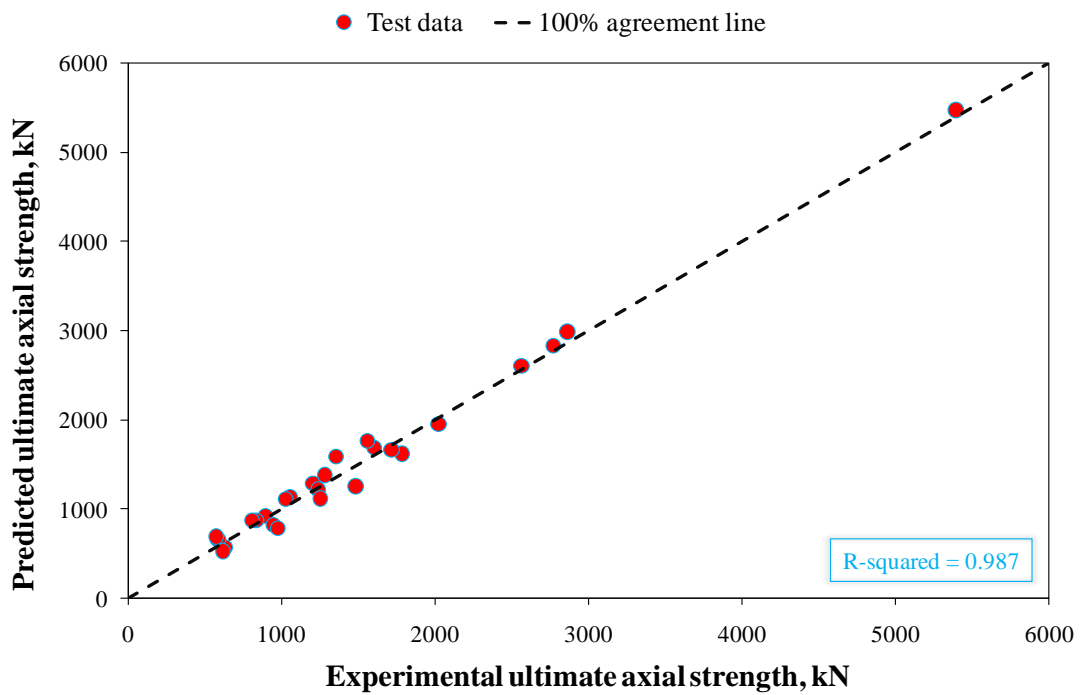


(b)

**Figure 4.27.** GEP prediction versus experimental ultimate axial strength values for: (a) train and (b) test sub-datasets

127

### 4.2.2 Comparison of GEP Model with Element Properties

In order to indicate how the prediction performance of the GEP model varied with respect to the mechanical properties of the element, the ultimate axial strengths extrapolated by applying the GEP model are shown in Figure 4.28a, 4.28b, and 4.28c according to the yield strength of outer/inner steel tubes and compressive strength of concrete annulus, respectively.

The graphical presentation exhibits that the GEP model has a good prediction performance whatever yield strength of outer and inner steel tubes. The yield strength values for outer steel tubes vary between 200 and 600 MPa as seen in Figure 4.28a and the GEP model has the estimated values close to the actual values for each outer steel tube yield strength values. The same interpretations could be done for the relation between actual and predicted ultimate axial strengths versus inner steel tube yield strength as can be clearly seen in Figure 4.28b. The concrete strength was another factor playing a significant role on the load carrying capacity of the CFDST columns with CHS. The concrete classes used in the studies changes from the low-strength concrete to the high-strength. Figure 4.28c pointed out that the GEP model could sensitively predict the ultimate axial strength of such types of columns without discriminating concrete strength.
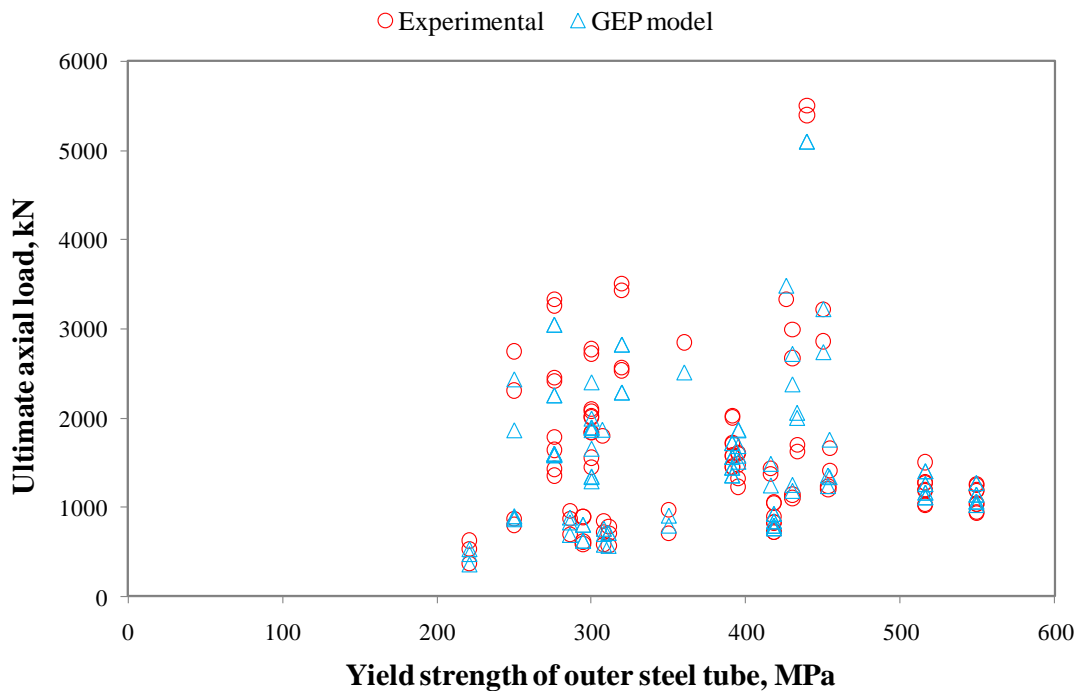


(a)
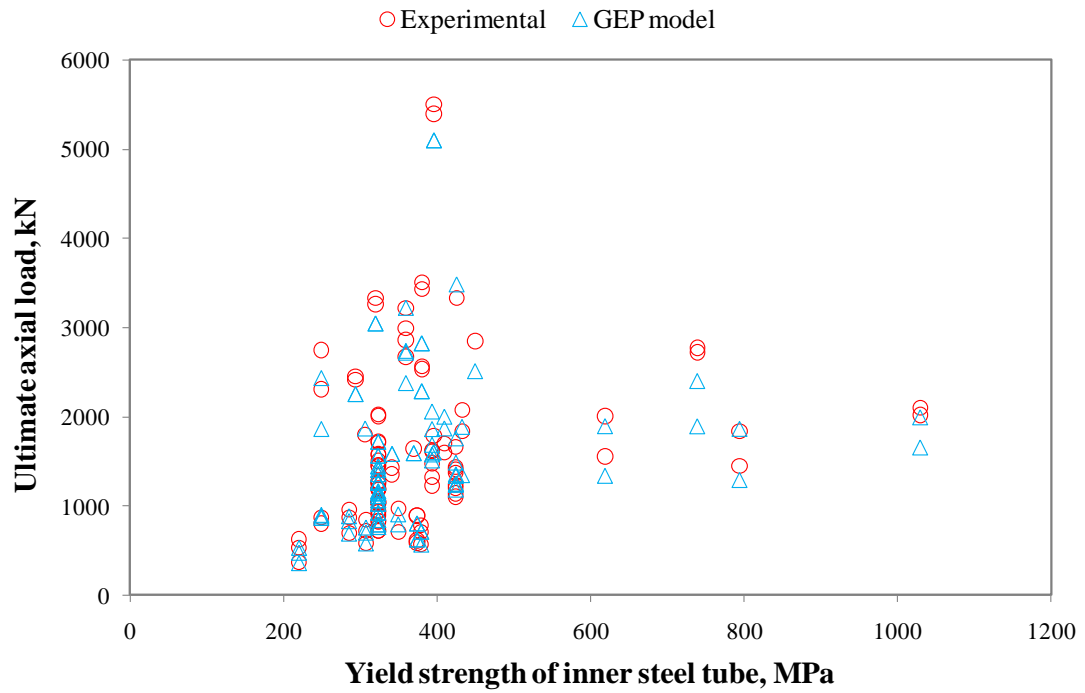
(b)
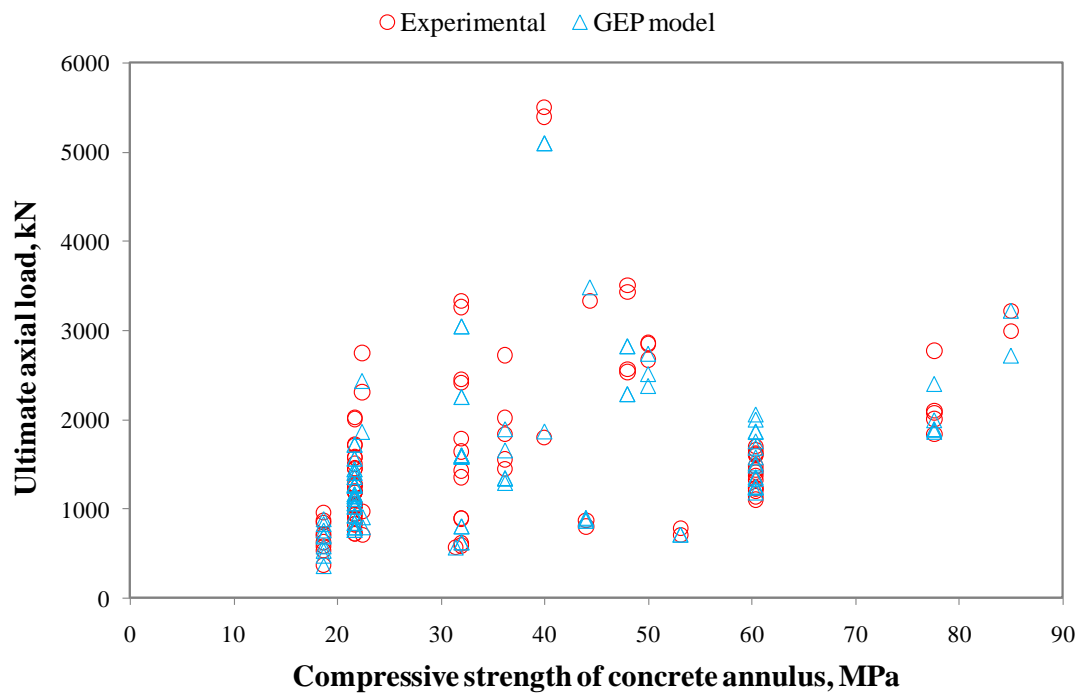


(c)

**Figure 4.28.** Experimental and GEP prediction ultimate axial strength versus: (a) yield strength of outer steel tube, (b) yield strength of inner steel tube, and (c) compressive strength of concrete annulus

129

As a result, it can be absolutely expressed that the proposed FEM model has a good prediction capability whatever the strengths of elements are.



(a)



(b)

130
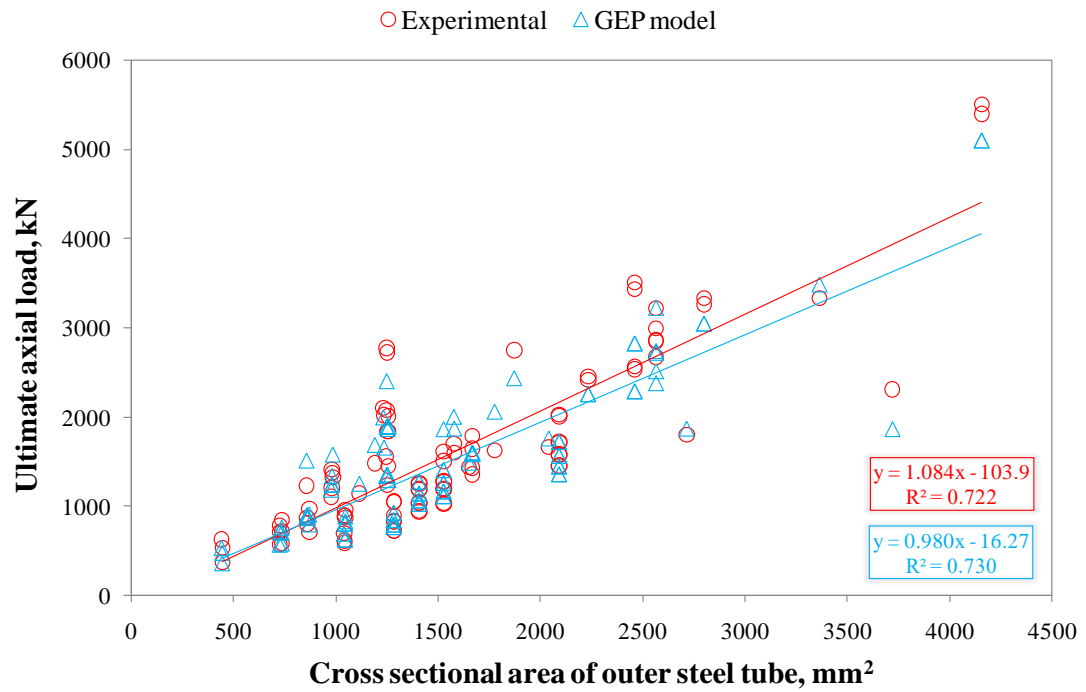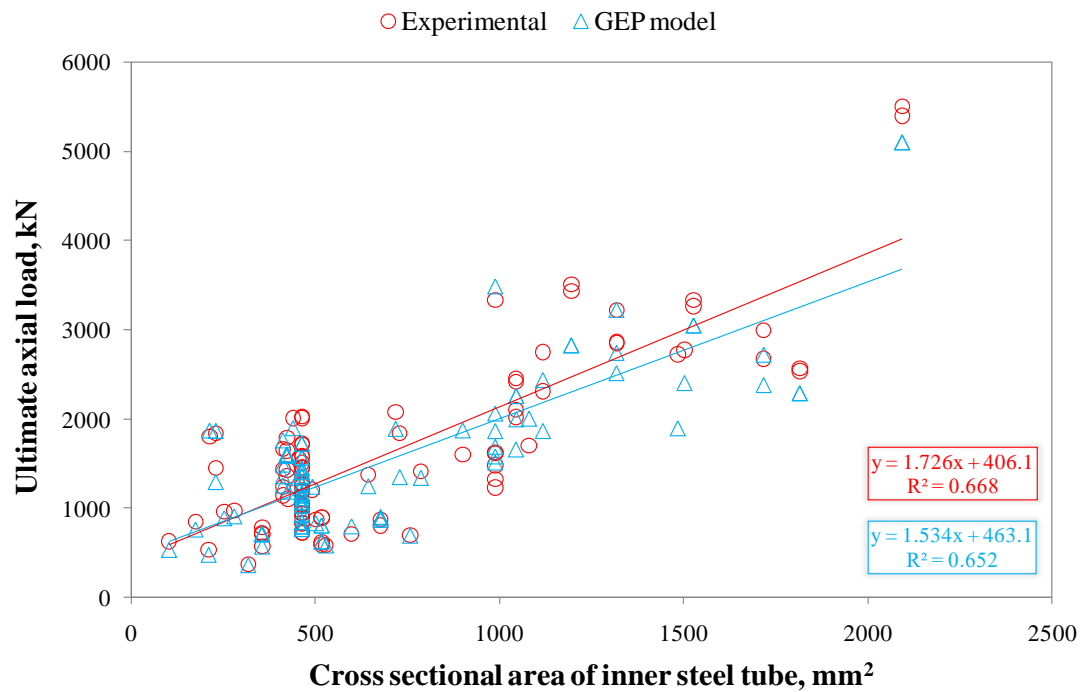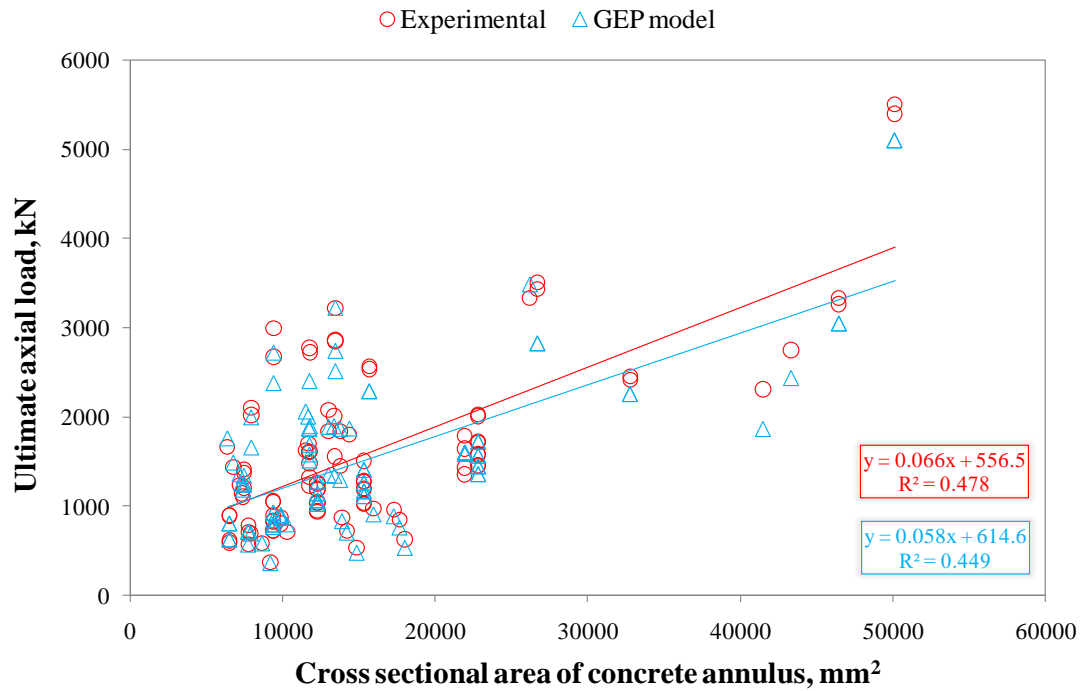
**Figure 4.29.** Experimental and GEP prediction ultimate axial strengths versus cross-sectional area of: (a) outer steel tube, (b) inner steel tube, and (c) concrete annulus

In addition, the cross-sectional areas of the outer/inner steel tubes and concrete annulus have remarkable influences on the load carrying capacity of the CFDST columns with CHS as much as the yield strength of steel tubes and compressive strength of concrete. Therefore, the graphical comparison of the actual and predicted ultimate axial strength values versus the cross-sectional area of the outer steel tube, the inner steel tube, and the concrete annulus are illustrated in Figure 4.29a, 4.29b, and 4.29c, respectively. There is a reasonable linearly increasing relation between the cross-sectional area of the members and the experimental ultimate axial strength. This relation could be seen for cross-sectional area of all members. Namely, when the cross-sectional area of the member increases, the ultimate axial strength also increases.

The same trend could be seen for the relation between the predicted ultimate axial strength and the cross-sectional area as well. The relation between the cross-sectional area and ultimate axial strength is almost similar for both actual and predicted values as can be comprehended from the R-sqaured values given in Figure 4.29a, 4.29b, and 4.29c.

131

The level of the relation between the cross-sectional area and ultimate axial strength could be understood from the R-squared values. It could be said that there is a normal relation level between the cross-sectional area and the load carrying capacity for steel tubes whereas the level of this relation for concrete could be accepted as poor. But the important point herein is that the R-squared values for predicted ultimate axial strength values are almost same with that for actual values. This close value R-squared means that the prediction performance of the model is good and reliable.

Although the load carrying capacity of the CFDST columns with CHS are significantly determined by the mechanical properties of the used materials and their cross-sectional areas, the length and the diameter of members used in the preparation of specimen as well as the amount of hollow part have also important influences on the ultimate axial strength of these columns. Because of that, Figures 4.30a, 4.30b, and 4.30c are presented to comprehend the effect of these parameters and how the GEP model results vary according to the changing in these parameters.

The GEP model had the ability to extrapolate the load carrying capacity of these columns without exception $L/D_o$ value. Namely, it cannot be specified about the developed GEP model that it is able to predict the ultimate axial strength of columns that have a certain $L/D_o$ value. The developed GEP model has a prediction performance by which the ultimate axial strength f CFDST columns can be determined whatever their $L/Do$ values are. This situation is also identical for $D_o/t_o$ and hollow ratio values as can be obviously experienced from the observing of Figures 4.30b and 4.30c.

As a result, it can be summarized that the model generated the GEP is not influenced from the sectional and geometric properties of materials and the developed GEP model has a general estimation performance. By this, it can be expressed that the developed GEP model can predict the load carrying capacity of CFDST column with various material strengths, cross-sections, and lengths. This is the superior side of the developed GEP model. Because the proffered models in the literature have some restriction for determination of the ultimate axial strength of such composite columns such as steel tube diameter, column length, concrete class, and steel tube yield strength.
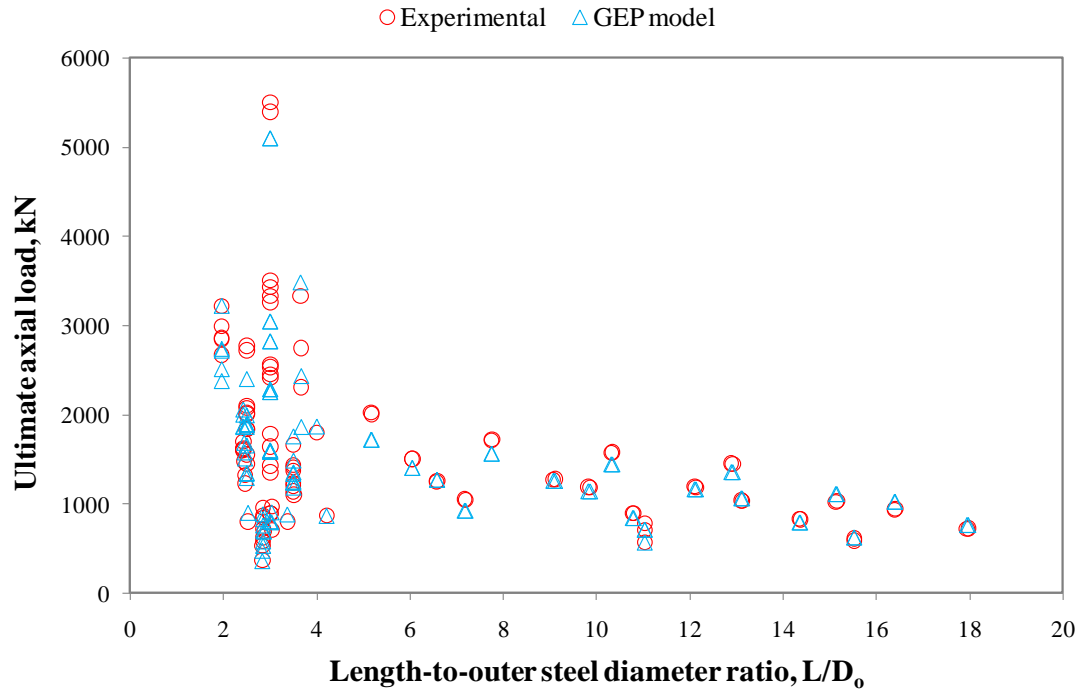
(a)
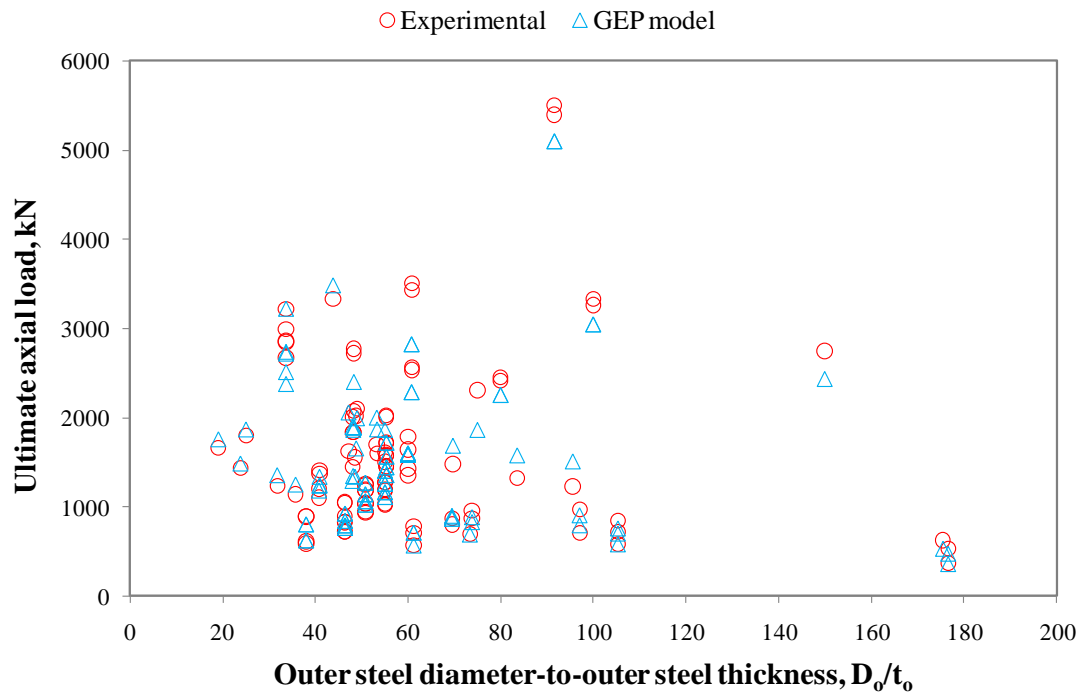


(b)
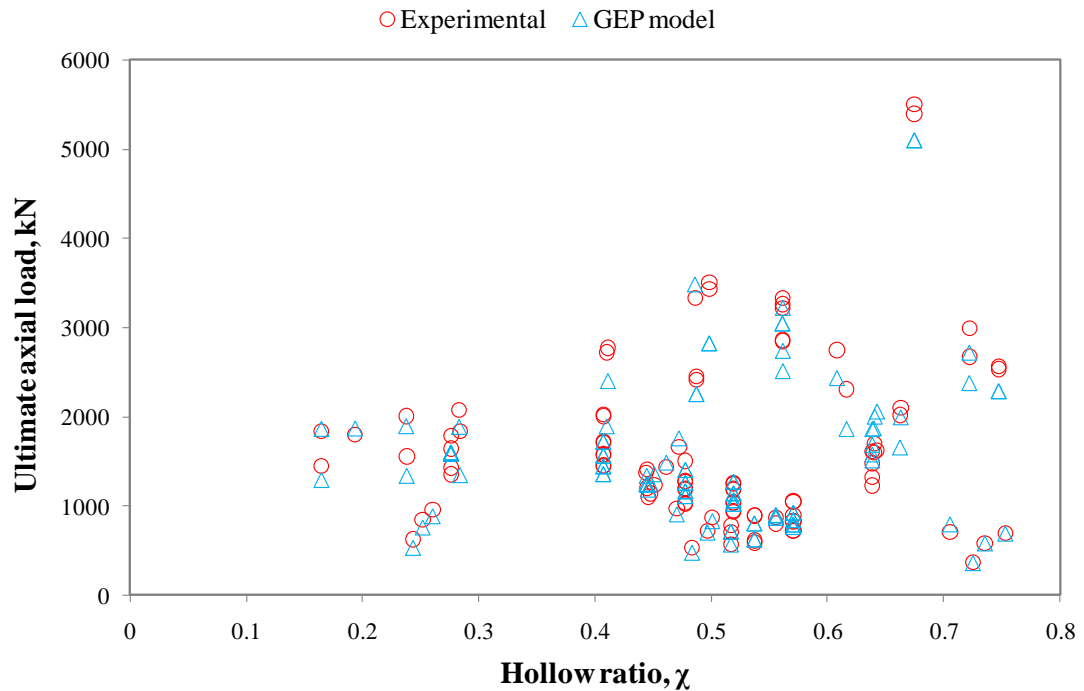
(c)

**Figure 4.30.** Experimental and GEP prediction ultimate axial strength versus: (a) length-to-outer steel tube ratio ($L/D_o$), (b) outer steel diameter-to-outer steel thickness ($D_o/t_o$), and (c) hollow ratio ($\chi$)

### 4.2.3 Comparison of GEP Model with Modified ACI (2002) Formula

The ultimate axial strength estimated by the GEP model and the modified ACI (2002) formula versus experimental ultimate axial strengths are given in Figure 4.31a whereas the normalized ultimate axial strength values of the GEP model and the modified ACI (2002) formula are plotted in Figure 4.31b. The easily visual comparison for the prediction performance of the GEP model against to the modified ACI (2002) formula is aimed by the graphical presentation of the results.

When Figure 4.31a is observed, it can be seen that the ultimate axial strengths extrapolated by the modified ACI (2002) formula are dispersed far away from the 100% agreement line while the strengths predicted by the GEP model are amassed close around to this line. Furthermore, the same situation can be inferred when Figure 4.31b is beheld. The many normalized values achieved from the modified ACI (2002) formula are dispersed throughout above of the +10% normalization limit line, which is the indication of underestimated ultimate axial strength values by this

formula. On the other hand, a few number of the GEP model values are at the outside of the normalization limit lines whereas the rest well scattered between the limitation lines.
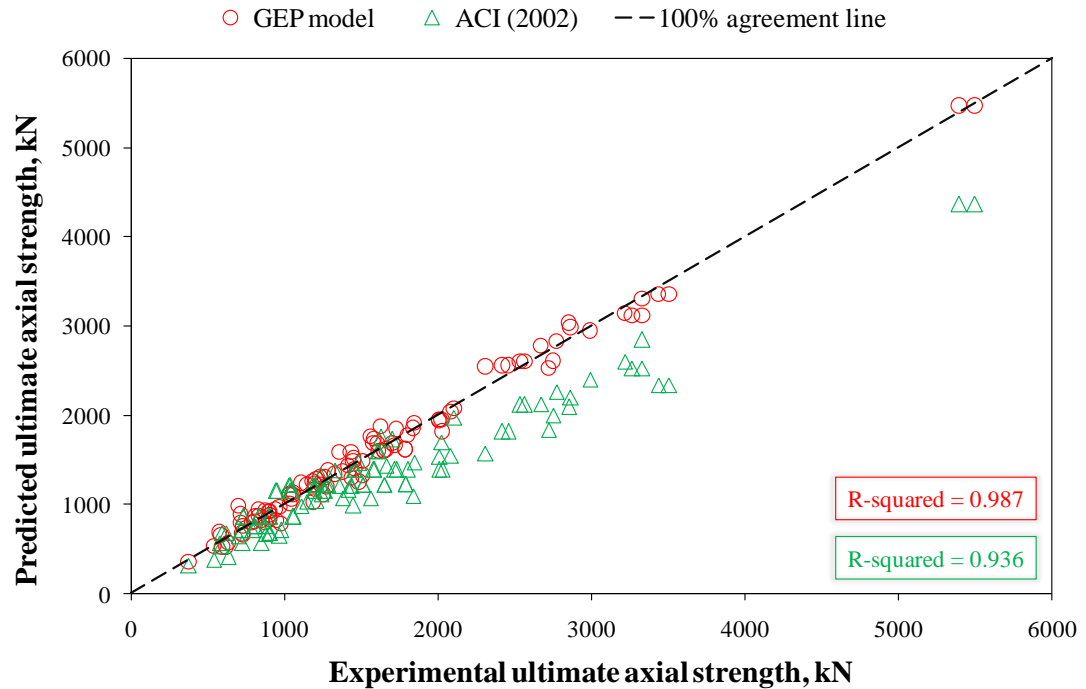


(a)
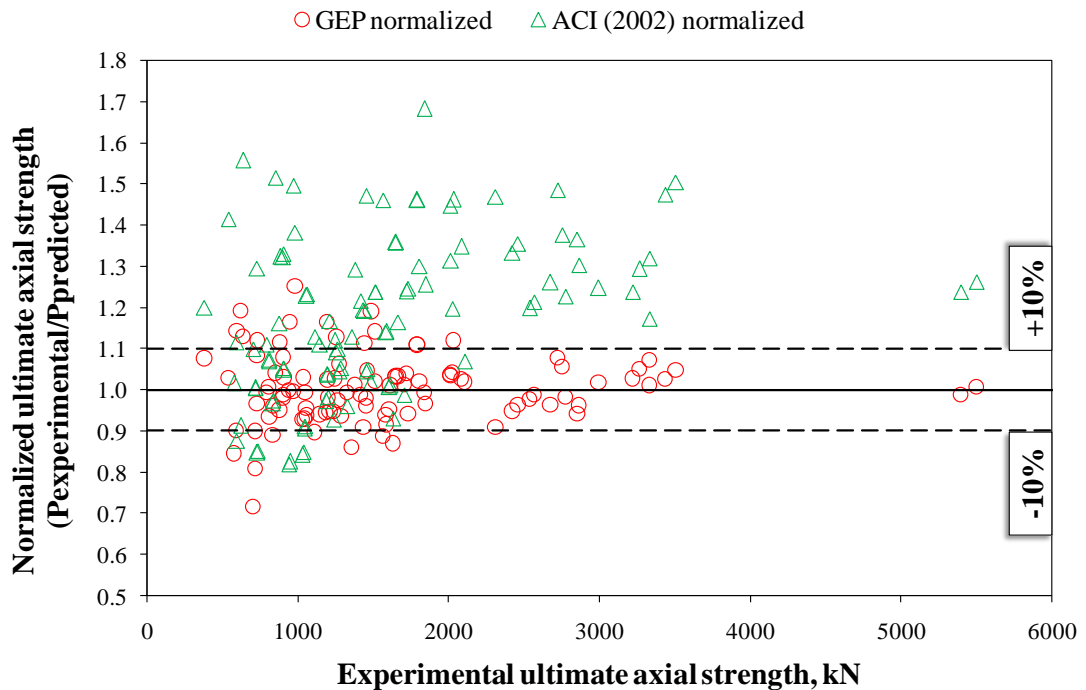


(b)

**Figure 4.31.** (a) predicted and (b) normalized ultimate axial strengths of GEP model and modified ACI (2002) formula versus experimental ultimate axial strengths

135

Besides, the R-squared values of both models are presented in Figure 4.31a. The difference between the R-squared values of the developed GEP model and the modified ACI (2002) formula describes the difference between prediction performances of both models. Briefly, it can be articulated about the developed GEP model having higher R-squared value that its estimation performance is much better than that of the modified ACI (2002) formula.

**4.2.4 Comparison of GEP Model with Modified Eurocode 4 (2004) Formula**

The ultimate axial strength estimated by the GEP model and the modified Eurocode 4 (2004) formula versus experimental ultimate axial strengths are given in Figure 4.32a whereas the normalized ultimate strength values of the GEP model and the modified Eurocode 4 (2004) formula are plotted in Figure 4.32b. The easily visual comparison for the prediction performance of the GEP model against to the modified Eurocode 4 (2004) formula is aimed by the graphical presentation of the results.

The graphical exhibition of the results reveals that both the GEP model and the modified Eurocode 4 (2004) formula has good prediction capability but the performance of the GEP model is unequivocally better especially when the R-squared values are taken into consideration. The R-squared value of GEP model is 0.987 whilst that of modified Eurocode 4 (2004) formula is 0.960. The results interspersion on the graph for the GEP model and the modified Eurocode 4 (2004) formula are identical, yet, some underestimated ultimate axial strengths are determined in the case of the modified Eurocode 4 (2004) formula used. This can be viewed in both Figure 4.32a and 4.32b.

In addition, both has a few number of strength values falling at outside of the normalization limits. But the number of strength values being out of the normalization limit lines for the GEP model is less than that for the modified Eurocode 4 (2004) formula. These assessments support that the GEP model has a better prediction performance than the modified Eurocode 4 (2004) formula.

Besides, the GEP model results amass around the 100% agreement line while the modified Eurocode 4 (2004) formula has some results far away from that line particularly ultimate axial strength value between 2000 and 4000 kN. This is the indication of that the generated GEP model has a robust and reliable estimation

capability than the modified Eurocode 4 (2004) formula. It can overtly be expressed that the GEP model has more accurate and believable results no matter what is the ultimate axial strength.
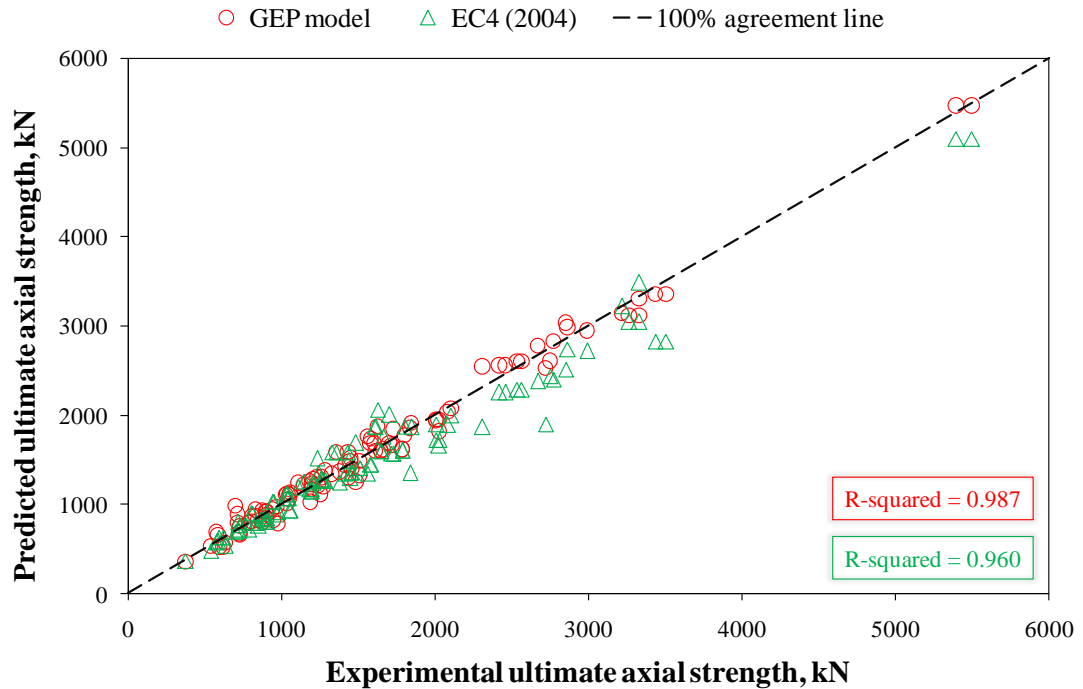


(a)
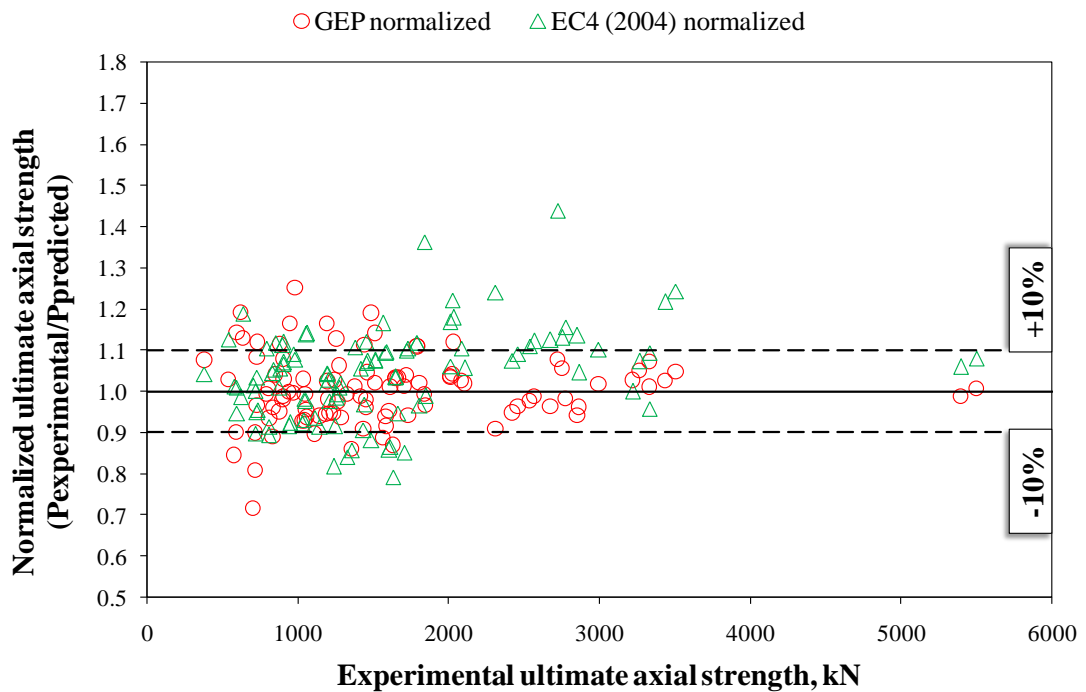
(b)

**Figure 4.32.** (a) predicted and (b) normalized ultimate axial strengths of GEP model and modified EC4 (2004) formula versus experimental ultimate axial strengths

### 4.2.5 Comparison of GEP Model with Modified AISC (2010) Formula

The ultimate axial strength estimated by the GEP model and the modified AISC (2010) formula versus experimental ultimate axial strengths are given in Figure 4.33a whereas the normalized ultimate axial strength values of the GEP model and the modified AISC (2010) formula are plotted in Figure 4.33b. The easily visual comparison for the prediction performance of the GEP model against to the modified AISC (2010) formula is aimed by the graphical presentation of the results.

The GEP model has the R-squared value of 0.987 while the modified AISC (2010) formula had the R-squared value of 0.950. Since the R-squared value directly reflects the correlation between the predicted and the actual results, it can be absolutely stated that the ultimate axial strengths determined by the developed GEP model are much better than that predicted by using the modified AISC (2010) formula.

The results interspersion on the graph for the GEP model is identical, but, a lot of underestimated ultimate axial strengths are determined in the case of the modified AISC (2010) formula used. This could be seen in both Figure 4.33a and 4.33b.



(a)

138

(b)
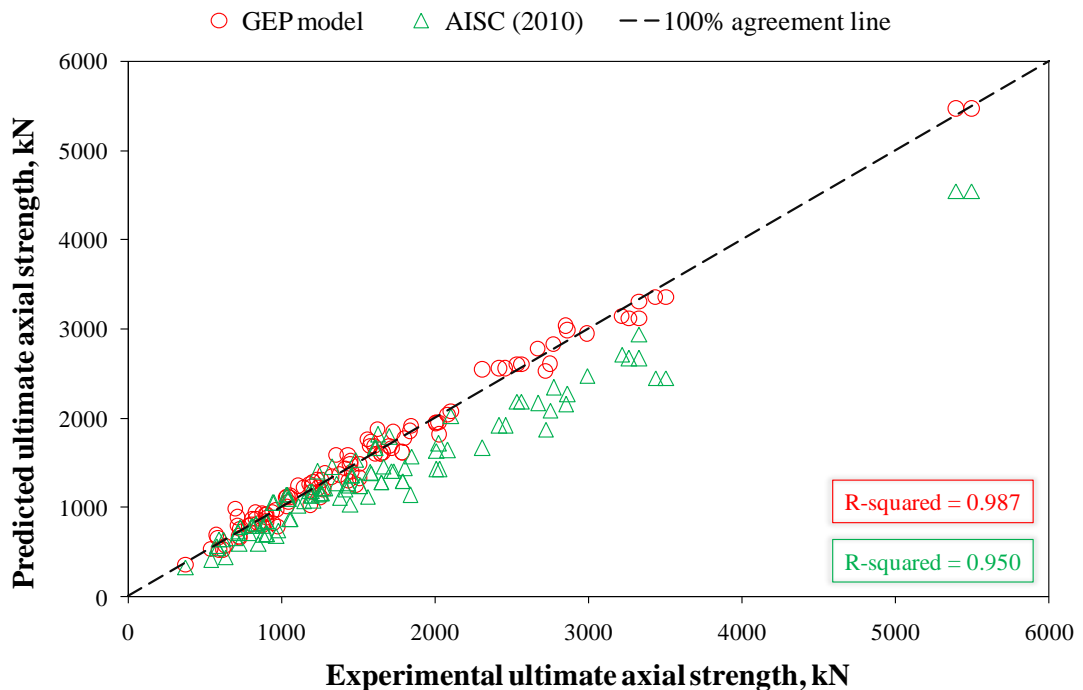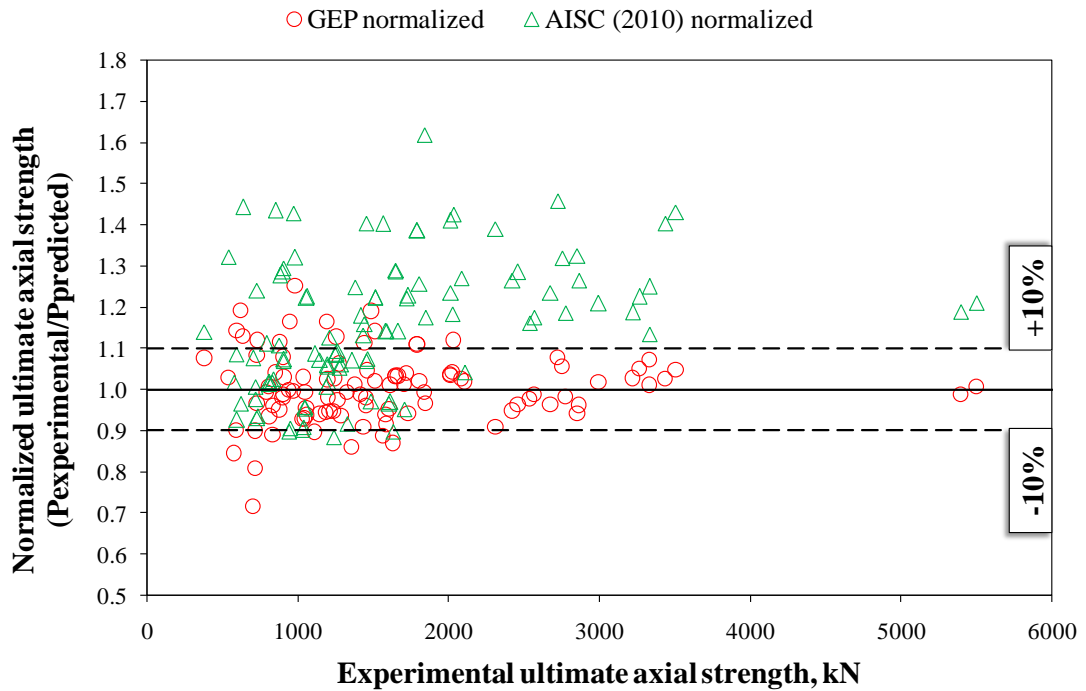
**Figure 4.33.** (a) predicted and (b) normalized ultimate axial strengths of GEP model and modified AISC (2010) formula versus experimental ultimate axial strengths

The results of the GEP model generally amass around the 100% agreement line (Figure 4.33a) and mostly fall between the normalization limit lines (Figure 4.33b). But the results of the modified AISC (2010) formula are usually dispersed far away from the 100% agreement line (Figure 4.33a) and frequently fall out of the normalization limit lines (4.33b). For this reason, it can be emphasized about the developed GEP model that its performance to predict the ultimate axial strength is also better than that of the modified AISC (2010) formula.

### 4.2.6 Comparison of GEP Model with Model of Uenaka et al. (2010)

The ultimate axial strength estimated by the GEP model and the model of Uenaka et al. (2010) versus experimental ultimate axial strengths are given in Figure 4.34a whereas the normalized ultimate strength values of the GEP model and the model of Uenaka et al. (2010) are plotted in Figure 4.34b. The easily visual comparison for the prediction performance of the GEP model against to the model of Uenaka et al. (2010) is aimed by the graphical presentation of the results.

(a)
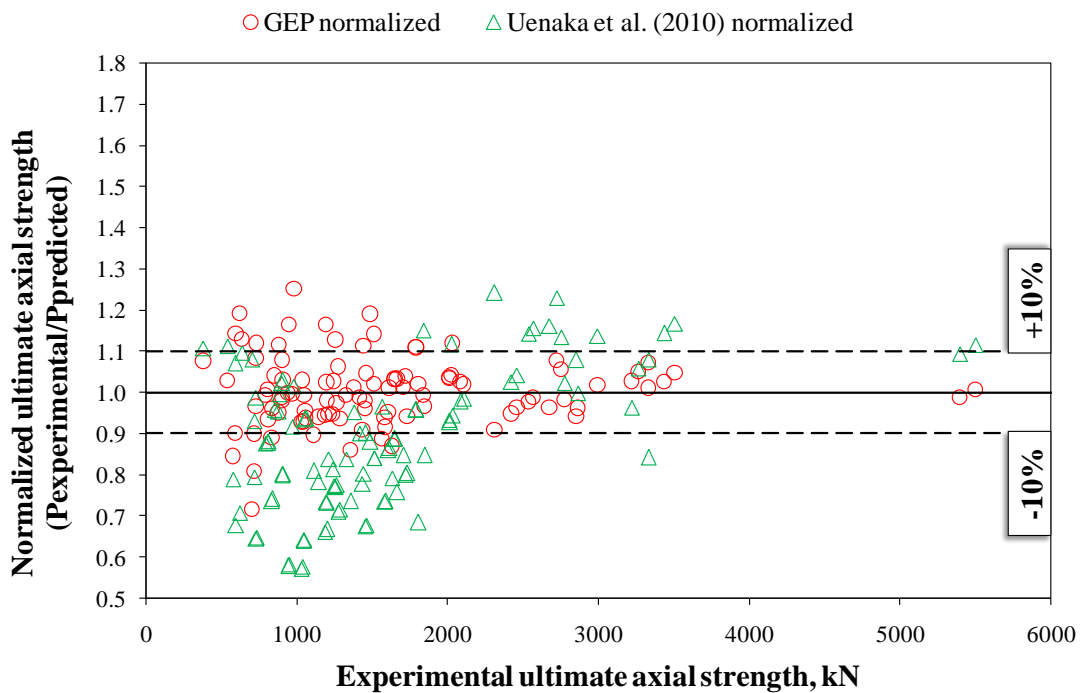


(b)

**Figure 4.34.** (a) predicted and (b) normalized ultimate axial strengths of GEP model and Uenaka et al. (2010) model versus experimental ultimate axial strengths

The results indicate that the model of Uenaka et al. (2010) predictes the ultimate axial strengths more than the actual values. The number of overestimated ultimate

axial strength values was more and this resulted in lower R-squared value of 0.888. When the R-squared value of the model proposed by Uenaka et al. (2010) is compared with that of the developed GEP model, it can be clearly perceived that the developed GEP model has the better prediction performance than the model of Uenaka et al. (2010). For this reason, it can be certainly stated that the developed GEP model has more accurate and reliable results than the empirical model suggested by Uenaka et al. (2010).

### 4.2.7 Comparison of GEP Model with Model of Han et al. (2011b)

The ultimate axial strength estimated by the GEP model and the model of Han et al. (2011b) versus experimental ultimate axial strengths are given in Figure 4.35a whereas the normalized ultimate strength values of the GEP model and the model of Han et al. (2011b) are plotted in Figure 4.35b. The easily visual comparison for the prediction performance of the GEP model against to the model of Han et al. (2011b) is aimed by the graphical presentation of the results.

The good prediction performance of the model proposed by Han et al. (2011b) could be succeed up to 2000 kN value of the ultimate strength as presented in Figure 4.35a. However, after this level of ultimate axial strength, the prediction capability of the model worsens while the GEP model still has a good estimation throughout the all strength levels.

In Figure 4.35a, the R-squared values of both models are also given. According to the R-squared values, it could be said that the performance of the GEP model to extrapolate the ultimate axial strength was better than the model of Han et al. (2011b). The model proposed by Han et al. (2011b) had many underestimated ultimate axial strength values as could clearly be seen in Figure 4.35b. Although the GEP model also had over and underestimated ultimate axial strength values, the number of these over and underestimated values and the residual ultimate axial strength values were less than the model of Han et al. (2011b).

For this reason, it could be unequivocally stated for the developed GEP model that it is more reliable and robust model than the empirical model recommended by Han et al. (2011b).
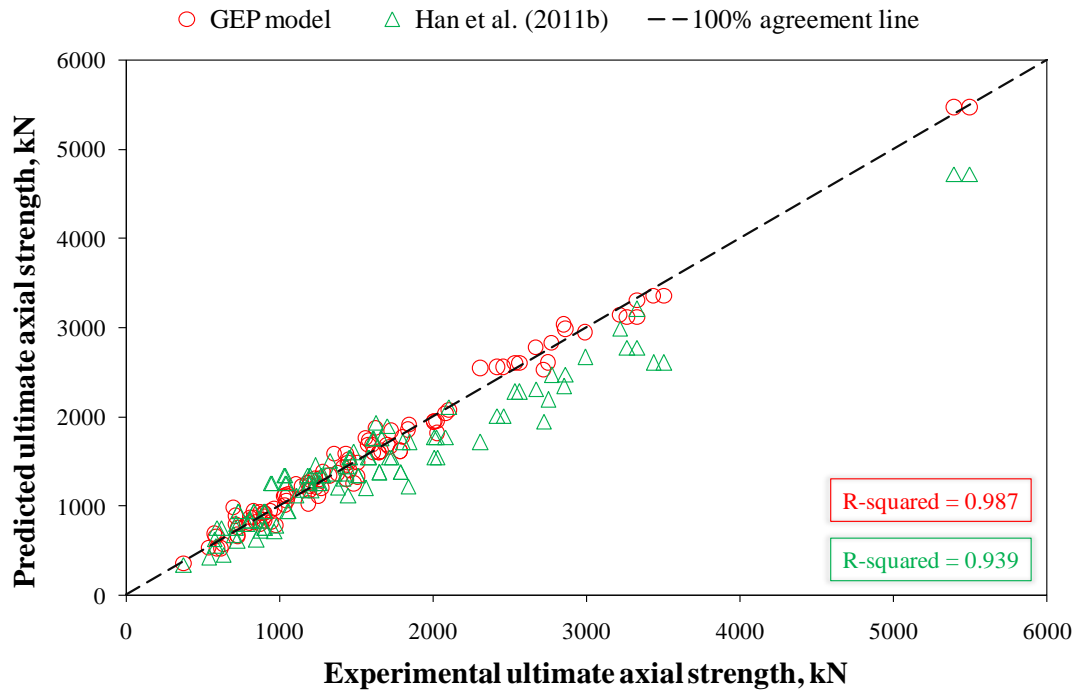
(a)
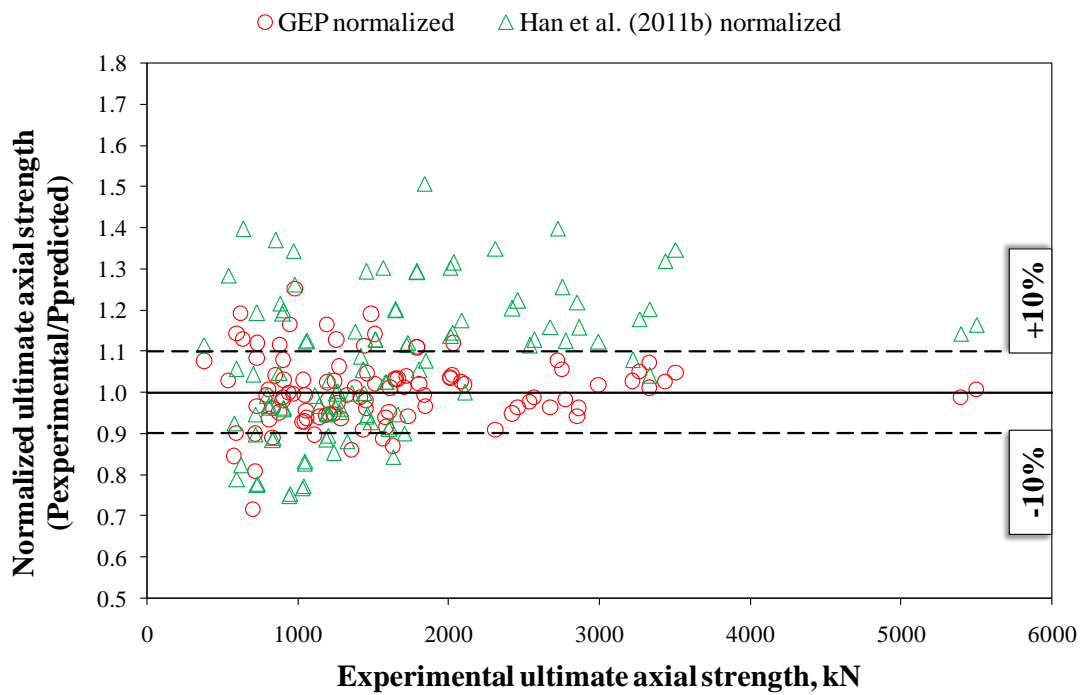


(b)

**Figure 4.35.** (a) predicted and (b) normalized ultimate axial strengths of GEP model and Han et al. (2011b) model versus experimental ultimate axial strengths

### 4.2.8 Comparison of GEP Model with Model of Yu et al. (2013)

The ultimate axial strength estimated by the GEP model and the model of Yu et al. (2013) versus experimental ultimate axial strengths are given in Figure 4.36a whereas the normalized ultimate strength values of the GEP model and the model of Yu et al. (2013) are plotted in Figure 4.36b. The easily visual comparison for the prediction performance of the GEP model against to the model of Yu et al. (2013) is aimed by the graphical presentation of the results.

Figure 4.36a indicates the relationship between the predicted and experimental strength values. According to observation of this figure, it can be seen that the predicted strength values for both models are amassed around the 100% agreement line, yet, when Figure 4.36b in which the normalized versus the experimental ultimate axial strength values are plotted is observed, it can be obviously seen that a great number of normalized ultimate strength values predicted by model of Yu et al. (2013) are at the outside of the normalization limit lines. This indicates that there are a lot of over and underestimated ultimate axial strength values of the model proffered by Yu et al. (2013).
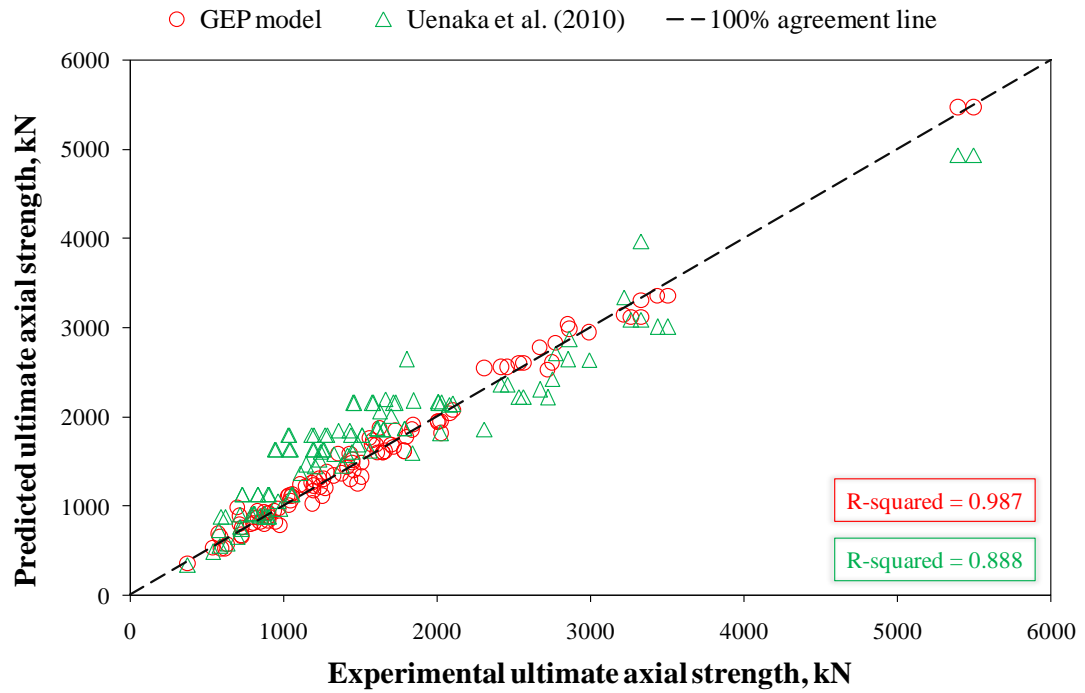


(a)

(b)
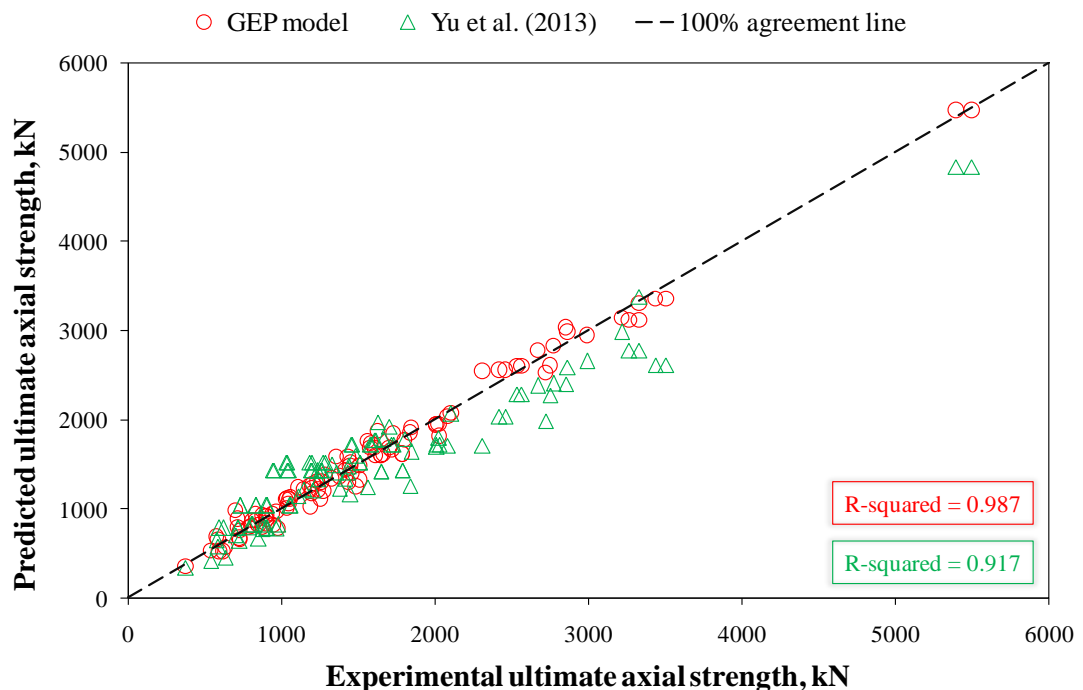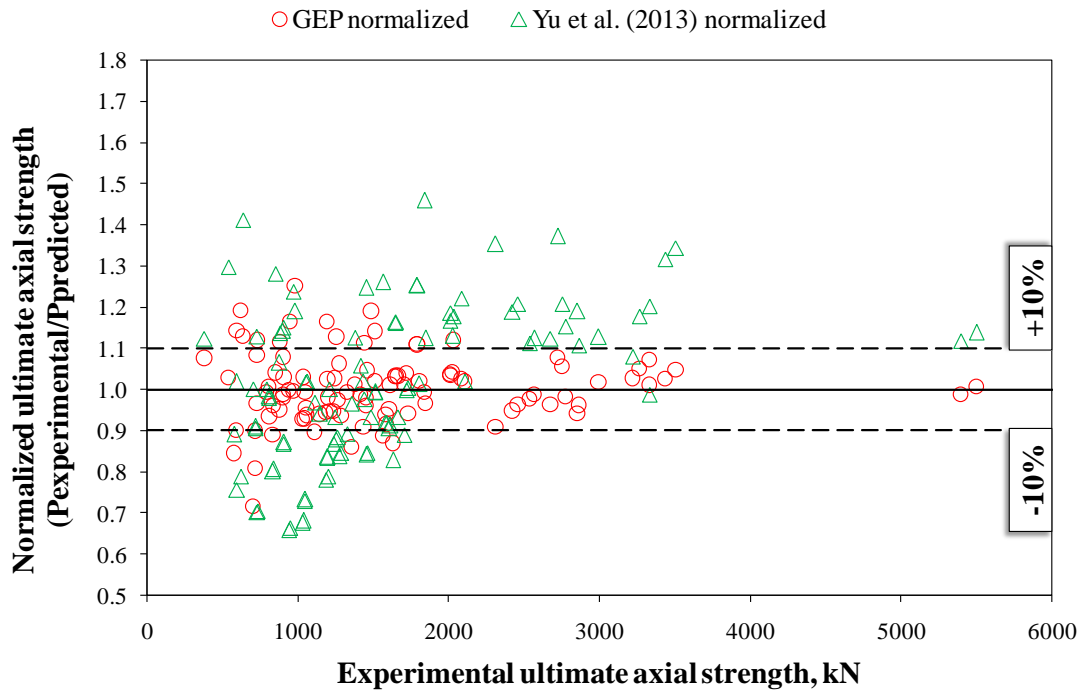
**Figure 4.36.** (a) predicted and (b) normalized ultimate axial strengths of GEP model and Yu et al. (2013) model versus experimental ultimate axial strengths

In addition, the R-squared value of the developed GEP model is greater than that of the model of Yu et al. (2013) as given in Figure 4.36a. This is also the indication of why the prediction performance of the developed GEP model is better than that of the model of Yu et al. (2013). These findings also support the reliability and accuracy of the developed GEP model.

**4.2.9 Comparison of GEP Model with Model of Hassanein et al. (2013b)**

The ultimate axial strength estimated by the developed GEP model and the model of Hassanein et al. (2013b) versus experimental ultimate axial strengths are given in Figure 4.37a whereas the normalized ultimate strength values of the developed GEP model and the model suggested by Hassanein et al. (2013b) are plotted in Figure 4.37b. The easily visual comparison for the prediction performance of the GEP model against to the model of Hassanein et al. (2013b) is aimed by the graphical presentation of the results.

144
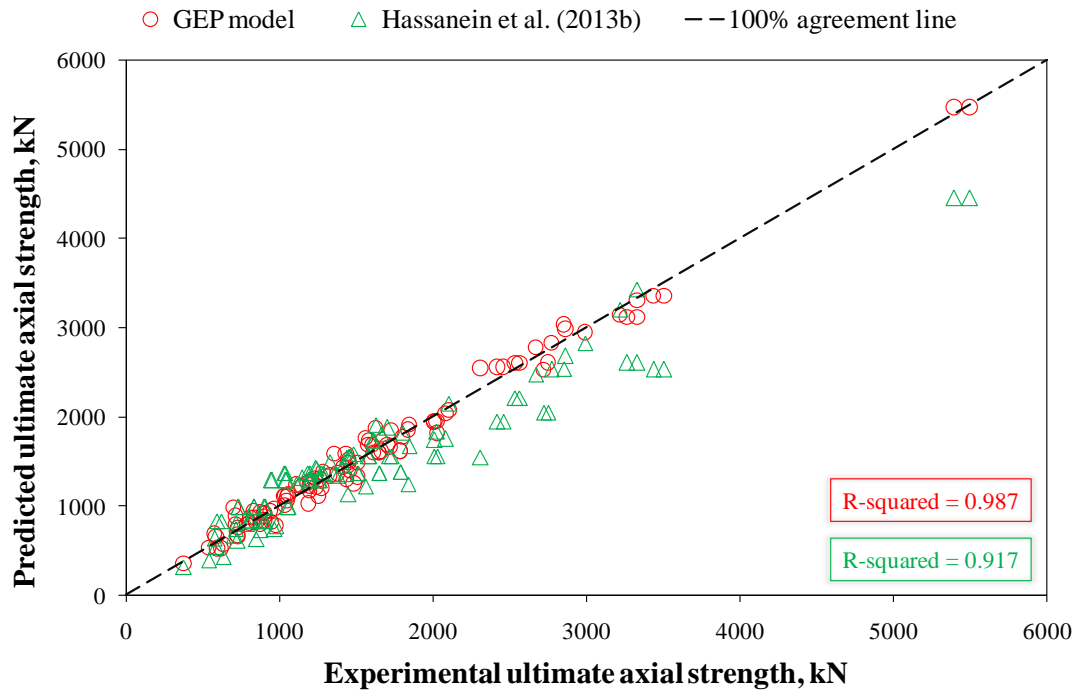
(a)
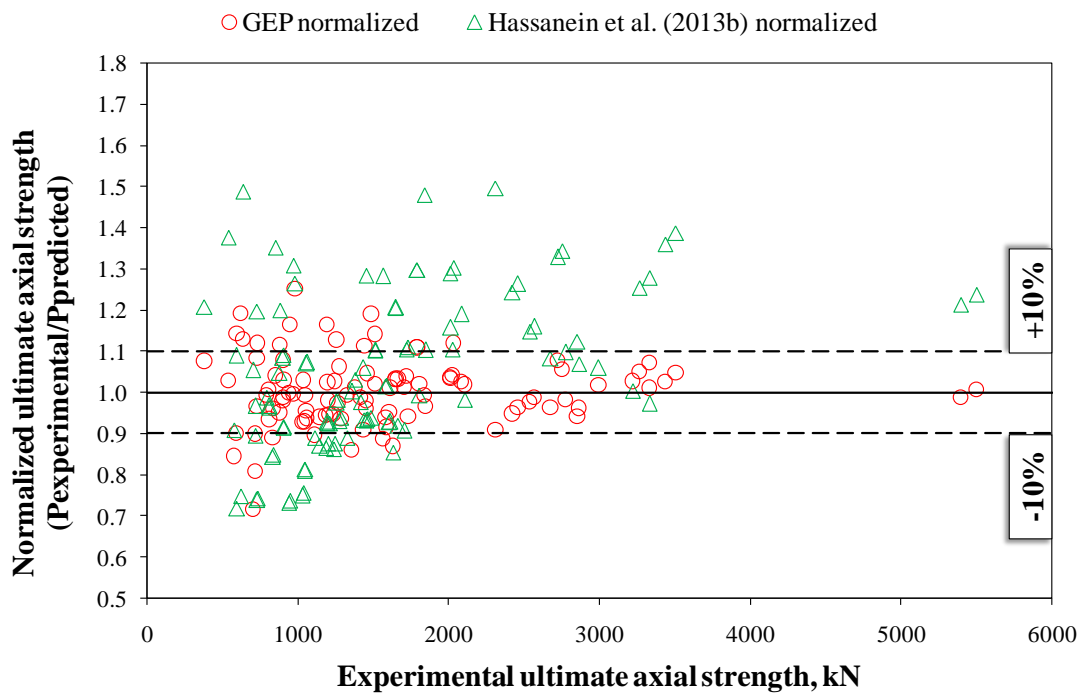


(b)

**Figure 4.37.** (a) predicted and (b) normalized ultimate axial strengths of GEP model and Hassanein et al. (2013b) model versus experimental ultimate axial strengths

The results obviously indicate that the developed GEP model is also better than the model of Hassanein et al. (2013b) regarding prediction performance. The correlation

between the predicted and the actual strengths also show how the performance of the developed GEP model regarding the prediction capability is better than that of the model of Hassanein et al. (2013b).

In addition, when Figure 4.37b is viewed, it would be seen that there are a lot of normalized values achieved from the model of Hassanein et al. (2013b) dispersed throughout outside of the ±10% normalization limit lines. On the other hand, a few number of the developed GEP model values are at the outside of the normalization limits whereas the rest well scattered between the limitation lines.

Briefly, it can be said that so much overestimation and/or underestimation could decrease the reliability and accuracy of the model and it can be obviously seen when the R-squared values of both models are compared.

### 4.2.10 Statistical Comparison of Models

In addition to graphical comparison of the results, the statistically evaluation of the model is crucially necessary. Therefore, the ultimate axial strength results extrapolated by the GEP model, the modified formulas, and the proposed empirical models are statistically evaluated in this section. The fundamental statistical parameters such as MAPE, MSE, RMSE, COV, and R-squared values of which formulas were given in Chapter 3 were used to evaluate the prediction performance of the models and compare their capabilities.

The values of these parameters are tabulated in Table 4.4. In order to visualize these tabulated values, MAPE, MSE, and RMSE values are shown in Figure 4.38a, 4.38b, and 4.38c, respectively, while COV and R-sqaured values are indicated in Figure 4.39a and 4.39b, respectively.

These statistical parameters of the existing models were then compared with that of the GEP model. The GEP model exhibited superior performance against to the modified formulas and the models recommended by the researchers. Figure 4.38a, 4.38b, and 4.38c showed the comparison of the MAPE, MSE, and RMSE values of the GEP with the modified formulas and suggested empirical models.

**Table 4.4.** Statistical parameters of the prediction performance of proposed GEP model and existing design codes and suggested empirical models in the previous studies

| Statistical parameters | Mean absolute percent error (MAPE) | Mean square error (MSE) | Root mean square error (RMSE) | Coefficient of variation (COV) | Coefficient of determination (R-squared) |
|---|---|---|---|---|---|
| **GEP** | 6.43 | 11543 | 85.7 | 0.084 | 0.987 |
|    **Train** | 5.72 | 10860 | 81.0 | 0.075 | 0.987 |
| **Test** | 8.52 | 13567 | 99.9 | 0.109 | 0.987 |
| **ACI (2002)** | 16.81 | 168726 | 301.0 | 0.192 | 0.936 |
| **EC4 (2004)** | 8.68 | 45291 | 151.4 | 0.104 | 0.960 |
| **AISC (2010)** | 14.41 | 129403 | 262.5 | 0.139 | 0.950 |
| **Uenaka et al. (2010)** | 21.46 | 128636 | 291.2 | 0.186 | 0.888 |
| **Han et al. (2011b)** | 13.48 | 87481 | 220.6 | 0.160 | 0.939 |
| **Yu et al. (2013)** | 15.43 | 90708 | 234.3 | 0.180 | 0.917 |
| **Hassanein et al. (2013b)** | 14.54 | 104162 | 232.5 | 0.178 | 0.917 |

The statistical results revealed that the GEP model was the best model at the prediction of the ultimate axial strength of the CFDST columns with CHS among the other models since the GEP had the lowest MAPE, MSE, and RMSE values, namely, lower prediction errors.

When the MAPE, MSE, and RMSE values are considered, it can be stated that within the modified formulas of the codes; the best prediction performance belongs to the modified Eurocode 4 (2004) formula while within the proposed models by the researchers; the model of Han et al. (2011b) is the best regarding the estimation capability. Among the modified formulas and the models recommended by the researchers, the worst performance to estimate the ultimate axial strength of CFDST columns appertains to the model of Uenaka et al. (2010) while the best one is the modified Eurocode 4 (2004) formula. The GEP model has the highest accuracy,

reliability, and robustness in the case of the comparison with the modified formulas and the models recommended by the researchers according to the MAPE, MSE, and RMSE values.
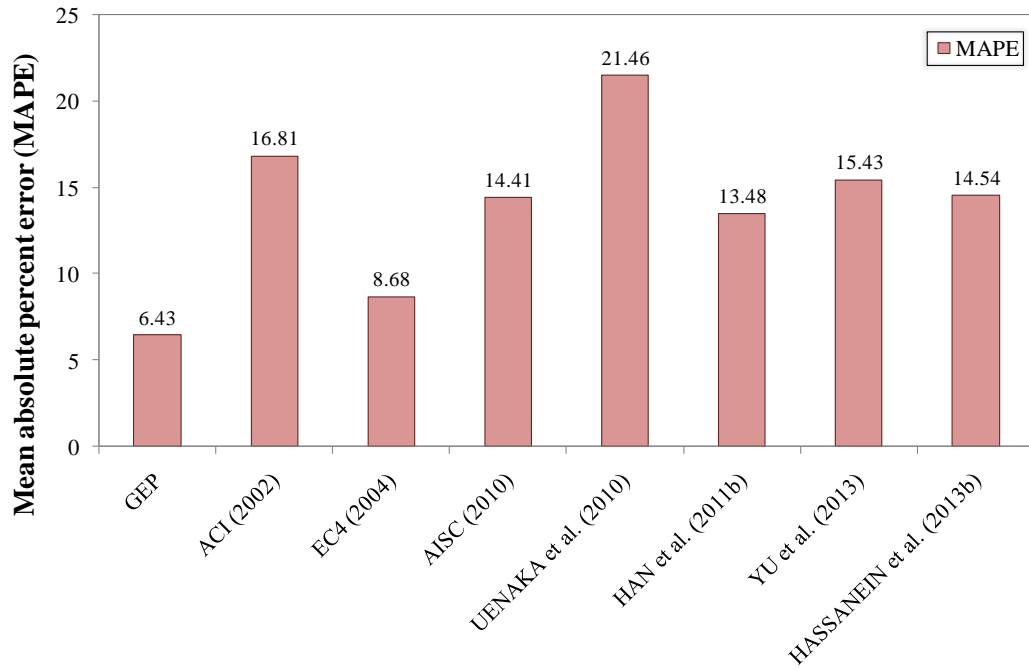


(a)
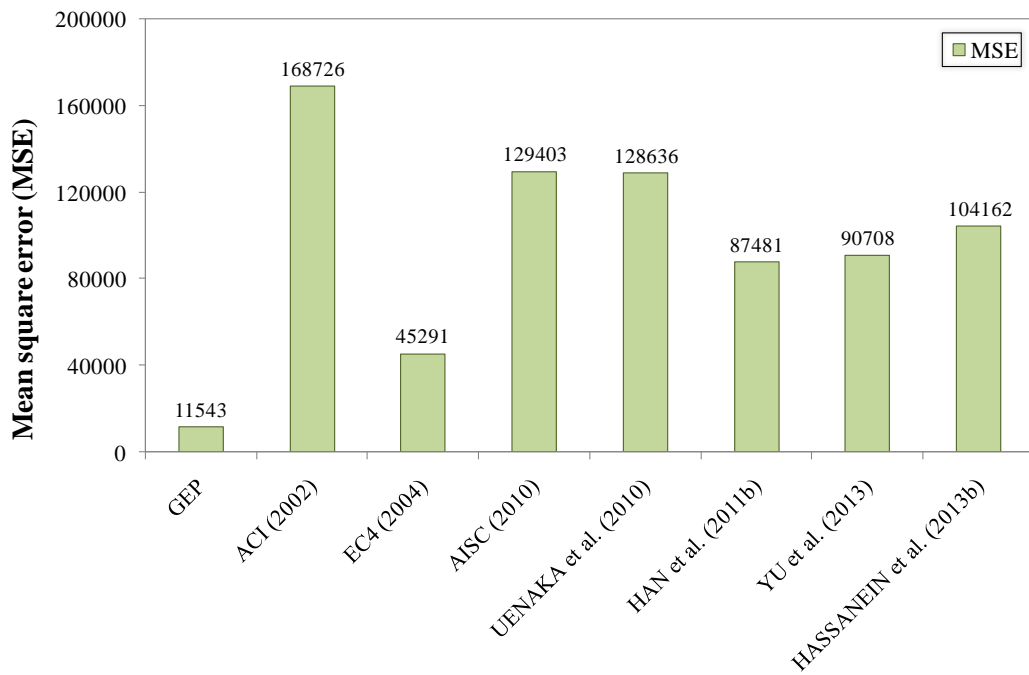


(b)
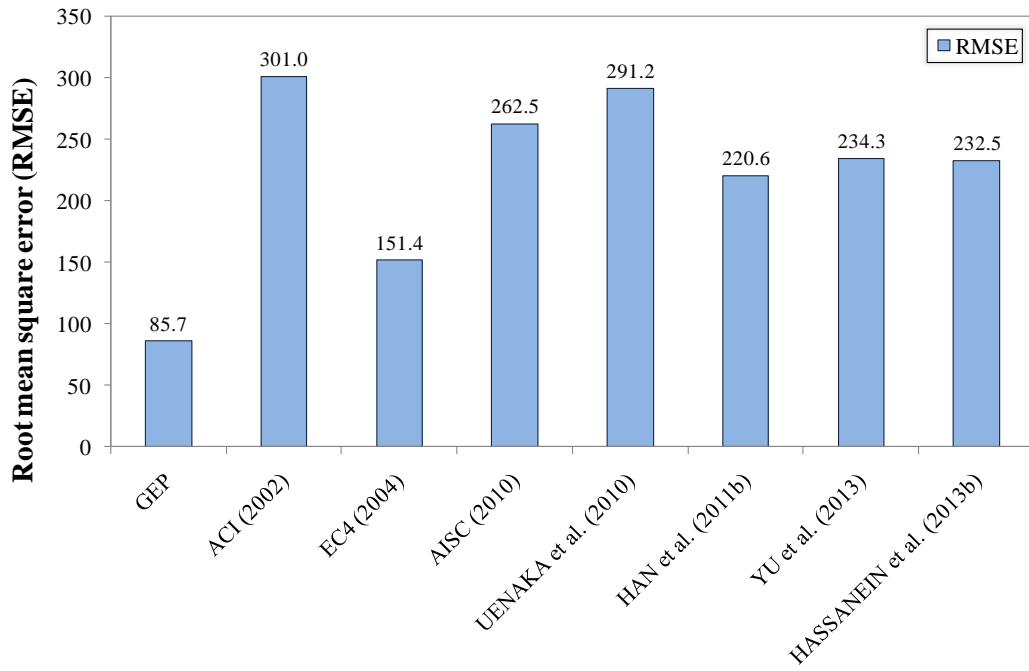
(c)

**Figure 4.38.** Statistically comparison GEP model with the modified formulas and suggested empirical models with regard to: (a) MAPE, (b) MSE, and (c) RMSE

In addition to the MAPE, MSE, and RMSE, the COV of the normalized ultimate axial strengths and R-squared values also indicate that the estimation capability of the developed GEP model is better than the others.



(a)

(b)
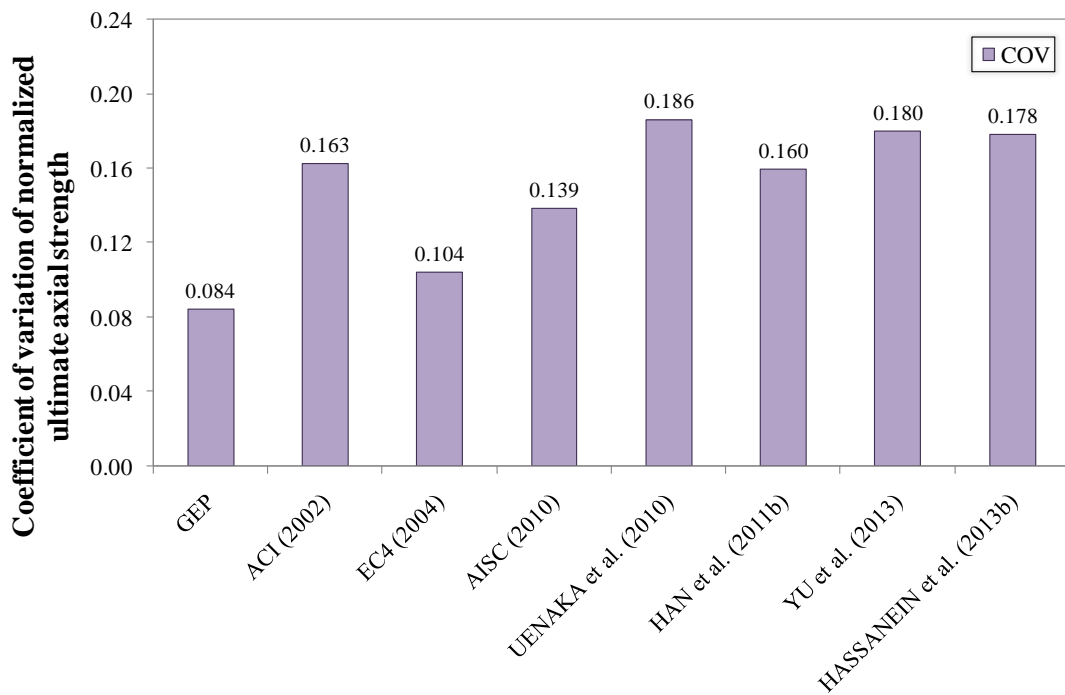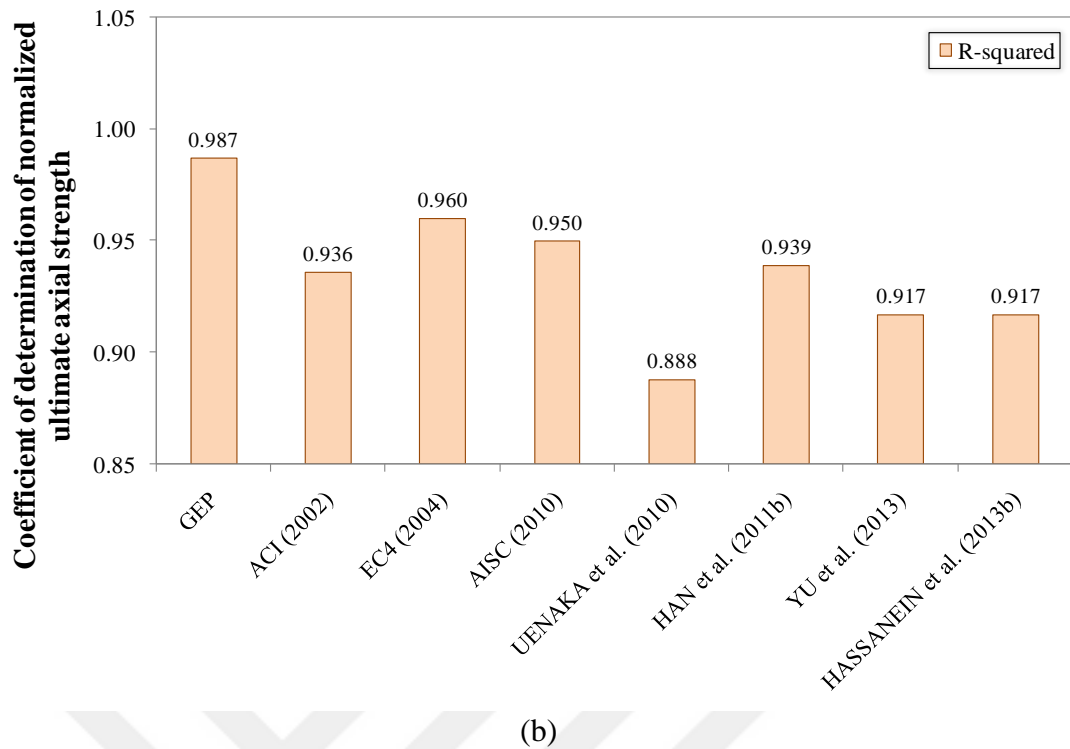
**Figure 4.39.** Statistically comparison GEP model with the modified formulas and suggested empirical models with regard to: (a) COV and (b) R-squared

As known, the R-squared value approaching to the value 1 is the indication of better estimation capability. For this, reason when Figure 4.39b is examined, it can be obviously seen that the highest R-squared value is attained in the developed GEP model. This situation means that the prediction performance of the GEP model is the best.

Besides, the COV value of the ultimate axial strengths also gives an idea about the prediction performance of the model by approaching to or moving away from 0. When the model has the good prediction performance, the COV value would approach to 0. For this reason, it can be clearly seen from Figure 4.39b, the lowest COV value is determined for the GEP model meaning that it has a better prediction performance. Among the modified formulas and the models suggested by the researchers, the modified Eurocode 4 (2004) formula has the highest R-squared and the lowest COV value while the empirical model of Uenaka et al. (2010) has the lowest R-sqared and the highest COV values. For these reasons, the reliability, accuracy, and consistency of the proposed GEP model are higher than the others.

Finally, the percent error caused by the models during the prediction of the ultimate axial strength is grouped according to the strength partitions and they are given in Figure 4.40. The ultimate axial strength values are divided into five partitions with the range of 750 kN and the number of data falling in each partition class is also shown in Figure 4.40 as frequency.
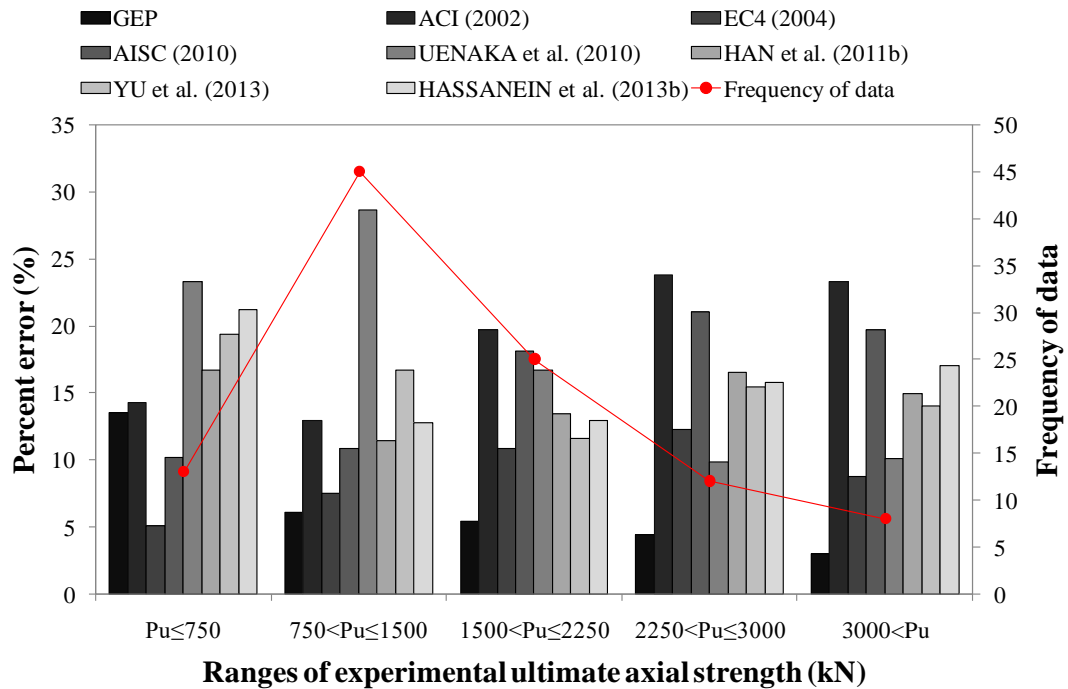


**Figure 4.40.** Error analysis of proposed GEP model, modified code formulas, and suggested empirical models

It can be clearly seen that the modified Eurocode 4 (2004) formula exhibites lower percent error value only in the case of the ultimate axial strength value ≤ 750 kN while the proposed GEP model shows lower percent error values in the other intervals. For the ultimate axial strength values ≤ 1500 kN, the higher percent error values are obtained from the model of Uenaka et al. (2010) whereas for the strength values > 1500 kN, the worst percent error results are procured from the modified ACI (2002) formula. The percent error values of the GEP model decrease by increasing of the ultimate strength and the lowest percent error value of 2.98% is achieved at the ultimate axial strength >3000kN. It can be concluded that when the ultimate axial strength of the CFDST columns with CHS increases, the prediction performance of the GEP model also increases.

## 4.3 Artificial Neural Network (ANN) Model Results

The section herein includes the comparison of the ANN model used in the prediction of the ultimate axial strength of the CFDST columns with CHS regarding the mechanical and sectional properties of elements used in the preparation of the specimen and the equations modified from the codes and existing proposed empirical models. As mentioned in Chapter 3, the data set used in the creating the ANN model was arbitrarily divided into train and test sub-datasets. The train dataset was handled to employ for the enhancement of the developed model whereas the test dataset was used to observe the fitness, predictability, robustness and repeatability of the proposed mathematical model. Moreover, the train and test sub-datasets were also statistically analyzed in order to observe these sub-datasets represent all data or not and the results were given in Table 3.5. In this section, firstly the extrapolated values of the train and test sub-datasets are compared with actual values achieved from the experimental test. Then after, the whole predicted values are firstly compared with the material properties and then compared with the existing formulas that are used to predict the ultimate axial strength of the CFDST columns with CHS. The ultimate axial strength values calculated by Equation 3.16 derived from the ANN model including both train and test values are tabulated in Table 4.5 including also the experimental test results. The normalized ultimate axial strength values, which are calculated by dividing the experimental strength to the predicted strength given in Table 4.5, are presented in Figure 4.41 in order to reveal how the normalized values are dispersed on the normalization line.

**Table 4.5.** Ultimate axial strength values of experiment and ANN prediction

| Sample | | | Experimental ultimate axial strength $(P_u)_{EXP}$, kN | Predicted ultimate axial strength $(P_u)_{ANN}$, kN |
|---|---|---|---|---|
| Reference | Number | Identification | | |
| Zhao et al. (2002a) | 1 | C1C7 | 1415.0 | 1405.4 |
| | 2 | C2C7 | 1380.0 | 1351.7 |
| | 3 | C3C7 | 1210.0 | 1206.7 |
| | 4 | C4C7 | 1110.0 | 1153.4 |
| | 5 | C5C8 | 1705.0 | 1645.6 |
| | 6 | C6C8 | 1605.0 | 1619.2 |

**Table 4.5.** (cont'd) Ultimate axial strength values of experiment and ANN prediction

| | Sample | | Experimental ultimate axial strength $(P_u)_{EXP}$, kN | Predicted ultimate axial strength $(P_u)_{ANN}$, kN |
|---|---|---|---|---|
| Reference | Number | Identification | | |
| Lin and Tsai (2003) | 7 | DS-06-2-2-C | 2311.0 | 2330.7 |
| | 8 | DS-06-4-2-C | 2750.0 | 2734.8 |
| Tao et al. (2004) | 9 | cc2a | 1790.0 | 1807.7 |
| | 10 | cc2b | 1791.0 | 1807.7 |
| | 11 | cc3a | 1648.0 | 1618.6 |
| | 12 | cc3b | 1650.0 | 1618.6 |
| | 13 | cc4a | 1435.0 | 1437.5 |
| | 14 | cc4b | 1358.0 | 1437.5 |
| | 15 | cc5a | 904.0 | 898.7 |
| | 16 | cc5b | 898.0 | 898.7 |
| | 17 | cc6a | 2421.0 | 2428.1 |
| | 18 | cc6b | 2460.0 | 2428.1 |
| | 19 | cc7a | 3331.0 | 3297.1 |
| | 20 | cc7b | 3266.0 | 3297.1 |
| | 21 | pcc2-1a | 620.0 | 624.9 |
| | 22 | pcc2-1b | 595.0 | 624.9 |
| Lu et al. (2010b) | 23 | C2-C4-SCC1-Ref | 3333.0 | 3342.4 |
| Uenaka et al. (2010) | 24 | c10-375 | 635.0 | 648.6 |
| | 25 | c10-750 | 540.0 | 531.2 |
| | 26 | c10-1125 | 378.3 | 366.6 |
| | 27 | c16-375 | 851.6 | 883.0 |
| | 28 | c16-750 | 728.1 | 705.0 |
| | 29 | c16-1125 | 589.0 | 563.1 |
| | 30 | c23-375 | 968.2 | 955.6 |
| | 31 | c23-750 | 879.1 | 857.5 |
| | 32 | c23-1125 | 703.6 | 753.4 |
| Zhao et al. (2010) | 33 | O1I1-S | 1665.0 | 1682.5 |
| | 34 | O2I1-S | 1441.0 | 1398.6 |
| | 35 | O3I1-S | 1243.0 | 1219.0 |
| | 36 | O4I1-S | 1145.0 | 1179.2 |
| | 37 | O5I2-S | 1629.0 | 1677.1 |
| | 38 | O6I2-S | 1613.0 | 1611.9 |
| | 39 | O7I2-S | 1487.0 | 1436.5 |
| | 40 | O8I2-S | 1328.0 | 1339.7 |
| | 41 | O9I2-S | 1236.0 | 1282.8 |

**Table 4.5.** (cont'd) Ultimate axial strength values of experiment and ANN prediction

| Sample | | | Experimental ultimate axial strength $(P_u)_{EXP}$, kN | Predicted ultimate axial strength $(P_u)_{ANN}$, kN |
|---|---|---|---|---|
| Reference | Number | Identification | | |
| Han et al. (2011a) | 42 | DCc-0 | 578.0 | 570.3 |
| | 43 | DCc-1 | 789.0 | 743.4 |
| | 44 | DCc-2 | 715.0 | 743.4 |
| Han et al. (2011b) | 45 | C1-1 | 2537.0 | 2557.6 |
| | 46 | C1-2 | 2566.0 | 2557.6 |
| | 47 | C2-1 | 3436.0 | 3460.7 |
| | 48 | C2-2 | 3506.0 | 3460.7 |
| Dong and Ho (2012) | 49 | D50-5-0 | 2852.0 | 2840.3 |
| Li et al. (2012) | 50 | C1-1 | 5499.0 | 5451.5 |
| | 51 | C1-2 | 5396.0 | 5451.5 |
| Dong and Ho (2013) | 52 | D-A-50-0 | 2865.0 | 2894.2 |
| | 53 | D-B-50-0 | 2674.0 | 2652.6 |
| | 54 | D-A-85-0 | 3218 | 3205.3 |
| | 55 | D-B-85-0 | 2994 | 3002.4 |
| Wang et al. (2014) | 56 | 0HA0 | 980.0 | 948.8 |
| | 57 | 0HB0 | 715.0 | 740.6 |
| Essopjee and Dundu (2015) | 58 | S139.2-1.0 | 1059.2 | 1037.7 |
| | 59 | S139.2-1.0 | 1056.1 | 1037.0 |
| | 60 | S139.2-1.5 | 905.5 | 935.3 |
| | 61 | S139.2-1.5 | 901.6 | 934.7 |
| | 62 | S139.2-2.0 | 831.7 | 831.6 |
| | 63 | S139.2-2.0 | 837.4 | 832.0 |
| | 64 | S139.2-2.5 | 732.1 | 720.4 |
| | 65 | S139.2-2.5 | 729.0 | 721.3 |
| | 66 | S152.4-1.0 | 1263.5 | 1285.4 |
| | 67 | S152.4-1.0 | 1254.9 | 1285.7 |
| | 68 | S152.4-1.5 | 1195.6 | 1154.4 |
| | 69 | S152.4-1.5 | 1191.2 | 1152.9 |
| | 70 | S152.4-2.0 | 1047.3 | 1042.4 |
| | 71 | S152.4-2.0 | 1041.6 | 1041.7 |
| | 72 | S152.4-2.5 | 941.4 | 935.4 |
| | 73 | S152.4-2.5 | 949.0 | 935.0 |
| | 74 | S165.1-1.0 | 1512.3 | 1490.0 |

154

**Table 4.5.** (cont'd) Ultimate axial strength values of experiment and ANN prediction

| Sample | | | Experimental ultimate axial strength $(P_u)_{EXP}$, kN | Predicted ultimate axial strength $(P_u)_{ANN}$, kN |
|---|---|---|---|---|
| Reference | Number | Identification | | |
| Essopjee and Dundu (2015) | 75 | S165.1-1.0 | 1510.6 | 1489.6 |
| | 76 | S165.1-1.5 | 1286.4 | 1316.7 |
| | 77 | S165.1-1.5 | 1275.1 | 1318.5 |
| | 78 | S165.1-2.0 | 1187.2 | 1182.8 |
| | 79 | S165.1-2.0 | 1199.8 | 1184.0 |
| | 80 | S165.1-2.5 | 1028.0 | 1062.2 |
| | 81 | S165.1-2.5 | 1036.5 | 1061.2 |
| | 82 | S193.7-1.0 | 2010.0 | 2015.6 |
| | 83 | S193.7-1.0 | 2030.0 | 2017.8 |
| | 84 | S193.7-1.5 | 1730.0 | 1727.1 |
| | 85 | S193.7-1.5 | 1720.0 | 1728.0 |
| | 86 | S193.7-2.0 | 1581.6 | 1554.8 |
| | 87 | S193.7-2.0 | 1584.1 | 1553.5 |
| | 88 | S193.7-2.5 | 1451.4 | 1438.5 |
| | 89 | S193.7-2.5 | 1458.7 | 1439.7 |
| Abbas et al. (2016) | 90 | CB2-40NG-AB-CP | 1805.0 | 1814.7 |
| Wang et al. (2016) | 91 | HC22X4-C40 | 1450.0 | 1436.7 |
| | 92 | HC32X6-C40 | 1562.0 | 1567.1 |
| | 93 | HC38X8-C40 | 1838.4 | 1836.6 |
| | 94 | HC55X11-C40 | 2724.0 | 2720.3 |
| | 95 | HC89X4-C40 | 2024.9 | 2034.8 |
| | 96 | HC22X4-C80 | 1845.1 | 1855.8 |
| | 97 | HC32X6-C80 | 2012.5 | 2010.2 |
| | 98 | HC38X8-C80 | 2083.4 | 2081.7 |
| | 99 | HC55X11-C80 | 2775.0 | 2782.7 |
| | 100 | HC89X4-C80 | 2107.4 | 2097.5 |
| Hastemoğlu (2017) | 101 | DSCFT 3 | 807.0 | 825.4 |
| | 102 | DSCFT 4 | 810.0 | 829.2 |
| | 103 | DSCFT 5 | 877.0 | 836.2 |

The normalized ultimate axial strength results obtained from the ANN model perform a good interspersion around the normalization line. There is no normalized value at outside of the normalization limit lines of ±10%. According to this perfect

155

dispersion, it could be certainly specified that the model created by ANN has nearly perfect estimation performance.
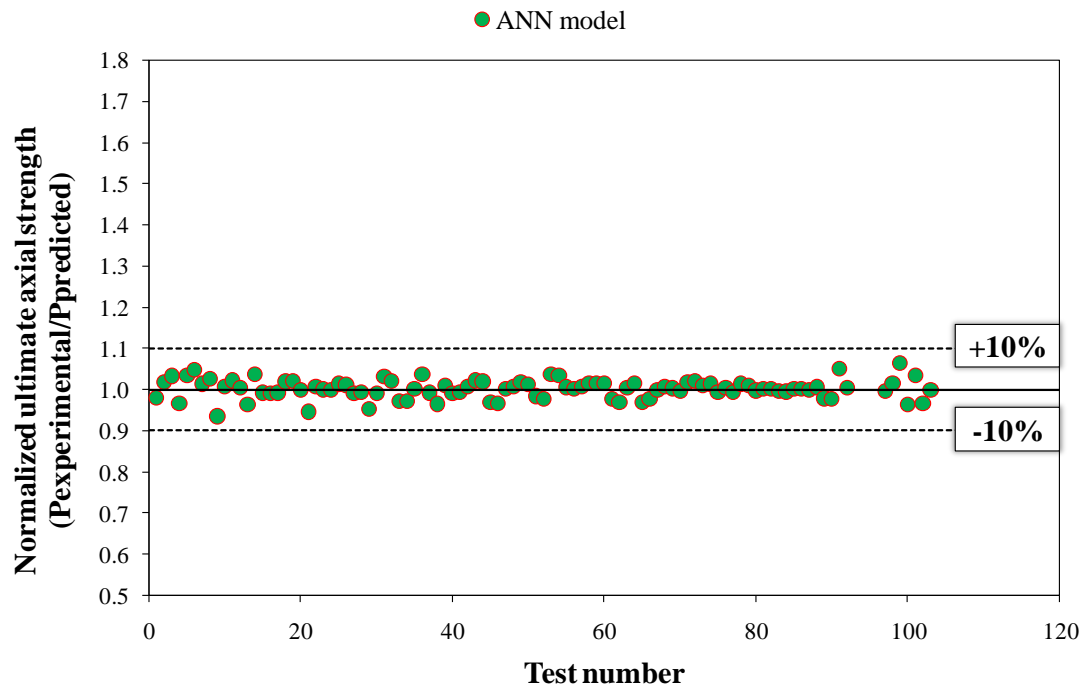


**Figure 4.41.** Prediction performance of ANN model based on normalized ultimate axial strength values

### 4.3.1 Comparison of Train and Test Sub-datasets for ANN Model

Figure 4.42a and 4.42b are the graphically presentation of the estimated ultimate axial strengths for train and test sub-datasets with respect to experimental strengths, respectively. The extrapolated values of both sub-datasets indisputably match with the experimental results as shown in the following figures. This perfect matching means that the estimated ultimate axial strengths are almost same with the experimental strengths. In addition, the comparison of the predicted and actual strength values is demonstrated in Figure 4.43a and 4.43b for the train and test sub-datasets, respectively.

The model developed by using ANN has the capability to predict the ultimate axial strength value at various strength levels as can be seen in Figure 4.42a and 4.42b. From the lowest strengths to the highest, the ANN model performs perfect prediction capableness for both train and test sub-datasets.
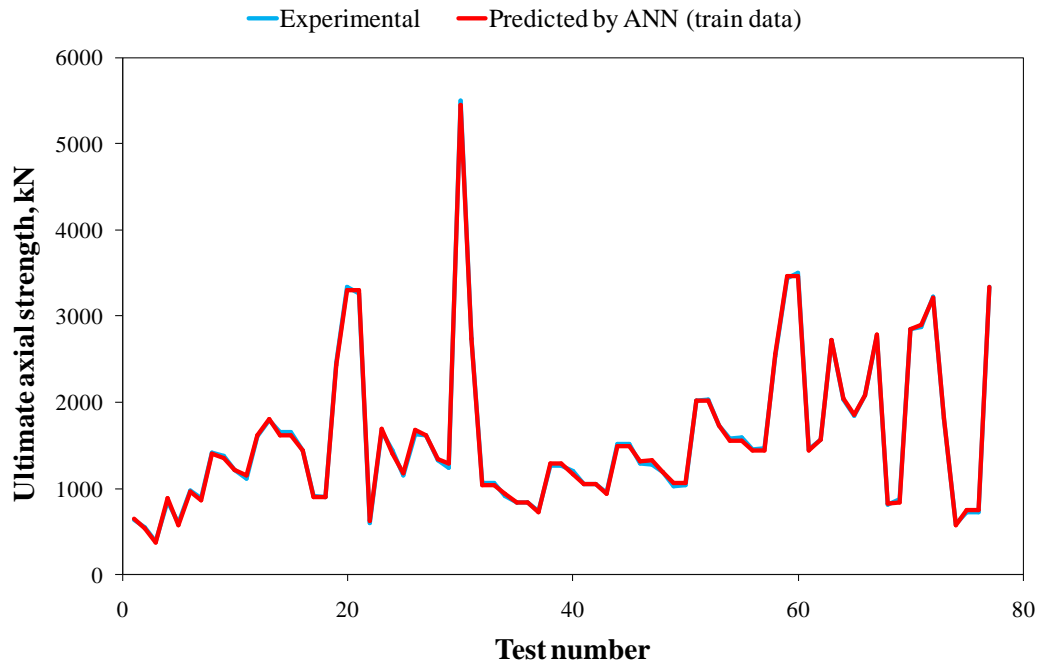
(a)
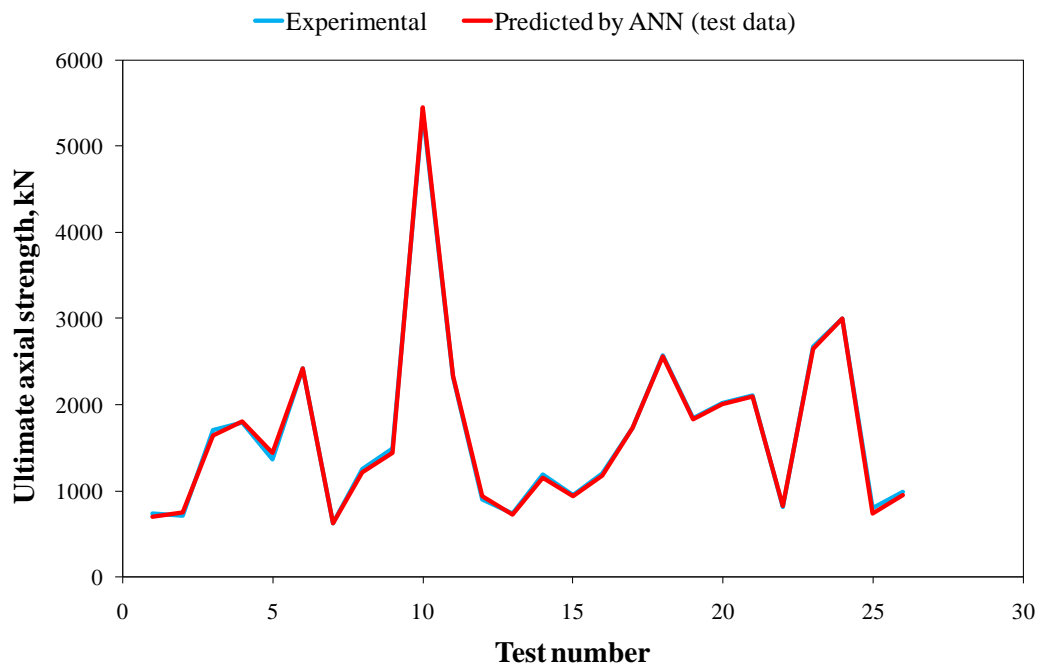


(b)

**Figure 4.42.** ANN prediction and experimental ultimate axial strength values of: (a) train and (b) test sub-datasets

In addition, the comparison of the predicted and actual strength values for the train and test sub-datasets are demonstrated in Figure 4.43a and 4.43b, respectively. In order to evaluate the correlation between the experimental and the predicted strength

values based on the R-squared values, Figure 4.43a and 4.43b include also the R-squared values.
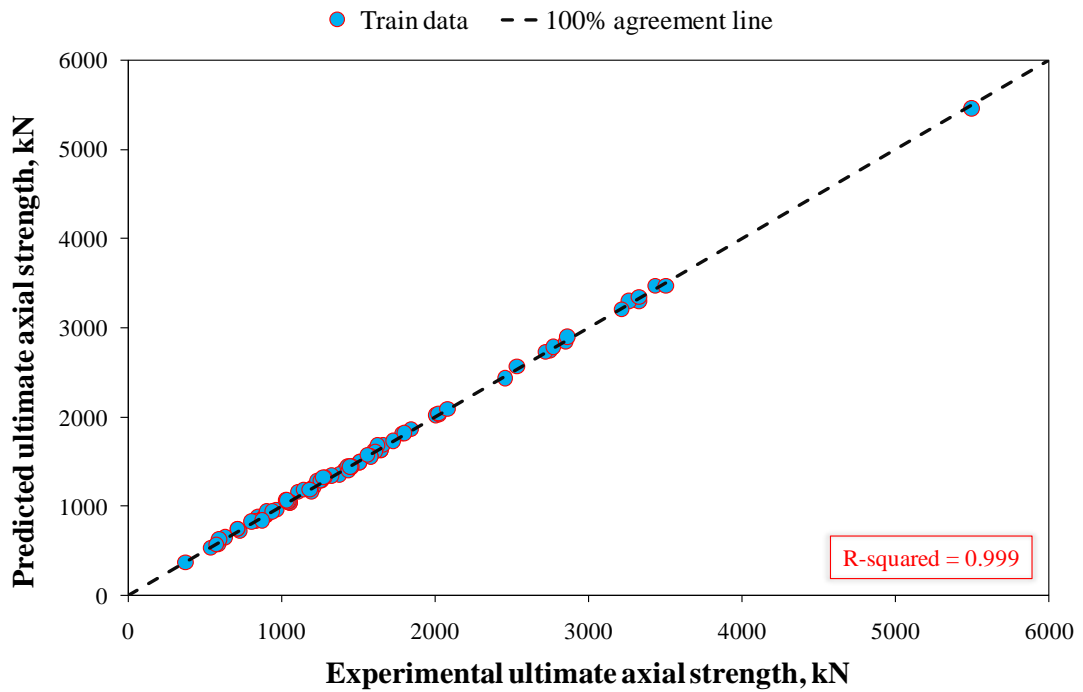


(a)
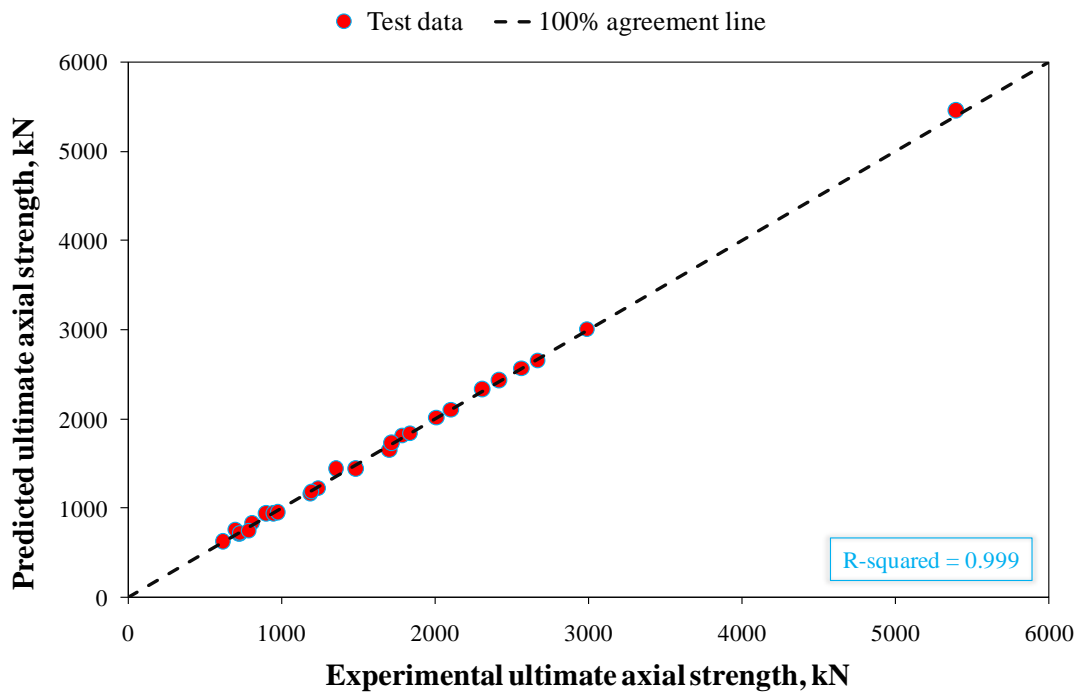


(b)

**Figure 4.43.** ANN prediction versus experimental ultimate axial strength values for: (a) train and (b) test sub-datasets

As seen from Figure 4.43a and 4.43b, the train and test sub-datasets has the R-squared value of 0.999 in the developing of the ANN model. This indicates that the train and test sub-datasets strongly reflect all dataset and also it is the manifestation of a strong correlation between the actual and predicted values. In addition, the robustness and appropriate correctitude of the ANN model can be stated by obtaining the proximate R-squared values.

### 4.3.2 Comparison of ANN Model with Element Properties

In order to indicate how the prediction performance of the FEM model varies with respect to the mechanical properties of the element, the ultimate axial strengths extrapolated by applying the FEM model are shown in Figure 4.44a, 4.44b, and 4.44c according to the yield strength of outer/inner steel tubes and compressive strength of concrete annulus, respectively.

It can be easily perceived from Figure 4.44 that the ANN model has nearly perfect estimation capacity whatever yield strength of outer and inner steel tubes. The yield strength values for outer steel tubes alter between 200 and 600 MPa, as seen in Figure 4.44a and the ANN model has almost same estimated values with the actual values for each outer steel tube yield strength.
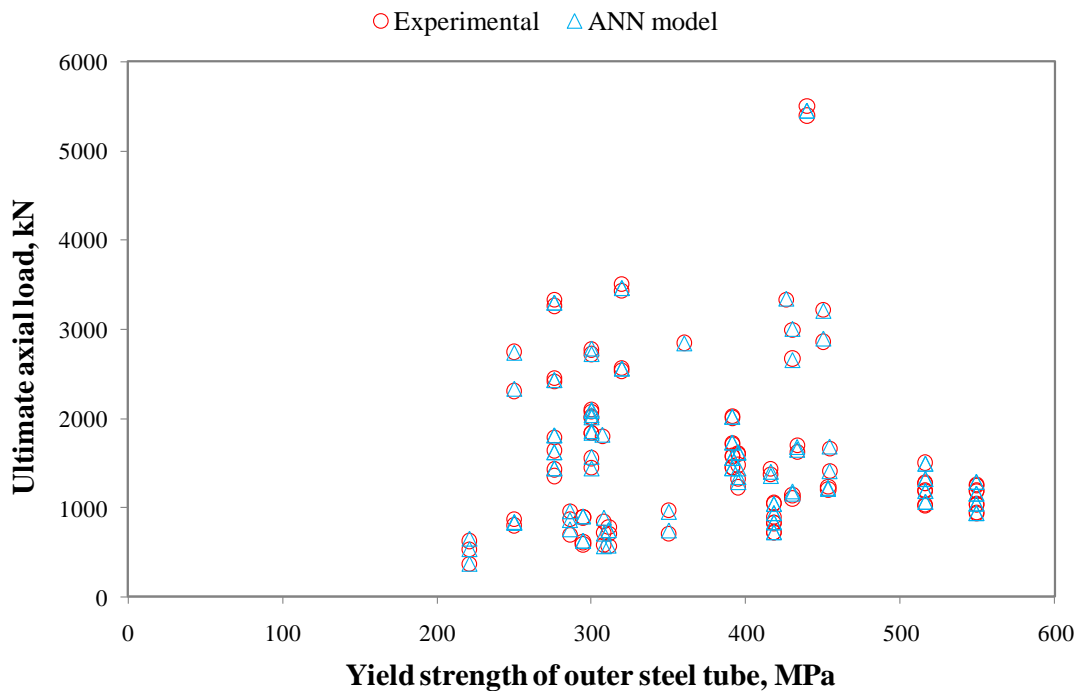


(a)
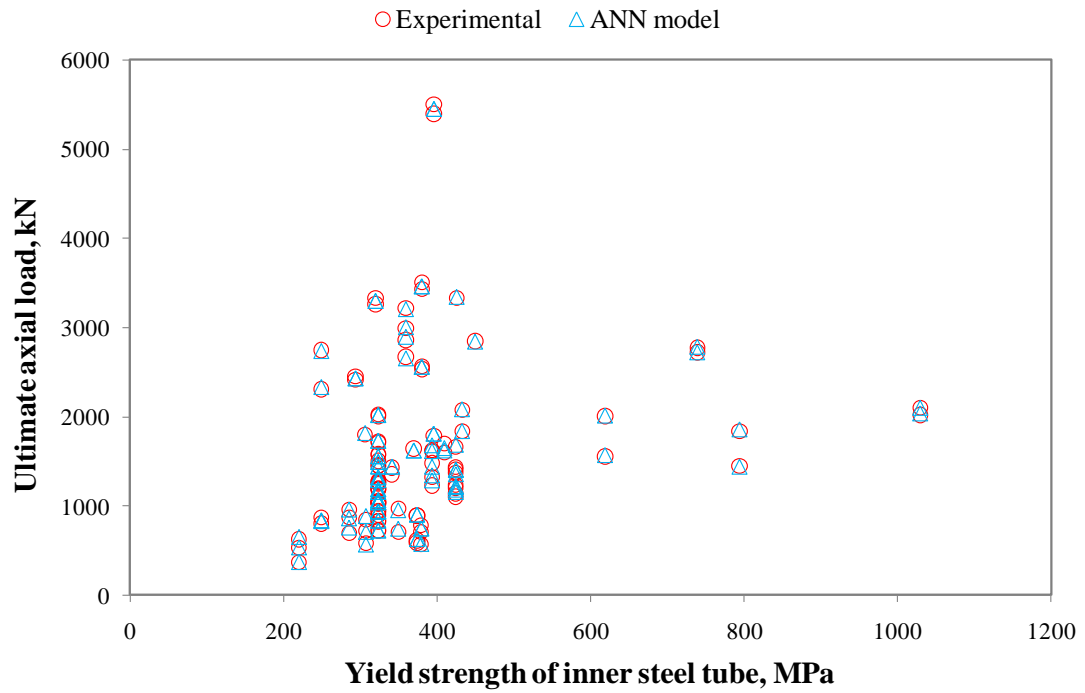
(b)
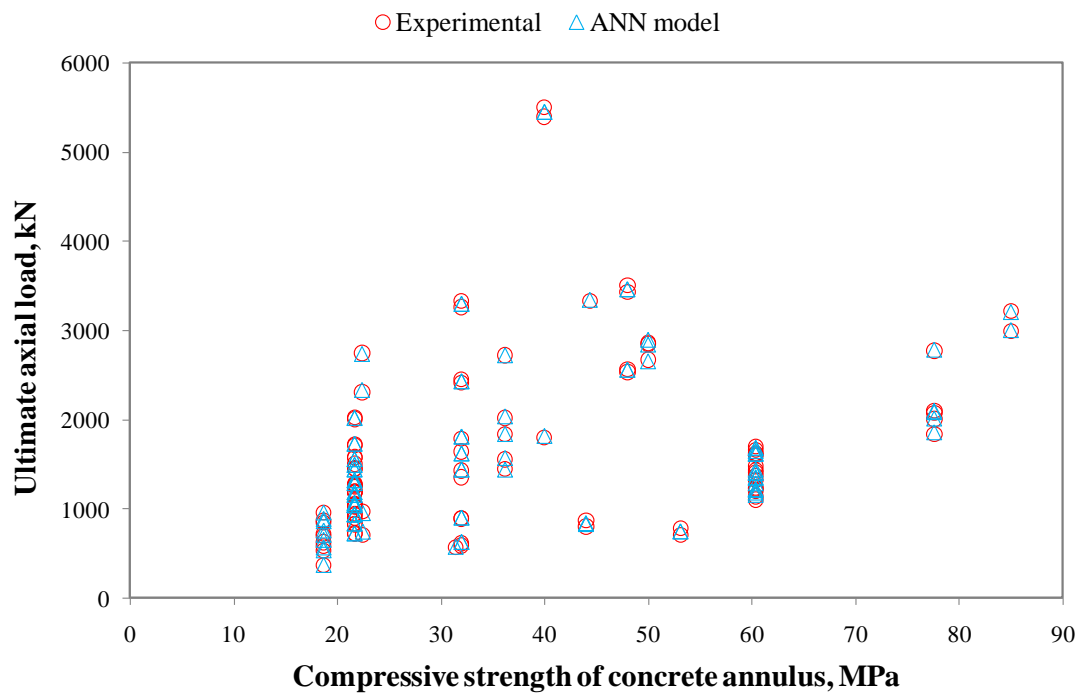


(c)

**Figure 4.44.** Experimental and ANN prediction ultimate axial strength versus: (a) yield strength of outer steel tube, (b) yield strength of inner steel tube, and (c) compressive strength of concrete annulus

160

The same situation can be valid for the relation between the actual and the predicted ultimate axial strengths versus inner steel tube yield strength as can be clearly seen in Figure 4.44b. Moreover, the compressive strength of the concrete has a significant effect on the load carrying capacity of the CFDST columns with CHS. The concrete compressive strength values used in the studies vary between 18 and 85 MPa. Figure 4.44c points out that the ANN model can properly estimate the ultimate axial strength of such types of columns without discriminating concrete compressive strength.

As well, the cross-sectional areas of the outer/inner steel tubes and concrete annulus has remarkable influences on the load carrying capacity of the CFDST columns with CHS as much as the yield strength of steel tubes and compressive strength of concrete.

Therefore, the graphical comparison of the actual and predicted ultimate axial strength values versus the cross-sectional area of the outer steel tube, inner steel tube, and concrete annulus are illustrated in Figure 4.45a, 4.45b, and 4.45c, respectively.
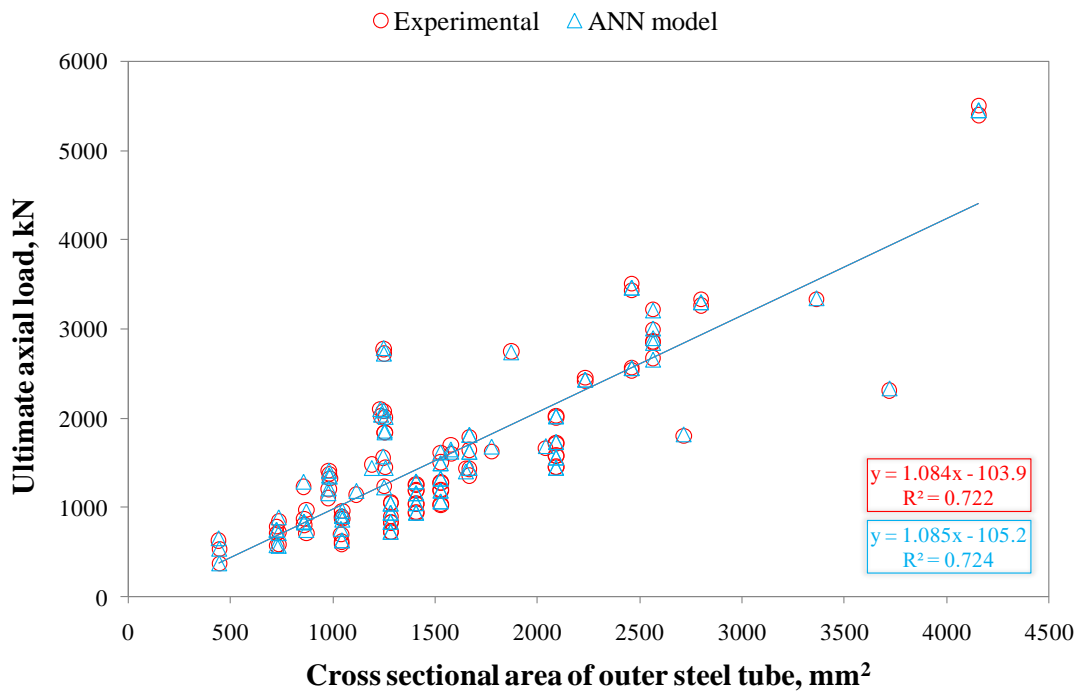


(a)
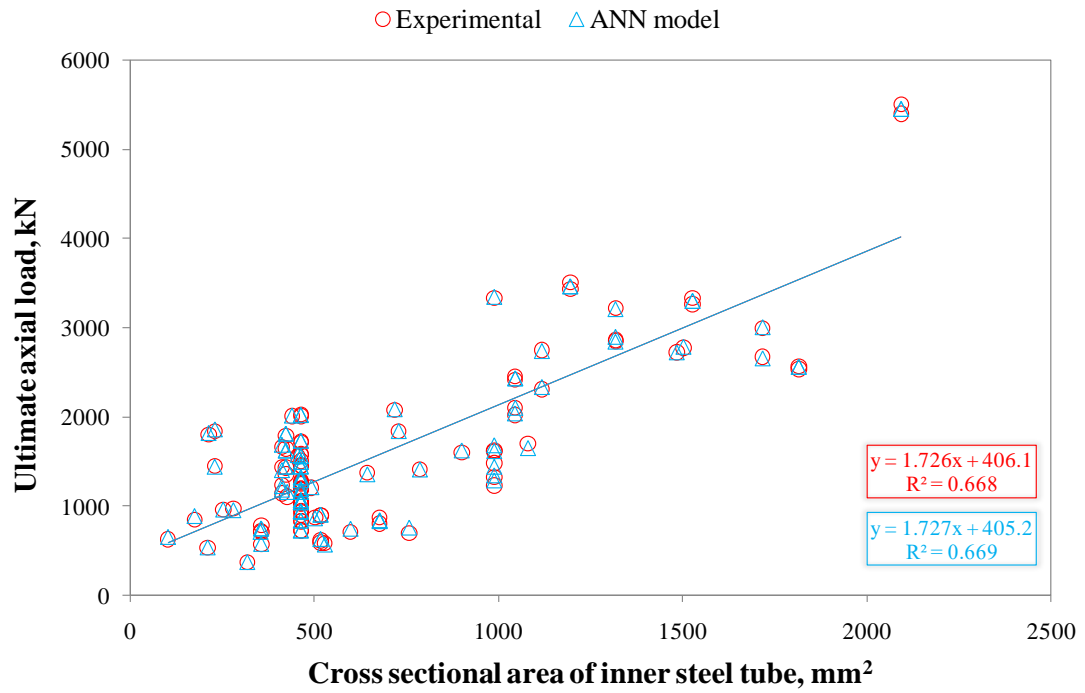
(b)
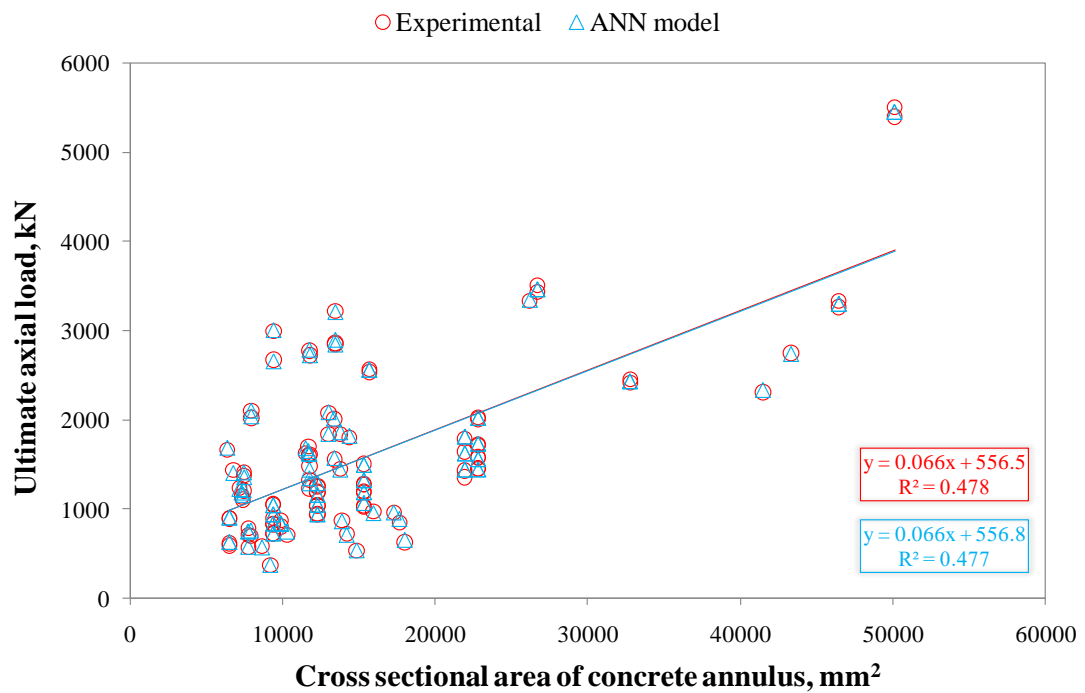


(c)

**Figure 4.45.** Experimental and ANN prediction ultimate axial strengths versus cross-sectional area of: (a) outer steel tube, (b) inner steel tube, and (c) concrete annulus

There is a reasonable linearly increasing relation between the cross-sectional area of the members and the experimental ultimate axial strength. This relation can be seen

for cross-sectional area of all members. The same trend could be observed for the predicted ultimate axial strength as well. The relation between the cross-sectional area and ultimate axial strength is almost similar for both actual and predicted values. This can be understood from the R-squared values of both actual and predicted results as given in Figure 4.45a, 4.45b, and 4.45c. The level of the relation between the cross-sectional area and ultimate axial strength can be comprehended from the R-squared values. It can be said that the relation between the cross-sectional area and the load carrying capacity for steel tubes is in the normal level whereas there is a poor relation level between the cross-sectional area of the concrete and the ultimate axial strength. The R-squared values for predicted ultimate axial strengths are almost same with that for actual strengths.

Although the load carrying capacity of the CFDST columns with CHS are significantly determined by the mechanical properties of the used materials and their cross-sectional areas, the length and the diameter of members used in the preparation of specimen as well as the amount of hollow part have also important influences on the ultimate axial strength of these columns. Because of that, Figures 4.46a, 4.46b, and 4.46c are presented to comprehend the effect of these parameters and how the ANN model results vary according to the changing in these parameters.
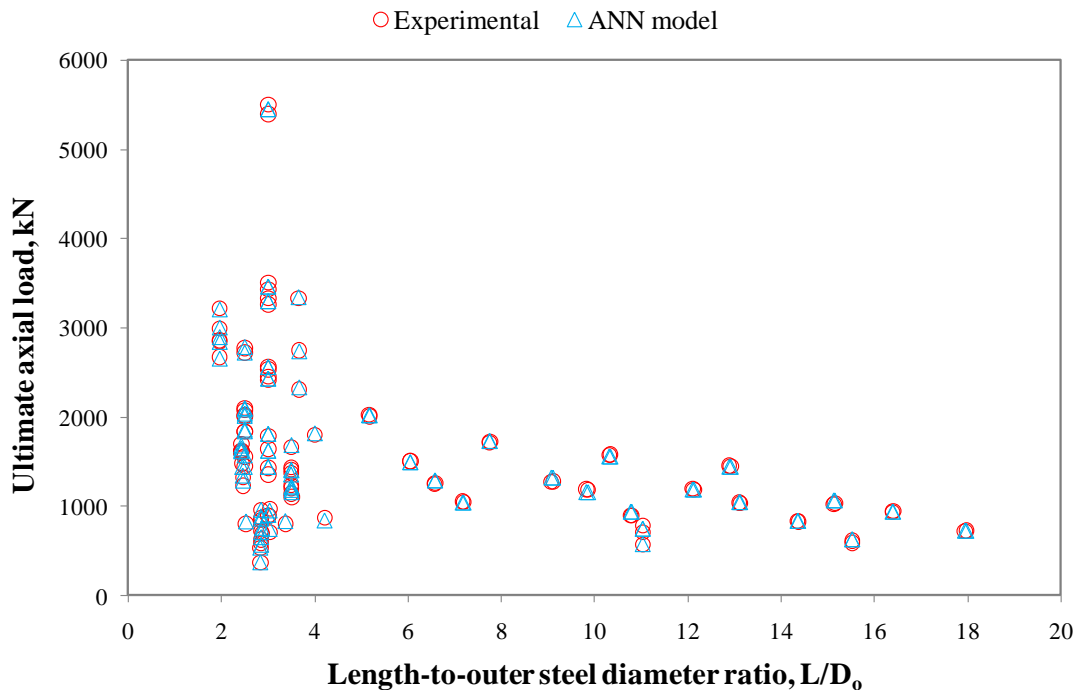


(a)
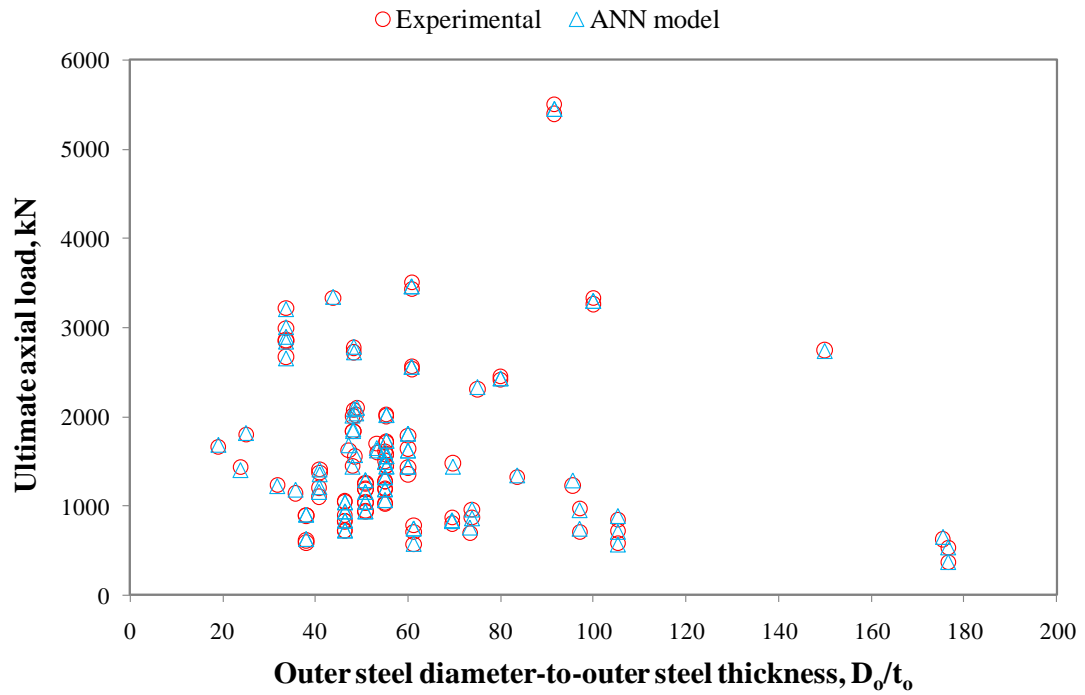
(b)
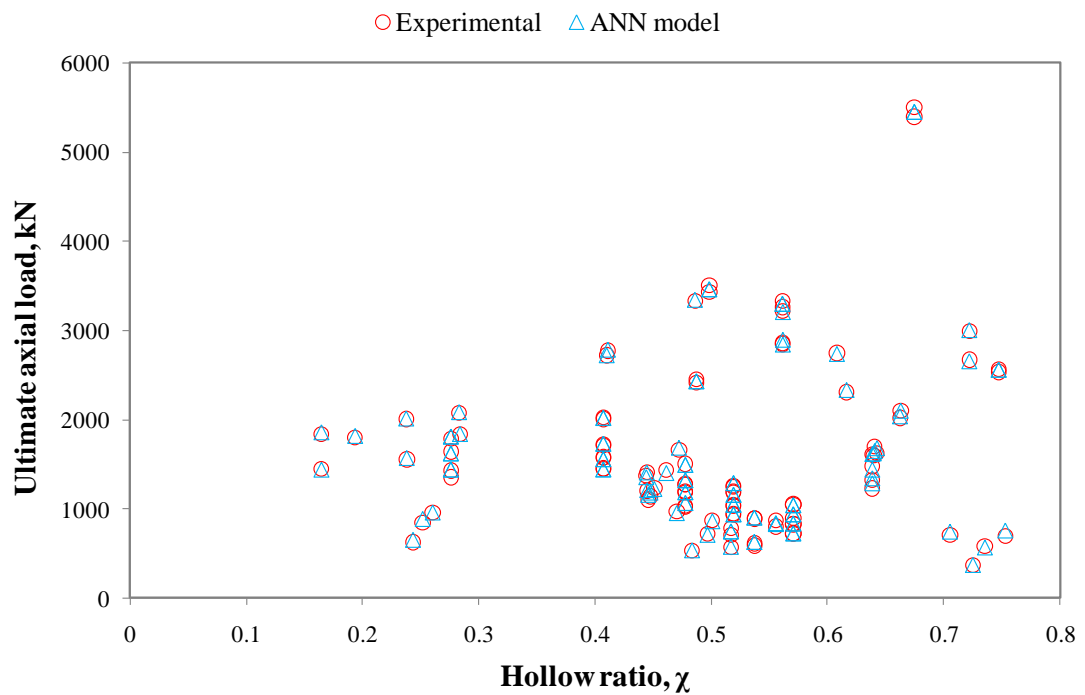


(c)

**Figure 4.46.** Experimental and ANN prediction ultimate axial strength versus: (a) length-to-outer steel tube ratio (L/D$_o$), (b) outer steel diameter-to-outer steel thickness (D$_o$/t$_o$), and (c) hollow ratio (χ)

According to Figure 4.46a, 4.46b, and 4.46c, it can be discerned that how the performance of the ANN model regarding the prediction of the ultimate axial strength of the CFDST columns with CHS alters when the sectional properties of the elements are changed. The ANN model has the ability to extrapolate the load carrying capacity of these columns without exception $L/D_o$ value. Namely, it cannot be said about the ANN model that it is able to predict the ultimate axial strength of columns that has a certain $L/D_o$ value. This situation is also identical for $D_o/t_o$ and hollow ratio values as can be obviously experienced from the observing of Figures 4.46b and 4.46c. As a result, it could be summarized that the generated ANN model is not influenced from the sectional and geometric properties of the members and the proposed model has a general estimation capability.

### 4.3.3 Comparison of ANN Model with Modified ACI (2002) Formula

The ultimate axial strengths predicted by the ANN model and the modified ACI (2002) formula versus experimental ultimate axial strengths and the normalized ultimate strength values of the ANN model and the modified ACI (2002) formula are presented in Figure 4.47a and 4.47b, respectively. The easily visual comparison for the prediction performance of the ANN model against to the modified ACI (2002) formula is the purpose of the presenting the results as graph.



(a)

165
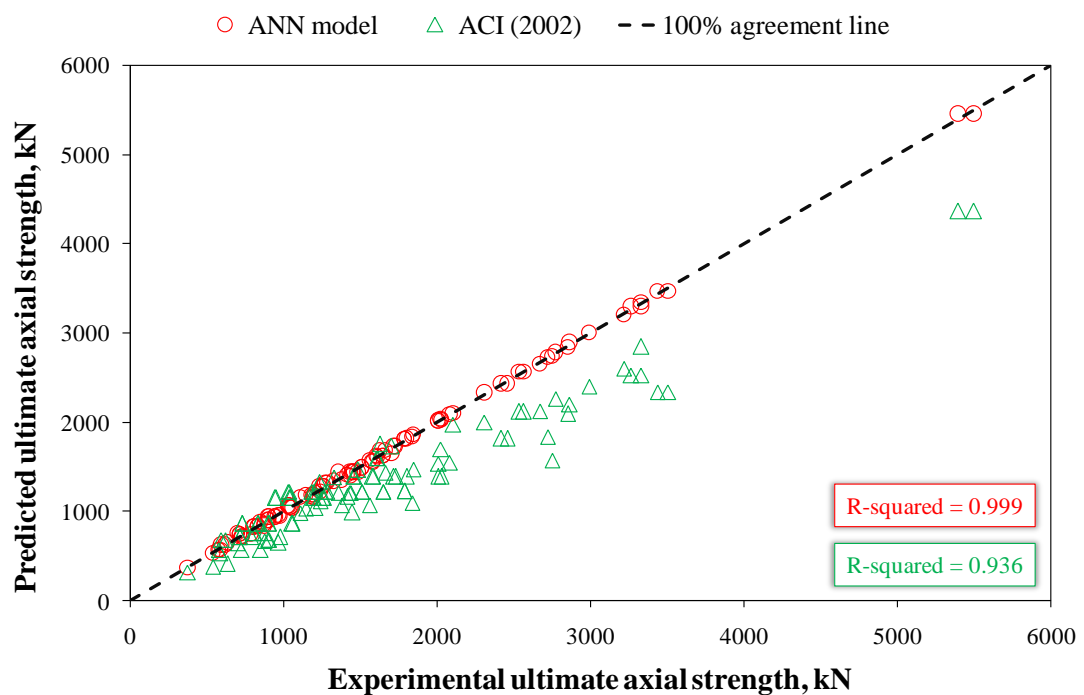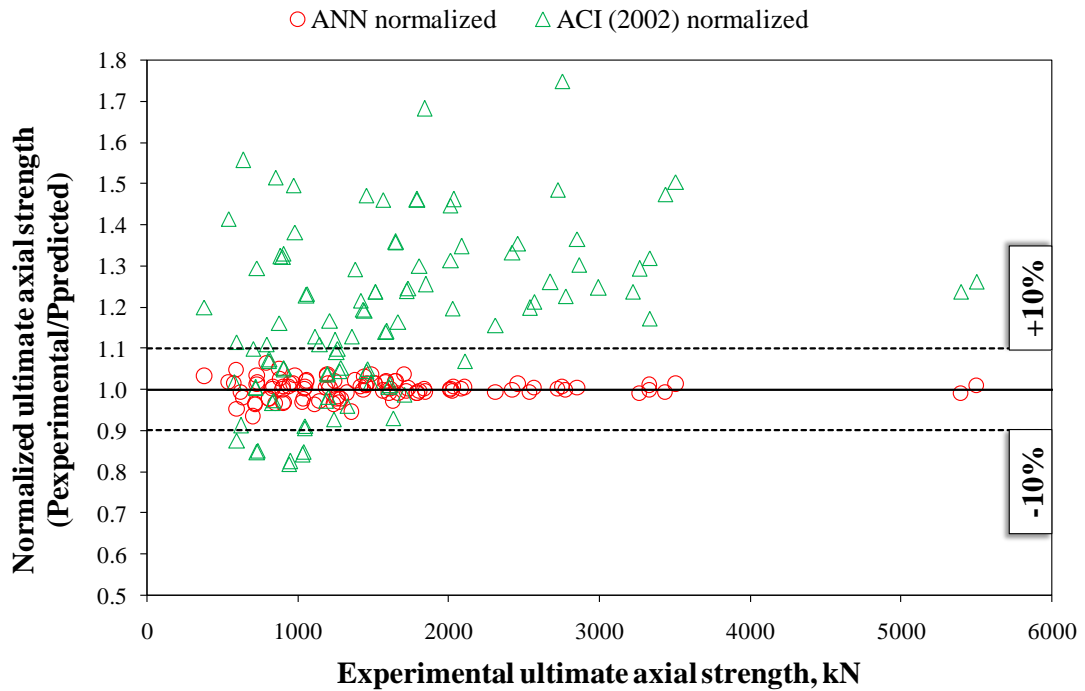
(b)

**Figure 4.47.** (a) predicted and (b) normalized ultimate axial strengths of ANN model and modified ACI (2002) formula versus experimental ultimate axial strengths

The results indicated that the ANN model has a superior prediction performance against to the modified ACI (2002) formula. While the results of the generated ANN model dispersed as a straight line on the 100% agreement line, the results of the modified ACI (2002) formula spread a large area away from the 100% agreement line as can be seen in Figure 4.47a.

In addition, the normalized ultimate axial strength results exhibited that the ANN model has overestimated and underestimated values so close to the experimental results whereas the modified ACI (2002) formula has over and underestimated values far away from the experimental results. This illustrates that the ANN model is more reliable and accurate than the modified ACI (2002) formula.

**4.3.4 Comparison of ANN Model with Modified Eurocode 4 (2004) Formula**

The ultimate axial strength predicted by the ANN model and the modified Eurocode 4 (2004) formula versus experimental ultimate axial strength and the normalized ultimate strength values of the ANN model and the modified Eurocode 4 (2004) formula are presented in Figure 4.48a and 4.48b, respectively. The easily visual

166

comparison for the prediction performance of the ANN model against to the modified Eurocode 4 (2004) formula is the purpose of the presenting the results as graph.

The predicted ultimate axial strengths of the ANN model distribute on the 100% agreement line and it means that the predicted strengths attained by the ANN model are almost same with the experimental strengths. However, the ultimate axial strengths predicted by the modified Eurocode 4 (2004) are dispersed a little far away from the 100% agreement line as shown in Figure 4.48a. This visual observation indicates how the prediction performance of the ANN model is good.

Moreover, when the Figure 4.48b is viewed, it would be noticed that all normalized values of the ANN model fell between the upper and lower normalization limit lines whereas great numbers of normalized values of the modified Eurocode 4 (2004) formula are at outside of the normalizations limit lines. The modified Eurocode 4 (2004) formula is the best existing formula in the literature used to extrapolate the ultimate axial strength of the CFDST columns with CHS. But when Figures 4.48a and 4.48b are observed, it can be easily noticed that the generated ANN model is much better than the modified Eurocode 4 (2004) formula.
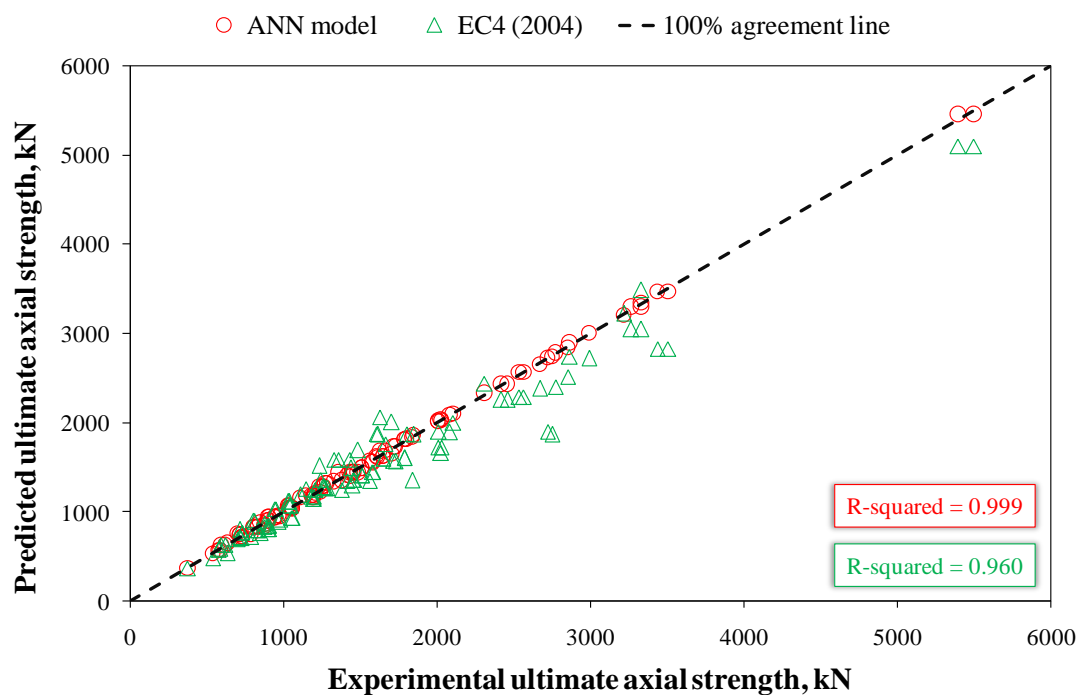


(a)

(b)

**Figure 4.48.** (a) predicted and (b) normalized ultimate axial strengths of ANN model and modified EC4 (2004) formula versus experimental ultimate axial strengths

## 4.3.5 Comparison of ANN Model with Modified AISC (2010) Formula

The ultimate axial strength predicted by the ANN model and the modified AISC (2010) formula versus experimental ultimate axial strength and the normalized ultimate strength values of the ANN model and the modified AISC (2010) formula are presented in Figure 4.49a and 4.49b, respectively. The easily visual comparison for the prediction performance of the ANN model against to the modified AISC (2010) formula is the purpose of the presenting the results as graph.

Figure 4.49a indicates that the predicted ultimate axial strength of the ANN model dispersed on the 100% agreement line like a straight line, yet, the results of modified AISC (2010) formula disperses not only near to the 100% agreement line but also far away from it. This is the demonstration of how the estimation capability of the ANN model was better. When Figure 4.49b is viewed, it can be readily seen that numerous normalized ultimate axial strength values of the modified AISC (2010) formula fall out of the normalization limit lines of ±10%. But all normalized values of the ANN model are between these limit. According to these findings, it can be unequivocally

said that the performance of the ANN model in the prediction of the ultimate axial strength of the CFDST columns with CHS is much better than that of the modified AISC (2010) formula.



(a)
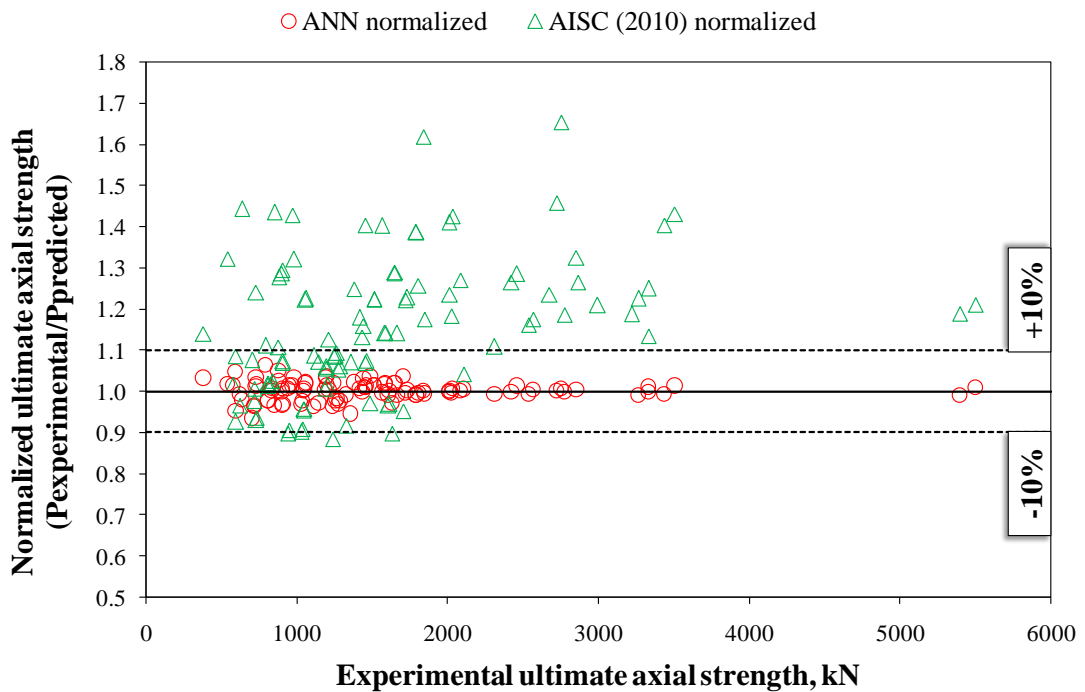


(b)

**Figure 4.49.** (a) predicted and (b) normalized ultimate axial strengths of ANN model and modified AISC (2010) formula versus experimental ultimate axial strengths

### 4.3.6 Comparison of ANN Model with Model of Uenaka et al. (2010)

The ultimate axial strength predicted by the ANN model and the proposed empirical model of Uenaka et al. (2010) versus experimental ultimate axial strength and the normalized ultimate strength values of the ANN model and the proposed empirical model of Uenaka et al. (2010) are presented in Figure 4.50a and 4.50b, respectively. The easily visual comparison for the prediction performance of the ANN model against to the model of Uenaka et al. (2010) is the purpose of the presenting the results as graph.

The R-squared values given in Figure 4.50a indicate how much the prediction performance of the generated ANN model is better than the empirical model of Ueneka et al. (2010). The R-squared value of the model recommended by Ueneka et al. (2010) is 0.888 whilst that of the generated ANN model is 0.999. There are many predicted ultimate axial strength values much more than or less than the experimental values while there is a slight difference between the experimental strength and the predicted strength by the generated ANN model that could be negligible.



(a)
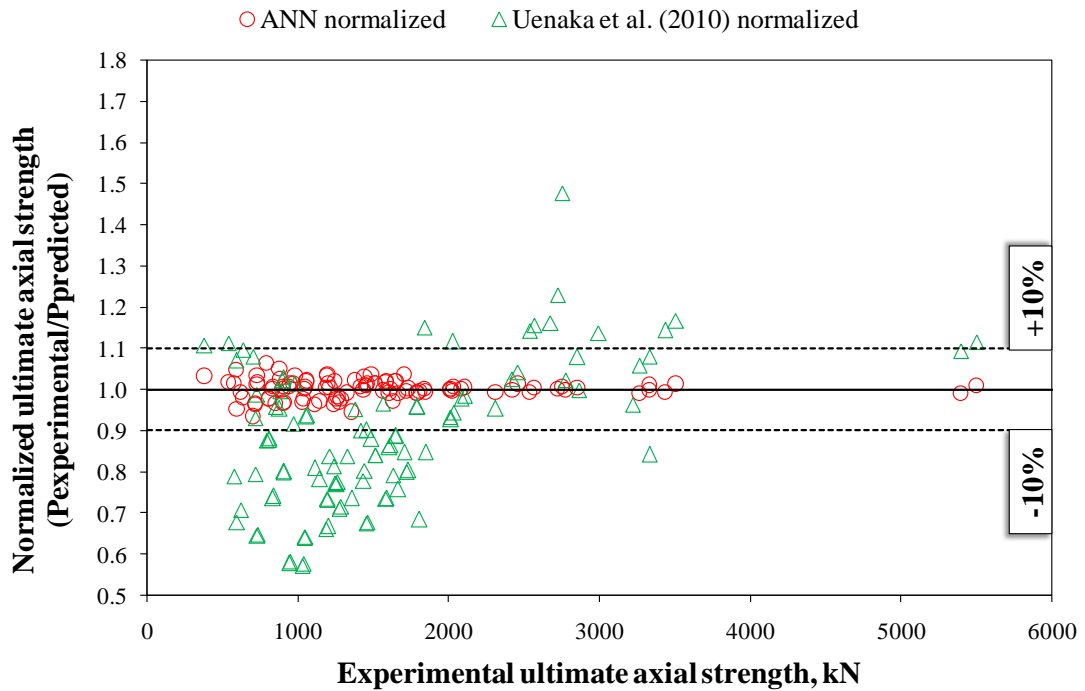
(b)

**Figure 4.50.** (a) predicted and (b) normalized ultimate axial strengths of ANN model and Uenaka et al. (2010) model versus experimental ultimate axial strengths

The difference in the prediction performance of the generated ANN model and the model of Uenaka et al. (2010) could be openly viewed in Figure 4.50b. While the scattering of the normalized ultimate axial strength values attained from the ANN model is near to the perfect, the interspersion of the normalized values obtained from the model of Uenaka et al. (2010) is very poor. As a result, it can be certainly expressed that the prediction performance of the ANN model is much better than that of the model suggested by Uenaka et al. (2010).

**4.3.7 Comparison of ANN Model with Model of Han et al. (2011b)**

The ultimate axial strength predicted by the ANN model and the proposed empirical model of Han et al. (2011b) versus experimental ultimate axial strength and the normalized ultimate strength values of the ANN model and the proposed empirical model of Han et al. (2011b) are pr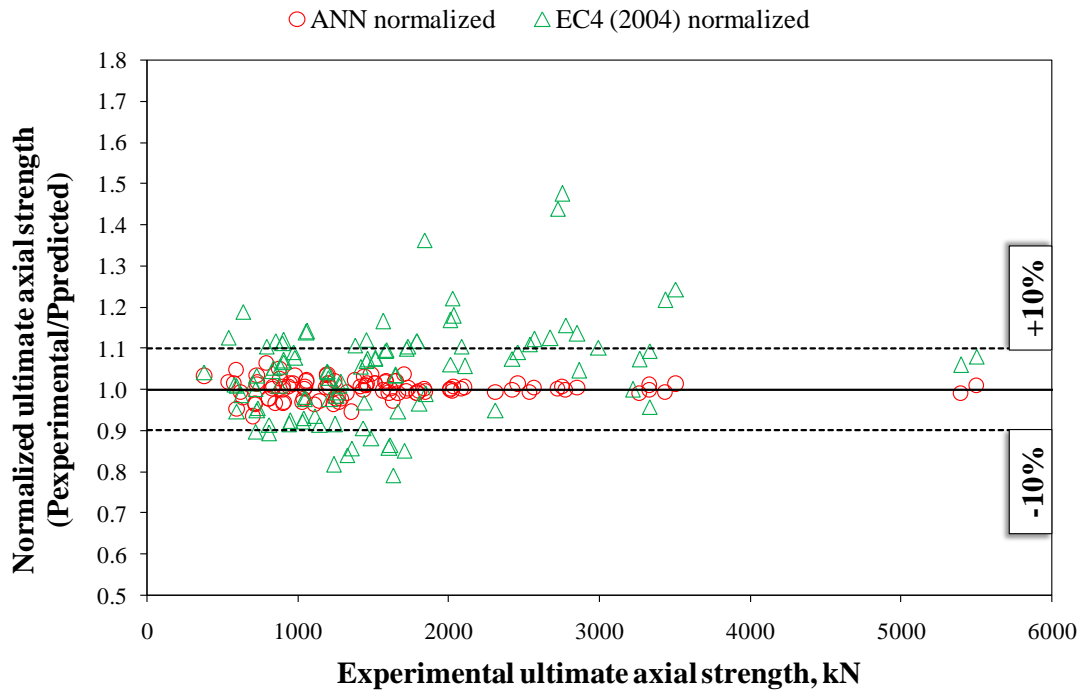esented in Figure 4.51a and 4.51b, respectively. The easily visual comparison for the prediction performance of the ANN model against to the model of Han et al. (2011b) is the purpose of the presenting the results as graph.

(a)
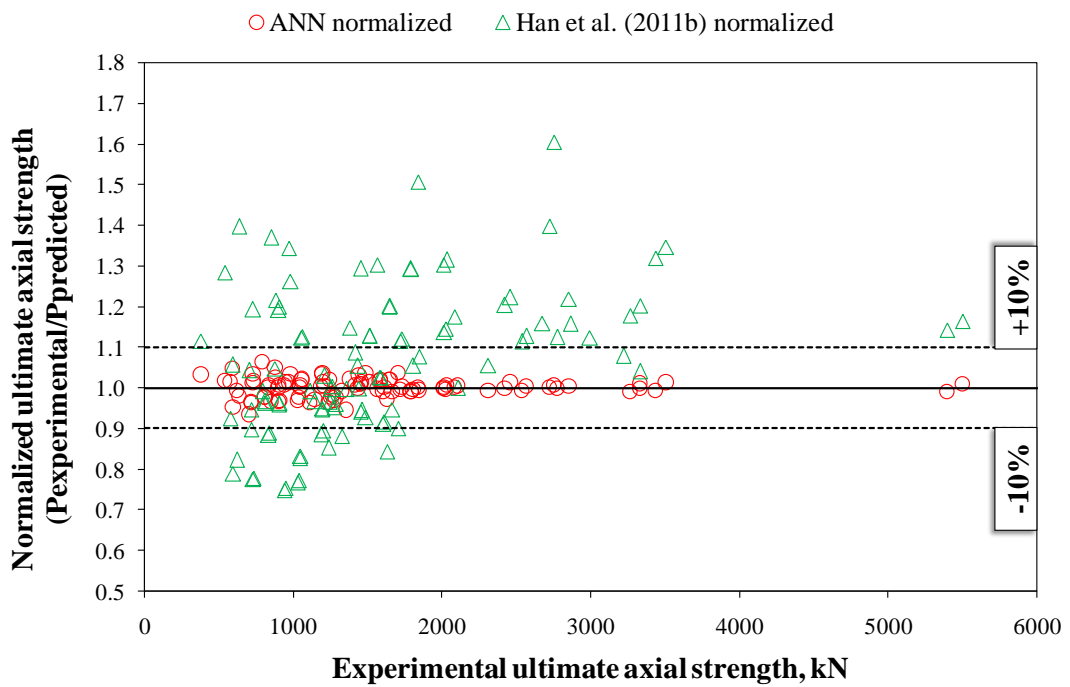


(b)

**Figure 4.51.** (a) predicted and (b) normalized ultimate axial strengths of ANN model and Han et al. (2011b) model versus experimental ultimate axial strengths

Figure 4.51a indicates that the predicted ultimate axial strength of the ANN model disperse on the 100% agreement line like a straight line, but the results of the model of Han et al. (2011b) intersperse both near to the 100% agreement line and far away

from it. This is the indication of how the prediction performance of the generated ANN model is better.

The model proposed by Han et al. (2011b) has many underestimated ultimate axial strength values as clearly be seen in Figure 4.51b. However, the ANN model also has over and underestimated ultimate axial strength values of which variation could be neglected, namely the residual ultimate strength values of the generated ANN model are so small when it is compared with the residual strength values of the model proposed by Han et al. (2011b). For this reason, it can be indisputably said for the ANN model, it is much more reliable and robust model than the model proffered by Han et al. (2011b).

### 4.3.8 Comparison of ANN Model with Model of Yu et al. (2013)

The ultimate axial strength predicted by the ANN model and the proposed empirical model of Yu et al. (2013) versus experimental ultimate axial strength and the normalized ultimate strength values of the ANN model and the proposed empirical model of Yu et al. (2013) are presented in Figure 4.52a and 4.52b, respectively. The easily visual comparison for the prediction performance of the ANN model against to the model of Yu et al. (2013) is the purpose of the presenting the results as graph.

Figure 4.52a indicates the relation between the predicted and experimental strengths. According to observing this figure, it can be seen that the scattering of the predicted ultimate axial strength values calculated by the generated ANN model is like a straight line and amasses so close to the 100% agreement line. However, a wider dispersion of the results of the model of Yu et al. (2013) can be observed in Figure 4.52a. The difference in the prediction performance of the ANN and Yu et al. (2013) models could be clearly viewed in Figure 4.52b. The figure reveals that while all normalized ultimate axial strength values of the ANN model are between the normalization limit lines of ±10%, there is only a few number of the normalized strength values of the model of Yu et al. (2013) falling between these limit lines. This demonstrates that there are a lot of over and underestimated ultimate axial strength values of the model proposed by Yu et al. (2013). According to graphical presentations of the prediction performance, it could be absolutely said for the generated ANN model that its reliability and accuracy are much better than that of the model suggested by Yu et al. (2013).
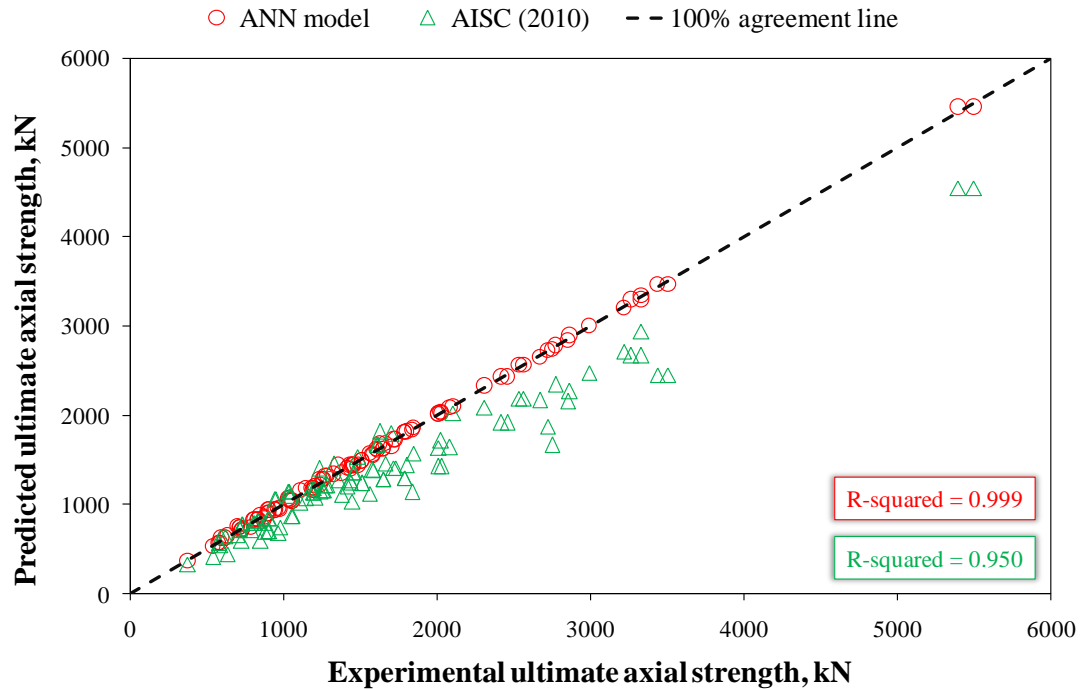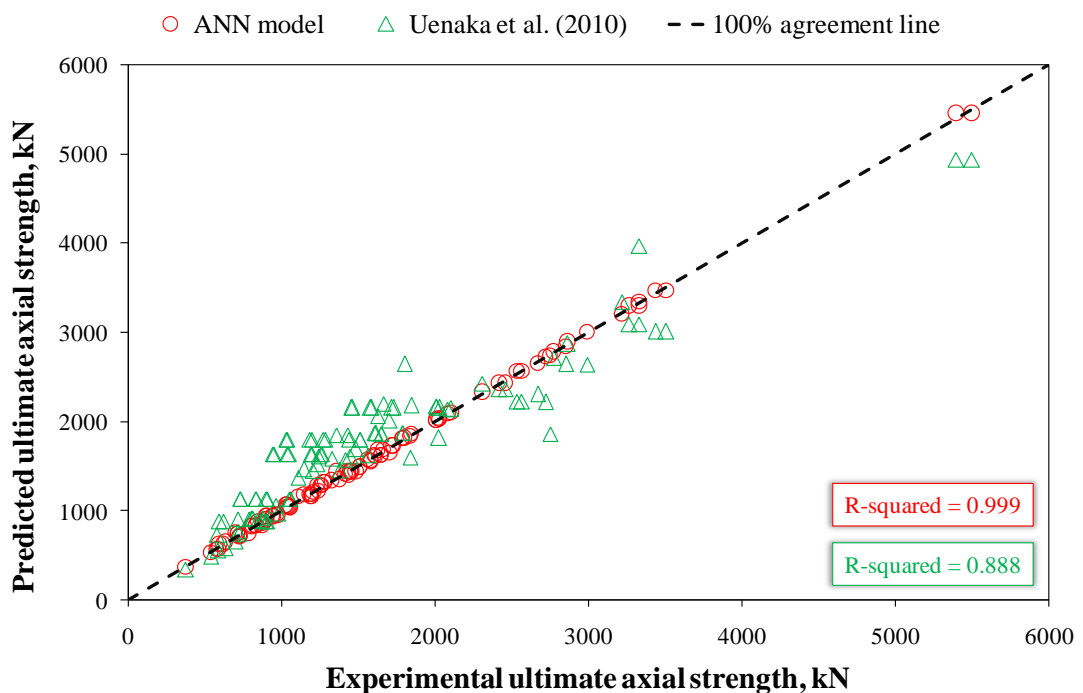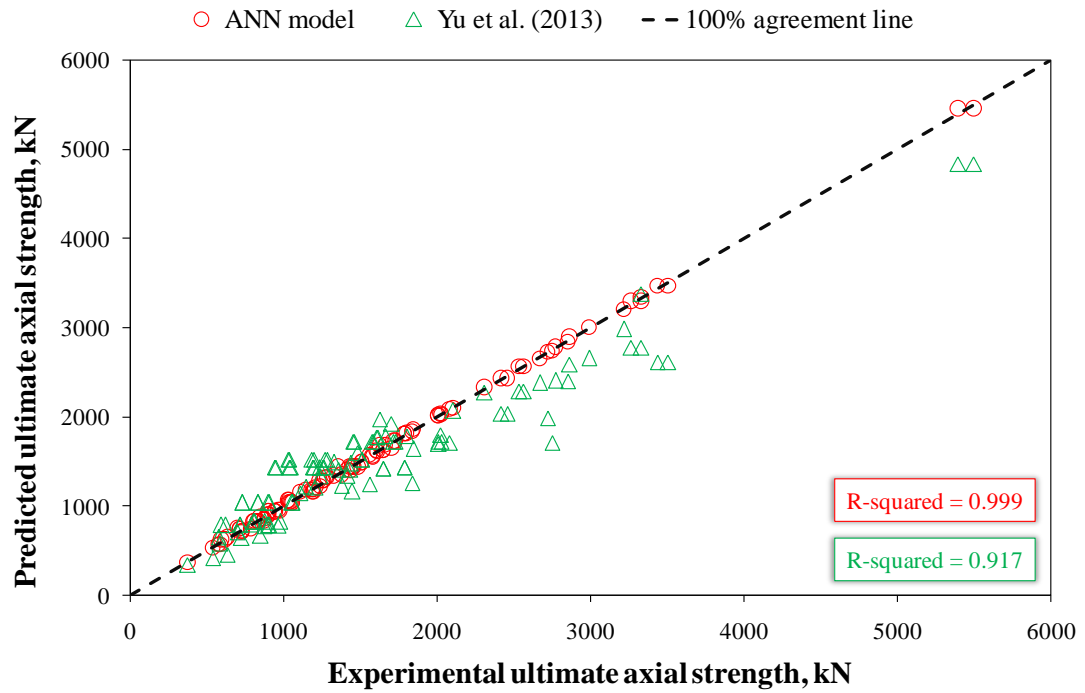
(a)
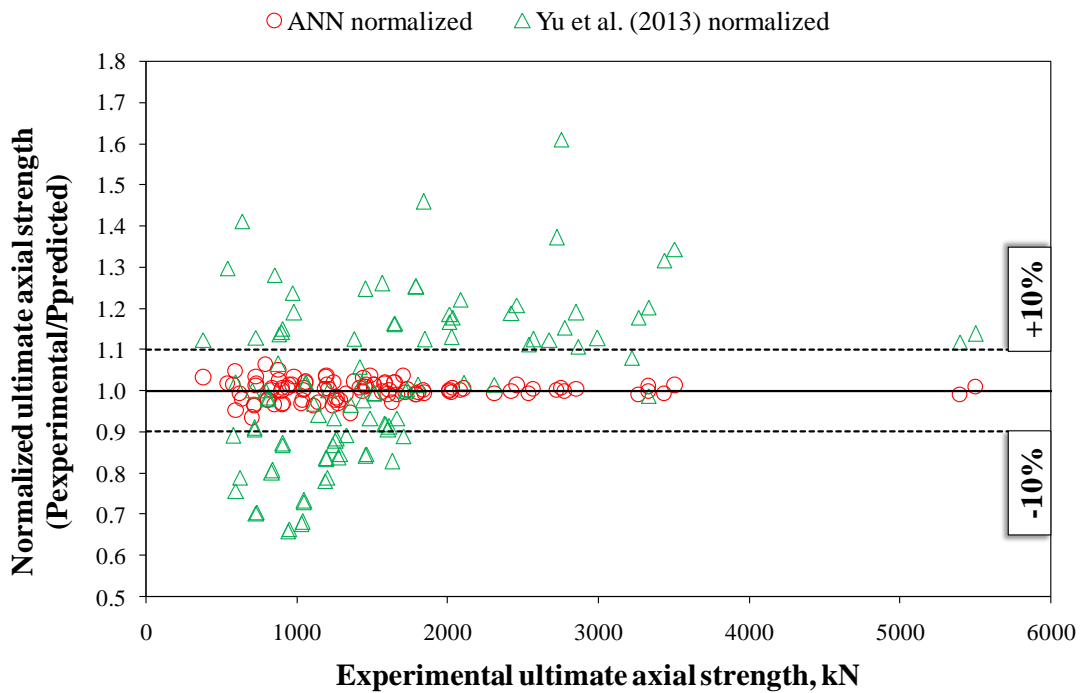


(b)

**Figure 4.52.** (a) predicted and (b) normalized ultimate axial strengths of ANN model and Yu et al. (2013) model versus experimental ultimate axial strengths

## 4.2.9 Comparison of GEP Model with Model of Hassanein et al. (2013b)

The ultimate axial strength predicted by the ANN model and the proposed empirical model of Hassanein et al. (2013b) versus experimental ultimate axial strength and the normalized ultimate strength values of the ANN model and the proposed empirical model of Hassanein et al. (2013b) are presented in Figure 4.53a and 4.53b, respectively. The easily visual comparison for the prediction performance of the ANN model against to the model of Hassanein et al. (2013b) is the purpose of the presenting the results as graph.

The ultimate axial strength predicted according to the model proposed by Hassanein et al. (2013b) indicates similar performance with that of Yu et al. (2013). But it could be briefly specified that the model of Hassanein et al. (2013b) has a bad prediction performance when it is compared with the ANN model. In addition, when Figure 4.53b is viewed, it would be seen that there are a lot of normalized values achieved from the model of Hassanein et al. (2013b) dispersed throughout outside of the ±10% normalization limit line. On the other hand, all normalized value of the ANN model is at the inside of the normalization limit lines. For this reason, in the general view of the prediction, the ANN model has a superior estimation capability with respect to predict the ultimate axial strength values of the CFDST columns with CHS.
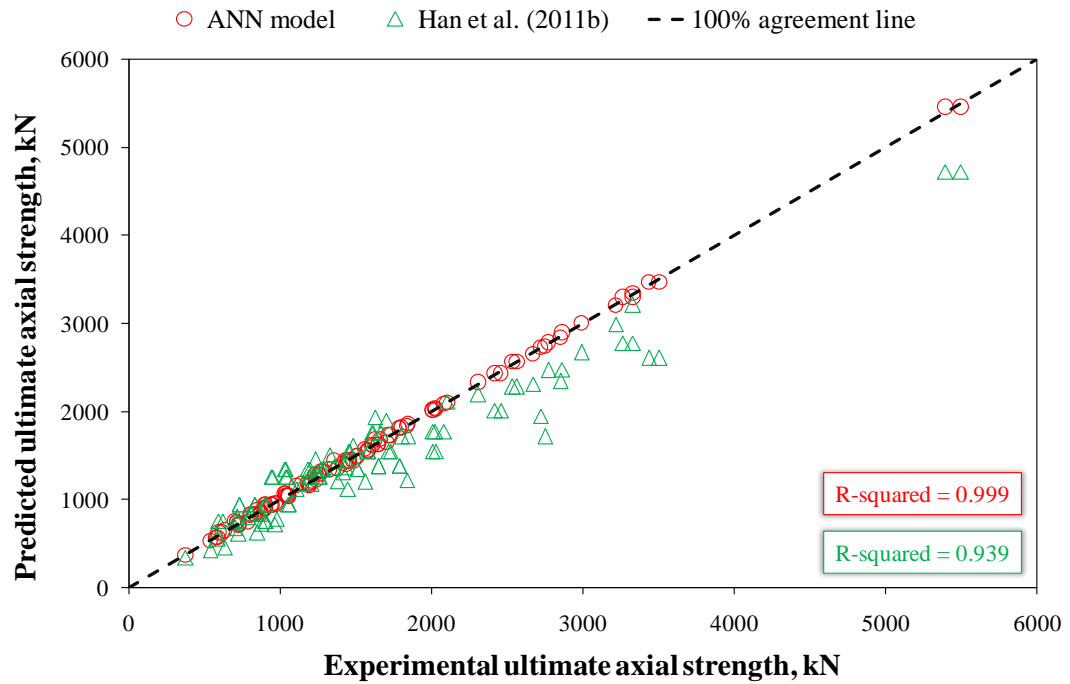


(a)

175
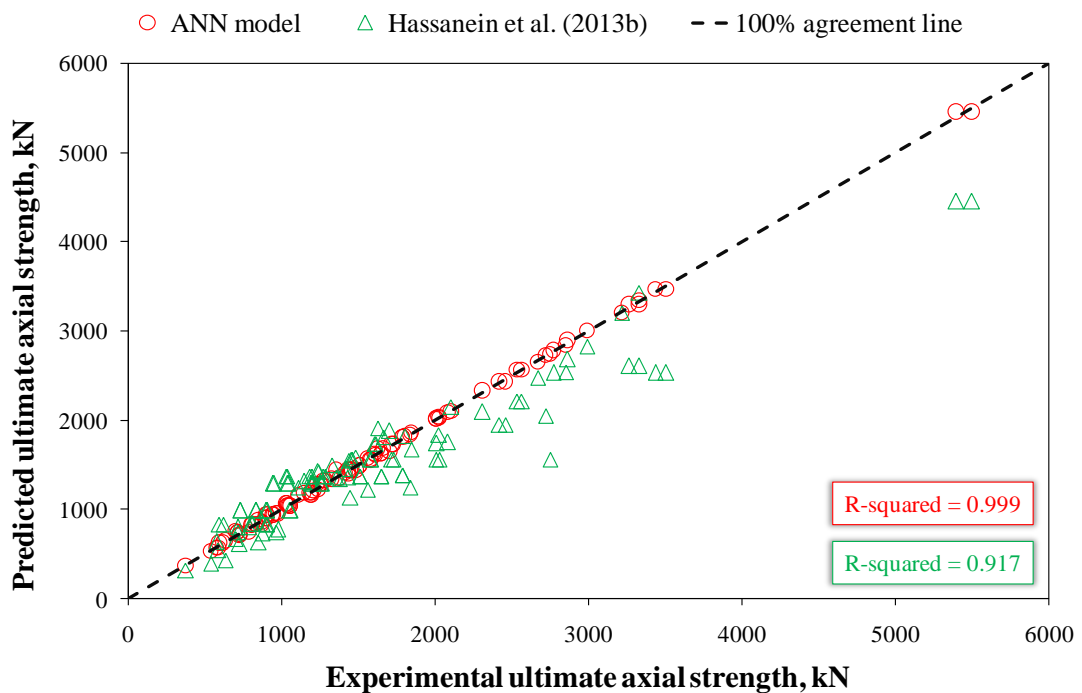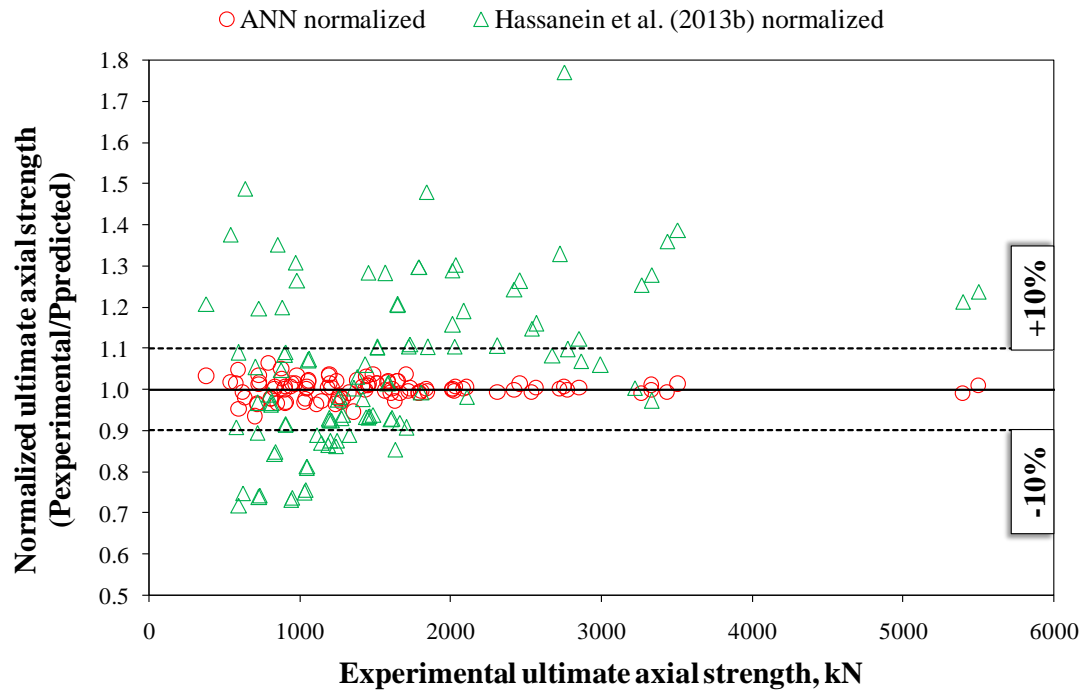
(b)

**Figure 4.53.** (a) predicted and (b) normalized ultimate axial strengths of ANN model and Hassanein et al. (2013b) model versus experimental ultimate axial strengths

## 4.2.10 Statistical Comparison of Models

In addition to graphical comparison of the results, the statistically evaluation of the model is crucially necessary. Therefore, the ultimate axial strength results extrapolated by the ANN model, the modified formulas, and the proposed empirical models are statistically evaluated in this section. The fundamental statistical parameters such as MAPE, MSE, RMSE, COV, and R-squared values of which formulas were given in Chapter 3 are used to evaluate the prediction performance of the models and compare their capabilities. The values of these parameters are tabulated in Table 4.6.

In order to visualize these tabulated values, MAPE, MSE, and RMSE values are shown in Figure 4.54a, 4.54b, and 4.54c, respectively, while COV and R-sqaured values are indicated in Figure 4.55a and 4.55b, respectively.

The MAPE, MSE, and RMSE values indicated the ANN model is incomparably better than the modified formulas and the proposed empirical models. These statistical parameters indicate the errors, which is occurred by the model during the

prediction, and according to these parameters, it can be easily said that the ANN model has a wonderful prediction performance. Because the amount of error occurred at during the prediction by the modified formulas and the proposed models is at a tremendous rate when compared with the amount of error caused by the ANN model prediction.

**Table 4.6.** Statistical parameters of the prediction performance of proposed ANN model and existing design codes and suggested empirical models in the previous studies

| Statistical parameters | Mean absolute percent error (MAPE) | Mean square error (MSE) | Root mean square error (RMSE) | Coefficient of variation (COV) | Coefficient of determination (R-squared) |
|---|---|---|---|---|---|
| **ANN** | 1.69 | 688 | 21.1 | 0.022 | 0.999 |
| **Train** | | | | | |
| **Test** | 1.56 | 567 | 19.8 | 0.020 | 0.999 |
| | 2.06 | 1044 | 25.2 | 0.028 | 0.999 |
| **ACI (2002)** | 16.81 | 168726 | 301.0 | 0.192 | 0.936 |
| **EC4 (2004)** | 8.68 | 45291 | 151.4 | 0.104 | 0.960 |
| **AISC (2010)** | 14.41 | 129403 | 262.5 | 0.139 | 0.950 |
| **Uenaka et al. (2010)** | 21.46 | 128636 | 291.2 | 0.186 | 0.888 |
| **Han et al. (2011b)** | 13.48 | 87481 | 220.6 | 0.160 | 0.939 |
| **Yu et al. (2013)** | 15.43 | 90708 | 234.3 | 0.180 | 0.917 |
| **Hassanein et al. (2013b)** | 14.54 | 104162 | 232.5 | 0.178 | 0.917 |

The COV value gives an idea about the prediction performance of the model by approaching to or moving away from 0. There is an inverse proportion between the COV value and the prediction performance. When the COV value approaches to 0, the model would has a good prediction performance. For this reason, it could be clearly seen from Figure 4.55a, the lowest COV value of the normalized ultimate axial strength is determined for the ANN model that means it has a superior

prediction performance than the modified formulas and the proposed empirical models.
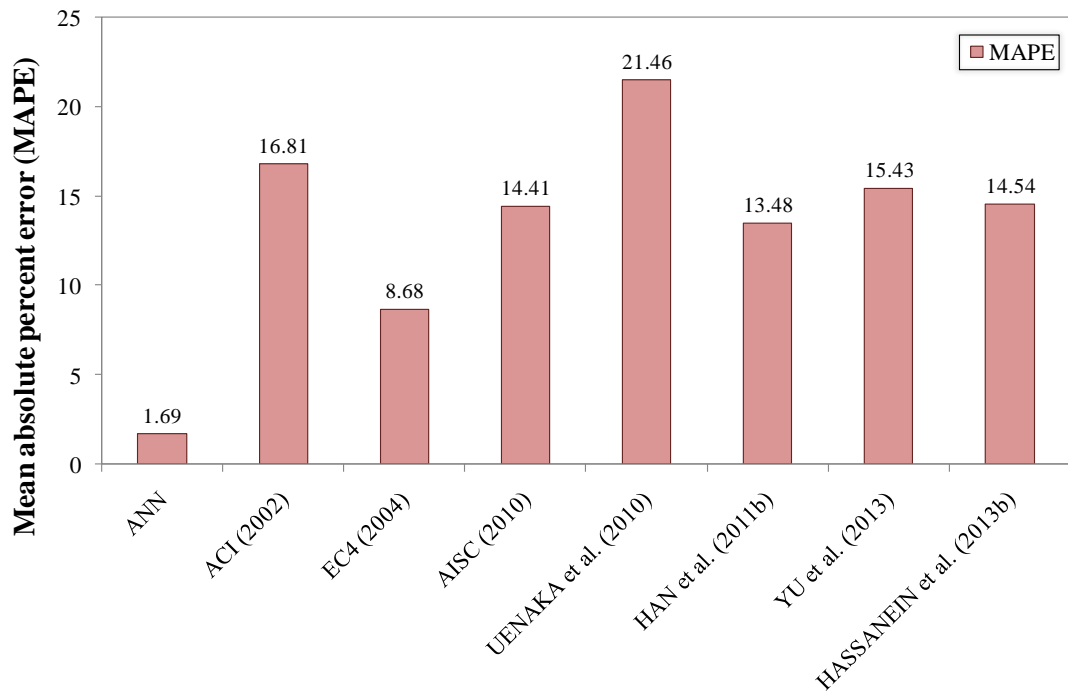


(a)
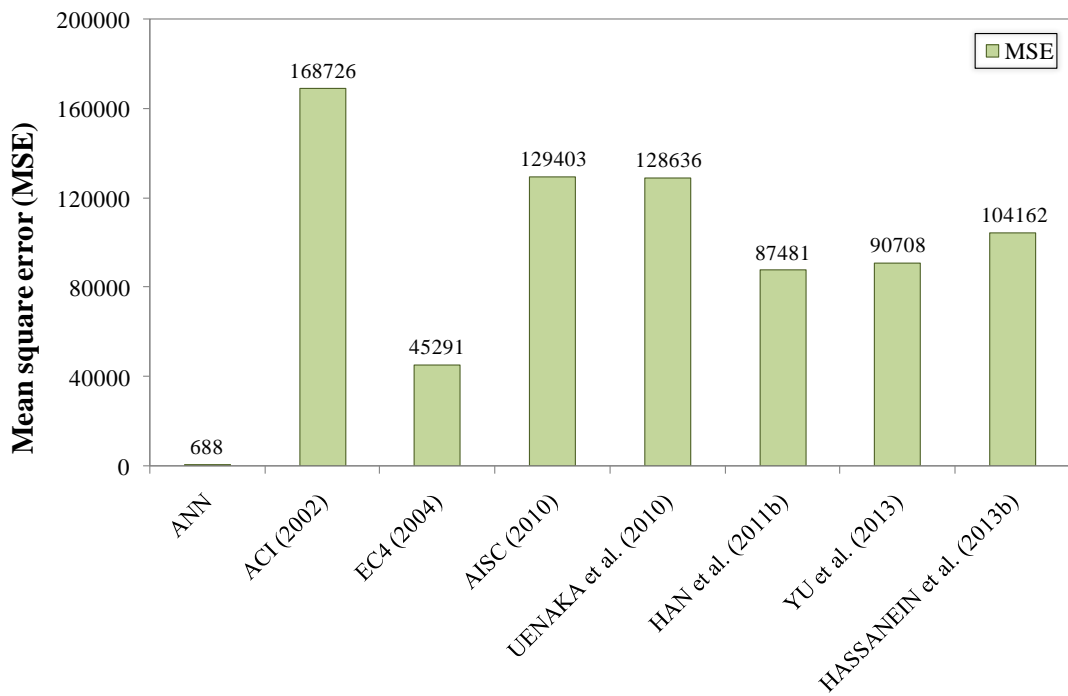


(b)
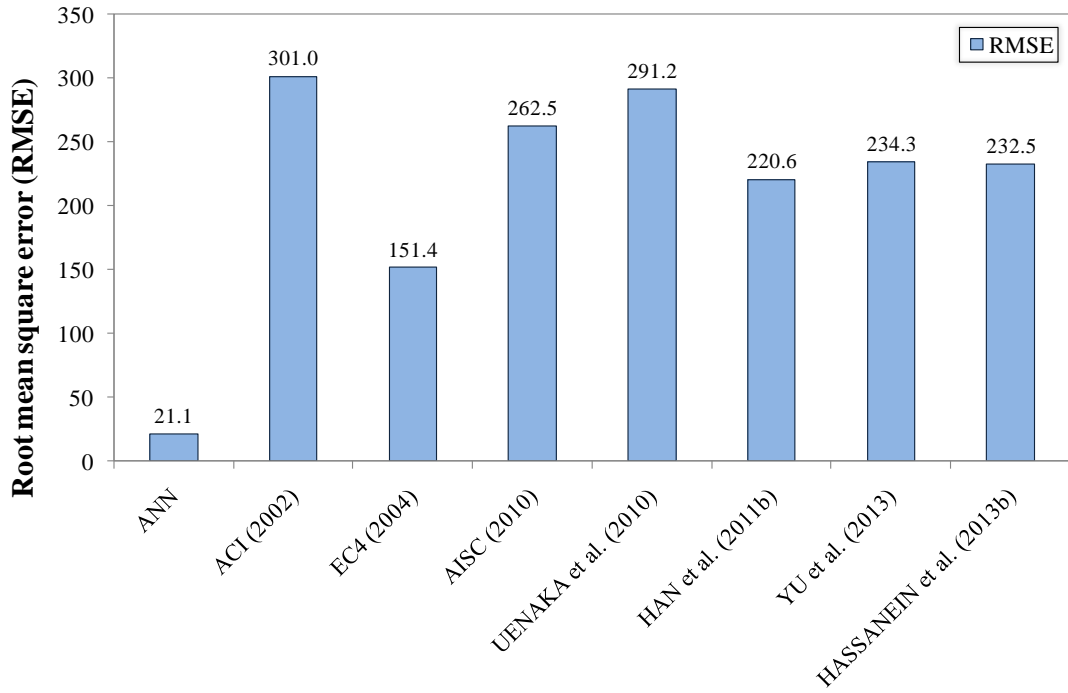
(c)

**Figure 4.54.** Statistically comparison ANN model with the modified formulas and suggested empirical models with regard to: (a) MAPE, (b) MSE, and (c) RMSE
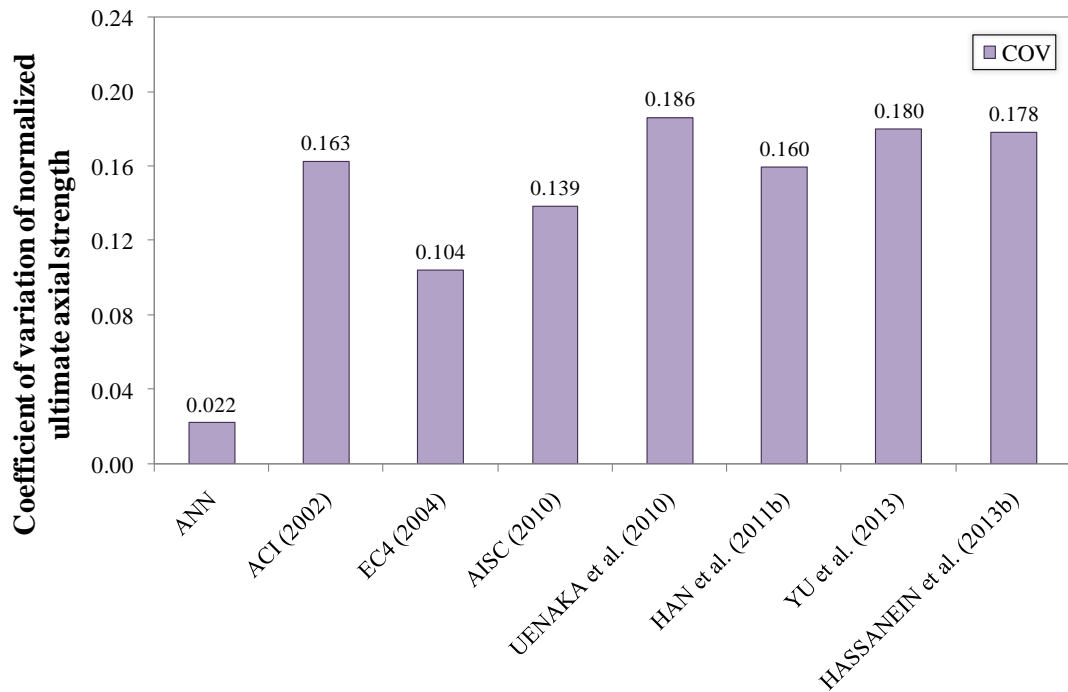


(a)
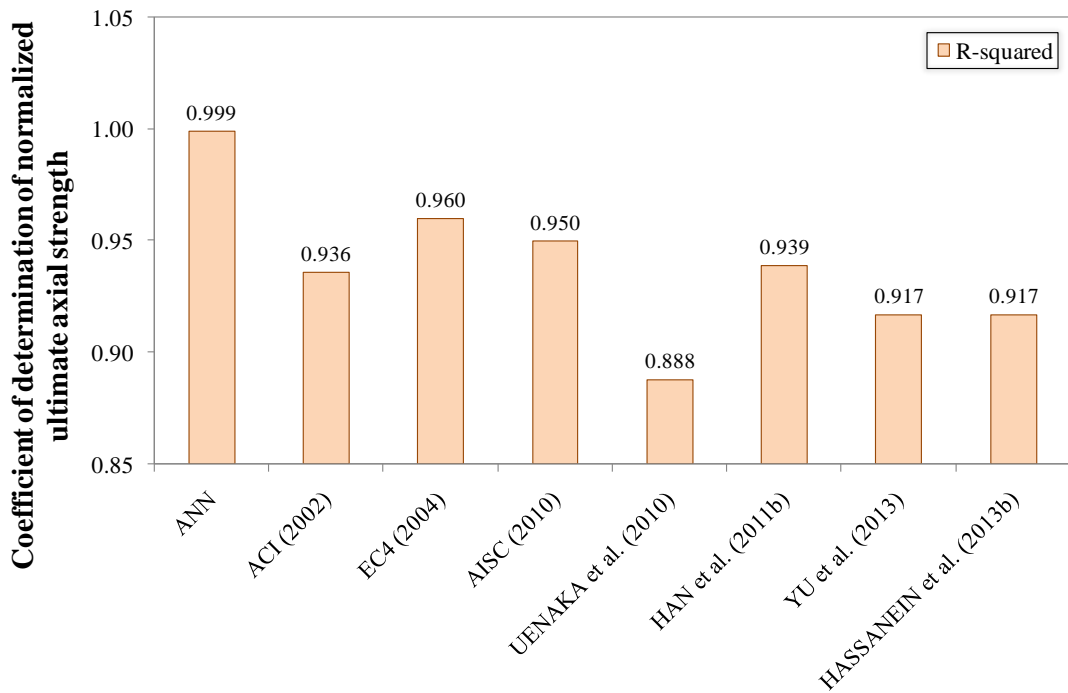
(b)

**Figure 4.55.** Statistically comparison ANN model with the modified formulas and suggested empirical models with regard to: (a) COV and (b) R-squared

Besides, it is known that the R-squared value varies between 0 and 1. While 0 means no relation between the actual and predicted results, 1 implies absolute relation between the actual and the predicted results. When the R-squared value of the ANN model is considered, it would be inferred that there is almost absolute relation between the experimental and the predicted ultimate axial strengths of the CFDST columns with CHS. This situation indicates also the prediction capability of the ANN model. According to the R-squared value, it can be stated about the ANN model that it has a very high reliability and accuracy.

Finally, the percent error caused by the models during the prediction of the ultimate axial strength is grouped according to the strength partitions and they are given in Figure 4.56. The ultimate axial strength values are divided into five partitions with the range of 750 kN and the number of data falling in each partition class is also shown in Figure 4.56 as frequency.

It can be clearly seen that the ANN model has lower percent error value for all ultimate axial strength partitions. Moreover, the percent error value of the ANN model decreases by increasing of the ultimate strength and the lowest percent error

value of 0.52% is procured at the ultimate axial strength more than 2000 and less than 3000 kN.
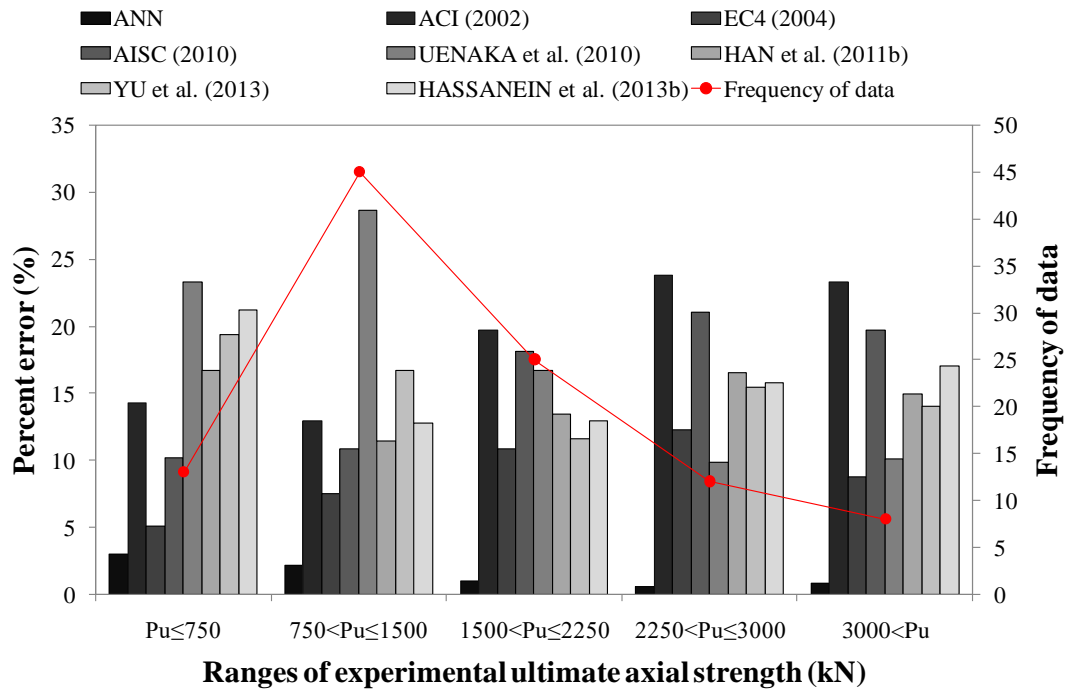


**Figure 4.56.** Error analysis of proposed ANN model, modified code formulas, and suggested empirical models

## 4.4 Comparison of Generated Models

The section herein includes the comparison of the models generated in this thesis. Till here, the generated models were firstly compared with the experimental results, and then their prediction performances were observed with respect to the CFDST columns with CHS features. Then after, they were compared with the available empirical models used in the literature. The comparison of the proposed models with the modified formula and the suggested empirical models, which are available in the literature, revealed that all three models developed in this thesis has the prediction performance better than the existing models. Therefore, in this section, their prediction performances are compared against to each other.

Figure 4.57a, 4.57b, and 4.58c illustrate the experimental ultimate axial strengths and the ultimate axial strengths predicted by the FEM, GEP, and ANN models, respectively. When Figure 4.57 is observed entirely, it can be easily seen that the

181

GEP model has prediction performance better than the FEM model while the ANN model has estimation performance better than both.

In these figures, the blue lines are used to denote the experimental ultimate axial strength while the red lines are utilized to designate the predicted ultimate axial strengths. In Figure 4.57a, for some ultimate axial strength values, the blue lines can be easily visible. This exhibits that the predicted strength values in these points are less or more than the actual strength values.

But when Figure 4.57b is examined, fewer blue lines are visible. This situation reveals that the ultimate axial strength values predicted by the GEP model are more close to the actual strength values. It would be openly noticed that the visibility level of the blue lines is considerable barely reduced when Figure 4.57c is considered.

Based on the change in the visibility of the blue lines, it can be unequivocally stated that the prediction performance of the proposed ANN model is the best among the other two models proposed in this study.
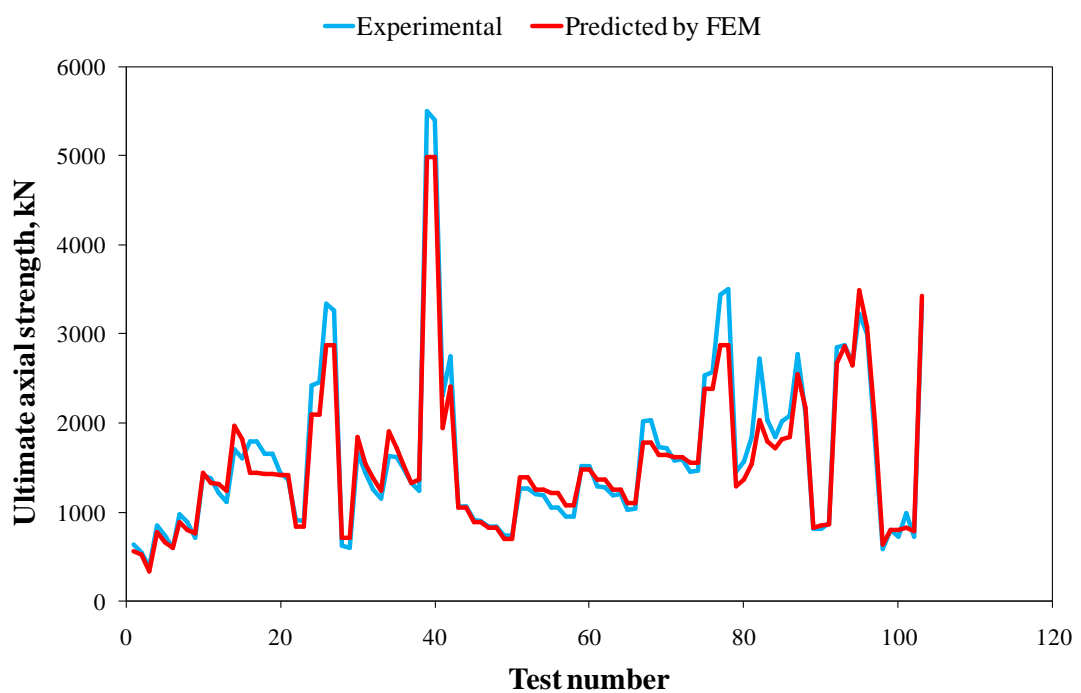


(a)
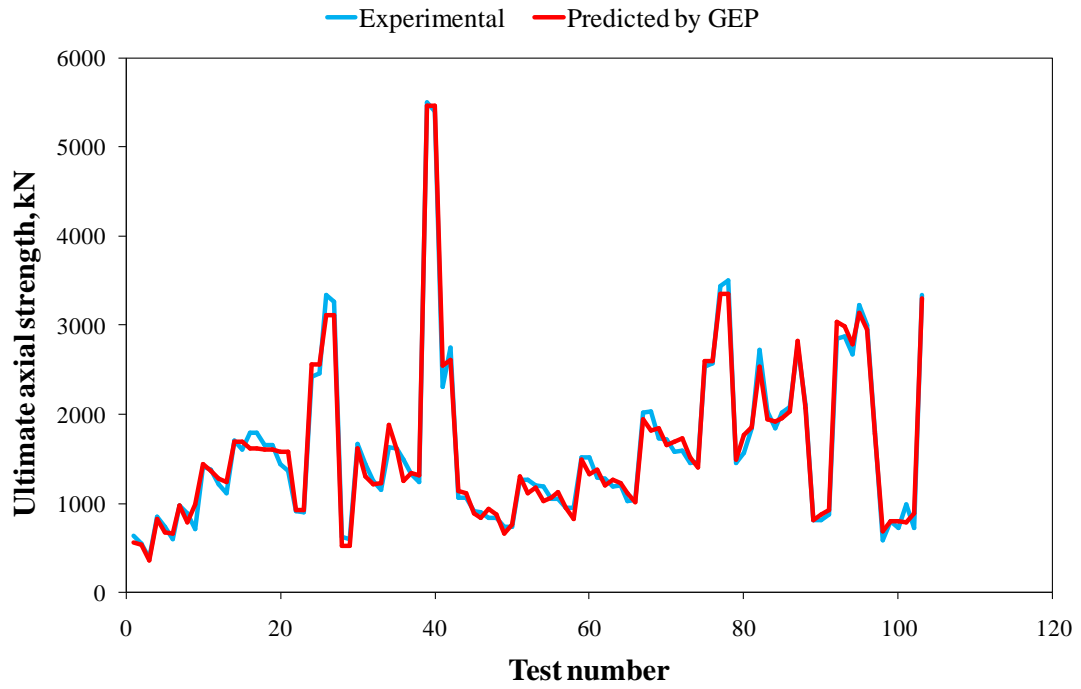
(b)
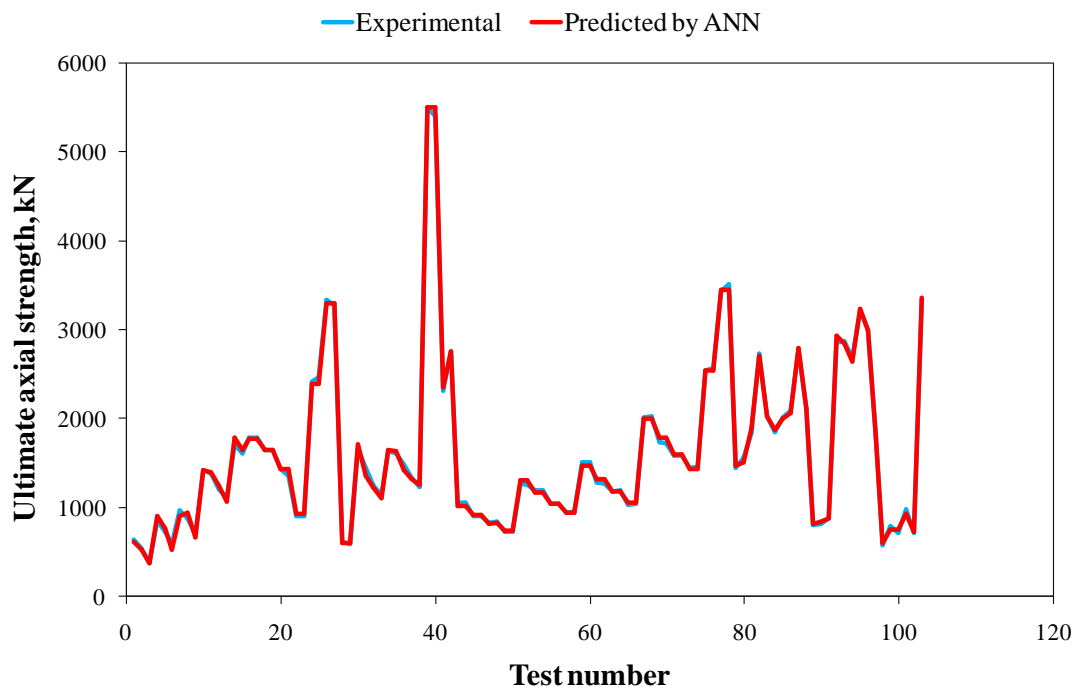
(c)

**Figure 4.57.** Ultimate axial strength of experiment and prediction by: (a) FEM, (b) GEP, and (c) ANN models

Moreover, the ultimate axial strength predicted by the FEM, GEP, and ANN models versus the experimental ultimate axial strengths are illustrated in Figure 4.58. When

the figure is viewed, it can be easily noticed that the results achieved by the GEP and ANN models are dispersed on 100% agreement line, but the some results of the FEM model are some more away from 100% agreement line. This situation means that the residual ultimate axial strength values, namely difference between the experimental and predicted strength values, procured by the proposed FEM model are more than that obtained by the generated GEP and ANN models. In other words, the prediction performances of the generated GEP and ANN models are much better than that of the proposed FEM model. In addition, when the pointers of the GEP (blue circle) and ANN (red triangle) results are looked at, it would be clearly comprehended that the estimation capability is of the ANN model better than that of the GEP model since the red triangle pointers amass on the 100% agreement line while the blue circle pointers accumulate around the 100% agreement line.
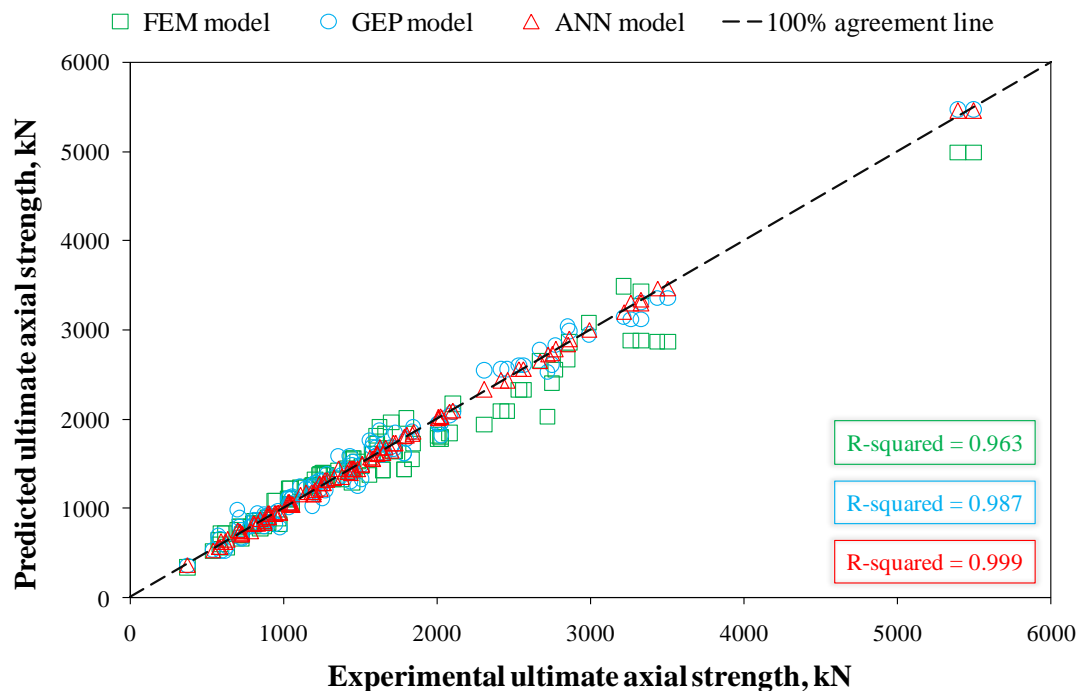


**Figure 4.58.** Predicted versus experimental ultimate axial strength

Additionally, the normalized ultimate axial strength values of the FEM, GEP, and ANN models are shown in Figure 4.59. The figure shows that both FEM and GEP models have great numbers of normalized results remaining at the outside of the normalization limits of ±10% while the ANN model had no normalized result remaining at the outside of these limits. This situation reveals how the prediction

performance, robustness, accuracy, and reliability of the generated ANN model are good.
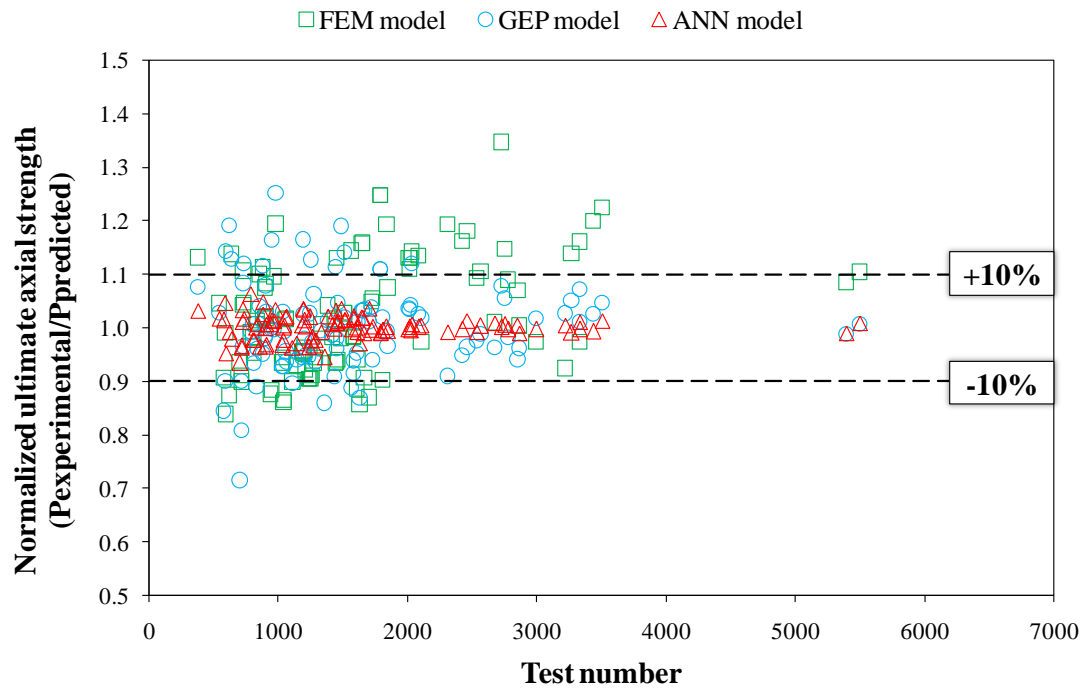


**Figure 4.59.** Normalized ultimate axial strengths of FEM, GEP, and ANN models

In order to obviously indicate the residual between the experimental and the predicted ultimate axial strength values, all results are presented in Figures 4.60a, 4.60b, 4.60c, and 4.60d with respect to the test number order given in Tables 4.1, 4.3, and 4.5. In figures, the black dot pointer is used to exhibit the experimental values while the green square, blue circle, and red triangle pointers are utilized to show the predicted values of the FEM, GEP, and ANN models, respectively. When the figures are beheld, it would be openly seen that the black dot and red triangle indicators almost perfectly match with each other, but the same matching between the black dot and green square or blue circle could not be stated.

When the figures were carefully examined, the matching between the black dot and green square or blue circle could be seen, yet the number of these matches is incomparable regarding the match number of red triangle. Namely, it could be briefly stated that the values of residual strength between the experimental and ANN prediction are less than that between the experimental and FEM or GEP prediction. By this way, it could be understood that the error occurrence during the prediction by the ANN model is much less than the error occurring during the prediction by the

185

FEM and the GEP models. And, this is the exhibition of the good and reliable prediction performance of the generated ANN model.
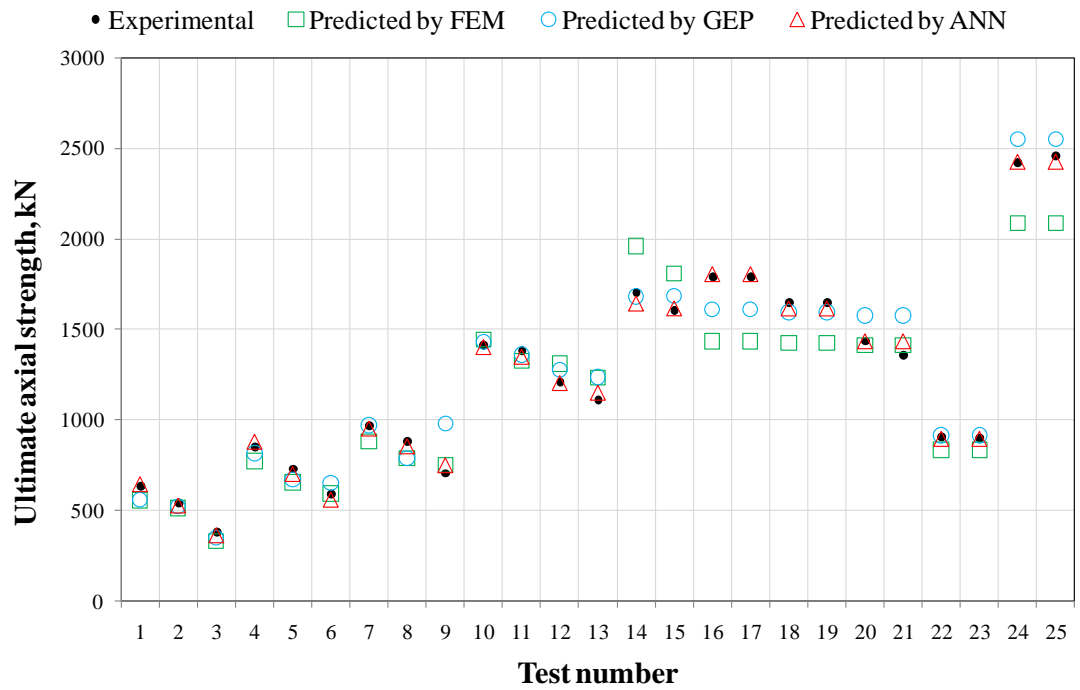


(a)
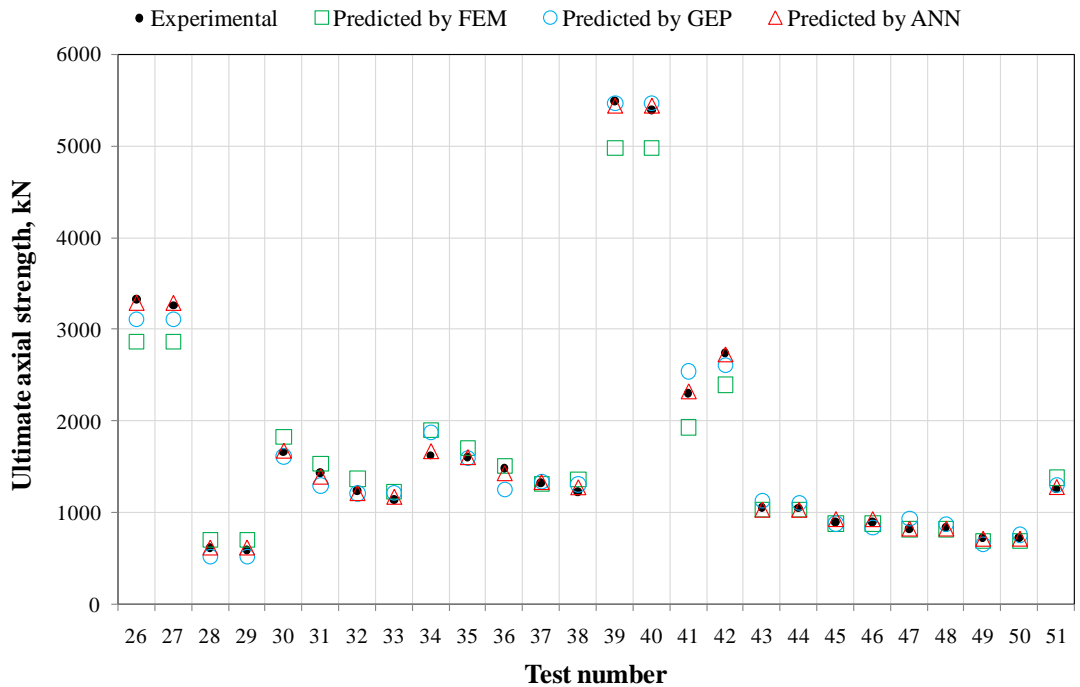


(b)
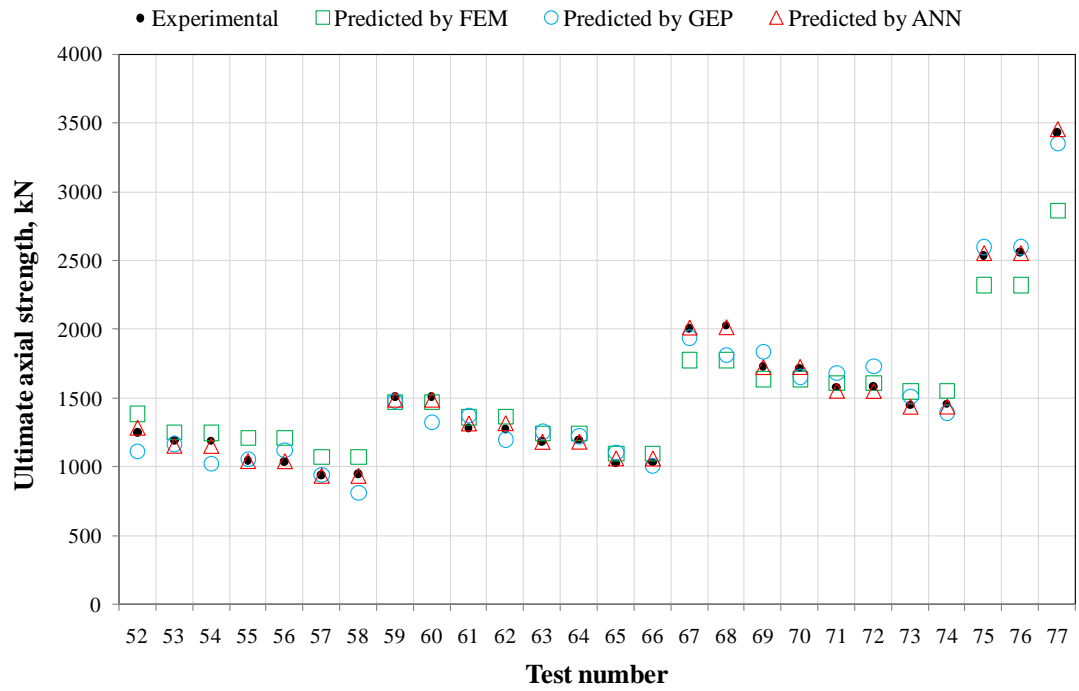
(c)
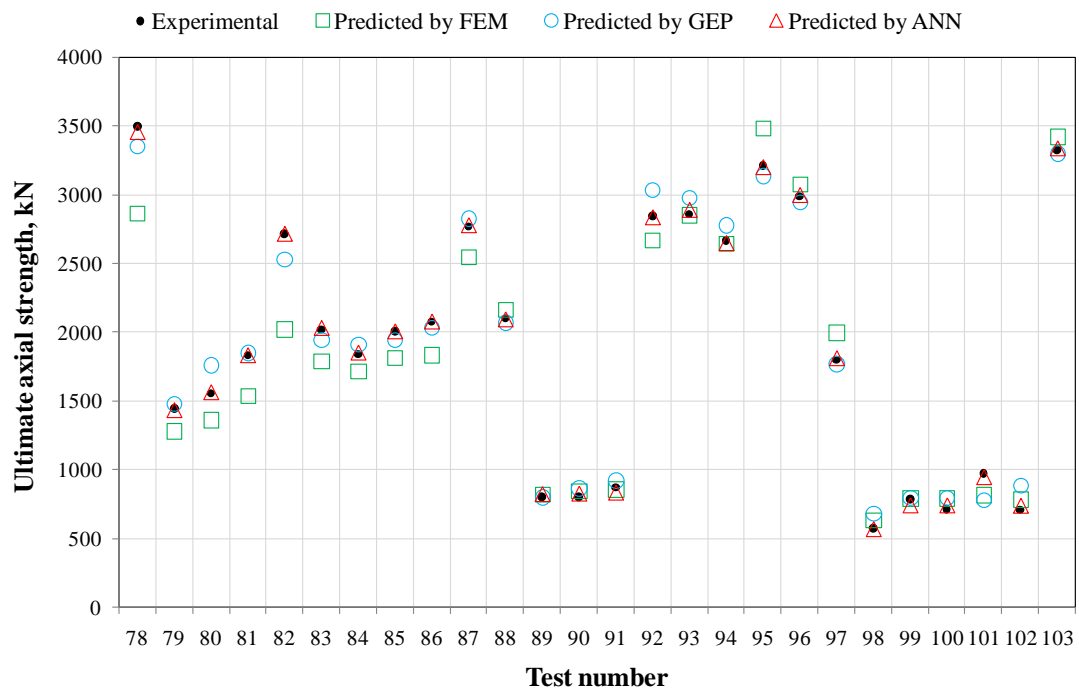


(d)

**Figure 4.60.** Ultimate axial strength values versus test number: (a) from 1 to 25, (b) from 26 to 51, (c) from 52 to 77, and (d) from 78 to 103

In order to exhibit the differences between the prediction performance of the FEM, GEP and ANN models, their results are also evaluated statistically. The some

187

previously calculated basic statistical parameters such as MAPE, MSE, RMSE, COV, and R-squared are also presented in Table 4.7. In order to visualize these tabulated values, MAPE, MSE, and RMSE values are shown in Figure 4.61a, 4.61b, and 4.61c, respectively, while COV and R-sqaured values are indicated in Figure 4.62a and 4.62b, respectively.

**Table 4.7.** Statistical parameters of the prediction performance of proposed FEM, GEP, and ANN models

| Statistical parameters | Mean absolute percent error (MAPE) | Mean square error (MSE) | Root mean square error (RMSE) | Coefficient of variation (COV) | Coefficient of determination (R-squared) |
|---|---|---|---|---|---|
| **FEM** | 8.51 | 41515 | 145.9 | 0.104 | 0.963 |
| **GEP** | 6.43 | 11543 | 85.7 | 0.084 | 0.987 |
| **ANN** | 1.69 | 688 | 21.1 | 0.022 | 0.999 |

Comparing the MAPE, MSE, and RMSE values of the FEM, GEP, and ANN models also benchmarks their estimation capableness. The lowest error values occurr in the ANN model whereas the highest take place in the FEM model. This also indicates which model has good, reliable, robust, and accurate prediction performance. The lowest amount of error is the demonstration of the highest prediction performance. Therefore, according to the MASE, MSE, and RMSE values, it can be indisputably specified that while the prediction performance of the ANN model is highest as against to the FEM and GEP models, the prediction performance of the FEM model was lowest when compared with the GEP and ANN models.

The reliability, robustness, and accuracy of the estimation performance of the generated ANN model are also supported by the COV of the normalized ultimate axial strength and R-squared values. When Figure 4.62a and 4.62b are viewed, it would be noticed that the lowest COV value and the highest R-squared values are achieved in the ANN model. Especially, the R-squared value of the ANN model is so close to value 1 which means the perfect correlation between the actual and predicted values.
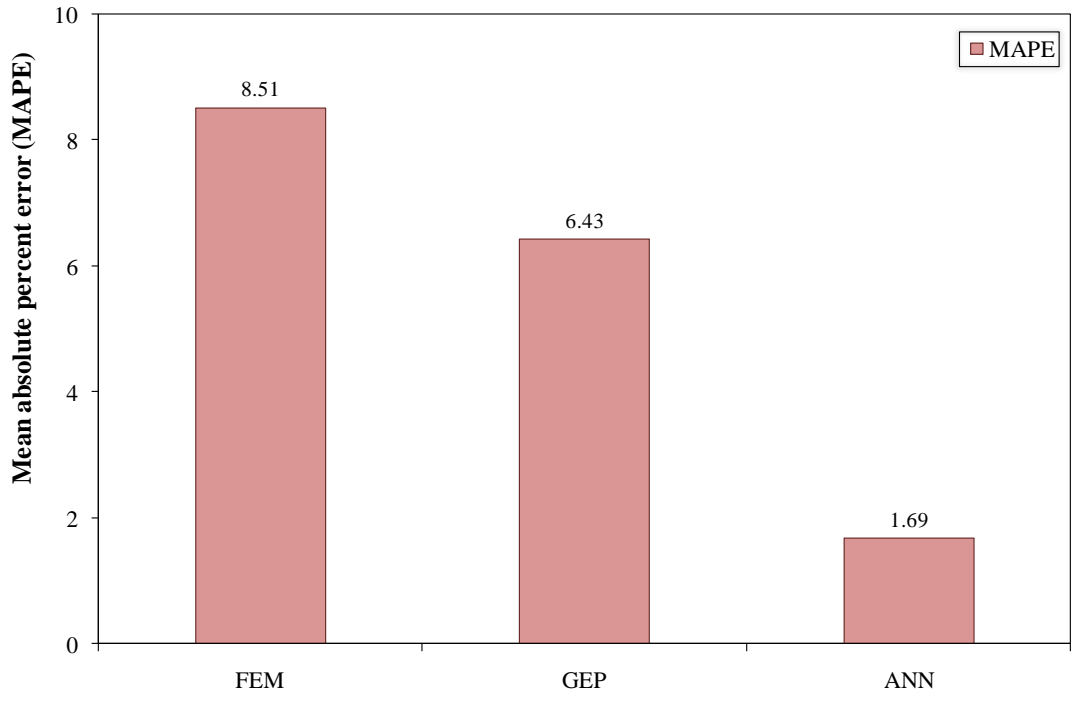
(a)
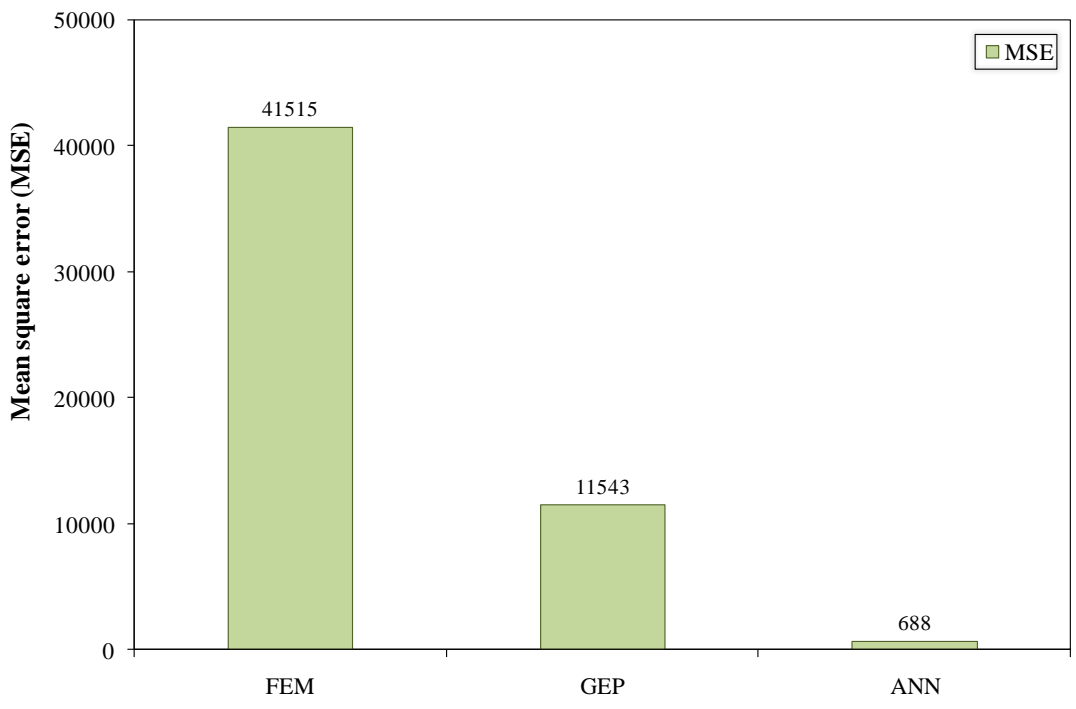


(b)
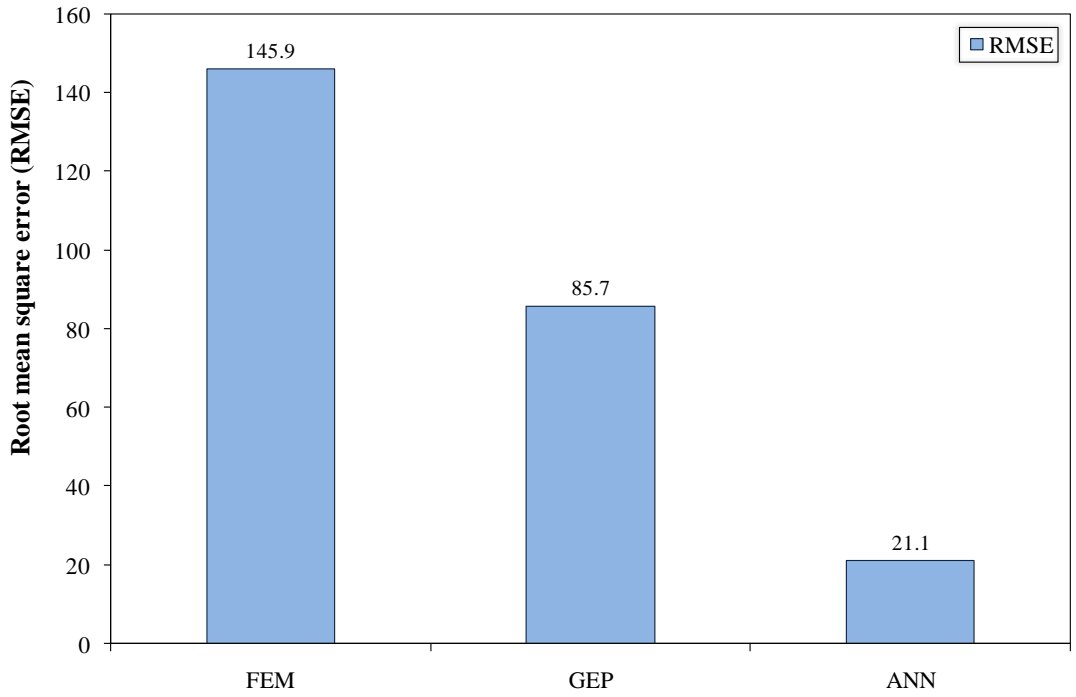
(c)

**Figure 4.61.** Statistically comparison of FEM, GEP, and ANN models with regard to: (a) MAPE, (b) MSE, and (c) RMSE
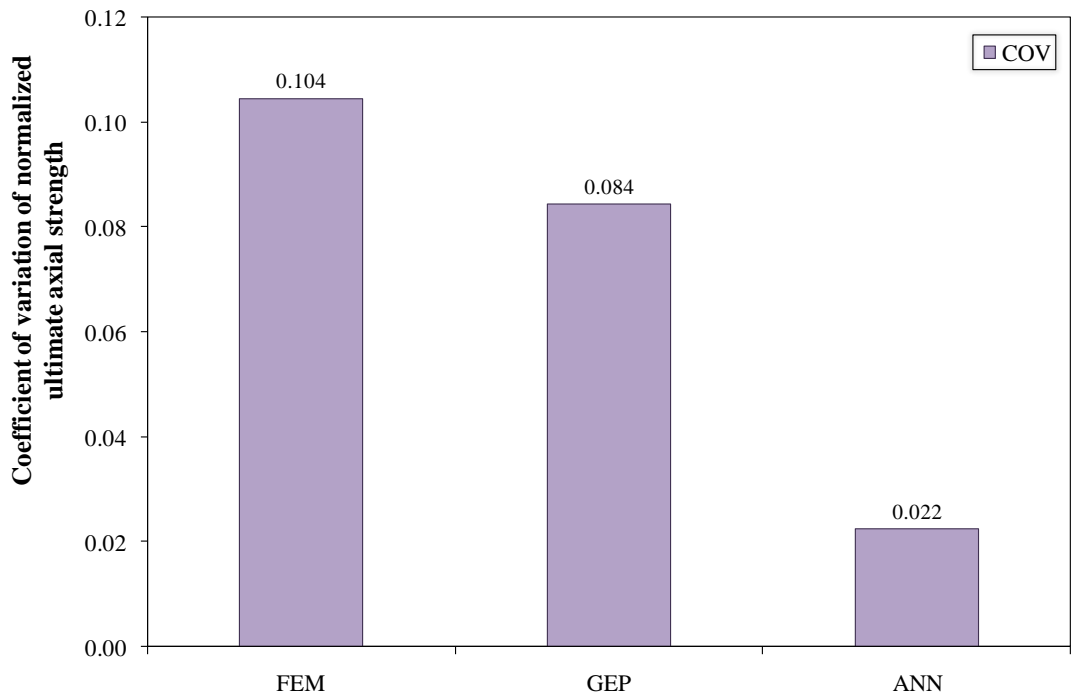


(a)
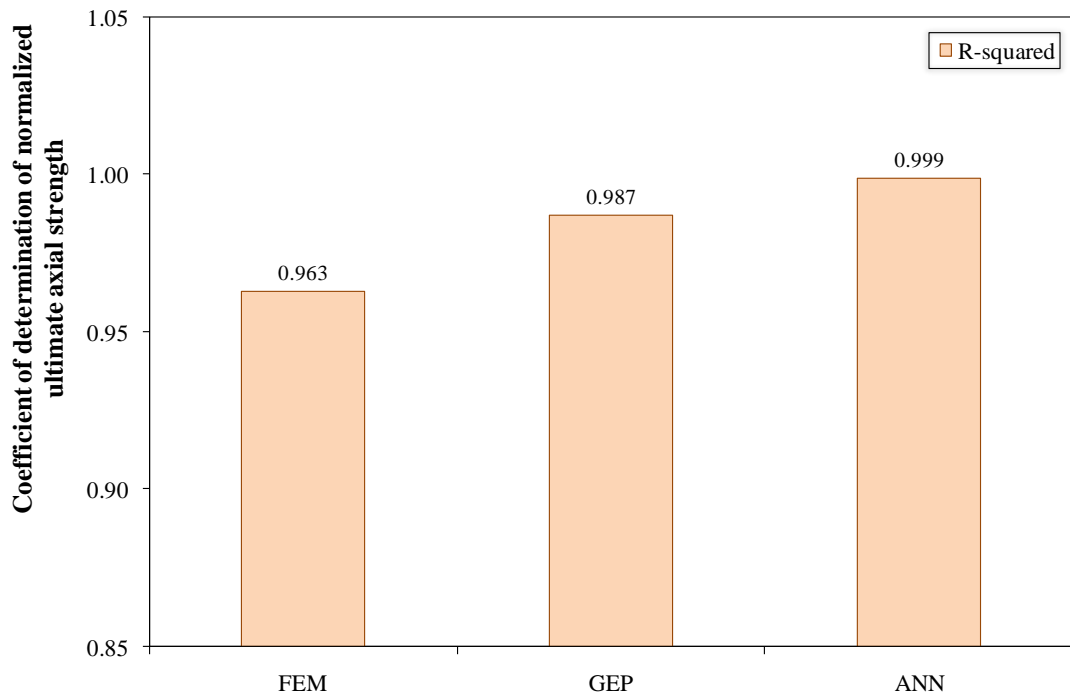
(b)

**Figure 4.62.** Statistically comparison of FEM, GEP, and ANN models with regard to: (a) COV and (b) R-squared

Finally, the percent error caused by the models during the prediction of the ultimate axial strength is grouped according to the strength partitions and they are given in Figure 4.63. The ultimate axial strength values are divided into five partitions with the range of 750 kN and the number of data falling in each partition class is also shown in Figure 4.63 as frequency.

The proposed FEM model exhibits lower percent error value than the generated GEP model only in the case of the ultimate axial strength value $\leq$ 750 kN while in the other intervals the proposed FEM model shows the highest percent error values. Besides, it can be clearly seen that lower percent error value for all ultimate axial strength partitions are attained in the generated ANN model. Furthermore, the lowest percent error value of 0.58% is procured at the ultimate axial strength between 2250 and 3000 kN. According to the statistical evaluation of the model, the prediction performance of the ANN model and its reliability, robustness, and accuracy are the best as against to the FEM and GEP.
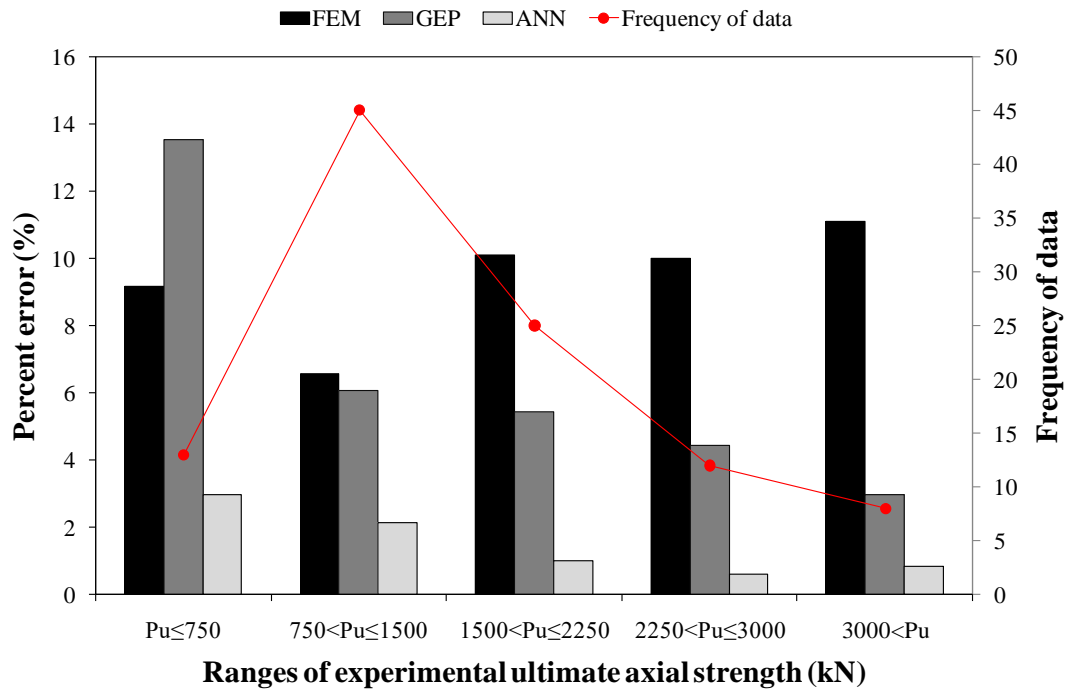
**Figure 4.63.** Error analysis of proposed FEM, GEP, and ANN models

# CHAPTER 5

## PARAMETRIC STUDY AND STATISTICAL ANALYSIS

### 5.1 Parametric Study

In this section, in order to investigate the effect of various parameters, namely, the thickness and diameter of outer and inner steel tubes, concrete compressive strength, on the ultimate axial strength of CFDST columns with CHS, a parametric study was conducted. Therefore, 72 CFDST columns with CHS were designed in ABAQUS CAE (Abaqus, 2014) in order to identify the effectiveness of parameters on the ultimate axial strength of such columns. In these columns, the length of specimen and yield strengths of outer and inner steel tubes were kept constant while the diameters and thicknesses of outer and inner steel tubes and the compressive strength of the concrete annulus were the variable parameters. Two outer steel tube diameters with values of 200 and 300 mm, three different outer steel tube thicknesses with values of 2, 3, and 4 mm, two inner steel tube diameters with values of 80 and 120 mm, and three different inner steel tube thicknesses with values of 1, 2, and 3 mm were chosen in order to investigate and visualize the effect of sectional properties of CFDST columns with CHS. By changing the outer steel tube diameter with keeping the length of specimen constant, mainly length-to-outer steel tube diameter ratio was changed. In addition to examine the sectional properties, two different concrete compressive strength with values of 25 and 50 MPa were considered in the designing of columns to reveal the effect of concrete compressive strength on the ultimate axial strength of CFDST columns.

The each CFDST column specimen was designed according to the specifications given in Chapter 3, Section 3.2.1. The ultimate axial strength of each specimen was predicted after the simulation by ABAQUS CAE software (Abaqus, 2014). Table 5.1 involves the details of each specimen and the ultimate axial strength of simulated CFDST column specimens attained from the finite element analysis by using ABAQUS CAE software (Abaqus, 2014).

**Table 5.1.** Properties of CFDST columns used in parametric study

| Sample No | Yield strength | | Diameter | | Thickness | | Concrete compressive strength | Length of specimen | Predicted ultimate axial strength, |
|---|---|---|---|---|---|---|---|---|---|
| | Outer steel tube $f_{syo}$ (MPa) | Inner steel tube $f_{syi}$ (MPa) | Outer steel tube $D_o$ (mm) | Inner steel tube $D_i$ (mm) | Outer steel tube $t_o$ (mm) | Inner steel tube $t_i$ (mm) | $f_c'$ (MPa) | $L$ (mm) | $P_{u,pred}$ (kN) |
| 1 | 365 | 365 | 200 | 80 | 2 | 1 | 25 | 600 | 1288 |
| 2 | 365 | 365 | 200 | 80 | 2 | 2 | 25 | 600 | 1374 |
| 3 | 365 | 365 | 200 | 80 | 2 | 3 | 25 | 600 | 1461 |
| 4 | 365 | 365 | 200 | 80 | 3 | 1 | 25 | 600 | 1584 |
| 5 | 365 | 365 | 200 | 80 | 3 | 2 | 25 | 600 | 1679 |
| 6 | 365 | 365 | 200 | 80 | 3 | 3 | 25 | 600 | 1772 |
| 7 | 365 | 365 | 200 | 80 | 4 | 1 | 25 | 600 | 1909 |
| 8 | 365 | 365 | 200 | 80 | 4 | 2 | 25 | 600 | 2008 |
| 9 | 365 | 365 | 200 | 80 | 4 | 3 | 25 | 600 | 2105 |
| 10 | 365 | 365 | 200 | 120 | 2 | 1 | 25 | 600 | 1156 |
| 11 | 365 | 365 | 200 | 120 | 2 | 2 | 25 | 600 | 1295 |
| 12 | 365 | 365 | 200 | 120 | 2 | 3 | 25 | 600 | 1439 |
| 13 | 365 | 365 | 200 | 120 | 3 | 1 | 25 | 600 | 1463 |
| 14 | 365 | 365 | 200 | 120 | 3 | 2 | 25 | 600 | 1615 |
| 15 | 365 | 365 | 200 | 120 | 3 | 3 | 25 | 600 | 1763 |
| 16 | 365 | 365 | 200 | 120 | 4 | 1 | 25 | 600 | 1759 |
| 17 | 365 | 365 | 200 | 120 | 4 | 2 | 25 | 600 | 1906 |
| 18 | 365 | 365 | 200 | 120 | 4 | 3 | 25 | 600 | 2059 |

**Table 5.1.** (cont'd) Properties of CFDST columns used in parametric study

| Sample No | Yield strength | | Diameter | | Thickness | | Concrete compressive strength $f_c'$ (MPa) | Length of specimen L (mm) | Predicted ultimate axial strength, $P_{u,pred}$ (kN) |
| | Outer steel tube $f_{syo}$ (MPa) | Inner steel tube $f_{syi}$ (MPa) | Outer steel tube $D_o$ (mm) | Inner steel tube $D_i$ (mm) | Outer steel tube $t_o$ (mm) | Inner steel tube $t_i$ (mm) | | | |
|---|---|---|---|---|---|---|---|---|---|
| 19 | 365 | 365 | 300 | 80 | 2 | 1 | 25 | 600 | 2469 |
| 20 | 365 | 365 | 300 | 80 | 2 | 2 | 25 | 600 | 2556 |
| 21 | 365 | 365 | 300 | 80 | 2 | 3 | 25 | 600 | 2642 |
| 22 | 365 | 365 | 300 | 80 | 3 | 1 | 25 | 600 | 2993 |
| 23 | 365 | 365 | 300 | 80 | 3 | 2 | 25 | 600 | 3079 |
| 24 | 365 | 365 | 300 | 80 | 3 | 3 | 25 | 600 | 3165 |
| 25 | 365 | 365 | 300 | 80 | 4 | 1 | 25 | 600 | 3429 |
| 26 | 365 | 365 | 300 | 80 | 4 | 2 | 25 | 600 | 3521 |
| 27 | 365 | 365 | 300 | 80 | 4 | 3 | 25 | 600 | 3613 |
| 28 | 365 | 365 | 300 | 120 | 2 | 1 | 25 | 600 | 2351 |
| 29 | 365 | 365 | 300 | 120 | 2 | 2 | 25 | 600 | 2495 |
| 30 | 365 | 365 | 300 | 120 | 2 | 3 | 25 | 600 | 2627 |
| 31 | 365 | 365 | 300 | 120 | 3 | 1 | 25 | 600 | 2854 |
| 32 | 365 | 365 | 300 | 120 | 3 | 2 | 25 | 600 | 2992 |
| 33 | 365 | 365 | 300 | 120 | 3 | 3 | 25 | 600 | 3127 |
| 34 | 365 | 365 | 300 | 120 | 4 | 1 | 25 | 600 | 3298 |
| 35 | 365 | 365 | 300 | 120 | 4 | 2 | 25 | 600 | 3452 |
| 36 | 365 | 365 | 300 | 120 | 4 | 3 | 25 | 600 | 3601 |

**Table 5.1.** (cont'd) Properties of CFDST columns used in parametric study

| Sample No | Yield strength | | Diameter | | Thickness | | Concrete compressive strength | Length of specimen L | Predicted ultimate axial strength, |
|---|---|---|---|---|---|---|---|---|---|
| | Outer steel tube $f_{syo}$ (MPa) | Inner steel tube $f_{syi}$ (MPa) | Outer steel tube $D_o$ (mm) | Inner steel tube $D_i$ (mm) | Outer steel tube $t_o$ (mm) | Inner steel tube $t_i$ (mm) | $f_c'$ (MPa) | (mm) | $P_{u,pred}$ (kN) |
| 37 | 365 | 365 | 200 | 80 | 2 | 1 | 50 | 600 | 1906 |
| 38 | 365 | 365 | 200 | 80 | 2 | 2 | 50 | 600 | 1992 |
| 39 | 365 | 365 | 200 | 80 | 2 | 3 | 50 | 600 | 2078 |
| 40 | 365 | 365 | 200 | 80 | 3 | 1 | 50 | 600 | 2150 |
| 41 | 365 | 365 | 200 | 80 | 3 | 2 | 50 | 600 | 2237 |
| 42 | 365 | 365 | 200 | 80 | 3 | 3 | 50 | 600 | 2323 |
| 43 | 365 | 365 | 200 | 80 | 4 | 1 | 50 | 600 | 2368 |
| 44 | 365 | 365 | 200 | 80 | 4 | 2 | 50 | 600 | 2456 |
| 45 | 365 | 365 | 200 | 80 | 4 | 3 | 50 | 600 | 2542 |
| 46 | 365 | 365 | 200 | 120 | 2 | 1 | 50 | 600 | 1607 |
| 47 | 365 | 365 | 200 | 120 | 2 | 2 | 50 | 600 | 1742 |
| 48 | 365 | 365 | 200 | 120 | 2 | 3 | 50 | 600 | 1874 |
| 49 | 365 | 365 | 200 | 120 | 3 | 1 | 50 | 600 | 1855 |
| 50 | 365 | 365 | 200 | 120 | 3 | 2 | 50 | 600 | 1989 |
| 51 | 365 | 365 | 200 | 120 | 3 | 3 | 50 | 600 | 2121 |
| 52 | 365 | 365 | 200 | 120 | 4 | 1 | 50 | 600 | 2070 |
| 53 | 365 | 365 | 200 | 120 | 4 | 2 | 50 | 600 | 2217 |
| 54 | 365 | 365 | 200 | 120 | 4 | 3 | 50 | 600 | 2367 |

**Table 5.1.** (cont'd) Properties of CFDST columns used in parametric study

| Sample No | Yield strength | | Diameter | | Thickness | | Concrete compressive strength $f_c'$ (MPa) | Length of specimen L (mm) | Predicted ultimate axial strength, $P_{u,pred}$ (kN) |
|---|---|---|---|---|---|---|---|---|---|
| | Outer steel tube $f_{syo}$ (MPa) | Inner steel tube $f_{syi}$ (MPa) | Outer steel tube $D_o$ (mm) | Inner steel tube $D_i$ (mm) | Outer steel tube $t_o$ (mm) | Inner steel tube $t_i$ (mm) | | | |
| 55 | 365 | 365 | 300 | 80 | 2 | 1 | 50 | 600 | 4013 |
| 56 | 365 | 365 | 300 | 80 | 2 | 2 | 50 | 600 | 4100 |
| 57 | 365 | 365 | 300 | 80 | 2 | 3 | 50 | 600 | 4185 |
| 58 | 365 | 365 | 300 | 80 | 3 | 1 | 50 | 600 | 4530 |
| 59 | 365 | 365 | 300 | 80 | 3 | 2 | 50 | 600 | 4617 |
| 60 | 365 | 365 | 300 | 80 | 3 | 3 | 50 | 600 | 4686 |
| 61 | 365 | 365 | 300 | 80 | 4 | 1 | 50 | 600 | 4924 |
| 62 | 365 | 365 | 300 | 80 | 4 | 2 | 50 | 600 | 5012 |
| 63 | 365 | 365 | 300 | 80 | 4 | 3 | 50 | 600 | 5098 |
| 64 | 365 | 365 | 300 | 120 | 2 | 1 | 50 | 600 | 3743 |
| 65 | 365 | 365 | 300 | 120 | 2 | 2 | 50 | 600 | 3877 |
| 66 | 365 | 365 | 300 | 120 | 2 | 3 | 50 | 600 | 4009 |
| 67 | 365 | 365 | 300 | 120 | 3 | 1 | 50 | 600 | 4249 |
| 68 | 365 | 365 | 300 | 120 | 3 | 2 | 50 | 600 | 4382 |
| 69 | 365 | 365 | 300 | 120 | 3 | 3 | 50 | 600 | 4514 |
| 70 | 365 | 365 | 300 | 120 | 4 | 1 | 50 | 600 | 4632 |
| 71 | 365 | 365 | 300 | 120 | 4 | 2 | 50 | 600 | 4766 |
| 72 | 365 | 365 | 300 | 120 | 4 | 3 | 50 | 600 | 4898 |

The predicted ultimate axial strengths attained from the simulation by using ABAQUS CAE versus the outer steel tube thickness is given in Figures 5.1a and 5.1b in the case of $L/D_o = 3$ and $L/D_o = 2$, respectively.

These figures also include the variation in the ultimate axial strength regarding both inner steel tube diameter and concrete compressive strength. It can be overtly seen from Figures 5.1a and 5.1b that increasing both outer and inner steel tubes thicknesses leads to the increasing of the ultimate axial strength.

In the case of $L/D_o = 3$, $D_i = 80$ mm, and $f_c' = 25$ MPa, increasing the outer steel tube thickness from 2 to 4 mm conduces to 48, 46, and 44% increment of the ultimate axial strength when the inner steel tube thicknesses are 1, 2, and 3 mm, respectively. When the $L/D_o$ ratio is decreased from 3 to 2, these increment rates in the ultimate axial strength are 39, 38, and 37% when the inner steel tube thicknesses are 1, 2, and 3 mm, respectively.

The results also indicate that when the $L/D_o$ ratio is decreased from 3 to 2, namely when the diameter of outer steel tube is increased without changing the length of specimen, the remarkable enhancement in the ultimate axial strength is observed.
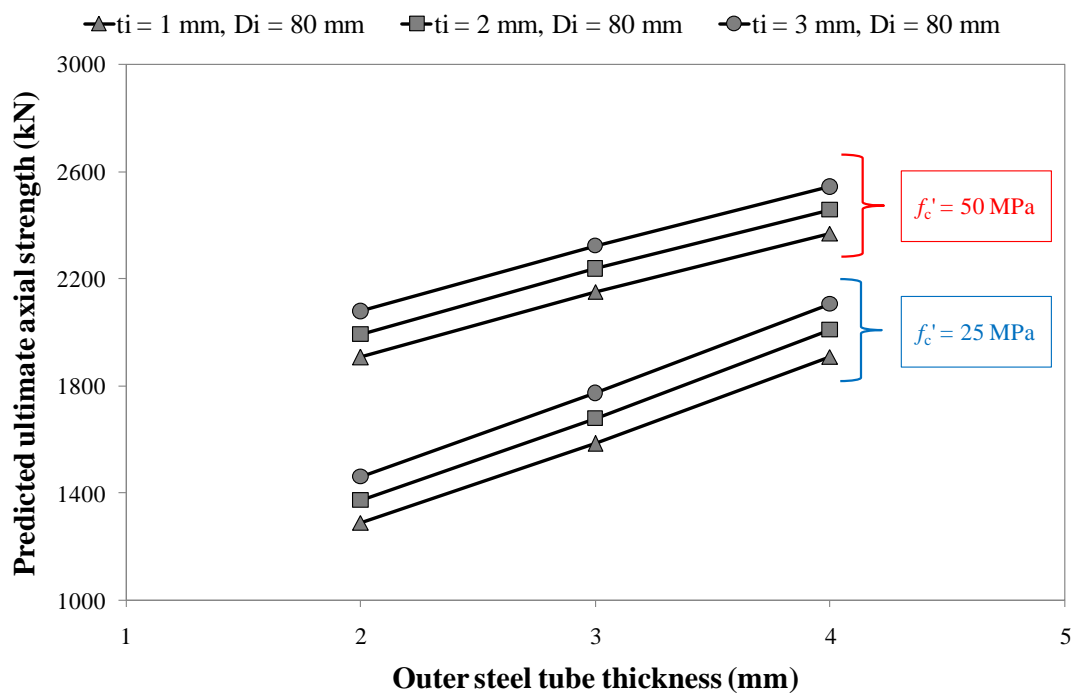


(a)
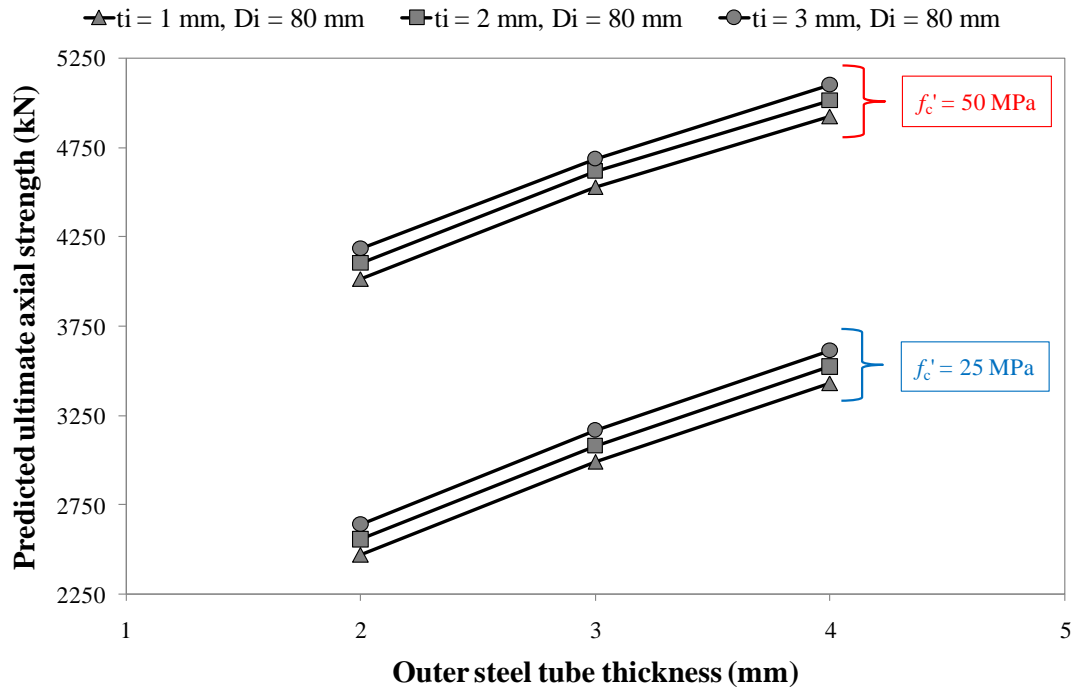
(b)

**Figure 5.1.** Ultimate axial strength predicted by FEM model vs. outer steel tube thickness for: (a) $L/D_o = 3$, $D_i = 80$ mm and (b) $L/D_o = 2$, $D_i = 80$ mm

Another finding is that using concrete with higher compressive strength significantly increases the ultimate axial strength of the CFDST columns. In the case of $L/D_o = 3$, $D_i = 80$ mm, and $f_c' = 50$ MPa, increasing the outer steel tube thickness from 2 to 4 mm leads to 24, 23, and 22% increasing of the ultimate axial strength when the inner steel tube thicknesses are 1, 2, and 3 mm, respectively. When the $L/D_o$ ratio is decreased from 3 to 2, these increment rates in the ultimate axial strength are 23, 22, and 22% when the inner steel tube thicknesses are 1, 2, and 3 mm, respectively.

Another changeable parameter is the diameter of inner steel tube ($D_i$). Figures 5.2a and 5.2b demonstrate the predicted ultimate axial strength of the CFDST columns according to the outer steel tube thickness when the $D_i$ is 120 mm and other parameters are same as in Figures 5.1a and 5.1b. The results show that increasing the $D_i$ from 80 to 120 mm decreases the load carrying capacity of the CFDST columns. The effect of the concrete compressive strength can also be observed when the $D_i$ is 120 mm. The higher compressive strength means the higher ultimate axial strength of the CFDST columns. Besides, when Figures 5.2a and 5.2b are examined, it can be obviously seen that increasing the diameter of the outer steel tube ($D_o$) from 200 to

300 mm by keeping the length of specimen constant leads to doubling of the load carrying capacity of the CFDST columns.



(a)



(b)
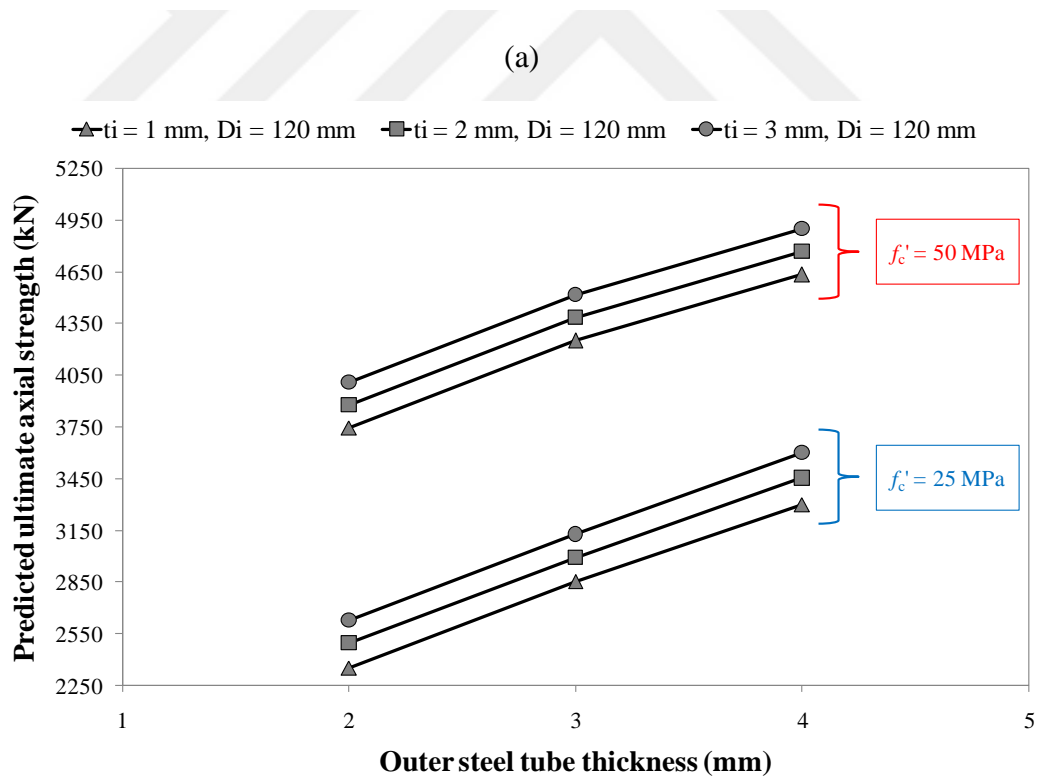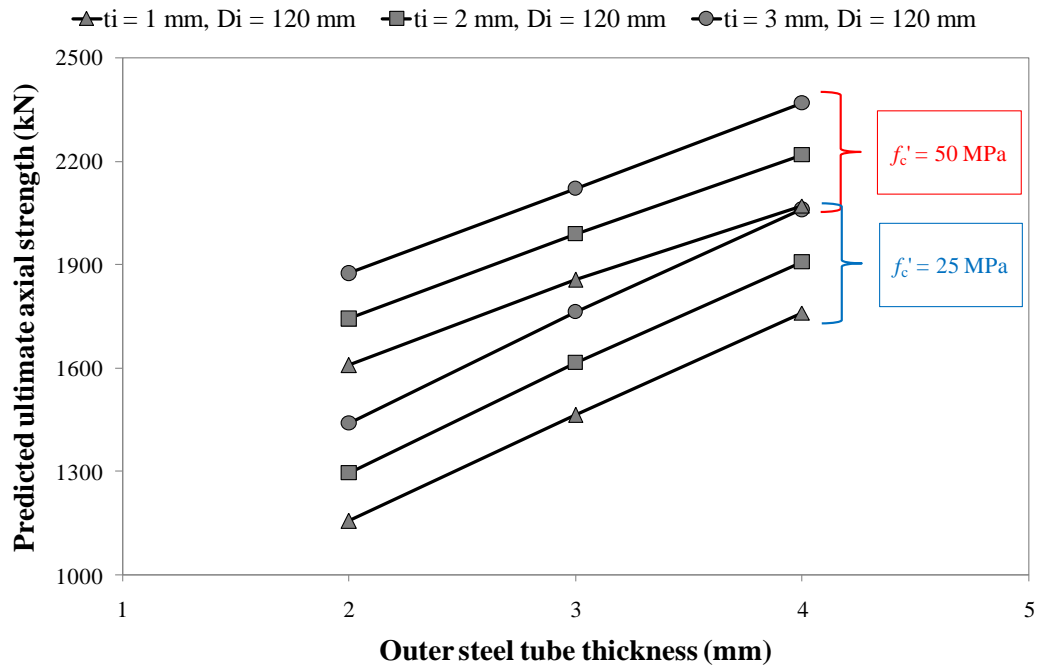
**Figure 5.2.** Ultimate axial strength predicted by FEM model vs. outer steel tube thickness for: (a) $L/D_o = 3$, $D_i = 120$ mm and (b) $L/D_o = 2$, $D_i = 120$ mm

When Figures 5.1a, 5.1b, 5.2a, and 5.2b are totally considered, it can be clearly comprehended that increasing the inner steel tube thickness is not effective on the ultimate axial strength as much as increasing the outer steel tube thickness. The increment rates in the ultimate axial strength by increasing the outer steel tube thickness are in the range of 37-52% and 22-29% in the case of $f_c' = 25$ and 50 MPa, respectively, whereas when the thickness of the inner steel tube is increased, the increment rates in the ultimate axial strength are between 5-24% and 3-17% for $f_c' = 25$ and 50 MPa, respectively.

In order to clearly indicate the change in the ultimate axial strength of the CFDST columns with regard to altering of $L/D_o$, $D_i$, $t_o$, $t_i$, and $f_c'$, Figures 5.3a and 5.3b are plotted. It can be expressed that the slight increase in the ultimate axial strength can be seen when the inner steel tube thickness is increased while a significant enhancement in the load carrying capacity of CFDST columns can be observed when the outer steel tube thickness is increased.

Besides, it is obvious that the most significant increasing in the ultimate axial strength is seen when the $L/D_o$ is reduced or $D_o$ is increased and the compressive strength of the concrete annulus is increased.
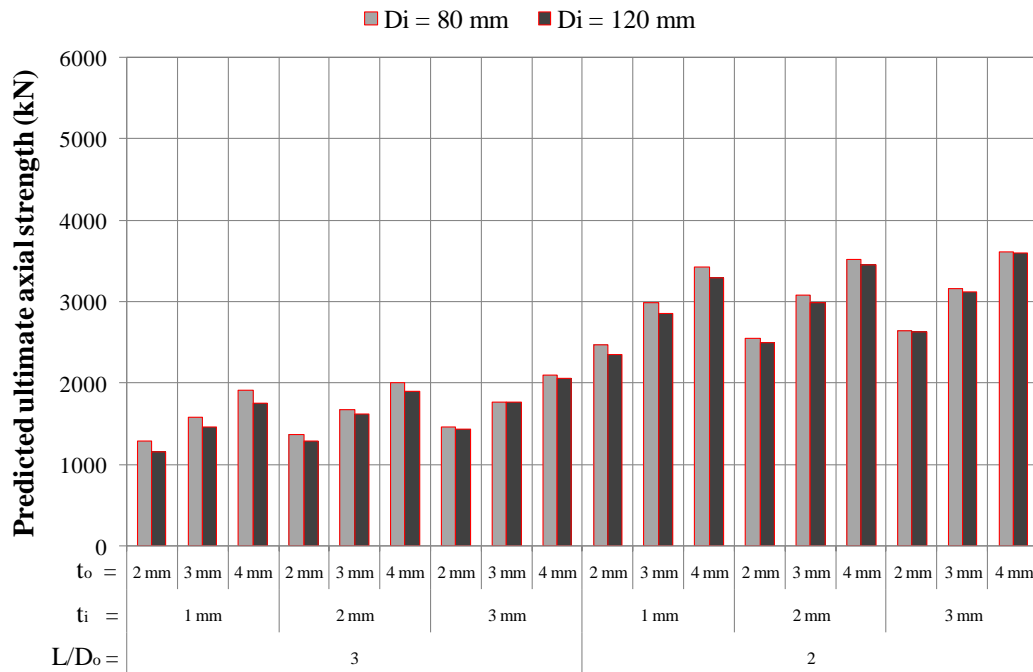


(a)
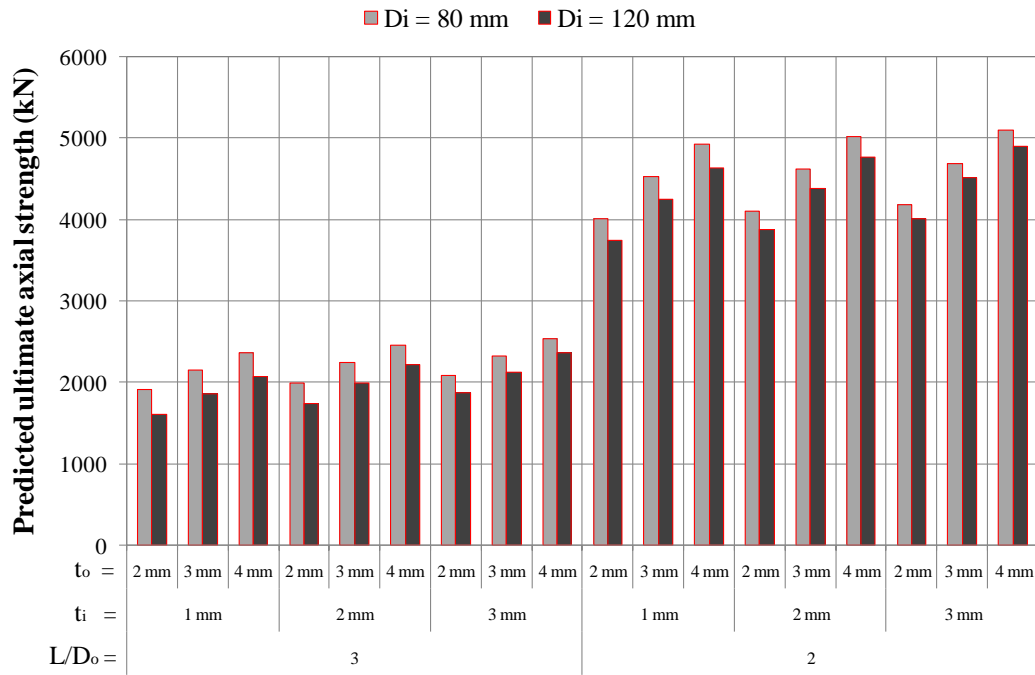
(b)

**Figure 5.3.** Variation in ultimate axial strength predicted by FEM model with regard to $L/D_o$, $D_i$, $t_o$, $t_i$ values in the case of: (a) $f_c' = 25$ MPa and (b) $f_c' = 50$ MPa

The similar findings about the ultimate axial strength regarding the change in such properties can be found in the experimental studies available in the literature. For instance, Uenaka et al. (2010) investigated the influences of diameter and yield strength of outer steel tube and the diameter and thickness of inner steel tube. In some specimens of this experimental study, the diameter of inner steel tube was increased from 39 to 77 mm and then from 77 to 114 mm by keeping the other parameters constant, the gradual decreasing in the ultimate axial strength was observed. But the individual effect of other changeable parameters could not be explained since three of them were altered with together.

In experimental study of Zhao et al. (2002a), in two CFDST column specimens, the individual effect of inner steel tube thickness could be comprehended. In these two specimens, the diameter of outer steel tube, inner steel tube yield strength and diameter, length of specimen and concrete compressive strength were constant whereas the yield strength and diameter of outer steel tube were 454 MPa and 114.5 mm for one specimen, respectively, and 453 MPa and 114.4 mm for other specimen, respectively. The variation in the yield strength and diameter of outer steel tube could be negligible and accepted as constant. In this situation, the only changeable

parameter was the thickness of inner steel tube and it was 5.9 mm for first specimen and 3.5 mm for second one. This means that the inner steel tube thickness was decreased from 5.9 to 3.5 mm, which conduced to the reducing of the ultimate axial strength.

In another study of Zhao et al. (2010), in two CFDST column specimens, all parameters were kept constant except the thickness of outer steel tube, which were 6.0 mm for one sample and 3.6 mm for other sample. The CFDST column specimen manufactured with 6-mm outer steel tube performed higher ultimate axial strength than that produced with 3.6-mm outer steel tube. Namely, increasing the outer steel tube diameter enhanced the load carrying capacity of the CFDST columns. Similar result was found in the study of Lin and Tsai (2003), the thickness of outer steel tube was increased from 2 to 4 mm with keeping the other properties constant and the increasing in the ultimate axial strength was observed.

As well, in the study of Han et al. (2011b), the effect of inner steel tube diameter was investigated and it was revealed that reducing the inner steel tube diameter from 159 to 106 mm significantly increased the ultimate axial strength of CFDST columns. This situation was also observed in the experimental study of Dong and Ho (2013). The inner steel tube diameter with the values of 88.9 and 114.3 mm were used in the manufacturing of CFDST column specimen. In this study, it was found out that the lower diameter of inner steel tube resulted in higher ultimate axial strength. Besides, Dong and Ho (2013) investigated the effect of concrete compressive strength in same study. Two concrete compressive strength grades of 50 and 85 MPa was chosen in their study. The CFDST column specimen manufactured with concrete having higher compressive strength ensued to higher load carrying capacity. The similar results were also found in the study of Han et al. (2011a) and Wang et al. (2014). The experimental programs of Han et al. (2011a) and Wang et al. (2014) were conducted by using two concrete compressive strength values of 39.3-66.4 MPa and 40.5-79.9 MPa, respectively, and it was revealed that the specimens manufactured by using the concrete having higher compressive strength performed higher ultimate axial strength values.

**5.2 Statistical Analysis**

The influences of independent parameters such as the diameters and thicknesses of outer and inner steel tubes and the compressive strength of concrete annulus are graphically illustrated in the previous section. Here, the results are statistically evaluated. For this, the analysis of variance (ANOVA) was used to indicate effectiveness of independent variables on the dependent variable. The analysis method known as general linear model analysis of variance (GLM-ANOVA) was utilized in the statistically evaluation of the results. The software named "Minitab" including GLM-ANOVA method was employed in performing the statistical analysis (Minitab, 2018). The GLM-ANOVA is a diagnostic tool that decreases the control variance in order to help a control factor dominance to be quantified.

In this study, the diameter and thickness of the outer and inner steel tubes and the concrete compressive strength were designated as independent variable while the ultimate axial strength of the double skin composite columns was identified as dependent variable. Besides, the significance level of 0.05 was adjusted in the analysis to reveal which independent variable is statistically important parameter on the dependent variable. The results obtained from the statistically analysis of the proposed FEM model are presented in Table 5.2. The significance of the independent parameters can be comprehended taking into consideration of the P-values. If the P-value of any independent variable is greater than the level of significance, it can be stated that this variable has an insignificant effect on the dependent variable. In the contrary case, namely, when the P-value of any independent variable is less than the level of significance, it can be incontrovertibly specified that this parameter can be approved as a significant variable on the dependent variable.

The statistical analysis results show that all independent variables has a significant effect on the ultimate axial strength of the CFDST columns since the p-values of each independent variable is less than the significance level value of 0.05. Even though all independent variables are statistically significant parameter on the ultimate axial strength, it should be also stated the degree of effectiveness of each independent variable. Therefore, the contributions of the independent variables on the ultimate axial strength of the CFDST columns are given as percentage under the last column in Table 5.2. The higher percent contribution of the independent variable

implies the higher effectiveness of this variable on the dependent variable. According to the percent contribution values presented in Table 5.2, it can be easily said that the most significant parameter that affects the ultimate axial strength of the CFDST columns is the diameter of the outer steel tube. However, the influences of inner steel tube diameter and thickness can be accepted as negligible since their percent contributions values are too small when they are compared with the percent contributions of the outer steel tube diameter and the concrete compressive strength. The second most significant independent variable is the concrete compressive strength with the percent contribution value of 17.8 and the effectiveness of the outer steel tube thickness can be approved as moderate due to having 7.2 percent contribution value.

**Table 5.2.** Statistical analysis of the ultimate axial strength of the CFDST columns predicted by the proposed FEM model

| Dependent Variable | Independent variable | Sequential Sum of Squares | Computed F | P-value | Significance | Contribution (%) |
|---|---|---|---|---|---|---|
| $P_{u,Pred}$ | $D_o$ | 62291401 | 796.5 | 0.000 | YES | 68.3 |
| | $D_i$ | 451250 | 5.8 | 0.019 | YES | 0.5 |
| | $t_o$ | 6559575 | 41.9 | 0.000 | YES | 7.2 |
| | $t_i$ | 623141 | 4.0 | 0.023 | YES | 0.7 |
| | $f_c'$ | 16273513 | 208.1 | 0.000 | YES | 17.8 |
| | Error | 5005538 | - | - | - | 5.5 |
| | Total | 91204418 | - | - | - | - |

The statistical analysis of the ultimate axial strength results achieved by using the proposed FEM model indicates that all independent parameters, namely, the diameter and the thickness of the outer and inner steel tubes and the concrete compressive strength, are the significant parameters in the determination of the ultimate axial strength of the CFDST columns according to the P-values, but the most significant parameter is the diameter of the outer steel tube and the lowest significant parameter can be accepted as the diameter and thickness of the inner steel tube regarding the percent contribution values.

# CHAPTER 6

## CONCLUSIONS

The study herein exhibited three explicit models for the ultimate axial strength of the concrete filled double skin steel tubular (CFDST) columns with circular hollow section (CHS). In the proposing of the models, finite element method (FEM), gene expression programming (GEP), and artificial neural network (ANN) were used. In the development of the models, the experimental test results available in the literature were compiled and utilized as the dataset. With reference to the aforementioned results, discussions, evaluations, and comparisons, the following conclusions could be drawn:

- Totally 103 experimental test results from 16 different studies were compiled to produce the dataset in the developing of the models.

- Three formulas suggested by the codes (ACI, 2002; Eurocode 4, 2004; AISC, 2010) to be used in the prediction of the concrete filled single skin steel tubular columns involving reinforcing bars were modified so that it could be practicable to the CFDST columns with CHS.

- Among these prediction formulas modified from the codes, the best prediction performance was achieved from the modified Eurocode 4 (2004) formula.

- Four empirical models proposed by the researchers (Uenaka et al., 2010; Han et al., 2011b; Yu et al., 2013; Hassanein et al., 2013b) to be used in the prediction of the CFDST columns with CHS were chosen with the purpose of comparison.

- Among the empirical proposed models, the best estimation capability was obtained from the model suggested by Han et al. (2011b).

- The FEM model was created by using ABAQUS CAE 16 named software whereas the GEP and ANN models were generated by using GeneXproTools 5.0 and MATLAB v.17 named software, respectively.

- It was exhibited that the FEM technique could be useful tool in order to develop a estimation model of the CFDST columns with CHS to be able to predict the ultimate axial strength while the GEP and ANN techniques could be beneficial tools in the derivation of empirical mathematical formulation in order to predict the ultimate axial strength of the CFDST columns with CHS regarding the several section sizes and material properties.

- The veridical and logical results were attained in the FEM, GEP, and ANN models, namely, the values of predicted strength were not zero or less than zero. Besides, the proposed GEP and ANN models comprise of many mathematical functions that need to be transferred to the computer in order to save time and eliminate the human factor.

- The estimated results procured from the FEM model were compared with the results extrapolated by using the modified formulas of codes and the empirical models of the researchers. The results of comparisons indicated that the FEM model has better prediction capableness than the modified formulas and the proposed empirical models.

- In addition, the results of FEM model were also statistically compared with the modified formulas and empirical models in terms of MAPE, MSE, RMSE, COV, and R-squared values. The statistical evaluation of the results revealed that the FEM model has the lowest error that occurred during the prediction and the highest R-squared value that is the indication of the correlation between the actual and predicted values.

- The predicted results of the GEP model were compared with the results extrapolated by using the modified formulas of codes and the empirical models of the researchers. The results of comparisons showed that the prediction performance of the GEP model is much better than that of the modified formulas and empirical models.

- Furthermore, the estimated results of the GEP model, the modified formulas, and the proposed empirical models were also statistically evaluated in terms of MAPE, MSE, RMSE, COV, and R-squared values. The statistical evaluation of the results indicated that among these prediction methods, the GEP model has the lowest error that occurred during the prediction and the

highest R-squared value that is the indication of the correlation between the actual and predicted values.

- The comparison of the predicted results determined by using the ANN model with the results extrapolated by using the modified formulas of codes and the empirical models of the researchers revealed that the ANN model has almost perfectly estimation capableness, robustness, accuracy, and reliability than the modified formulas and the proposed empirical models.

- Besides, the estimated results of the ANN model, the modified formulas, and the proposed empirical models were also statistically evaluated in terms of MAPE, MSE, RMSE, COV, and R-squared values. The statistical evaluation of the results indicated that among these prediction methods, the ANN model has the lowest error that occurred during the prediction and the highest R-squared value that is the indication of the correlation between the actual and predicted values.

- The R-squared values, which is the remarkable parameter for these type of models, of 0.936, 0.960, 0.950, were attained for the modified ACI (2002), Eurocode 4 (2004), and AISC (2010) formulas, respectively, whereas the R-squared values of 0.888, 0.939, 0.917, and 0.917 were procured for the empirical models proposed by Uenaka et al. (2010), Han et al. (2011b), Yu et al. (2013), and Hassanein et al. (2013b), respectively. On the other hand, the FEM, GEP, and ANN models had the R-squared values of 0.963, 0.987, and 0.999, respectively.

- The percent error values for various ultimate axial strength intervals were also used to evaluate the prediction capability of the models. It could be professed that while the other models indicated fluctuating estimation capability with respect to the strength intervals, the proposed models exhibited stable prediction performance no matter what the strength intervals.

- When the generated models in this thesis were compared with each other, it was obviously comprehended that the ANN model is more reliable, accurate, and robust model than the FEM and GEP models. Besides, the prediction capability of the ANN model was better than the others and this was supported by statistical evaluation.

- Even though the proposed models in this thesis with 103 data compiled from the available experimental researches in the literature had a reliable and better prediction performance than existing ones, indeed, the robustness, reliability, and accuracy as well as the generalization capability of such models could be improved by extending the dataset utilized in the training of the model.

- The verified FEM model indicated that the ultimate axial strengths of the CFDST columns were affected by the outer and inner steel tubes diameters and thicknesses and the concrete compressive strength. According to the FEM model, when the outer steel tube diameter and thickness increased, the ultimate axial strength also increased. The FEM model results also showed that increasing the concrete compressive strength increased the load carrying capacity of the CFDST columns.

- The predicted results were also statistically analyzed by means of general linear model analysis of variance technique. The analyzing of the FEM model results indicated that all independent parameters have significant effect on the ultimate axial strength of the CFDST columns according to P-values, but the highest effectiveness degree belongs to the outer steel tube diameter regarding the percent contribution. Also, it is noticed that the effectiveness level of the inner steel tube diameter and thickness can be disregarded.

# REFERENCES

Abaqus. (2014). Analysis user's manuals and example problems manuals, version 6.14. Dassault Systemes Simulia Corp., Providence, RI, USA.

Abbas, H., Al-Salloum, Y., Alsayed, S., Alhaddad, M., Iqbal, R. (2016). Post-heating response of concrete-filled circular steel columns. *KSCE Journal of Civil Engineering.* 1-12.

ACI-318. (2002) Building code requirements for reinforced concrete. *ACI.*

AIJ. (2002) Standard for structural calculation of steel reinforced concrete structures. (In Japanese).

AISC. (2010). Load and resistance factor design specification, for structural steel buildings. *American Institute of Steel Construction, Chicago, USA.*

Boyd, P.F., Cofer, W.F., Mclean, D.I. (1995). Seismic performance of steel-encased concrete columns under flexural loading. *ACI Structural Journal.* **92(3)**, 355-64.

Chen, W.F., Chen, C.H. (1973). Analysis of concrete filled steel tubular beam-columns. *International Association for Bridger and Structural Engineering Publications.* **33(11)**, 37-52.

Convolutional Neural Networks for Visual Recognition. 2018. http://cs231n.github.io/neural-networks-1/.

D'Aniello, M., Güneyisi E.M., Landolfo, R., Mermerdaş, K. (2014). Analytical prediction of available rotation capacity of cold-formed rectangular and square hollow section beams. *Thin-Walled Structures.* **77**, 141-152.

Damaraju, A.V. (2013). Investigation on the stability of noncompact and slender concrete filled tubes subjected to axial loads. MSc Thesis, University of Cincinnati, India.

Dong, C.X., Ho, J.C.M. (2012). Uni-axial behaviour of normal-strength CFDST columns with external steel rings. Steel and Composite Structures. **13(6)**, 587-606.

Dong, C.X., Ho, J.C.M. (2013). Improving interface bonding of double-skinned CFST columns. *Magazine of Concrete Research.* **65(20)**, 1199-1211.

Elchalakani, M., Zhao, X.L., Grzebieta, R.H. (2001). Concrete filled circular steel tubes subjected to pure bending. *Journal of Constructional Steel Research.* **57(11)**, 1141-68.

Elchalakani, M., Zhao, X.L., Grzebieta, R.H. (2002). Tests on concrete filled double-skin (CHS outer and SHS inner) composite short columns under axial compression. *Thin-Walled Structures.* **40(5)**, 415-41.

Ellobody, E., Young, B. (2006a). Nonlinear analysis of concrete-filled steel SHS and RHS columns. *Thin Walled Structures.* **44**, 919-30.

Ellobody, E., Young, B. (2006b). Design and behavior of concrete-filled cold-formed stainless steel tube columns. *Engineering Structures.* **28**, 716-28.

Elmas, Ç. (2003). Yapay sinir ağları. *Seçkin Yayıncılık, Ankara.* 21-39.

Elremaily, A., Azizinamini, A. (2002). Behavior and strength of circular concrete-filled tube columns. *Journal of Constructional Steel Research.* **58(12)**, 1567-91.

Ergezer, H., Dikmen, M., Özdemir, E. (2003). Yapay sinir ağları ve tanıma sistemleri. *Pivolka.* 14-17.

Ersoy, U., Özcebe, G., Tankut, T. (2010). Reinforced concrete. *METU Press Ankara, Turkey.*

Essopjee, Y., Dundu, M. (2015). Performance of concrete-filled double-skin circular tubes in compression. *Composite Structures.* **133,** 1276-83.

Eurocode 3. (2004). Design of steel structure – Part 1.1: general rules and rules for buildings. *London: British Standard Institution, ENV 1993-1-1.*

Eurocode 4. (2004). Design of composite steel and concrete structures – Part 1.1: general rules and rules for buildings. *London: British Standard Institution, ENV 1994-1-1.*

Ferreira, C. (2001). Gene expression programming; a new adaptive algorithm for solving problems. *Complex Systems.* **12(2)**, 87-129.

Fujimoto, T., Mukai, A., Nishiyama, I., Sakino, K. (2004). Behavior of eccentrically-loaded concrete-filled steel tubular columns. *Journal of Structural Engineering.* **2**, 203-12.

Furlong, R.W. (1967). Strength of steel-encased-concrete beam columns. *Journal of Structural Division.* **93**, 113-24.

Gardner, N.J., Jacobson, E.R. (1967). Structural behavior of concrete-filled steel tubes. *American Concrete Institute Journal.* **64(7)**, 404-12.

Gen, M., Cheng, R. (1997). Genetic algorithms and engineering desing. *Wiley, USA.*

GepSoft. 2018. GeneXproTools 5.0. http://www.gepsoft.com/.

Giakounnelis, G., Lam, D. (2004). Axial capacity of circular concrete-filled tube columns. *Journal of Constructional Steel Research.* **60(7)**, 1049-68.

Goode, C.D., Lam, D. (2008). Concrete-filled tube columns: Tests compared with Eurocode 4. *Composite Construction in Steel and Concrete VI Proceeding Engineering International Conference, ASCE, Reston, VA.* 317-25.

Güneyisi, E.M., Gültekin, A., Mermerdaş, K. (2016). Ultimate capacity prediction of axially loaded CFST short columns. *International Journal of Steel Structures.* **16(1)**, 99-104.

Han, L.H. (2000). The influence of concrete compaction on the strength of concrete-filled steel tubes. *Advances in Structural Engineering.* **3(2)**, 131-7.

Han, L.H., Huang. H., Zhao, X.L. (2009). Analytical behavior of concrete-filled double skin steel tubular (CFDST) beam-columns under cyclic loadin. *Thin-Walled Structures.* **47(6-7)**, 668-680.

Han, L.H., Huo, J.S. (2003). Concrete-filled HSS columns after exposure to ISO-834 standard fire. *Journal of Structural Engineering.* **129(1)**, 68-78.

Han, L.H., Li, Y.J., Liao, F.Y. (2011a). Concrete-filled double skin steel tubular (CFDST) columns subjected to long-term sustained loading. *Thin-Walled Structures.* **49**, 1534-43.

Han, L.H., Ren, Q.X., Li, W. (2011b). Tests on stub stainless steel-concrete-carbon steel double-skin tubular (DST) columns. *Journal of Constructional Steel Research.* **67**, 437-52.

Han, L.H., Tao, Z., Huang, H., Zhao, X.L. (2004). Concrete-filled double skin (SHS outer and CHS inner) steel tubular beam-columns. *Thin-Walled Structures.* **42(9)**, 1329-55.

Han, L.H., Yang, Y.F. (2005). Cyclic performance of concrete-filled steel CHS columns under flexural loading. *Journal of Constructional Steel Research.* **61(4)**, 423-52.

Han, L.H., Yang, Y.F., Tao, Z. (2003). Concrete-filled thin-walled steel SHS and RHS beam-columns subjected to cyclic loading. *Thin-Walled Structures.* **41(9)**, 801-33.

Han, L.H., Yao, G.H., Zhao, X.L. (2005). Tests and calculations for hollow structural steel (HSS) stub columns filled with self-consolidating concrete (SCC). *Journal of Constructional Steel Research.* **61(9)**, 1241-69.

Han, L.H., Zhao, X.L. (2003). Recent developments in concrete-filled steel tubular structures in China. *International Conference on Advances in Structures, Sydney, Australia.* 899-907.

Hassanein, M.F., Kharoob, O.F. (2014a). Analysis of circular concrete-filled double skin tubular slender columns with external stainless steel tubes. *Thin-Walled Structures.* **79**, 23-37.

Hassanein, M.F., Kharoob, O.F. (2014b). Compressive strength of circular concrete-filled double skin tubular shorts columns. *Thin-Walled Structures.* **77**, 165-73.

Hassanein, M.F., Kharoob, O.F., Liang, Q.Q. (2013a). Behaviour of circular concrete-filled lean duplex stainless steel tubular short columns. *Thin-Walled Structures.* **68**, 113-23.

Hassanein, M.F., Kharoob, O.F., Liang, Q.Q. (2013b). Circular concrete-filled double skin tubular short columns with external stainless steel tubes under axial compression. *Thin-Walled Structures.* **73**, 252-63.

Hastemoğlu, H. (2017). Behaviour of double skinned composite columns with concrete filled tubular columns. *Journal of Architectural Engineering Technology.* **6(2)**, 194-204.

Haykin, S. (2000). Neural networks: a comprehensive foundation. *New Jersey: Macmillan College Publications Cooperation.*

Hebb, D. O. (1949). The organization of behavior. *New York: John Wiley and Sons Inc.*

Ho, J.C.M., Lai, M.H. (2013). Behaviour of uni-axially loaded CFST columns connected by tie bars. *Journal of Constructional Steel Research.* **83**, 37-50.

Hsiao, P.C., Hayashi, K.K., Nishi, R., Lin, X.C., Nakashima, M. (2015). Investigation of concrete-filled double-skin steel tubular columns with ultrahigh-strength steel. *Journal of Structural Engineering.* **141(7)**, 04014166.

Hu, H.T., Huang, C.H., Wu, M.H., Wu, Y.M. (2003). Nonlinear analysis of axially loaded concrete-filled tube columns with confinement effect. Journal of Structural Engineering. 129(10), 1322-9.

Hu, H.T., Schnobrich, W.C. (1989). Constitutive modeling of concrete by using nonassociated plasticity. *Journal of Materials in Civil Engineering.* **1(4)**, 199-216.

Kato, B. (1995). Compressive strength and deformation capacity of concrete-filled tubular stub columns. Part I: Strength and rotation capacity of concrete-filled tubular columns. *Journal of Structural and Construction Engineering.* **468**, 183-91.

Kızrak, A. (2018). Şu kara kutuyu açalım: yapay sinir ağları. https://medium.com/deep-learning-turkiye/%C5%9Fu-kara-kutuyu-a%C3%A7alim-yapay-sinir-a%C4%9Flar%C4%B1-7b65c6a5264a.

Koza, J.R. (1992). Genetic programming; on the programming of computers by means of natural selection. *MIT Press, USA.*

Li, W., Ren, Q.X., Han, L.H., Zhao, X.L. (2012). Behaviour of tapered concrete-filled double skin steel tubular (CFDST) stub columns. *Thin-Walled Structures.* **57**, 37-48.

Liang, Q.Q. (2009). Performance-based analysis of concrete-filled steal tubular beam-columns. Part I: theory and algorithms. *Journal of Constructional Steel Research.* **65(2)**, 363-73.

Liang, Q.Q., Fragomeni, S. (2009). Nonlinear analysis of circular concrete-filled steel tubular short columns under axial loading. *Journal of Constructional Steel Research.* **65(12)**, 2186-96.

Lin, C.Y. (1988). Axial capacity of concrete infilled cold-formed steel columns. *Proceeding of Ninth Internation Specialty Conference on Cold-Formed Steel Structures. St. Louis, Missouri, USA.*

Lin, M.L., Tsai, K.C. (2001). Behaviour of double-skinned composite steel tubular columns subjected to combined axial flexural loads. *First International Conference on Steel and Composite Structures, Pusan, Korea.* 1145-52.

Lin, M.L., Tsai, K.C. (2003). Mechanical behavior of double-skinned composite steel tubular columns. *Joint NCREE-JRC Conference, Taipei, Taiwan.*

Lu, H., Han, L.H., Zhao, X.L. (2009). Analytical behavior of circular concrete-filled thin-walled steel tubes subjected to bending. *Thin-Walled Structures.* **47(3)**, 346-58.

Lu, H., Zhao, X.L., Han, L.H. (2010a). Fire performance of self-consolidating concrete filled double skin tubular columns: experiment. *Fire Safety Journal.* **45(2)**, 106-15.

Lu, H., Zhao, X.L., Han, L.H. (2010b). Testing of self-consolidating concrete-filled double skin tubular stub columns exposed to fire. *Journal of Constructional Steel Research.* **66**, 1069-80.

Lu, Z.H., Zhao, Y.G., (2010). Suggested empirical models for the axial capacity of circular CFT stub column. *Journal of Constructional Steel Research.* **66**, 850-62.

Luksha, L.K., Nesterovich, A.P. (1991). Strength testing on larger-diameter concrete filled steel tubular members. *Proceeding 3$^{rd}$ International Conference on Steel-concrete Composite Structures.*

Maladkar, K. (2018). Types of activation functions in neural networks and rationale behind it. https://www.analyticsindiamag.com/most-common-activation-functions-in-neural-networks-and-rationale-behind-it/.

Mander, J.B., Priestly, M.J.N., Park, R. (1988). Theoretical stress-strain model for confined concrete. *Journal of Structural Engineering.* **114(8)**, 1804-26.

Marson, J., Bruneau, M. (2004). Cyclic testing of concrete-filled circular steel bridge piers having encased fixed-base detail. *Journal of Bridge Engineering.* **1**, 14-23.

MathWorks. 2018. MatlabV.R2017. http://www.mathworks.com/help/.

McCulloch, W.S., Pitts, W.H. (1943). A logical calculus of the ideas immanent in nervous activity. *Bulletin of Mathematical Biophysics.* **5**, 115-133.

Minitab. (2018). Statistical Tool. *Quality Plaza, 1829 Pine Hall Rd., State College, PA 16801-3008, USA*

Mitchell, M. (1996). An introduction to genetic algorithms. *MIT Press, USA.*

Montague, P. (1975). A simple composite construction for cylindrical shells subjected to external pressure. *Journal of Mechanical Engineering Science.* **17(2)**, 105-13.

Montague, P. (1978). The experimental behavior of double-skinned, composite, circular cylindrical shells under external pressure. *Journal of Mechanical Engineering Science.* **20(1)**, 21-34.

Morino, S., Sakino, K., Mukai, A., Yoshioka, K. (1997). Experimental studies of CFT column systems: U.S.-Japan cooperative earthquake research. *ASCE, New York, USA.* 1106-10.

Nakanishi, K., Kitada, T., Nakai, H. (1999). Experimental study on ultimate strength and ductility of concrete filled steel columns under strong earthquakes. *Journal of Constructional Steel Research.* **51(3)**, 297-319.

Nie. J.G., Liao, Y.B. (2008). Bearing capacity calculations for concrete filled double skin tubes. *Journal of Tsinghua University (Science and Technology).* **48(3)**, 312-5. [In Chinese]

O'Shea, M.D., Bridge, R.Q. (2000). Design of circular thin-walled concrete filled steel tubes. *Journal of Structural Engineering.* **11**, 1295-303.

Pagoulatou, M., Sheehan, T., Dai, X.H., Lam, D. (2014). Finite element analysis on the capacity of circular concrete-filled double-skin steel tubular (CFDST) stub columns. *Engineering Structures.* **72**, 102-12.

Prion, H.G.L., Boehme, J. (1994). Beam-column behavior of steel tubes filled with high strength concrete. *Canadian Journal of Civil Engineering.* **21(2)**, 207-18.

Rirchart, F.E., Brandzaeg, A., Brown, R.L. (1928). A study of the failure of concrete under combined compressive stresses. *Bull. 185. Champaign: University of Illinois Engineering Experimental Station, IL, USA.*

Roeder, C.W., Lehman, D.E., Bishop, E. (2010). Strength and stiffness of circular concrete-filled tubes. *Journal of Structural Engineering.* 1545-53.

Saenz, L.P. (1964). Discussion of 'Equation for the stress-strain curve of concrete' by P. Desayi, and S. Krishman. *Journal of the American Concrete Institute.* **61**, 1229-35.

Schalkoff, R. J. (1997). Artificial neural networks. *Columbus: McGraw-Hill*.

Shakir-Khalil, H. (1991). Composite columns of double-skinned shells. *Journal of Constructional Steel Research.* **19**, 133-52.

Susac, M. Z., Sarlija, N., Bensic, M., Tortorelli, S. (2005). Selecting neural network architecture for investment profitability predictions. *Journal of Information and Organizational Sciences*. **29(2)**, 83-95.

Tang, J., Hino, S., Kuroda, I., Ohta, T. (1996). Modeling of stress-strain relationships for steel and concrete in concrete filled circular steel tubular columns. *Steel Construction Engineering, JSSC.* **3(11)**, 35-46.

Tao, Z., Han, L.H. (2006). Behaviour of concrete-filled double skin rectangular steel tubular beam-columns. *Journal of Constructional Steel Research.* **62(7)**, 631-46.

Tao, Z., Han, L.H., Zhao, X.L. (2004). Behaviour of concrete-filled double skin (CHS outer and CHS inner) steel tubular stub columns and beam-columns. *Journal of Constructional Steel Research.* **60(8)**, 1129-58.

Tomlinson, M., Chapman, M., Wright, H.D., Tomlinson, A., Jefferson, A. (1989). Shell composite construction for shallow draft immersed tube tunnels. *ICE International Conference on Immersed Tube Tunnel Techniques, Manchester, UK.*

Uenaka, K., Kitoh, H., Sonoda, K. (2010). Concrete filled double skin circular stub columns under compression. *Thin-Walled Structures.* **48**, 19-24.

Wah, B.W., Mehra, P. (1992). Artificial neural networks: concepts and theory. *Los Alamitos, California, USA.*

Wang, F., Young, B., Gardner, L. (2016). Experimental investigation of concrete-filled double skin tubular stub columns with stainless steel outer tubes. *Eighth International Conference on Steel and Aluminium Structures Hong Kong, China.*

Wang, J., Liu, W., Zhou, D., Zhu, L., Fang, H. (2014). Mechanical behaviour of concrete filled double skin steel tubular stub columns confined by FRP under axial compression. *Steel and Composite Structures.* **14(4)**, 431-52.

Wei, S., Mau, S.T., Vipulanandan, C., Mantrala, S.K. (1995). Performance of new sandwich tube under axial loading: experiment. *Journal of Structural Engineering, ASCE.* **121(12)**, 1806-14.

Wheeler, A., Bridge, R. (2006). The behavior of circular concrete-filled thin-walled steel tubes in flexure. *Composite Construction in Steel and Concrete V Proceeding 5th Engineering International Conference, ASCE, Reston, VA.* 412-23.

Wright, H., Oduyemi, T., Evans, H.R. (1991a). The design of double skin composite elements. *Journal of Constructional Steel Research.* **19**, 111-32.

Wright, H., Oduyemi, T., Evans, H.R. (1991b). The experimental behaviour of double skin composite elements. *Journal of Constructional Steel Research.* **19**, 91-110.

Yagishita, F., Kitoh, H., Sugimoto, M., Tanihira, T., Sonoda, K. (2000). Double skin composite tubular columns subjected to cyclic horizontal and constant axial forces. *Composite and Hybrid Structures.* **1**, 497-503.

Yagishita, F., Kitoh, H., Suimoto, M., Tanihira, T., Sonoda, K. (2002). Double-skin composite tubular columns subjected cyclic horizontal force and constant axial force. *Sixth ASCCS conference Los Angeles, USA.* 497-503.

Yang, J., Xu, H., Peng, G. (2008) Behavior of concrete-filled double skin steel tubular columns with octagon section under axial compression. *Frontiers of Architecture and Civil Engineering in Chine.* **2(3)**, 205-10.

Yu, M., Zha, X., Ye, J., Li, Y. (2013). A unified formulation for circle and polygon concrete-filled steel tube columns under axial compression. *Engineering Structures.* **49**, 1-10.

Zadeh, L.A. (1994). Soft computing and fuzzy logic. *IEEE Software.* **11(6)**, 48-56.

Zhang, G.W., Xiao, Y., Kunnath, S. (2009). Low-cycle fatigue damage of circular concrete-filled tube columns. *ACI Structural Journal.* **106(2)**, 151-9.

Zhao, X.L., Grzebieta, R.H. (2002). Strength and ductility of concrete-filled double skin (SHS inner and SHS outer) tubes. **Thin-Walled Structures. 40(2)**, 199-213.

Zhao, X.L., Grzebieta, R.H., Elchalakani, M. (2002a). Tests of concrete-filled double skin CHS composite stub columns. *Steel and Composite Structures.* **2(2)**, 129-42.

Zhao, X.L., Grzebieta, R.H., Ukur, A., Elchalakani, M. (2002b). Tests of concrete-filled double skin (SHS outer and CHS inner) composite stub columns. *Advances in Steel Structures.* **1**, 567-74.

Zhao, X.L., Han, L.H. (2006). Double skin composite construction. *Progress in Structural Engineering and Materials.* **8**, 93-102.

Zhao, X.L., Tong, L.W., Wang, X.Y. (2010). CFDST stub columns subjected to large deformation axial loading. *Engineering Structures.* **32(3)**, 692-703.

Zhu, W.Z., Peter, J.M.B. (2003). Permeation properties of self-compacting concrete. *Cement and Concrete Research.* **33(6)**, 921-6.

## PERSONAL INFORMATION

Name and surname     : Süleyman İPEK

Nationality          : T.C.

Birth place and date : Diyarbakır/1987

Marital status       : Single

Phone number         : +9 (542) 313 44 21

Fax                  : -

Email                : sipek@bingol.edu.tr

## EDUCATION

|              | Graduate school         | Year |
|--------------|-------------------------|------|
| Master       | University of Gaziantep  | 2013 |
| Bachelor     | University of Gaziantep  | 2010 |
| High school  | Yunus Emre Lisesi        | 2004 |

## WORK EXPERIENCE

| Years         | Place                   | Enrollment          |
|---------------|-------------------------|---------------------|
| 2018-Present  | Bingöl University        | Research Assistant  |
| 2011-2018     | University of Gaziantep  | Research Assistant  |
| 2010-2011     | Bingöl University        | Research Assistant  |

## PUBLICATIONS

### A. International Journals

**1. Süleyman İpek**, Esra Mete Güneyisi (2019) "Ultimate axial strength of concrete-filled double skin steel tubular column sections" Advances in Civil Engineering https://doi.org/10.1155/2019/6493037.

**2.** Asra Al-Goody, Esra Mete Güneyisi, **Süleyman İpek** (2018) "Comparison of ultimate strength results from ACI and Eurocode 4 for steel tubular columns filled with SCC" MATEC Web of Conference Vol. 162.

**3.** Erhan Güneyisi, Mehmet Gesoğlu, Hussein Ghanim, **Süleyman İpek**, Ihsan Taha (2016) "Influence of the artificial lightweight aggregate on fresh properties and compressive strength of the self-compacting mortars" Construction and Building Materials Vol. 116, pp. 151-158.

**4.** Erhan Güneyisi, Mehmet Gesoğlu, Nahla Hilal, **Süleyman İpek** (2015) "Evaluation of the rheological behavior of fresh self-compacting rubberized concrete by using the Herschel-Bulkley and modified Bingham models" Archives of Civil and Mechanical Engineering Vol. 16, pp. 9-19.

**5.** Mehmet Gesoğlu, Erhan Güneyisi, Osman Hansu, **Süleyman İpek**, Dileer Sabah Asaad (2015) "Influence of waste rubber utilization on the fracture and steel-concrete bond strength properties of concrete" Construction and Building Materials Vol. 101, pp. 1113-21.

**6.** Erhan Güneyisi, Mehmet Gesoğlu, Asraa Al-Goody, **Süleyman İpek** (2015) "Fresh and rheological behavior of nano-silica and fly ash blended self-compacting concrete" Construction and Building Materials Vol. 95, pp. 29-44.

**7.** Erhan Güneyisi, Mehmet Gesoğlu, Turan Özturan, **Süleyman İpek** (2015) "Fracture behavior and mechanical properties of concrete with artificial lightweight aggregate and steel fiber" Construction and Building Materials Vol. 84, pp. 156-168.

**8.** Mehmet Gesoğlu, Erhan Güneyisi, Ganjeena J. Khoshnaw, **Süleyman İpek** (2014) "Abrasion and freezing-thawing resistance of pervious concretes containing waste rubbers" Construction and Building Materials Vol. 73, pp. 19-24.

**9.** Erhan Güneyisi, Mehmet Gesoğlu, Qais Kareem, **Süleyman İpek** (2014) "Effect of different substitution of natural aggregate by recycled aggregate on performance characteristics of pervious concrete" Materials and Structures Vol. 49, pp. 521-536.

**10.** Erhan Güneyisi, Mehmet Gesoğlu, Kasım Mermerdaş, **Süleyman İpek** (2014) "Experimental investigation on durability performance of rubberized concrete" Advances in Concrete Construction Vol. 2, pp. 187-201.

**11.** Mehmet Gesoğlu, Erhan Güneyisi, Ganjeena J. Khoshnaw, **Süleyman İpek** (2014) "Investigating properties of pervious concrete containing waste tire rubbers" Construction and Building Materials Vol. 63, pp. 206-213.

**12.** Erhan Güneyisi, Mehmet Gesoğlu, **Süleyman İpek** (2013) "Effect of steel fiber addition and aspect ratio on bond strength of cold-bonded fly ash lightweight aggregate concretes" Construction and Building Materials Vol. 47, pp. 358-65.

**B. International Congress, Conference, and Symposium**

**1.** Kasım Mermerdaş, **Süleyman İpek**, Mehmet Burak Bozgeyik, "Comparison of multi linear regression and genetic programming for estimation of compressive strength of concrete produced with various cement type and mix proportions," 6th International GAP Engineering Conference, Şanlıurfa, Turkey, 2018.

**2.** Kasım Mermerdaş, **Süleyman İpek**, "Fracture properties of high strength metakaolin and silica fume concretes," 3$^{rd}$ International Conference on Chemical, Civil and Environmental Engineering, Antalya, Turkey, 2016.

**3.** Asra Al-Goody, Erhan Güneyisi, Mehmet Gesoğlu, **Süleyman İpek**, "Sorptivity index of self-compacting concretes with nano-silica and fly ash," 2$^{nd}$ International Conference on Buildings, Construction, and Environmental Engineering, American University of Beirut, Lebanon, 2015.

**4.** Erhan Güneyisi, Mehmet Gesoğlu, Mostapha Fahmi, **Süleyman İpek,** "Mechanical and fracture properties of carbon fiber reinforced self-compacting concrete composites," 10$^{th}$ International Conference on Composite Science and Technology, Lisboa, Portugal, 2015.

**5.** Erhan Güneyisi, Mehmet Gesoğlu, Kasım Mermerdaş, **Süleyman İpek**, "Properties of lightweight aggregates made with cold bonded pelletization of fly ash, metakaolin, and cement," International Conference and Exhabition on Application of Efficient and Renewable Energy Technologies in Low Cost Buildings and Constructions, Gazi University, Ankara, 67-75, 2013.

**6.** Erhan Güneyisi, Mehmet Gesoğlu, Kasım Mermerdaş, **Süleyman İpek**, "Transport properties of plain and silica fume concretes incorporating waste tire rubber," 27th International Conference on Solid Waste Technology and Management, Philadelphia, USA, 599–608, 2012.

**7.** Shimal J. Younus, Erhan Güneyisi, Mehmet Gesoğlu, Kasım Mermerdaş, **Süleyman İpek**, "Resistance of natural rubber latex modified lightweight concrete to chloride ingress", 7th Asian Symposium on Polymers in Concrete (ASPIC 2012), İstanbul Technical University, İstanbul, 473-480, 2012.

**FOREIGN LANGUAGE**

Turkish, Kurdish, English

**HOBİLER**

Reading, Photography, Music, Woodwork, Writing